Application of Biochar to Stabilize Mercury in Riverbank Sediments and Floodplain Soils from South River, VA under Conditions Relevant to Riverine Environments

by

Alana Ou Wang

A thesis
presented to the University of Waterloo
in fulfillment of the
thesis requirement for the degree of
Doctor of Philosophy
in
Earth Sciences (Water)

Waterloo, Ontario, Canada, 2019

Examining Committee Membership

The following served on the Examining Committee for this dissertation. The decision of the Examining Committee is by majority vote.

External Examiner:	Dr. Upal Gosh
	Professor
Supervisor:	Dr. Carol Ptacek
	Professor
Internal Members:	
	Dr. David Blowes
	Professor
	Dr. Dogan Paktunc
	Adjunct professor
Internal-external Member：	
	Dr. Neil Tomson
	Professor

AUTHOR'S DECLARATION

This thesis consists of material all of which I authored or co-authored: see Statement of Contributions included in the thesis. This is a true copy of the thesis, including any required final revisions, as accepted by my examiners.

I understand that my thesis may be made electronically available to the public

Statement of Contributions

This dissertation consists of a series of manuscripts either published with co-authors or manuscripts prepared for submission to peer-reviewed journals. As the first author of each paper, I was responsible for conducting experiments, collecting samples for analysis, interpreting analytical results and writing manuscripts. Contributions for each chapter are summarized as below:

Chapter 1: This chapter was written solely by Alana Ou Wang with input from Carol Ptacek.

Chapter 2: The experiments was primarily conducted by Alana Ou Wang with input from Carol Ptacek, David Blowes, Richard Landis, James Dyer. Blair Gibson conducted X-ray absorption near edge structure across Hg L_{III}-edge for South River sediment. Jing Ma conducted sequential Hg extraction and solid MeHg analyses. Alana Ou Wang interpreted analytical results and wrote the manuscript. All other co-authors provided feedback prior to publishing.

Chapter 3: The experiments were primarily conducted by Alana Ou Wang with input from Carol Ptacek, David Blowes and Erin Mack. Dogan Paktunc suggested experimental designs for high energy resolution fluorescence detection X-ray absorption spectroscopy (HERFD-XAS) at Hg Lα fluorescence emission line, and Zou Finfrock further developed the HERFD-XAS experimental set-up. Alana Ou Wang collected samples for analyses and interpreted

analytical results. Alana Ou Wang wrote the manuscripts with feedback from Carol Ptacek, David Blowes, Zou Finfrock, Dogan Paktunc, and Erin Mack.

Chapter 4: The experiments were primarily conducted by Alana Ou Wang with input from Carol Ptacek, David Blowes, Dogan Paktunc and Erin Mack. Alana Ou Wang collected samples for analyses and interpreted analytical results. Alana Ou Wang wrote the manuscripts with feedback from Carol Ptacek.

Chapter 5: The experiments was primarily conducted by Alana Ou Wang with input from Carol Ptacek, David Blowes and Erin Mack. Alana Ou Wang collected samples for analyses and interpreted analytical results. Alana Ou Wang wrote the manuscripts with feedback from Carol Ptacek.

Chapter 6: This chapter was written solely by Alana Ou Wang with input from Carol Ptacek.

Abstract

Disposal of mercury (Hg) containing products related to industrial activities has led to large-scale watershed contamination across the globe, posing long-term risks to human health due to its persistent properties. Hg in terrestrial systems can re-enter aquatic systems directly through soil erosion and sediment resuspension, and indirectly through reductive dissolution of manganese (Mn) and iron (Fe) oxides, desorption from clays and other minerals, and breakdown of soil organic matter. Hg is transformed into methylmercury (MeHg), a well-known neurotoxin that accumulates through the food chain, mainly by microbially driven processes under anoxic conditions. Remediation of Hg in riverine environments is challenging due to dynamic redox oscillations caused by flooding and drainage which influence Hg mobility and bioavailability. Mercury sulfate ($HgSO_4$) was used by a textile plant in Waynesboro, VA between 1920-1950s, and as a result of inadvertent discharge elevated Hg concentrations have been observed in the South River watershed since 1970, long after cessation of $HgSO_4$ use. Biochars have been proposed for use in reactive capping mats or as soil amendments for *in situ* Hg stabilization. Studies evaluating the effectiveness of biochar for stabilizing Hg focus on the effectiveness under fully-saturated conditions, but how treatment systems respond to more environmentally relevant conditions, such as drying and rewetting, is less studied.

This dissertation evaluates selected biochars for Hg stabilization in river bank sediments and floodplain soils collected along the South River using laboratory-scale experiments under conditions relevant to riverine environments, including flooding and drainage, fully-

saturated anoxic, and drying and rewetting conditions. Five biochars selected for study were: hardwood biochar (OAK), sulfurized-hardwood biochar (MOAK), and biochar prepared from ethanol refinery by-products, including distillers` grains (DIS), anaerobic digestate (DIG), and a mixture of digestate and distillers` grains (75G25S). OAK was evaluated for potential application as a reactive capping mat as well as a soil amendment, and the other biochars were evaluated as soil amendments.

To evaluate OAK as a reactive capping mat which intercepts flow paths under flooding and drainage conditions, the treatment system consisted of two sets of modified humidity-cell experiments operated for 100 weekly cycles. The weekly cycles started with dry air, water-saturated air, and were followed by an aqueous leach at day 7 of each week. Each set contained a source column and a treatment column. Source columns contained river bank sediment and floodplain soil collected from different locations along the South River. Treatment columns contained 50% v/v OAK and non-reactive quartz sand. South River water (SRW) was used as input solution for the source column containing river bank sediment, and acidic rain water (ARW) was used as an input solution for the source column containing floodplain soil. Leachates collected from the source columns were used as input solutions for the treatment columns. More than 80% Hg was retained in the treatment columns with limited formation of MeHg in both aqueous and solid phases. Results of micro X-ray fluorescence mapping (μ-XRF) indicate Hg retained on OAK co-occurred with Si, S, Fe and Cu within the biochar porous structure. Results of S K-edge X-ray absorption near edge structure (XANES) analyses indicate lower fractions of sulfoxide for OAK in treatment systems than in untreated OAK. These synchrotron-based analyses indicate that Hg

accumulation in OAK when used as a reactive capping mat under flooding and drainage conditions can be attributed to retention of the Hg as particulates in the biochar porous structure as well as formation of complexes with O-containing functionalities on the biochar.

OAK and MOAK were evaluated as soil amendments in a floodplain soil under anoxic saturated conditions using laboratory-scale microcosm experiments followed by drying and rewetting of the biochar-amended systems. Floodplain soil was mixed with or without biochars and equilibrated with SRW under anoxic conditions for up to 200 d, and solid materials collected at selected reaction intervals were dried under oxic conditions for 90 d and rewet under anoxic conditions for an additional 90 d. Limited Hg removal was observed in OAK-amended systems. Addition of MOAK enhanced Hg removal under anoxic conditions without promoting MeHg production. After drying and rewetting, Hg in OAK-amended systems was remobilized, likely due to association with dissolved organic carbon (DOC), while Hg in MOAK-amended systems remained at low concentrations. Increases in solid MeHg concentrations coupled with increases in aqueous Mn, Fe, SO_4^{2-} and HS^- concentrations in MOAK-amended systems were observed. 16s RNA pyrosequencing analysis suggests shifts in Hg methylating community composition toward sulfur-reducing bacteria (SRB). Drying and rewetting alters the structure of the microbial community, therefore generating conditions favourable for MeHg production in MOAK-amended systems.

DIG, DIS, and 75G25S were evaluated as alternative soil amendments in floodplain soil following the same experimental protocol used to evaluate OAK and MOAK as soil amendments. Addition of digestate-based biochar (DIG and 75G25S) led to greater Hg

uptake and lower MeHg concentrations than the addition of DIS. After drying and rewetting, increases in DOC concentrations were observed in digestate-biochar amended systems, while concentrations of Hg remained at low concentrations, suggesting Hg in digestate-based biochars was less likely affected by the release of DOC. Concentrations of MeHg in these biochar-amended systems remained at low concentrations, and solid MeHg content was 50% lower after drying and rewetting than under initial anoxic conditions. These experiments suggest that digestate-based biochars can potentially be used as soil amendment in fully-saturated anoxic environments with limited impacts from drying and rewetting on the system performance.

MOAK and DIG were further evaluated as soil amendments under periodic wetting and drying conditions due to their greater control of Hg under anoxic conditions. The periodic wetting and drying conditions were mimicked using a modified humidity-cell experiment. Each wetting and drying cycle contained a wetting, leaching and drainage period, and a total of ten cycles was conducted. In wetting periods, SRW was added and the system was allowed to stagnate for 14 d, and then drained by gravity during leaching periods, after which solid materials were dried before the next wetting period. An early period of elevated leachate concentrations of THg, MeHg, DOC, and Mn, was observed in the soil control and biochar-amended systems. Limited Hg removal (up to 57%) was observed in the biochar-amended systems at steady state. Minimal MeHg (<0.6 ng L^{-1}) was observed in soil control and DIG-amended systems, while MeHg concentrations were up to 158 ng L^{-1} in the MOAK-amended system during the early flush. THg and MeHg concentrations in the early flush were positively correlated with DOC and Mn concentrations. Concentrations of SO_4^{2-}

increased with decreases in pH and alkalinity in the MOAK-amended system. Initial release of elevated (SO_4^{2-}) was observed in the DIG-amended system. S K-edge XANES spectra indicate polysulfur is the predominant S form in the biochar-amended systems. Results of 16s rRNA pyrosequencing suggest the microbial community in the MOAK-amended system shifted toward sulfur oxidizers, while the microbial community in the DIG-amended system was similar to the soil control. The greater abundances of sulfur oxidizers in the MOAK-amended system suggest MOAK is more available for microbial organisms to promote microbially-driven oxidation under periodic wetting and drying conditions.

Results of this study suggest that Hg removal under conditions relevant to riverine environment depends on application methods, biochar properties and biogeochemical conditions. Biochars may be used as reactive material embedded in geotextiles for river bank stabilization and as soil amendments. Dynamic oscillations representative of riverine environments indirectly influences the effectiveness of Hg removal and may result in unintended consequences. Careful characterization of biochar properties and local environments are recommended prior to implementing large-scale biochar applications.

Acknowledgements

I would like to express my deepest appreciation to my supervisor Dr. Carol Ptacek for her continuous support for my PhD study and research. Her guidance has provided fulfilling advice regarding my science and career development. Dr. Carol Ptacek has provided numerous opportunities for me to learn and to teach. I am particularly impressed by her perceptiveness and intelligence. Without her guidance, it would not have been possible for me to finish this dissertation.

I am grateful for constructive feedback from other committee members, Dr. David Blowes, Dr. Richard Amos, and Dr. Dogan Paktunc. Dr. David Blowes always provided valuable feedback related to experimental design and data interpretation. Dr. Richard Amos taught me to pay attention to the big picture. Dr. Dogan Paktunc provided valuable comments related to solid-phases analyses. I would like to give special thanks to my external committee member Dr. Upal Gosh for his valuable comments related to this thesis. I also really appreciate the valuable suggestions related to manuscript consolidation from my internal-external committee member Dr. Neil Tomson.

I would like to thank everyone who helped me to complete this dissertation. I would like to thank former and current members from the Geochemistry Groundwater Remediation group, including Joanne Angai, Janis Rachel Baldwin, Krista Elena, Sara Fellin, Janice Cooper, Stefan DeYoung, Dr. Blair Gilson, Laura Groza, Nidhu Jagoda, Amy Kenwell, Dr. Peng Liu, David Hilger, Joy Hu, Jing Ma, Mason McAlary, Dr. Eva Pakostova, Roberta Parigi, Emily Saurette, Julie Van de Valk, and Brent Verbuyst for their assistance on sample collection and

data analysis. I would like to thank staff members working at synchrotron facilities, including Dr. Yongfeng Hu and Dr. Zou Finfrock at CLS, Dr. Matthew Newville, Dr. Antonio Lanzirotti, Dr. Steve Heald, Michael Pape, and Dr. George Sterbinsky at the Advanced Photon Source for their help with experimental set-ups. I would like to thank Dr. Michael Schinlder and his former student Sara Lanteigene from Laurentian University for conducting powder XRD analysis for selected South River bank sediments and floodplain soils. I would like to Bryce Meeker from Earth, Energy & Environment, LLC (Shawnee, KS, USA) for providing biochars prepared from ethanol refinery by-products. I also want to thank Ms. Gillian Larkin, member of the Editor's Association of Canada, for providing editorial and technical comments in Chapters 2 to 5. I would like to thank members of South River Science Team for their continued advice and contributions, especially for those who formerly worked at E. I. du Pont de Nemours and Company, including Elizabeth Erin Mack, James A Dyer, Nancy Grosso and Richard Landis.

Finally, I would like to give my special thanks to the following sources for supporting this research. Funding for this research was provided by the Natural Sciences and Engineering Research Council of Canada (NSERC), E. I. du Pont de Nemours and Company Canada, and an Ontario Research Fund (ORF) Research Excellence grant awarded to C. Ptacek and D. Blowes. Synchrotron-related experiments used resources operated for the U.S. Department of Energy (DOE) Office of Science by Argonne National Laboratory supported by the U.S. DOE under Contract No. DE-AC02-06CH11357 and the Canadian Light Source (CLS) and its funding partners. CLS Student Travel Support was awarded to Alana Ou Wang for supporting trips to synchrotron facilities.

Dedication

To my parents, Dan Zhang and Qiping Wang, my husband Dr. Long Pu, and my other family members, Hei Hei, Hui Hui, and Dan Dan for their endless love and support.

Table of Contents

List of Figures

List of Tables

List of Abbreviations

α-HgS	Cinnabar
β-HgS	Metacinnabar
μ-XRF	Micro X-ray fluorescence
μ-XANES	Micro X-ray absorption near edge structure
θ	Volumetric water content
%RSD	Relative standard deviation
75G25S	Biochar prepared from 75% digestate gains and 25% distillers` grains
ANOVA	Analysis of variance
DIG	Biochar prepared from 100% digestate grains
DIS	Biochar prepared from 100% distillers` grains
DOC	Dissolved organic carbon
FeRB	Iron-reducing bacteria
HERFD-XAS	High energy solution fluorescence detection X-ray absorption spectroscopy
MeHg	Methylmercury
MOAK	Sulfurized-hardwood biochar
MOTO	Floodplain soil collected at 1.65 km downstream of the historical contamination site
NSS	Normalized-square sum
OAK	Hardwood biochar used in Chapters 2 and 3
OTUs	Operational taxonomic units
r	Pearson product moment correlation coefficients
SR6	River bank sediment collected at 0.16 km downstream of the historical contamination site
SRB	Sulfate-reducing bacteria
TEM	Transmission electron microscopy
THg	Total Hg
unf	Unfiltered
XANES	X-ray absorption near edge structure
HMT	Source column with MOTO in Chapter 2
H6S	Source column with SR6 in Chapter 2
THC-HMT	Treatment column using leachates from HMT in Chapter 2
THC-H6S	Treatment column using leachates from H6S in Chapter 2
SRWCTRs	Microcosm systems with SRW in Chapters 3 and 4
SedCTRs	Microcosm systems with floodplain soil collected at 36.5 km downstream of the historical contamination site and SRW in Chapters 3 and 4
10%OAKs	Microcosm systems with 10% dry weight OAK of floodplain soil and equilibrated with SRW in Chapter 3
10%MOAKs	Microcosm systems with 10% dry weight MOAK of floodplain soil and equilibrated with SRW in Chapter 4

10%DIG	Microcosm systems with 10% dry weight DIG of floodplain soil and equilibrated with SRW in Chapter 4
10%DIS	Microcosm systems with 10% dry weight DIS of floodplain soil and equilibrated with SRW in Chapter 4
10%75G25S	Microcosm systems with 10% dry weight 75G25S of floodplain soil and equilibrated with SRW in Chapter 4
WatCTRs	Microcosm systems with ultrapure water only in Chapters 3 and 4
HCSed	Humidity-cell with floodplain soils collected at 36.5 km downstream of the historical contamination site in Chapter 5
HCDIG	Humidity-cell with floodplain soil and amended with 10% dry weight DIG in Chapter 5
HCMOAK	Humidity-cell with floodplain soil and amended with 10% dry weight MOAK in Chapter 5

Chapter 1 Introduction

1.1 Mercury Contamination at the Global Scale

Mercury (Hg) contamination related to human activities has been globally documented (Kocman et al., 2013). Mining Hg deposits has been reported as early as 3000 years ago in the Peruvian Andes, followed by the world`s largest Hg mining district in Spain, Almadén, which operated more than 2000 years ago (Cooke et al., 2009; Gray et al., 2004). Hg emissions were primarily related to volatilization from natural Hg deposits prior to the industrial revolution. After the industrial revolution, Hg release increased dramatically, mainly due to the widespread use of Hg-containing products in industrial activities, causing contamination in air, soil and water bodies (Table 1.1) (Horowitz et al., 2014; Kocman et al., 2013, 2017; Streets et al., 2017). Only 30% of the cumulative total Hg released after the industrial revolution has directly entered the atmosphere, whereas the remaining 70% has entered terrestrial and aquatic systems (Fig. 1.1) (Streets et al., 2017). On an annual basis, only 42% of the release from historical contaminated sites had entered the atmosphere through volatilization, while the majority directly enters aquatic systems, creating long-term catchment-scale contamination mainly through hydrological events (Kockman et al., 2013). Artisanal and small-scale gold mining has been identified as the primary source of Hg in aquatic systems, followed by disposal of Hg-containing products (Adler Miserendino et al., 2018; Kockman et al., 2017). After 1970, atmospheric Hg release declined by phasing out Hg in commercial products, however, Hg release derived from historical contaminated sites to terrestrial and aquatic systems has remained elevated (Horowitz et al., 2014; Streets et al., 2017).

In North America, Hg contamination related to disposal of Hg-containing products from industrial activities results in elevated concentrations of Hg in river water, soil, and fish tissues in numerous watersheds. For example, at a former Department of Energy nuclear weapons plant in Oak Ridge (TN, USA) 100 metric tons of Hg were released to the East Fork Poplar Creek, resulting in up to 2500 µg L^{-1} Hg in river water and up to 3000 µg g^{-1} in floodplain soils downstream of the site (Turner and Southworth, 1999). Hg was extensively used in large-scale historical Au mining in California before 1960, resulting in elevated filtered total Hg concentrations (up to 8000 ng L^{-1}) associated with colloidal HgS in downstream stream water, and MeHg/Hg in invertebrates collected in the watershed were >50% (Alpers et al., 2005; Lowry et al., 2004). $HgSO_4$ was discharged into the South River (VA, USA) by a textile plant from 1920s-1950s, resulting in elevated Hg in downstream sediments, floodplain soils, stream water, shallow groundwater, and fish tissues (Carter, 1977; Flanders et al., 2010; Lazareva et al., 2019). A chlor-alkali plant in Arvida (Québec, Canada) discharged 300 metric tons of Hg to the Saguenay Fjord (Québec, Canada) between 1947and 1976, resulting in 120 metric tons of Hg in surrounding soils (Mucci et al., 2015). More than 60 µg L^{-1} of Hg has been observed in the Gossan Creek (New Brunswick, Canada) due to discharge of a shallow groundwater plume derived from gold mine tailings (Al et al., 2006). A chlor-alkali plant in Dryden (Ontario, Canada) released 9 to11 metric tons of Hg between 1963-1970 into the English Wabigoon River (Ontario, Canada), and elevated Hg has been observed in fish tissues between 1970-2010 which potentially poses risks to human health (Neff et al., 2012; Takaoka et al., 2014).

It is important to control Hg release from historical contaminated sites as well as suppress MeHg production, however, traditional soil remediation technologies might not be adaptable for riverine environments, the focus of this thesis. For example, it is difficult to apply physical separation methods at the watershed scale, because physical extraction is usually applied only at highly localized sites (Akcil et al., 2014; Hempel and Thoeming, 1999). Soil washing, combined with physical extraction, has been globally applied at pilot or small-field scales (Dermont et al., 2008). Addition of strong chemicals, such as iodine (I-), EDTA, nitric acid (HNO_3), aqua regia, hydrochloric acid (HCl), and sodium hydroxide (NaOH), remove Hg from soil but alter soil properties, in many cases causing unintended contamination (Akcil et al., 2014; Mulligan et al., 2001; Wang et al., 2012). Thermal desorption removes Hg from the solid matrix as volatile phases at high temperatures and gaseous wastes are usually treated in a secondary treatment plant, which is expensive to operate at field-scales (Mulligan et al., 2001; Wang et al., 2012).

Increased efforts to improve remediation techniques for Hg have been undertaken to lower costs and environmental risks. *In situ* stabilization/immobilization has grown due to the potential for decreased costs and revegetation (Dermont et al., 2008). Application of *in situ* sorbent amendments may reduce transport and biouptake with limited destruction of the natural systems (Ghosh 2011). This thesis focuses on evaluating *in situ* Hg stabilization approaches in riverine environments, with an overall to propose sustainable remediation options for large-scale application in riverine environments.

1.2 Background on Hg Biogeochemistry

Hg is classified as a chalcophile element and occurs in three different oxidation states(Hg(0), Hg(I) and Hg(II)) as well as organomercury in natural environments. Hg(0), highly volatile and insoluble at room temperature, is the dominant atmospheric form of Hg (Fitzgerald and Lamborg, 2013). Hg(I) is not common because Hg(I) easily converts to Hg(0) and Hg(II) depending on prevailing redox conditions.

Hg(II) is the most common oxidation state of Hg in natural environments. Large Hg(II) deposits are usually comprised of cinnabar (α-HgS) and metacinnabar (β-HgS). In aquatic systems, Hg(II) tends to form neutral (e.g., HgS^0, $Hg(SH)_2^0$, HgS_x^0) and charged anionic aqueous species (e.g., HgS_2H^-, HgS_2^{2-}, HgS_xH^- and $Hg(S_x)_2H^{2-}$) with S that are dependant on pH and concentration of total sulfides in aqueous solution (Drott et al., 2013; Jay et al., 2000). In addition to total sulfides, Hg(II) forms complexes with reduced S groups in dissolved organic matter (e.g., $Hg(NOM\text{-}RS)_2$) (Liem-Nguyen et al., 2017). In the absence of strong ligands, Hg(II) hydroxide complexes (e.g., $Hg(OH)_2$ and $HgOH^+$) are common in fresh water, and the Hg(II) chloride complexes (e.g., $HgCl_2$ and $HgCl_4^{2-}$) are expected to occur at low pH and in high chloride systems (Ravichandran, 2004).

Methylmercury (MeHg), one of the most studied organomercury compounds, is a neurotoxin that accumulates through the food chain (Mergler et al., 2007). Hg is transformed into MeHg mainly through passive biouptake in anoxic environments (Fleming et al., 2006; Gilmour et al., 2013a; Hsu-Kim et al., 2013). Microbial communities such as sulfate-reducing bacteria (SRB), iron-reducing bacteria (FeRB), methanogens, syntrophic acetogenic, and fermenters contain potential Hg methylators (Bravo et al., 2018; Fleming et

al., 2006; Gilmour et al., 2013a; Hamelin et al., 2011). SRB are the most studied methylating communities in freshwater systems (Gilmour et al., 1992). FeRB may methylate Hg at a similar rate as SRB (Fleming et al., 2006). Recently, methanogens and FeRB have been observed to contribute more MeHg production than SRB in boreal lake environments (Bravo et al., 2018).

Bioavailability of neutrally charged HgS^0 increases as particle size and structural order decrease. Changes in total sulfides and dissolved organic carbon (DOC) concentrations affect Hg-S-DOM equilibria, indirectly influencing Hg bioavailability (Benoit et al., 1999; Graham et al., 2012, 2017; Liem-Nguyen et al., 2017; Slowey, 2010). Low sulfide conditions favour formation of neutrally charged HgS^0, which is positively correlated with MeHg formation (Benoit et al., 1999, 2001). Increases in DOC concentrations and aromaticity under sulfidogenic conditions enhance Hg bioavailability by forming poorly crystalline β-HgS nanoparticles (Graham et al., 2012, 2017). In systems with both sulfide and organic matter, polysulfur, one of the primary intermediate species for sulfide oxidation, may attach to organic matter to form sulfurized organic matter (Graham et al., 2017; Slowey, 2010), which reacts with Hg to form neutrally charged Hg-thiol-DOM complexes ($Hg(NOM\text{-}RS)_2$) that are highly bioavailable (Graham et al., 2017; Liem-Nguyen et al., 2017).

1.3 Mercury Cycling in Riverine Environments

Hg derived from historical industrial sites can continuously contaminate watersheds, resulting in elevated Hg contents that persist in downstream riverbank sediments, floodplain soils, and, in some cases, estuarine environments (Al et al., 2006; Brooks and Southworth

2011; Eggleston 2009; Flanders et al., 2010; Horvat et al., 1999; Lazareva et al., 2019; Turner and Southworth, 1999). In addition to large spatial distribution across watersheds, Hg accumulates in discontinuous soil horizons along riverbanks (Fig 1.3a), mainly associated with layers rich in soil organic matter (SOM), Fe/Mn oxides, clay minerals and sulfides (Hesterberg et al., 2001; Kim et al., 2004; Lazareva et al., 2019; Lowry et al., 2004; Manceau et al., 2015; Rimondi et al., 2014; Skyllberg et al., 2006). Recent studies demonstrate Hg associated with SOM can convert to nanoparticulate β-HgS (Manceau et al., 2015). These nanoparticles can become mobile during flooding events and highly bioavailable to methylating communities (Hofacker et al., 2013; Graham et al., 2012; Poulin et al., 2016).

Transport and transformation of Hg in riparian soils are strongly influenced by the dynamic nature of hydrological and biogeochemical processes in riverine environments. Hg previously deposited in surface soils can directly enter water columns through riverbank erosion, surface water run-off, and turbidity flows, while Hg deposited in channel margins can enter water bodies through riverbank failure, disturbance of sediment, diffusion, and surface water/groundwater interactions (Fig. 1.2a-b) (Babiarz et al., 2012; Eggleston, 2009; Gibson et al., 2011; Mucci et al., 2015). Extended flooding in riverine environments can lead to anoxic conditions that stimulate anaerobic oxidation of organic matter (Eq. 1.1-4). Under these conditions, Hg in riparian soils can indirectly enter the water column through reductive dissolution of Hg-bearing Fe/Mn oxides, degradation of soil organic matter, reductive dissolution of metacinnabar (β-HgS) to $Hg^{(0)}_{aq}$, and release of Hg-bearing nanoparticles during flooding events (Fig. 1.2c) (Hofacker et al., 2013; Lazareva et al., 2019; Mucci et al., 2015; Poulin et al., 2016). Conditions favourable for Mn(IV), Fe(III), and SO_4^{2-} reduction

and methanogenesis (Eq. 1.1-4) have been reported to be associated with an increase in MeHg production (Bravo et al., 2018; Fleming et al., 2006; Gilmour et al., 1992, 2013a; Hamelin et al., 2011; Liu et al., 2017, 2018a; Poulin et al., 2016; Singer et al., 2016).

$$(CH_2O)_x(NH_3)_y(H_3PO_4)_z + 2xMnO_2 + 3xH^+ \rightarrow xHCO_3^- + 2xMn^{2+} + 2H_2O + yNH_3 + zH_3PO_4 \quad \text{Eq. 1.1}$$

$$(CH_2O)_x(NH_3)_y(H_3PO_4)_z + 4xFe(OH)_3 + 7xH^+ \rightarrow xHCO_3^- + 4xFe^{2+} + 10H_2O + yNH_3 + zH_3PO_4 \quad \text{Eq. 1.2}$$

$$2(CH_2O)_x(NH_3)_y(H_3PO_4)_z + xSO_4^{2-} \rightarrow 2xHCO_3^- + xHS^- + 2yNH_3 + 2zH_3PO_4 \quad \text{Eq. 1.3}$$

$$(CH_2O)_x(NH_3)_y(H_3PO_4)_z + xH_2O + \rightarrow xHCO_3^- + xCH_4 + yNH_3 + zH_3PO_4 \quad \text{Eq. 1.4}$$

Periodic drying and rewetting in riverine environments induce dynamic microbial stresses and redox oscillations, which further influence Hg mobility and bioavailability. Rewetting soil after long-term drought conditions rapidly increases bacterial activity and promotes DOC production (Fierer and Schimel, 2002; Iovieno and Bååth, 2008). Yu et al. (2014) observed cumulative respiration depends on end products from the previous drying and rewetting event, indicating microbial responses for frequent drying and rewetting may differ from a sudden drying or a rewetting event. Drying and rewetting also can shift the taxonomic structure of bacterial communities in soils, with differences observed for soils maintained under long-term drought conditions versus those undergoing frequent drying and rewetting events (Fierer et al., 2003; Zhou et al., 2016). Intermittent drying alters O_2 concentrations in the soil matrix and further leads to SOM oxidation/reduction reactions coupled to cycling of

soil N, Mn, Fe, and S (Fig. 1.2a-c). Newly precipitated Mn(IV) and Fe(III) oxides act as carriers for Hg and MeHg (Dent et al., 2014; Lazareva et al., 2019). Seasonal cycling of Mn(IV) and Fe(III) oxides enhances release of Hg and MeHg through reductive dissolution to aquatic systems (Lazareva et al., 2019; Poulin et al., 2016).

1.4 Removal of Hg using Biochars

Carbonaceous materials with great sorption capacities and large porous structures, such as activated carbon, have been studied as sediment capping materials to minimize transport and biouptake of Hg in contaminated sediments under saturated conditions (Ghosh, 2011; Gilmour et al, 2013b, 2018). Both untreated biochars and modified biochars (e.g., sulfurized biochars) may be used as alternative materials to activated carbon for controlling the release and transformation of Hg due to the great affinity of Hg to their surface functionalities (Gomez-Eyles et al., 2013; Liu et al., 2016, 2018b; Park et al., 2019). Studies on applying biochars to control Hg-contaminated soils have been conducted under fully-saturated conditions (Fig. 1.3) (Fellin, 2016; Liu et al., 2017, 2018a, 2019a; Ting et al, 2018; O'Connor et al., 2018), which may represent remediation applications in benthic zones.

Hg deposited in channel margins may be released continuously to stream water through riverbank failure, resuspension of sediment in contact with stream water, and advective transport of dissolved or colloidal Hg-bearing particles with interflow and groundwater discharge (Fig. 1.2a-c). This Hg can be stabilized by emplacing biochar as reactive material embedded in permeable fabrics and installed along riverbanks (Fig. 1.3). Laboratory column experiments using biochar as a reactive media demonstrate >95% Hg removal with limited

MeHg production under saturated-flow conditions (Desrochers, 2013; Paulson, 2014; Peterson et al., 2017).

Although the above studies demonstrate biochars may limit the discharge of Hg without promoting methylation under saturated conditions, these studies may not be representative of environments that are subject to changes in hydrological and biogeochemcial conditions as a result of periodic flooding and drying in riverine environments (Fig. 1.3). Beckers et al. (2019) observed limited impacts on aqueous Hg concentrations in biochar-amended systems as Eh values increased from -130 to 300 mV, while increases in MeHg were observed at the Eh window from 0 to 100 mV. Release of Hg and production of MeHg in these biochar-amended systems are positiviely correlated to concentrations of DOC and SO_4^{2-} (Becker et al., 2019). Cycling of DOC, Mn, Fe, and S stemming from frequent flooding and drying and fluctuations in water levels may influence the effectiveness of biochar for Hg stabilization. These studies suggest that applications of biochar in dynamic hydrological and biogeochemical settings require thorough evaluation prior to installation of large-scale remediation systems.

1.5 General Research Objectives

This study evaluates Hg stabilization using a range of biochars under different environmentally relevant conditions. The biochars investigated included hardwood biochar (OAK), sulfurized-hardwood biochar (MOAK), biochars prepared from 100% anaerobic digestate grains (DIG), 100% distillers` grains (DIS), and a mixture of 75% anaerobic digestate grains with 25% distillers` grains(75G25S).Previous studies demonstrate OAK and

MOAK have the potential for stabilizing Hg from aqueous solutions (Liu et al, 2016; 2018b). The current study complements the use of OAK and MOAK for *in situ* Hg stabilization under environmentally relevant conditions. Biochars prepared from ethanol refinery by-products, including biochars prepared from anaerobic digestate or distillers` grains have not been evaluated for Hg stabilization, but biochars prepared from anerobic digestate effectively decrease concentrations of Pb^{2+}, Cd^{2+}, Cu^{2+}, and Ni^{2+} in aqueous solutions mainly through surface adsorption (Lnyang et al., 2012; Ni et al., 2019). Biochars prepared from these ethanol refinery by-products can further provide sustainable waste management. Therefore, biochars, including DIG, DIS, and 75G25S, were also selected and evaluated for their potential as soil amendments for stabilizing Hg. Laboratory microcosms and dynamic column experiments were conducted to evaluate the extent of Hg stabilization under conditions that were designed to mimic long-term flooding and drainage, long-term fully saturated, drying and rewetting, and under multiple drying and rewetting cycles.

1.6 Site Descriptions

Contaminated floodplain soil and sediment was collected from the South River watershed (VA, USA) (Fig. 1.4). The South River starts from southern Stanton passing through Waynesboro and flowing to northern Port Republic. $HgSO_4$ was used as a catalyst in acetate production by a textile plant in Waynesboro (VA, USA) from 1920s-1950s. Elevated concentrations of Hg were observed in the South River water, downstream soil samples, shallow ground water and fish tissues more than 20 years after cessation of Hg use at the textile plant (Cater, 1977; Flanders et al., 2010; Lazareva et al., 2019). Changes in river morphology led to deposition of Hg in clay and silt fractions of channel margins more than

38 km downstream of the historical release site, with particularly high concentrations observed close to the river edge (e.g., Lazareva et al., 2019 of 1200 μg g^{-1} at 5.6 km downstream). Concentrations of Hg greater than background concentrations (0.2 μg g^{-1}) have also been observed further from the river edge notably within the 5-year floodplain but also extending further inland in 100-year floodplain soils (URS, 2018). Frequent inundation events and erosion of riverbanks containing this accumulated Hg have been postulated to be the primary sources of Hg released to the South River with an estimated minimum annual rate of 109.6 kg $year^{-1}$ (Eggleston, 2009; Pizzuto, 2012; Rhoades et al., 2009). Isotopic measurements suggest the source of Hg along the South River is derived from direct industrial discharge from the textile plant, but also an unknown Hg source, and mixing of these two sources (Washburn et al., 2017).

Concentrations of MeHg in the South River bank sediments are closely correlated to the solid-phase organic carbon and poorly crystalline Mn and Fe oxides (Lazareva et al., 2019). Both FeRB and SRB are the predominant microbial communities contributing to Hg methylation in South River sediments (Liu et al., 2017, 2018a; Paulson et al., 2016; Yu et al., 2012). Elevated concentrations of MeHg have been observed in fish, birds and amphibians in the watershed (e.g., Cristol et al., 2008; Bergeron et al., 2011; Jackson et al., 2011). Newman et al. (2011) demonstrate greater biomagnification factors in the South River floodplains than in the South River.

1.7 Dissertation Contents

This dissertation consists of an introduction (Chapter 1), four chapters (Chapters 2 to 5) that are presented in the form of manuscripts either published or prepared for submittal to peer-reviewed journals. The goals of the four research chapters are to answer the following questions:

1. Can hardwood biochar (OAK) be used as a reactive capping mat under environmentally relevant flooding and drainage conditions?
2. Can sulfurized-hardwood biochar (MOAK) enhance Hg removal when applied as a soil amendment under long-term anoxic conditions? How do drying and rewetting events affect the biochar-amended systems?
3. Can alternative biochars, such as biochars prepared from ethanol refinery by-products, be applied as soil amendments? How do drying and rewetting events affect the biochar-amended systems?
4. How do multiple wetting and drying cycles in floodplains affect Hg removal as well as biochar-amended systems?

Chapter 2 evaluates the use of hardwood biochar (OAK) as a reactive mat under environmentally relevant flooding and drainage conditions. Weekly laboratory-cyclic experiments (100 weeks) were conducted that started with dry air, water-saturated air, and followed by an aqueous leach at the end of each week to simulate frequent flooding and drainage conditions along riverbanks. Each set of experiments contains a source and a treatment column. Source columns contain Hg-contaminated riverbank sediments and

floodplain soils collected along the South River. South River water (SRW) and simulated acid rain water (ARW) were used as the aqueous leach for the source columns. Treatment columns contained 50% v.v OAK with non-reactive quartz sand. Leachate collected from the source columns at the end of each week were used as input solutions to the treatment columns.

Chapters 3 and 4 evaluate alternative biochars (e.g., OAK, MOAK, DIG, DIS, and 75G25S) as soil amendments to floodplain soils and impacts of drying and rewetting on biochar-amended systems using laboratory-scale microcosm experiments. Biochars were mixed with Hg-contaminated floodplain soil and equilibrated with SRW under anoxic conditions with different reaction intervals up to 200 d. Aqueous samples were collected for analysis, solid residues in reaction vessels at selected reaction intervals were dried under oxic conditions for 90 d and then rewet under anoxic conditions for an additional 90 d. S K-edge X-ray absorption near edge structure (XANES) and 16s rRNA pyrosequencing analyses were conducted on solid material after the initial wetting, drying and rewetting conditions to explain impacts of drying and rewetting on the biochar-amended systems.

Chapter 5 evaluates MOAK and DIG for application as soil amendments under multiple wetting and drying conditions due to their greater Hg removal than other biochars under fully-saturated anoxic conditions. Laboratory dynamic column experiments containing a total of ten wetting and drying cycles were conducted, and each wetting and drying cycle consisted of a 14-d wetting period, followed by leaching and drying periods. SRW was added to amended systems at the beginning of each wetting period and allowed to stagnate for 14 d. After 14 d, leachate was drained from the solid matrix by gravity, and the solid was then

dried in air prior to the next wetting period. Solid samples collected over the experimental duration were analyzed for S K-edge XANES and 16s rRNA to determine impacts of continuously wetting and drying in the biochar-amended systems.

Chapter 6 provides a summary of experimental results, contributions of the research to the science literature, descriptions of the environmental implications, and future research directions. The results of the series of experiments are compared and contrasted to provide insight into biochar applications for *in situ* Hg stabilization in dynamic riverine environments and recommendations are made to guide future large-scale applications.

Table 1.1 Commercial past and current global uses of Hg and processes (Reprinted from Horowitz et al., Environ. Sci. Technol. 2014, 48, 10242-10250. Copyright (2019) American Chemical Society.).

Category	Description
Chlor-alkali plants	Electrochemical production of caustic soda and chlorine with Hg cathode
Silver and large-scale gold mining	Extraction from ore by Hg amalgamation
Artisanal and small-scale gold mining (ASGM)	Hg amalgamation by individual miners
Vinyl chloride monomer and other chemical	Production of chemicals with Hg catalyst, felt hat manufacturing and laboratory uses
Paint	Hg fungicide in marine antifouling paint, interior and exterior latex paint
Lamps	All types of Hg-containing lightbulbs (fluorescent, high intensity discharge, etc.)
Batteries	Button cells and cylinders using Hg as cathode or to prevent corrosion
Wiring devices and industrial measuring devices	Switches and relays, thermostats, barometers, manometers
Medical devices	Thermometers and sphygmomanometers (blood pressure meters)
Pharmaceuticals and personal care products	Vaccines and medicines, soaps, cosmetics
Dental amalgam	Cavity fillings with Hg/Ag/Sn/Cu amalgam
Dyes/ vermilion	Pigments containing Hg compounds
Pesticides and fertilizer	Fungicides used in agriculture and pulp and paper
Explosives/ weapons	Munitions, blasting caps, fireworks
Other	Ritual, cultural, and miscellaneous uses

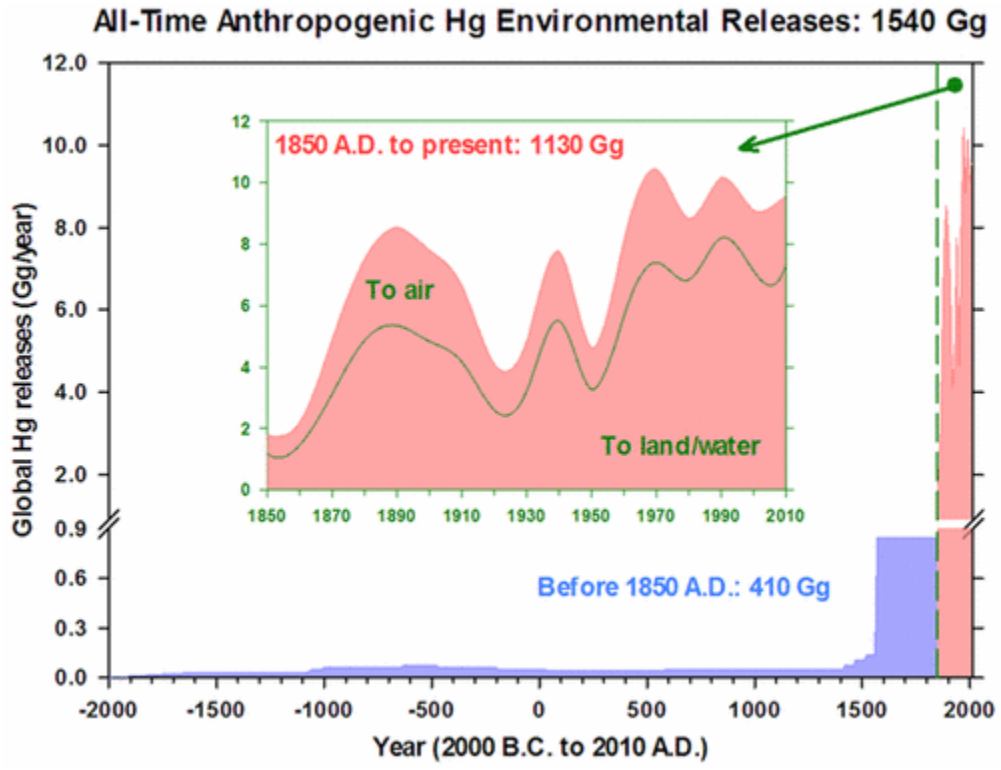

Fig. 1.1 Cumulative Hg release by human activities up to 2010 (Reprinted from Streets et al., Environ. Sci. Technol. 2017, 51, 5969-5977. Copyright (2019) American Chemical Society.).

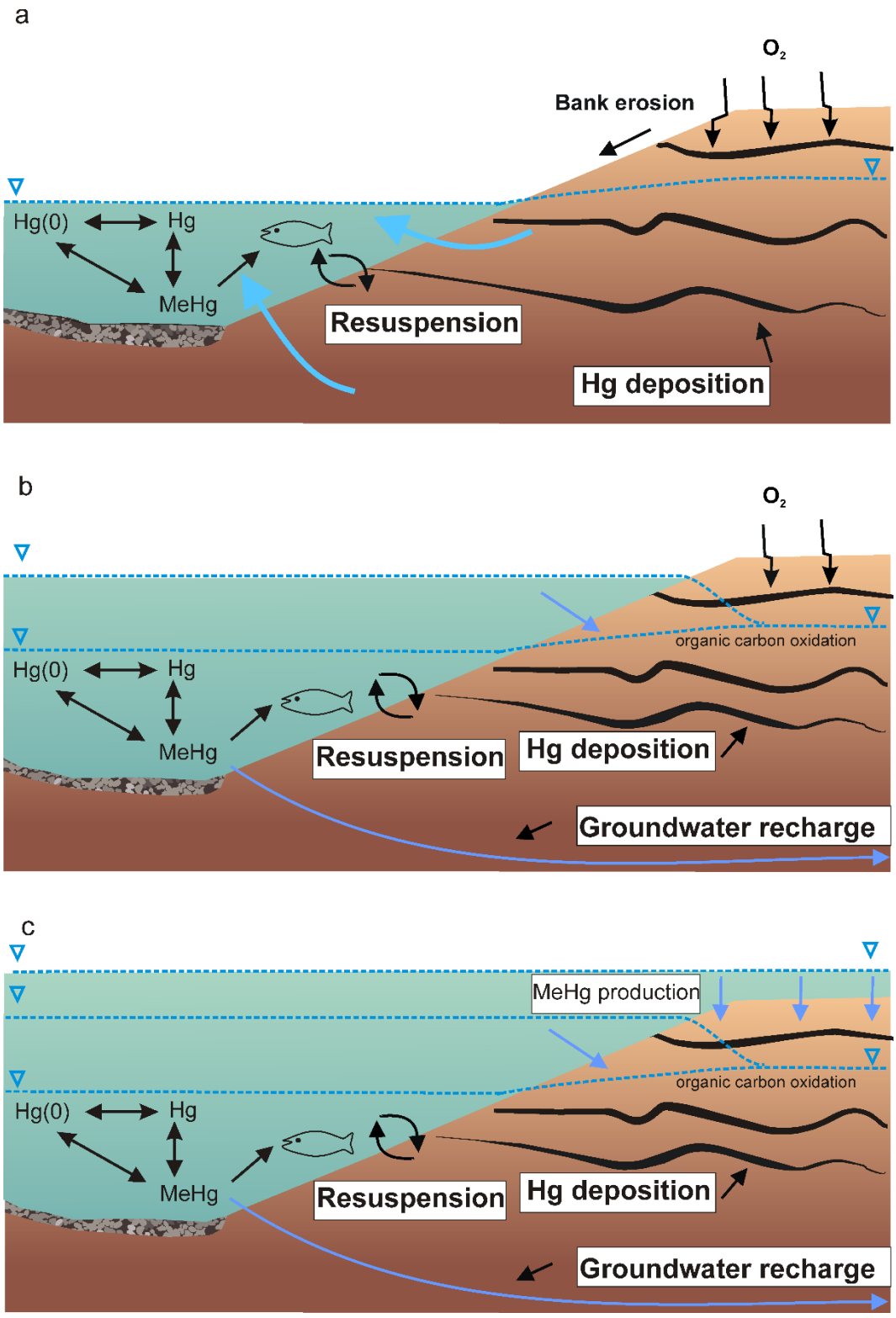

Fig. 1.2 Hg release in riverine environments under different hydrological events.

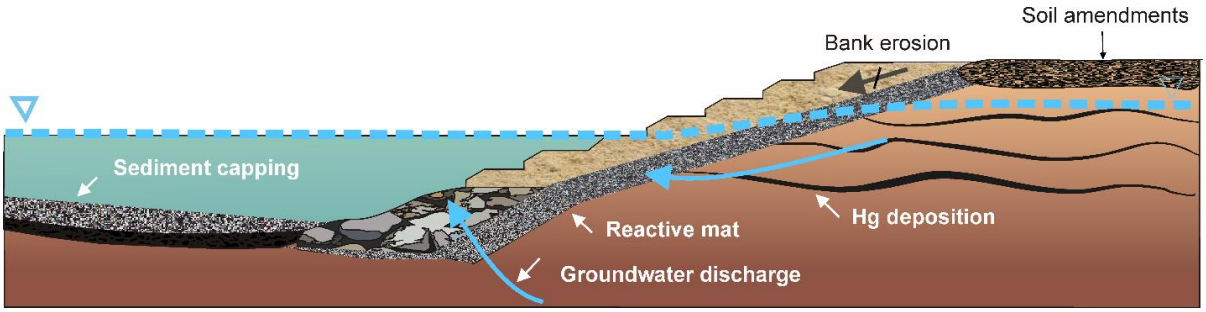

Fig. 1.3 Proposed approaches of biochar applications in riverine environments. Sediment capping refers to application of biochar above benthic sediment under fully-saturated conditions. Reactive mat refers to application of biochar as reactive material installed along riverbanks to minimize release of Hg. Soil amendments refers application of biochars directly in floodplain soils.

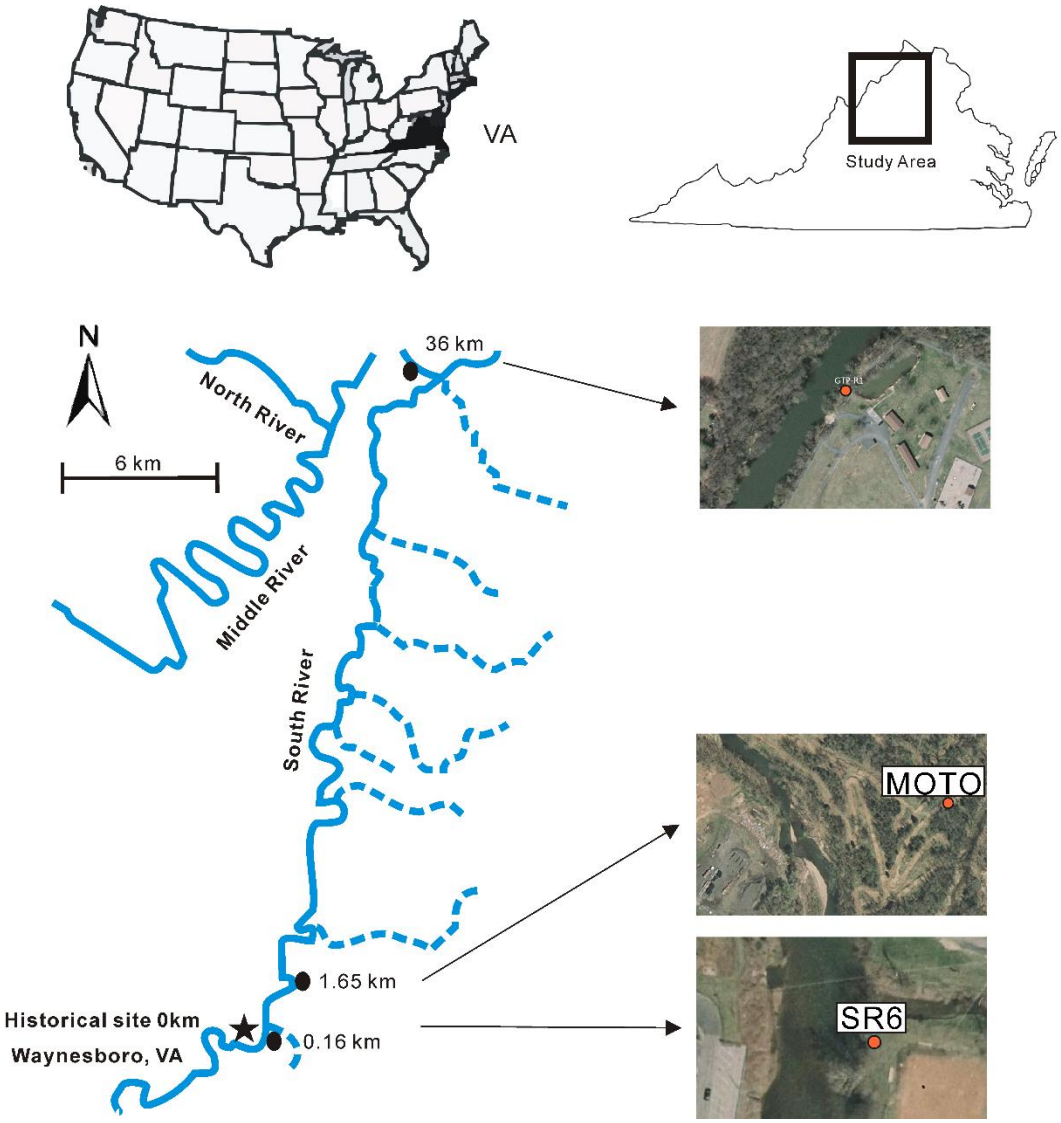

Fig. 1.4 South River watershed with selected river bank sediment (0.16 km) and floodplain soils (1.65 and 36 km) in this study.

Chapter 2 Application of hardwood biochar as a reactive capping mat to stabilize mercury derived from contaminated floodplain soil and riverbank sediments

This chapter is modified from:

Wang, A.O., Ptacek, C.J., Blowes, D.W., Gibson, B.D., Landis, R.C., Dyer, J.A., Ma, J., 2019. Application of hardwood biochar to stabilize mercury derived from contaminated floodplain soil and river bank sediments as a reactive mat in fluvial systems. Sci. Total Environ. 652, 549–561. doi:10.1016/J.SCITOTENV.2018.10.213

Summary

Hardwood biochar (pyrolyzed at 700 °C), a potential candidate for Hg removal, has been proposed for use as reactive capping mat along groundwater discharge zones or riverbanks to control release of Hg from contaminated riverbank sediments. Frequent flooding and drainage in fluvial settings can influence the effectiveness of remediation systems in contaminated riverbank sediments and floodplain soils. This study evaluated the effectiveness of Hg removal using hardwood biochar under hydrogeochemical conditions representative of those present within a reactive capping mat installed in a fluvial setting. Two sets of treatment columns, containing 50% v.v biochar and non-reactive quartz sand, were subjected to 100 weekly wetting/drying cycles that included dry air, water-saturated air, and drainage using leachate derived from two source columns as input solutions: 1. Passing simulated acid rain water through floodplain soil, 2. Passing river water through riverbank sediment. In both treatment columns, more than 80% of the Hg was retained on the biochar without promoting Hg methylation and the release of other unintended dissolved constituents (including N, P, DOC). Results from solid phase extraction analyses suggest that Hg

accumulated near the air/biochar-sand interface (0-2 cm) in the treatment columns at low loadings but was present at greater depths at higher loadings. Results of micro X-ray fluorescence (μ-XRF) mapping and micro X-ray absorption near edge structure (μ-XANES) for the biochar collected at depths 0-2 cm in treatment columns suggest retention of Hg-bearing particles derived from riverbank sediment and floodplain soil within the pore structure of the biochar. Sulfur K-edge XANES analysis of the unused biochar and biochar after treatment suggest formation of Hg-S complexes on the biochar surface. Based on these results, hardwood biochar is potentially an effective media for application in reactive mats for controlling Hg discharging from contaminated riverbank sediments.

2.1 Introduction

Mercury contamination in river water related to industrial activities has been widely documented around the world (Carter, 1977; Kocman et al., 2013; Morway et al., 2017). The release of Hg compounds to riverine systems can result in extensive accumulations of Hg in surrounding riverbank sediment and floodplain soils (Carter, 1977; Eggleston, 2009; Flanders et al., 2010; Mucci et al., 2015, Morway et al., 2017). Under reducing conditions, microorganisms in streams and soil pore water can methylate inorganic Hg species, such as nanoparticulate HgS, dissolved Hg(II), and dissolved $Hg^{(0)}$, to methylmercury (MeHg) in the presence of organic matter, posing health risks to humans and wildlife (Desrochers et al., 2015; Gilmour et al., 2013a; Guedron et al., 2011; Hu et al., 2013; Liu et al., 2016, 2018; Mosher et al., 2012; Paulson et al., 2016).

Mercury accumulates in alluvial sediments and floodplain soils mainly by adsorption on soil organic matter and Fe oxides (Mucci et al., 2015; Pizzuto, 2012). The release of Hg to pore water is controlled by multiple processes, including the release of suspended particles, release of particulate HgS, degradation of soil organic matter, reductive dissolution of Hg-rich Fe-oxides, and reduction of nanoparticulate metacinnabar (β-HgS) to $Hg^{(0)}_{aq}$ (Babiarz et al., 2012; Gibson et al., 2015; Hofacker et al., 2013; Lowry et al., 2004; Mucci et al., 2015; Poulin et al., 2016).

Frequent hydrological changes in fluvial settings can result in shifts in biogeochemical conditions, thus affecting the dynamic Hg cycle. During high runoff events, upstream soil erosion leads to increases in the release of suspended particles, thus causing the remobilization of Hg to river water associated with clay particles (Babiarz et al., 2012). Natural resuspension of sediments in freshwater bodies under oxic conditions can also result in the release of Hg to river water (Gibson et al., 2015). During extended inundation conditions, dissolved O_2 originally trapped within sediment pore spaces can be rapidly consumed by organic matter oxidation. Under these reducing conditions, mercury release to pore water is controlled by rates of soil organic matter degradation and reductive dissolution of reactive Fe-oxides, among other processes (Mucci et al., 2015; Poulin et al., 2016). Periods of extended flooding provide favourable conditions for methylation reactions at the sediment-water interface, mainly related to increases in bacterial activity (Johnson et al., 2010; Poulin et al., 2016; Singer et al., 2016).

Recent studies on *in situ* Hg stabilization focus on soil amendments for immobilizing Hg and minimizing production of MeHg (Bundschuh et al., 2015; Gilmour et al., 2013b, 2018;

Gomez-Eyles et al., 2013; Li et al., 2018; Liu et al., 2017, 2018; Wang et al., 2019; Zhang et al., 2018). Biochar, produced from natural raw organic materials with relatively large surface areas and abundant surface functionalities, has been widely evaluated as an alternative Hg immobilizing reagent due to its relatively low-cost and potential for local availability (Bundschuh et al., 2015; Gilmour et al., 2018; Gomez-Eyles et al., 2013; Liu et al., 2017, 2018; Zhang et a., 2018). Studies on Hg stabilization using biochar indicate biochar can reduce net MeHg production (Bundschuh et al., 2015; Gilmour et al., 2018; Gomez-Eyles et al., 2013; Liu et al., 2017, 2018; Zhang et al., 2013) as well as control the release of Hg from sediments (Liu et al., 2017, 2018).

Management of Hg release from riverbank sediments and floodplain soils is challenging due to the complexity of processes controlling the release and transformation of Hg. Mercury contamination at the watershed scale is usually distributed at isolated locations in a relatively large catchment (Flanders et al., 2010). Direct application of biochar as a soil amendment at isolated locations in a watershed scale may not be effective due to erosional losses caused by frequent flooding and drainage in riverine environments (Gilmour et al., 2018). Installing engineered reactive passive mats containing biochar as reactive materials along riverbanks has been proposed as a solution to retain biochar in designated locations and stabilize Hg under saturated flow conditions (Desrochers, 2013; Paulson 2014). The long-term effectiveness of Hg removal using reactive mats under flooding and drainage conditions is unclear. An evaluation of the robustness of the reactive mat is essential before installing in the field at larger scales.

Based on a previous 48-hour batch study, the hardwood biochar (pyrolyzed at 700°C) was selected due to its relatively high surface area and abundant surface functionalities, and low concentrations of SO_4^{2-} and organic acids compared to agricultural residue and manure-based biochars (Liu et al., 2015). The batch-scale experiments evaluating the hardwood biochar also show Hg removal that is similar to the removal observed using commercial activated carbon, but slightly less than agriculture residue biochars and manure-based biochars (Liu et al., 2016). However, due to the relatively low concentrations of SO_4^{2-}, DOC and acetate, the selected hardwood biochar, is less likely to promote Hg methylation in contaminated sediments under fully saturated static conditions (Liu et al., 2018a), and in experiments designed to evaluate a reactive capping mat under saturated flow conditions (Desrochers, 2013; Paulson, 2014). The effectiveness of biochar to stabilize Hg in fluvial settings, where frequent changes in hydrogeological and biogeochemical conditions occur, has not been widely evaluated.

This study evaluated the long-term effectiveness of Hg removal derived from riverbank sediment and floodplain soil using hardwood biochar as a passive reactive capping mat. Floodplain soils and sediments were used in laboratory apparatus modified from a standard humidity cell test method to provide the input source water for the experiment. Effluent from the source columns was directed to humidity test cells containing treatment materials. This configuration mimicked field weathering conditions and placement of reactive media representative of typical riverine systems.

2.2 Study Site

The South River, located in the Shenandoah Valley in Virginia, starts to the south of Stanton, passes through Waynesboro, and flows to north of Port Republic before it joins the South Fork Shenandoah River (Fig. A 1). A textile plant in Waynesboro, VA, used $HgSO_4$ as a catalyst to manufacture acetate fiber from 1929 to 1950. In the 1970s, elevated concentrations of Hg were observed in South River water, downstream soil samples, and fish tissue (Carter, 1977). Bank erosion has been postulated to be the primary source of Hg release from the alluvial sediments in the South River watershed to freshwater bodies downstream, corresponding to an estimated minimum annual input rate of 109.6 kg $year^{-1}$ (Eggleston, 2009; Rhoades et al., 2009). Concentrations of inorganic particulate Hg of up to 29.9 µg g^{-1} have been observed 16 km downstream from the historical release site (Flanders et al., 2010). Sulfate- and iron-reducing bacteria present in the riverbank sediments and floodplain soils contribute to the net production of MeHg (Desrochers et al., 2015; Paulson et al., 2016; Yu et al., 2012).

2.3 Material and Methods

2.4 Materials

Hardwood biochar, prepared from oak and maple hardwood and pyrolyzed at approximately 700°C, was obtained from Cowboy Charcoal LLC (Brentwood, TN, USA). The biochar was sieved between 0.5 and 2 mm. Riverbank sediment (SR6) was collected from the unsaturated zone of the South River from a depth of 0.3 m below ground surface at a location 0.16 km downstream from the point of historical Hg release; floodplain soil (MOTO) was collected from the center of a cut-off floodplain located 1.65 km downstream from the historical

release site (Fig. A 1; Table A 1). The riverbank sediments and floodplain soils were shipped to the University of Waterloo and stored below 4°C before use. The South River water (SRW) used in the experiment was collected upstream of the historical Hg release site on a bimonthly basis and shipped on ice to the University of Waterloo. SRW was stored at 4°C and in dark conditions prior to utilization in the experiment. Simulated acid rain water (ARW) was prepared by diluting a stock solution of 1 M H_2SO_4 and 1.14 M HNO_3 to a final pH of 4.6.

2.4.1 Experimental design

The humidity-cell-test method is a standardized laboratory procedure to evaluate the release of metals from mine wastes using a fixed-volume of aqueous leaching solution under simulated weathering conditions (Ardau et al., 2009; ASTM, 2012; Langman et al., 2015a,b; Maest and Nordstrom., 2017; Wilson et a., 2018). The first week of the test method includes adding three aliquots of ultrapure water to remove by-products generated during storage. Subsequent weekly cycles start with dry air, water-saturated air at 22°C, and the addition of an aliquot of ultrapure water at the end of each week that is drained by gravity.

In this study, minor modifications were made to the standard method. Acrylic columns were downscaled and had dimensions of 7.4 × 15.3 cm. Two source columns were packed with contaminated sediments that were leached under cyclic wetting/drying conditions. The leachate from the source columns was collected and used as the input solution for subsequent treatment columns that also were subjected to cyclic wetting/drying conditions (Fig. 2.1). One source column (HMT) was packed with MOTO. Sediments at the MOTO site are

subject to acid precipitation, therefore ARW was used as the input solution for HMT. Weekly cycles started with 3 d dry air, 4 d water-saturated air, and the addition of 125 mL ARW on day 7 of each week. The other source column (H6S) was packed with SR6 and had SRW as the input solution; its weekly cycle started with 1 d dry-air, 1 d water-saturated air, then 125 mL SRW added to the column on day 3 of each week. SRW was held in the column for 4 d to represent flooding conditions. On day 7, the leachate was drained by gravity and an aliquot collected for analysis, with the remaining volume used as the input solution for the treatment columns. The treatment columns were packed with 50% v/v biochar and non-reactive quartz sand and flushed with three 125-mL aliquots of ultrapure water during the first week to remove fine ash on the biochar. Aliquots of leachate collected from HMT and H6S were used as the input solutions for treatment humidity cells THC-HMT and THC-H6S, respectfully. The weekly cycle for the treatment columns started with dry air (3 d for THC-HMT and 1 d for THC-H6S), water-saturated air (4 d for THC-HMT and 5 d for THC-H6S), then 100 mL of leachate from HMT or H6S on day 7. Treatment effluents were drained by gravity on day 7 and collected for analysis.

2.4.2 Effluent sample collection

Effluent samples were collected in 250-mL Erlenmeyer flasks washed in 20% HCl. Samples for pH, Eh, total alkalinity, total Hg (THg), methylmercury (MeHg), cations, anions, dissolved organic carbon (DOC), NH_3-N, and PO_4-P were collected using 20-mL polypropylene/ polyethylene sterile Luer lock syringes (Norm-Ject, Thermo Fisher Scientific, Burlington, ON, Canada). pH and Eh were determined on unfiltered samples shortly after collection. Samples for analysis of total alkalinity, THg, MeHg, cations, anions, DOC, NH_3-

N, and PO_4-P were passed through 32-mm diameter syringe filters with 0.45-µm Supor® membranes (Acrodisc®, VWR, Burlington, ON, Canada). Unfiltered samples were also collected for THg and MeHg analyses in 15-mL vacuum and ionized amber borosilicate-glass vials with PTFE-lined caps (Qorpak®, VWR, Mississauga, ON, Canada). Samples for cation and anion analysis were collected in 15-mL polypropylene copolymer bottles (Nalgene®, VWR, Mississauga, ON, Canada). Samples for DOC, NH_3-N, and PO_4-P were collected in 15-mL amber borosilicate-glass vials with PTFE-lined caps. All samples, except for anion samples, were acidified to pH < 2 as follows: samples for THg and cations with ACS reagent grade 15.6 N HNO_3 (JT Baker®, VWR, Mississauga, ON, Canada); samples for MeHg with ACS reagent grade 12.1 N HCl (JT Baker®, VWR, Mississauga, ON, Canada); and samples for DOC, NH_3-N, and PO_4-P with OmniTrace Ultra™ 18.4 M H_2SO_4 (MilliporeSigma, VWR, Mississauga, ON, Canada). All samples were stored at < 4°C before analyses.

2.4.3 Solid sample collection

After 100 subsequent cycles, the treatment humidity cells (THC-HMT and THC-H6S) were sectioned into 2-cm intervals downward from the air/biochar-sand interface to the bottom of the column in a 3.5% H_2/balanced N_2 vinyl anaerobic chamber (COY, Mandel Scientific Company, Guelph, ON, Canada) to avoid further oxidation. The solid samples were frozen at -20°C prior until further analyses. Solid-phase samples collected at depths of 0-2, 2-4, 4-6, and 6-8 cm from the treatment columns were used for a five-step sequential extraction procedure, THg digestion, MeHg extraction, and S K-edge X-ray absorption near edge structure (XANES) analysis. Portions of materials from 0-2 cm were used to prepare polished

thin sections for micro X-ray absorption spectroscopy (μ-XAS) analysis. The polished thin sections were prepared by mounting freeze-dried biochar particles on 26 × 26 mm quartz slides with thicknesses of 30 μm (Vancouver Petrographics Ltd, Vancouver, Canada).

2.4.4 Analytical methods

pH was determined using a combination Ross electrode (Orion model 8156, Thermo Scientific, Waltham, MA, USA) calibrated with standard pH buffers (Thermo Fisher Scientific, Burlington, ON, Canada) at 7.00, 4.00, 10.01 and checked against buffer 7.01 where slopes for three-point calibrations were between 98 and 100%. Eh was determined using a combination platinum Ag/AgCl electrode (Orion 9678, Thermo Scientific, Burlington, ON, Canada) checked against ZoBell's (Nordstrom, 1977) and Light's (Light, 1972) solutions. All Eh values are reported relative to the standard hydrogen electrode. Alkalinity (as $CaCO_3$ mg L^{-1}) was analyzed on 0.45-μm filtered samples at the time of sample collection with a digital titrator using standardized 0.16 N H_2SO_4 (HACH, VWR, Mississauga, ON, Canada) and with bromocresol-green methyl red as an indicator.

Concentrations of trace elements were determined using inductively coupled plasma mass spectroscopy (ICP-MS, X Series 2, Thermo Scientific), and concentrations of major cations were determined using inductively coupled plasma optical emission spectrometry (ICP-OES, iCAP 6000, Thermo Scientific). Concentrations of anions were determined using ion chromatography (DIONEX^{TM} DX600, Thermo Scientific), with a hydroxide eluent (IonPac AG17 4 mm × 50, AS17 4 mm × 250) used for organic acids (lactate, acetate, propionate, and formate) and a carbonate eluent for major inorganic anions (IonPac AG9-HC 4 mm × 50,

AS9-HC 4 mm × 250). DOC was determined using a total organic carbon (TOC) analyzer (TOC-LCPH/CPN, Shimadzu Scientific Instruments, Inc. Columbia, MD, USA) following US EPA method 415.3 (US EPA, 2009). Reactive phosphorus PO_4-P (orthophosphate) was determined following the ascorbic acid method 4500-P E described in the Standard Methods for Examination of Water and Waste Water (APHA, 2005). Samples for NH_3-N were neutralized with 5 N NaOH (Hach, VWR, Mississauga, ON, Canada) before analysis. NH_3-N was determined using LR Test'n Tube™ vials (Hach, VWR, Mississauga, ON, Canada) following the salicylate method (Method 10023 from Hach DR 2800 manual) adapted from Reardon et al. (1966).

THg in different fractions was determined using cold vapour atomic fluorescence spectroscopy (CVAFS, Tekran® 2600, Tekran Instruments Corp, Scarborough, ON, Canada) following US EPA Method 1631 Revision E (US EPA, 2002). Quality assurance/quality control for THg analyses are summarized in supplementary information (Table A 2). The arithmetic mean for the instrument detection limit was 0.19 ± 0.1 ng L^{-1}. The recovery of certified reference material NIST 1614 D was 97% (n> 25). The arithmetic means of the relative percent standard deviation (% R.S.D) for triplicate samples for 0.45-µm and unfiltered THg were 10.7% and 7.82%, respectively. The recovery for matrix spike was 106%.

MeHg was determined using an automated MeHg analyzer (Tekran®2700, Tekran Instruments Corp., Scarborough, ON, Canada), after distillation using a temperature-controlled apparatus (Tekran ®2750, Tekran Instruments Corp, Scarborough, ON, Canada) and ethylating and purging following US EPA Method 1630 (US EPA, 2001). The analysis

detects both monomethylmercury (CH_3Hg^+) and dimethylmercury ($(CH_3)_2Hg$). The instrument detection limit was 0.02 ± 0.01 ng L^{-1} (n=7), and distillation standard recovery ranged from 83-125%. Matrix spikes ranged from 108-121%.

2.4.5 Calculation of Hg retained on biochar

Hg retained on biochar was estimated using the difference between concentrations of unfiltered Hg in the input solutions and in the treatment effluents, normalized to the masses of biochar in the treatment columns:

$$THg\ retained\ on\ biochar\ (\mu g\ g^{-1}) = \frac{(M_{Hgin} - M_{Hg\ out})}{M_{biochar}},$$

$$M_{Hgin}(\mu g) = \sum_{i=1}^{100} C_{input\ i} V_{input\ i},$$

$$M_{Hgout}(\mu g) = \sum_{i=1}^{100} C_{output\ i} V_{output\ i},$$

where M_{Hgin} (µg) is the mass of Hg loaded on the biochar, M_{Hgout} (µg) is the mass of Hg eluted from the biochar, $M_{biochar}$ is the mass of biochar in the treatment cell, $C_{input\ i}$ (µg L^{-1}) is the concentration of unfiltered THg in the input solution at week i, $V_{input\ i}$ (L) is the volume of the input solution added to the treatment cell on week i, $C_{output\ i}$ (µg L^{-1}) is the concentration of unfiltered THg in the treatment effluent on week i, and $V_{output\ i}$ (L) is the volume of treatment effluent collected on week i. Missing data points were interpolated assuming a linear relationship between two measured points.

2.4.6 Characterization of particles in leachates

Unfiltered samples derived from HMT (weeks 57, 81, and 111), H6S (week 57), THC-HMT (weeks 52 and 82), and THC-H6S (weeks 40 and 50) were characterized using transmission electron microscopy (TEM). TEM samples were prepared by placing 5-10 µL of unfiltered

aqueous sample on standard 200 mesh Cu grids (CANEMEC Inc., Montréal, QC, Canada) or on lacey formvar/carbon coated 200 mesh Ni grids (SPi®, SPi Supplies, London, ON, Canada). The prepared samples were analyzed using a Philips CM10 TEM operating at 60 KV at the University of Waterloo to obtain particle size information, with three to nine locations were randomly selected for each sample.

2.4.7 Solid-phase analyses

Solid-phase extractions, including a five-step sequential extraction, total Hg digestion, and MeHg digestion, were conducted on solid samples collected at different depths within the treatment humidity cells at the termination of the experiment. Duplicate extractions were conducted on each solid sample. Non-reactive quartz sand used in the treatment columns had limited impurity and retention. Therefore, concentrations can be corrected for the biochar mass in each column to represent concentrations retained on the biochar.

A five-step Hg sequential extraction procedure, developed by Bloom et al. (2003), was used to target water soluble (F1; WAT), stomach acid soluble (F2; STO), organo-chelated (F3; ORG), elemental (F4; ELE), and mercuric sulfide (F5; SUL) fractions using the following extractants: Ar-purged Milli-Q water (WAT), 0.1 M CH_3COH + 0.1 M HCl at pH 2 (STO), 0.1 M KOH (ORG), 12 M HNO_3 (ELE), and aqua regia (SUL). Concentrations of total Hg retained on the biochar were determined by digesting 0.5 g of solid material in aqua regia for 3 d. Solid-phase concentrations of MeHg were obtained by digesting 0.2 to 2 g of solid material using 20% KCl and 8 M H_2SO_4 with an addition of 0.2 M $CuSO_4$ for distillation, with the digestate analyzed using the method described above.

Statistical differences for the solid-phase concentrations on the biochar within each treatment column were determined using single-factor analyses of variance (ANOVA) at a 95% confidence level ($p<0.1$). Differences for the THg retained on the biochar determined using the sum of Hg extracted at each step from the five-step sequential extraction method and concentrations of Hg obtained from the THg digestion were analyzed using two-factor ANOVA at a 95% confidence level ($p<0.1$). Significant differences between the means of measured solid-phase concentration on the biochar at different depths within each treatment column were determined using Fisher's least significant difference (LSD) (Montgomery, 2012).

2.4.8 X-ray absorption spectroscopy (XAS)

2.4.8.1 Reference materials

Mercury reference compounds included mineral specimens of cinnabar (α-HgS) and corderoite ($Hg_3S_2Cl_2$) (Excalibur Mineral Corp., Peekskill, NY, USA) as well as reagent-grade mercury compounds HgO, $HgCl_2$, and $HgSO_4$ (Sigma-Aldrich, Oakville, ON, Canada). The spectrum of metacinnabar (β-HgS) was obtained from the Hephaestus utility of the Demeter software package (Ravel and Newville, 2005). Eighteen S reference compounds representing a wide range of oxidation states of S were analyzed (Table A 3). These references included natural mineral specimens, pyrrhotite ($Fe_{(1-x)}S$), α-HgS, pentlandite ($(Fe,Ni)_9S_8$), pyrite (FeS_2), marcasite (FeS_2), metacinnabar (β-HgS), elemental S (S_8), Na_2SO_3, $HgSO_4$, $FeSO_4$, $NiSO_4$, K_2SO_4, and gypsum ($CaSO_4 \cdot 2H_2O$) to represent inorganic S compounds. Organic S reference compounds included dibenzyl disulfide, L-cysteine, dibenzo

thiophene (Sigma-Aldrich, Oakville, ON, Canada), tetramethylene sulfoxide (Acros Organics, Thermo Fisher Scientific, Burlington, ON, Canada), and sodium methane sulfonate (Alfa Aesar, Fisher Scientific, Ottawa, ON, Canada).

2.4.8.2 Micro X-ray absorption spectroscopy (μ-XAS)

Micro X-ray absorption spectroscopy (μ-XAS) analyses, including micro X-ray fluorescence (μ-XRF) mapping and micro X-ray absorption near edge structure (μ-XANES) analysis, were conducted at beamline 13-ID-E at the Argonne National Laboratory, IL, USA. A four-element silicon drift detector (Vortex ME-4, SII Nanotechnology USA Inc., Northridge, CA, USA) and a focused ion beam measuring 2 × 2 μm were used to collect μ-XRF maps of Hg and other elements on the polished thin sections with a He bag placed around the sample stage to minimize radiation damage and reduce absorption by air. The μ-XRF maps for Si Kα and S Kα fluorescence lines were collected at 2550 eV, and the μ-XRF maps for Fe Kα, Cu Kα, and Hg Lα fluorescence lines were collected at 13,000 eV. Spots with elevated intensities of Hg were selected to collect μ-XANES across the S K-edge at 2472 eV and across the Hg L_{III}-edge at 12,284 eV.

2.4.8.3 X-ray absorption near edge structure (XANES)

Sulfur K-edge XANES spectra for bulk biochar samples and reference materials were collected at the Soft X-ray Microcharacterization Beamline (SXRMB) at the Canadian Light Source (CLS, Saskatoon, SK, Canada) using a Si (111) monochromator. A broad beam, measuring 3 × 2 mm, was used to collect spectra in fluorescence mode. Unused biochar and biochar collected at the termination of the experiments were analyzed. The biochar samples

and the reference materials were homogenized and smeared as thin films on conductive double-sided tape on a copper sample holder. The sample holder was then mounted in a chamber under vacuum during the analyses. Three scans were collected for each sample, and the scans merged before normalization.

Mercury L_{III}-edge XANES spectra for the floodplain soil (MOTO) and the riverbank sediment (SR6) were collected on beamline 20-ID-B,C-PNC/XSD at the Advanced Photon Source (Argonne National Laboratory, Lemont, IL, USA) using a 4-element Si drift detector (Vortex®, Hitachi High-Technologies Science America Inc., Chatsworth, CA, USA) in fluorescence mode. A defocused beam measuring 500 × 1,000 µm were used.

2.4.8.4 Spectra analyses

Data processing for µ-XANES spectra and bulk XANES spectra was performed using ATHENA (Ravel and Newville, 2005). Linear combination fitting analysis was conducted following the "Combo method" described by Manceau et al. (2012). Sulfur K-edge µ-XANES spectra and XANES spectra were also decomposed into several Gaussian peaks between 2466 and 2489 eV following Manceau and Nagy (2012). Two arctangent steps, representing reduced S species (2474 eV) and oxidized S species (2482.5 eV), were used to decompose spectra for reference compounds and the biochar samples. The collected spectra for reference compounds were first decomposed into Gaussian peaks to determine the whiteline positions indicative of different S species (Fig. A 2-4). Ten Gaussian peaks (Table A 4), representing sulfide minerals (2470.4, 2471.5, and 2472.3 eV), exocyclic S (2473.5 eV), heterocyclic S (2474 eV), sulfoxide (2476.1 eV), sulfite (2478.5 eV), sulfone (2480.2

eV), sulfonate (2481.4 eV), and sulfate (2482.7 eV), were used to decompose S K-edge μ-XANES spectra and XANES spectra for the biochar samples by constraining peak widths within a range of 0.65 to 0.8. Fitting qualities were estimated using a normalized-square sum (NSS) method described by Manceau and Nagy (2012):

$$NSS = \sum(fit - normalized)^2 / \sum normalized^2.$$

The area under a Gaussian peak for a given S species is proportional to the number of vacancies in 3p transitions, and thus increases with oxidation state (Waldo et al., 1991). Scaling factors (Fig. A 5; Table A 4), estimated by normalizing the area under each Gaussian peak to the area under the Gaussian peak of elemental S at 2472 eV, were used to account for the changes in absorption cross section and quantify fractions in each species following Manceau and Nagy (2012).

2.5 Results and Discussion

2.5.1 Overview of riverbank sediment and floodplain soil

Both SR6 and MOTO are abundant in Al, Fe, soil organic matter, and clay minerals with relatively low S contents (<400 μg g^{-1}) (Table A 1). SR6 and MOTO are fine-grained and classified as silty loam based on the USDA soil texture triangle (Soil Survey Division Staff., 1993). Hg L_{III}-edge X-ray absorption near edge structure (XANES) analysis revealed that Hg is mainly present as metacinnabar (β-HgS), cinnabar (α-HgS) and Hg sorbed on goethite (Fig. A 6).

2.5.2 Overview of hardwood biochar

Characterization of the hardwood biochar was conducted in previous studies (Liu et al., 2015, 2018). The hardwood biochar mainly contained C (99.9%) with lesser amounts of Ca (2900 μg g^{-1}) and K (2600 μg g^{-1}). The surface area of the hardwood biochar is 65 m^2 g^{-1}. The most abundant functional groups on the hardwood biochar were hydroxyl, aliphatic, and carboxylic groups.

2.5.3 Chemical composition of input solutions

Leachates derived from humidity cells containing floodplain soil (HMT) and riverbank sediment (H6S) had varying composition over the 100-week duration of the experiment (Table 2.1). Leachates derived from HMT and H6S had generally consistent concentrations of DOC, dissolved anions (Cl^-, NO_3^-, SO_4^{2-}), major cations (Na, Mg, Si, and K), and other trace elements with minor fluctuations. Slightly different values for pH, alkalinity, and concentrations of Al and Ca were observed for the leachates derived from HMT and H6S, mainly due to the different input solutions used for these source columns (Table 2.1). Results of TEM analysis indicate that leachate derived from HMT and H6S contained aggregates of nano-scale particles (Fig. A 7), which is consistent with the mobilization of Hg through the release of colloidal particles from flooded riverine soil (Hofacker et al., 2013; Lowry et al., 2004; Poulin et al., 2016).

The unfiltered leachates derived from HMT and H6S contained elevated concentrations of THg that varied over the duration of the experiment (Fig. 2.2). Effluent concentrations of unfiltered THg derived from HMT ranged from 11,800 to 55,300 ng L^{-1} over the 100-week experimental period. Unfiltered effluent concentrations of THg derived from H6S varied from

1500 to 14,600 ng L^{-1} with a mean value of 4600 ng L^{-1} from weeks 1 to 63, before rapidly increasing to 36,800 ng L^{-1} at week 84 and then dropping to 6160 ng L^{-1} at week 92. The relatively large variations in the chemical composition of leachates from HMT and H6S are attributed to the weekly application of simulated acidic rain water (ARW), river water (SRW) which induce oscillations in pore water chemistry and affect kinetic release rates. These variations are consistent with leachate chemistry derived from other humidity cell experiments (e.g., Ardau et al., 2009; Langman et al., 2015a,b; Maest and Nordstrom, 2017). Concentrations of unfiltered THg from HMT and H6S are similar to the release of total Hg under saturated flow conditions (Desrochers, 2013, 2015; Paulson, 2014; Paulson et al., 2016) and saturated static conditions (Liu et al., 2017) for sediments collected near South River, VA, USA, whereas the release of total Hg under saturated flow and static conditions mostly occurred in the fraction passing a 0.45-µm filter.

Concentrations of 0.45-µm filtered THg and from HMT ranged from 1520 to 9010 ng L^{-1}, with a maximum occurring at week 43. Concentrations of 0.45-µm filtered THg from H6S fluctuated less, ranging from 322 to 741 ng L^{-1} over the course of the experiment. The relatively low proportions of 0.45-µm to unfiltered THg in HMT and H6S suggest that the majority of Hg release under flooding and drainage conditions was present in particulate forms, whereas Hg release under saturated flow/static conditions was present in dissolved (or colloidal) forms.

2.5.4 Composition of effluent from treatment columns

Passage of the source column (HMT and H6S) effluent through the biochar columns, designed to represent a reactive mat, resulted in limited changes in aqueous chemical composition (Table 2.1; Fig. A 8-9). Concentrations of DOC (<10 mg L^{-1}), organic acids (<0.5 mg L^{-1}), NO_3^- (<10 mg L^{-1}), and Ca in the treated effluent were close to the effluent from the respective source columns. Concentrations of SO_4^{2-}, Mg, and K in the treated effluent were slightly higher than in effluent from the source columns. Lower concentrations of Al and Si were observed in the treated effluent, suggesting removal of these constituents through uptake of clay particles within the porous biochar structure. Application of the hardwood biochar resulted in limited release of NH_3-N (<0.3 mg L^{-1}) and PO_4-P (<2 mg L^{-1}).

Application of the hardwood biochar resulted in lower concentrations of both unfiltered and 0.45-µm filtered THg in the treatment effluent derived from the treatment columns (THC-HMT and THC-H6S) than from the source columns (HMT and H6S) (Fig. 2.2). The weekly removal varied over the duration of the experiment and is attributed to the variable Hg release from the source columns. Concentrations of unfiltered THg derived from THC-HMT varied from a minimum of 1440 ng L^{-1} at week 23 to a maximum of 35,100 ng L^{-1} at week 25, while concentrations of 0.45-µm filtered THg varied from a minimum of 95 ng L^{-1} at week 23 to a maximum of 2530 ng L^{-1} at week 25. Weekly Hg removal by THC-HMT ranged from 19 to 90% (unfiltered) and 50 to 90% (0.45-µm filtered). The minimum THg removal for both unfiltered and 0.45-µm filtered THg occurred at week 25 when the lowest Hg release from HMT occurred. Concentrations of unfiltered THg derived from THC-H6S varied from a minimum of 121 ng L^{-1} at week 19 to a maximum of 1230 ng L^{-1} at week 40,

while concentrations of 0.45-µm filtered THg varied from a minimum of 44 ng L^{-1} at week 16 to a maximum of 422 ng L^{-1} at week 75. Weekly Hg removal values in THC-H6S were >90% (unfiltered) and >66% (0.45-µm filtered).

The Concentrations of total Hg retained in the biochar were estimated by normalizing differences between concentrations of unfiltered THg in the source and the treatment effluents to the mass of biochar in the treatment columns. Mercury retained in the THC-HMT biochar was twice as the concentration retained in THC-H6S (Table 2.2), with this difference likely related to the relatively higher release of Hg from HMT (Table 2.1). The estimated total mass of Hg retained in the biochar represents > 80% Hg removal by the THC-HMT column and > 96% removal by the THC-H6S column (Table 2.2).

MeHg concentrations in treatment effluents were lower than those derived from the source columns (Table 2.1). Minor formation of MeHg in treatment effluents was observed for THC-HMT (< 1.0 ng L^{-1}) and THC-H6S (< 0.5 ng L^{-1}) (Fig. 2.3).

2.5.5 Solid-phase extractions

Concentrations of Hg retained on the biochar collected at the termination of the experiment show different distributions within the two treatment columns (Fig. 2.4). No significant differences were observed between two methods (the sum of Hg extracted from the five-step sequential extraction and the *aqua regia* digestion) used to determine total Hg retained on the biochar. Total Hg retained in biochar at different depths changed significantly ($p < 0.002$) for THC-HMT and THC-H6S. Mercury retained on the biochar collected from THC-HMT, which had a higher concentration of unfiltered THg in the input, was present throughout the

entire column length with minor differences. Mercury retained on the biochar collected from THC-H6S, which had a lower concentration of unfiltered THg in the input, was mainly distributed close to the air/biochar-sand interface (0-2 cm), with concentrations then decreasing with increasing depth.

Different concentrations of Hg retained in the biochar in THC-HMT and THC-H6S could be related to the differences in Hg loading to the treatment columns. The lower mass of Hg retained in the biochar in THC-H6S is likely related to lower Hg release from H6S than from HMT. Lower Hg removal observed in THC-HMT than in THC-H6S (Fig. 2.1; Table 2.2) could also be attributed to the relatively acidic pH values and alkalinity (Table 2.1) derived from HMT.

Results of Hg extraction on the biochar collected from THC-HMT and THC-H6S (Fig. 2.4) at the end of the experiment indicate the hardwood biochar had not reached its removal capacity for stabilizing Hg-bearing particles after 100 weeks (82 pore volumes for THC-HMT and 101 pore volumes for THC-H6S), especially for THC-H6S that had 30% of the Hg loading of THC-HMT. The decrease in Hg in the biochar at greater depth in THC-H6S suggests that Hg first accumulated near the air/biochar-sand interface (0-2 cm) at the beginning of the experiment until the removal capacity of biochar at this location was exceeded. Over time, Hg had penetrated further and accumulated at greater depths. The accumulation of the majority of Hg at 0-2 cm in THC-H6S is consistent with a previous study where the majority of Hg was observed to accumulate within the first 2 cm when the same hardwood biochar was used to stabilize Hg derived from river bank sediments under saturated flow conditions (Paulson., 2014).

Results of the five-step sequential extraction procedure indicate that Hg retained in the biochar was mainly present in the organic-chelated Hg (ORG), and elemental Hg (ELE) fractions (Fig. 2.4), with minimal amounts of water soluble Hg (WAT), weak acid extractable Hg (STO), and mercury sulfide and residual forms (SUL). For the biochar in THC-HMT, concentrations of Hg extracted from the ELE, and SUL fractions were significantly lower ($p < 0.004$) at depths of 0-2 and 6-8 cm than from 2-6 cm, whereas variations in the concentrations of Hg extracted from the ORG fraction were not significantly over the length of the column ($p > 0.01$). For the biochar in THC-H6S, concentrations of Hg extracted from the ORG, ELE, and SUL fractions decreased significantly ($p < 0.02$) from 0-2 cm to greater depths (Fig. 2.4). As the total Hg retained on the biochar in THC-H6S decreased, Hg on the biochar shifted from the ELE fractions toward to the ORG fractions. Percentage of Hg extracted from the ELE fraction decreased from 49 to 26%, whereas percent of Hg extracted from the ORG fraction increased from 46 to 66%. This shift in relative percentage of Hg extracted from the ELE toward ORG fractions as loading concentration decrease indicates Hg tends to bound to functional groups on biochar at lower concentrations.

The minimal presence of WAT and STO fractions for biochar in THC-HMT and THC-H6S suggest Hg retained on the biochar is present in less mobile forms. This observation is consistent with a study in which hardwood biochar was used as a reactive mat under saturated flow conditions (Paulson, 2014). In the same study, no significant release of Hg occurred when the biochar was exposed to SRW, and minimal release when it was exposed to ARW (Paulson, 2014).

Insoluble and fine-grained HgS phases with impurities, such as Fe and Zn, can be extracted in the ELE fraction when the total Hg concentration is less than 20 μg g^{-1} (Bloom et al., 2003; Kim et al., 2003). The floodplain soil mainly contains β-HgS (Fig. A 6), likely in nanoparticulate form (Fig. A 7) and associated with other metals, suggesting Hg extracted in the ELE step might also have targeted HgS phases.

Results for MeHg on the biochar suggest a minimal presence (< 0.02 ng g^{-1}) in solid samples collected at the termination of the experiment, with the distribution (Fig. 2.5) following a similar pattern to the total Hg distribution (Fig. 2.4). Changes in biochar MeHg concentrations in THC-HMT were insignificant with an overall mean of 0.15 ± 0.02 ng g^{-1}. MeHg in biochar in THC-H6S decreased significantly ($p = 0.037$) from the air/biochar-sand interface (0.10 ± 0.04 ng g^{-1}) to greater depths (0.01 ± 0.01 ng g^{-1}). The concentrations of MeHg on the biochar represented less than 0.01% of total Hg retained on the biochar. The concentrations of MeHg on biochar from THC-HMT and THC-H6S are similar to those in a study that used the same hardwood biochar for Hg removal under aerobic fully-saturated flow conditions (Paulson, 2014), and the concentrations were more than 100 times lower than those observed in a study of Hg removal in anoxic sediments using the hardwood biochar (Liu et al., 2018a). The relatively low concentrations of sorbed MeHg in biochar collected at the end of the experiment suggest the hardwood biochar might be a good candidate as a reactive material installed under flooding and drainage conditions without promoting MeHg production.

2.5.6 Synchrotron X-ray absorption spectroscopy analyses

Micro XRF maps were collected on polished thin sections prepared with hardwood biochar from the air/biochar-sand interface (0-2 cm) of the treatment columns at the termination of the experiment. Results of µ-XRF maps for THC-HMT indicate the presence of Si, Fe, S, Cu, and Hg within the porous structure of the biochar (Fig. 2.6). Mercury retained on the biochar co-occurred with S and Cu in isolated locations. Limited Hg hot spots were observed in µ-XRF maps collected for biochar from THC-H6S; however, the concentrations of total Hg retained were close to those from THC-HMT, which might be related to the heterogeneous distribution of Hg on the biochar.

Micro-XANES analyses across the Hg L_{III}-edge and S K-edge were performed at locations where greater abundances of Hg and S were observed. Results from the Hg L_{III}-edge µ-XANES results (Fig. 2.7) suggest Hg on the biochar is present in different forms, with linear combination fitting results in derivative mode indicating a composition of ~50% metacinnabar (β-HgS), 43% Hg sorbed on goethite, and 7% HgO. Linear combination fitting was conducted with/without HgO. Excluding HgO (reduced $X^2 = 1.7 \times 10^{-5}$; NSS = 4.4×10^{-2}) resulted in a fit that did not closely correspond to the normalized spectra. Including HgO (reduced $X^2 = 8.4 \times 10^{-6}$; NSS = 2.3×10^{-2}) resulted in improved fit to the normalized spectra. This result suggests that HgO was likely a contributing phase for Hg retention by the biochar. A similar composition of Hg phases retained on the biochar was identified at a second location for the biochar collected at 0-2 cm in THC-HMT. Metacinnabar and Hg sorbed on iron oxides (Fig. A 6) have been observed in the same floodplain soil sample obtained from the South River, Virginia, USA which are consistent with common Hg phases

observed in sediments at sites contaminated by industrial activities (Gibson et al., 2015; Kim et al., 2000; Lowry et al., 2004; Poulin et al., 2016; Rimondi et al., 2014; Santoro et al., 2010; Terzano et al., 2010). The presence of β-HgS and Hg sorbed on iron oxides on biochar suggest retention of particles derived from floodplain soil.

The differences in the predominant Hg forms in the biochar identified using the Hg sequential extraction analyses and linear combination fitting of Hg L_{III} edge μ-XANES spectra can be attributed to differences between these two techniques. Sequential Hg extraction method targets different phases of Hg in bulk samples of biochar, whereas Hg L_{III}-edge μ-XANES analyses directly indicate chemical speciation of Hg in a 2 μm × 2 μm beam size area where the spectra were collected (Fig. 2.7).

Sulfur K-edge μ-XANES spectra collected at the same locations where Hg L_{III}-edge μ-XANES were collected show peaks at 2470.4, 2473.5, and 2482.7 eV (Fig. A 10). The results of Gaussian peak fitting suggest the spectra are mainly composed of sulfide minerals, exocyclic S, and sulfate. The presence of these groups is consistent with observations by Cheah et al. (2014) for XANES spectra collected on biochar prepared with oak or corn stover. Minimal amounts of other S phases, such as sulfoxide, sulfite, sulfone, and sulfonate, might also be present at the location where S K-edge μ-XANES spectra were collected (Fig. A 10). Sulfur groups, including sulfide minerals, elemental S, exocyclic S, heterocyclic S, sulfoxide, sulfone, sulfonate, and sulfate, are common in soil containing natural organic matter (Prietzel et al., 2003; Manceau and Nagy, 2012). The S groups identified by μ-XANES analyses might have originated from S phases present in the floodplain soil.

Three main peaks at 2,473.5, 2,476.1, and 2,482.7 eV were observed on the S K-edge XANES spectra for the unused biochar (Fig. 2.8), and these correspond to exocyclic S functionalities, sulfoxide, and sulfate or ester S functionalities (Table A 4) (Cheah et al., 2014; Manceau and Nagy, 2012). The peak at 2,476.1 eV is less pronounced for the biochar collected at different depths from the treatment columns, indicating a loss of sulfoxide functional groups. Wider peak shoulders are observed at approximately 2,470.4 and 2,472.3 eV for the biochar after treatment relative to the unused biochar, suggesting either precipitation or physical accumulation of sulfide minerals during treatment (Fig. 2.8).

Results of Gaussian peak fitting and linear combination fitting both suggest decreases in fractions of reduced S functionalities and sulfoxide for the biochar in THC-HMT and THC-H6S at the termination of the experiment than for the unused biochar (Fig. 2.8b-d and 9; Table A 5). The decrease in the fraction of reduced S functionalities can be related to the formation of Hg-thiol complexes on the biochar (Liu et al., 2016). The disappearance of the sulfoxide peak for biochar collected at 0-2 cm (Fig. 2.8) and the decrease in sulfoxide fractions for the biochar collected at greater depths in THC-HMT and THC-H6S (Fig. 2.9) can be related to the formation of Hg-O complexes on biochar with sulfoxide functional groups. Sulfoxide has the potential to form O-bonded complexes with various metals, such as Fe, Cu, or Hg (Calligaris and Carugo, 1996; Calligaris, 2004). For example, the use of dimethyl sulfoxide to pre-treat *Aspergillus flavus* biomass improved the biosorption of Pb (II) and Cu (II) from aqueous solution (Akar and Tunali, 2006). An EXAFS study indicates Hg tends to form complexes with sulfoxide as a six-fold Hg-O coordination (Persson et al., 2008). Fractions of sulfoxide on the biochar are not statistically correlated with the total Hg

retained on the biochar, which could be related to competition between Hg and other metals present in input solutions derived from HMT and H6S, such as Fe or Mn (Table 2.1) as well as Hg forming complexes with other functional groups on the biochar as suggested by the five-step sequential extraction method (Fig. 2.4).

Results of Gaussian peak fitting and linear combination fitting also both suggest increases in the fractions of sulfide and intermediate S (sulfone and sulfonate) for the biochar in THC-HMT and THC-H6S at the termination of the experiment than for the unused biochar (Fig. 2. 8b-d and 9; Table A 5). The increase in the sulfide fraction is consistent with the accumulation of Hg-S on the biochar as suggested by the five-step sequential extractions (Fig. 2.4), µ-XRF maps, Hg L_{III}-edge µ-XANES (Fig. 2.6-7), and S K-edge µ-XANES (Fig. A.10). Formation of H-S from aggregation of Hg-thiolate occurs in the presence of organic matter (Manceau et al., 2015). The increase in sulfide fractions, coupled with decreases in reduced S fractions, in the biochar is also likely related to the formation of Hg-S through aggregation of Hg-thiolate complexes. The increase in intermediate S species within the biochar after treatment is consistent with the results of S K-edge µ-XANES (Fig. A 10). The increases in both sulfide and intermediate S fractions may be related to the accumulation of particles derived from the floodplain soil.

2.5.7 Long-term performance of the hardwood biochar

The results of this study can be used to assess whether hardwood biochar can be used to promote sustained removal of Hg when installed in a riverine environment. Under the rapid drainage conditions and short residence times (<5 h) used in this experiment, the hardwood

biochar stabilized >80% Hg derived from source columns over a 100-week duration. These results suggest that the hardwood biochar may be a highly effective material for long-term use as reactive mat under environmentally relevant flooding and drainage conditions.

Previous studies have shown that information extracted from laboratory-scale humidity cell experiments can provide a reasonable assessment of solute release and microbial processes for medium-scale (> 1000 kg and < 10, 000 kg) field studies (Langman et al., 2015a,b; Maest and Nordstrom, 2017; Wilson et al., 2018). A similar prediction using humidity cell data is not available for Hg release under field conditions. Variations in local geochemical properties, changes in seasonal temperatures and hydrographic conditions may limit direct transfer of humidity cell predictions. For example, extreme storm events associated with climate change can lead to dramatic increases in the release of Hg to aquatic environments (Krabbenhoft and Sunderland 2013), which may not be captured in laboratory testing. Therefore, field pilot studies are recommended before implementing large-scale engineered remediation projects using biochar for Hg stabilization.

2.5.8 Proposed mechanisms for Hg removal

The mechanisms involved in Hg stabilization using hardwood biochar under conditions representative of typical fluvial settings can be attributed to a combination of physicochemical processes, including the formation of complexes with functional groups on the biochar surfaces and the retention/filtration of particulate Hg within the biochar porous structure.

Mercury can form complexes with functional groups on the biochar surface, including carboxylic groups, thiol functionalities, and sulfoxide groups (Calligaris, 2004; Calligaris and Carugo, 1996; Liu et al., 2016, 2017; Persson et al., 2008; Uchimiya et al., 2012) via reactions including:

$$-COOH + Hg^{2+} \rightarrow -COOHg^{+} + H^{+},$$

$$-SH + Hg^{2+} \rightarrow -S(Hg) -,$$

$$-S - S - + Hg^{2+} \rightarrow -S(Hg)S -,$$

$$6(R - SO - R) + Hg^{2+} \rightarrow [Hg(OSR_2)_6{}^{2+}].$$

Carboxyl groups are one of the most abundant functional groups in the biochar (Liu et al. 2015), which are known to promote the removal of heavy metals in contaminated sediment (Uchimiya et al., 2012). Concentrations of Hg extracted from the ORG fraction for biochar in THC-HMT and THC-H6S (Fig. 2.4) may represent the release of Hg bound to carboxyl groups. Other functional groups, including sulfoxide and thiol, can also contribute to the removal of Hg. Results of S K-edge XANES for biochar in THC-HMT and THC-H6S (Fig. 2.8-9) and μ-XANES for selected locations on biochar at depth 0-2 cm (Fig. A 10) indicate a decrease in peak intensity at 2,476.1 eV compared to the spectra for the unused biochar, suggesting the formation of metal-sulfoxide complexes (Calligaris, 2004; Calligaris and Carugo, 1996; Persson et al., 2008). A decrease in reduced S functionalities with depth suggested by S K-edge XANES for the biochar in THC-HMT and THC-H6S (Fig. 2.9) may be related to the formation of metal and thiol functional complexes, as suggested in studies of

Hg removal from aqueous solution using the same type of biochar (Liu et al., 2016) and from riverbank sediment under strongly reducing conditions (Liu et al., 2017).

Particles derived from the floodplain soil were also retained within the biochar porous structure. Results of μ-XRF for the biochar collected from the air/biochar-sand interface (0-2 cm) indicate a visual correlation between Hg and S, and the presence of other metals and clay minerals within the porous structure (Fig. 2.6). Results from sequential extraction (Fig. 2.4) and Hg L_{III}-edge μ-XANES (Fig. 2.7) analyses suggest the presence of Hg-S phases in the biochar collected from the treatment columns, which might be related to the retention of metacinnabar (β-HgS) (Fig. 2.7) and other sulfide minerals as observed in the results of S K-edge μ-XANES (Fig. A 10) and S K-edge XANES (Fig. 2.8-9) analyses of floodplain soil (Fig. A 6).

The relative contributions of physicochemical processes controlling Hg removal appear to differ depending on the extent of Hg loading. At low loading, Hg is primarily bound to surface functional groups on the biochar. As loading increases, other metals derived from natural sediment, including Fe and Cu, compete with Hg for available sites on the biochar surface. At higher loading, when limited functionalities are available, the physical filtration of particulate-bound Hg-S phases and other metal-bearing phases becomes the dominant removal mechanism.

2.6 Conclusions

This study indicates that biochar prepared from hardwood can minimize the release and transport of particulate and dissolved Hg derived from riverbank sediments under the rapid

drainage flow conditions and short residence times representative of dynamic fluvial systems. Relatively low concentrations of MeHg observed in effluent from treatment columns and in solid material at the end of the experiment suggest the application of biochar does not promote methylation reactions. Relatively low concentrations of other dissolved constituents suggest that application of the hardwood biochar does not release undesirable constituents (e.g., N, P), thus minimizing the potential for unintended environmental consequences. The application of the hardwood biochar in flow-through systems, such as reactive mats, has the potential for controlling long-term Hg release and transport in fluvial settings characterized by frequent changes in hydrological and geochemical conditions.

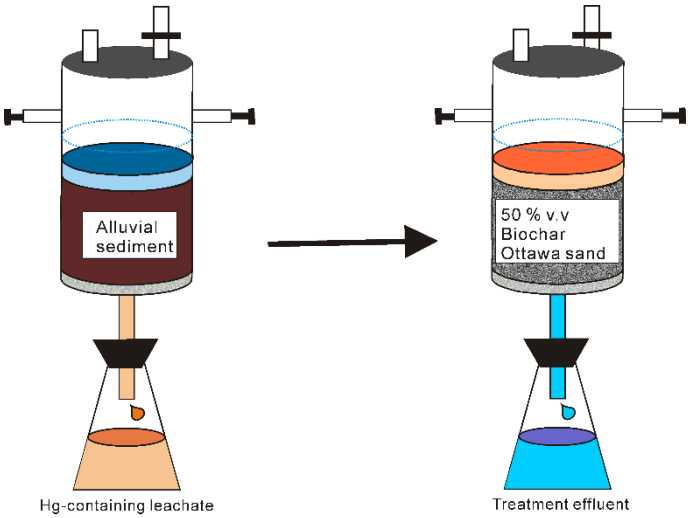

Fig. 2.1 Schematic diagram of experimental design.

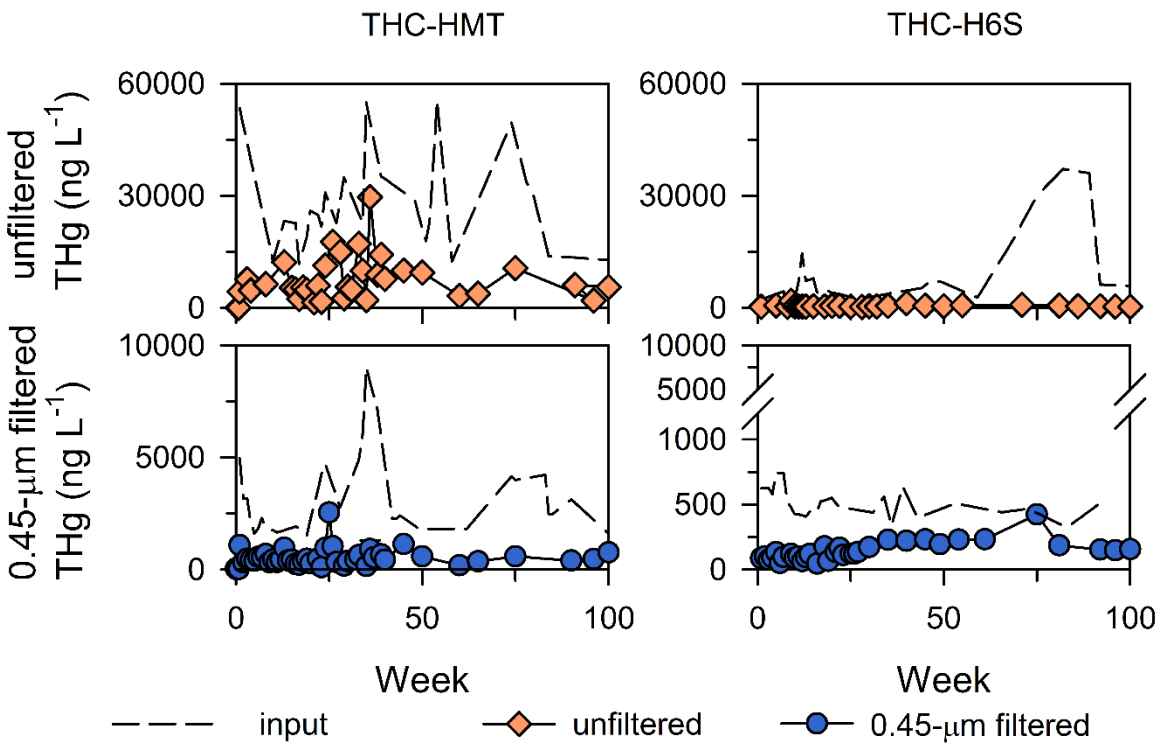

Fig. 2.2 Concentrations of unfiltered Hg (orange diamonds) and 0.45-µm filtered Hg (blue circles) in the effluent of treatment humidity columns (THC-HMT and THC-H6S) containing biochar. Dashed lines represent the concentration of Hg in the input solutions for the treatment columns. The input solutions were obtained by leaching floodplain soil MOTO (HMT) and riverbank sediment SR6 (H6S).

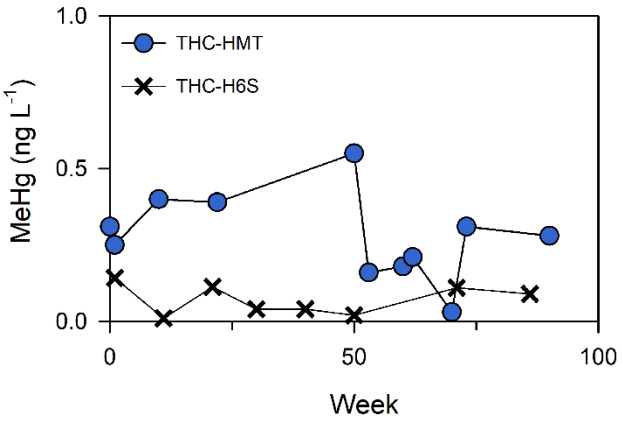

Fig. 2.3 Concentrations of methylmercury (MeHg) in 0.45-µm filtered effluent samples for treatment columns THC-HMT (blue circles) and THC-H6S (crosshairs).

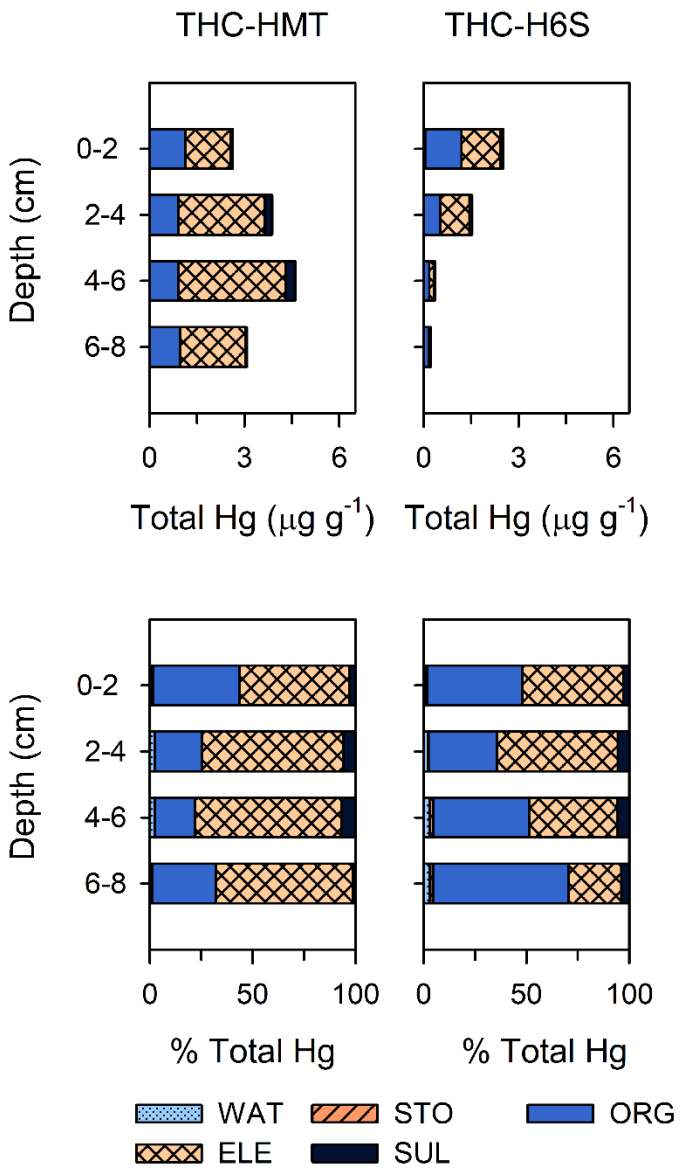

Fig. 2.4 Mean Hg concentrations and percentages extracted from the five-step sequential extraction targeting water soluble (F1; WAT), stomach acid soluble (F2; STO), organo-chelated (F3; ORG), elemental (F4; ELE), and mercuric sulfide (F5; SUL) fractions for biochar collected at different depths from the treatment columns at the termination of the experiments using input derived from source columns HMT and H6S.

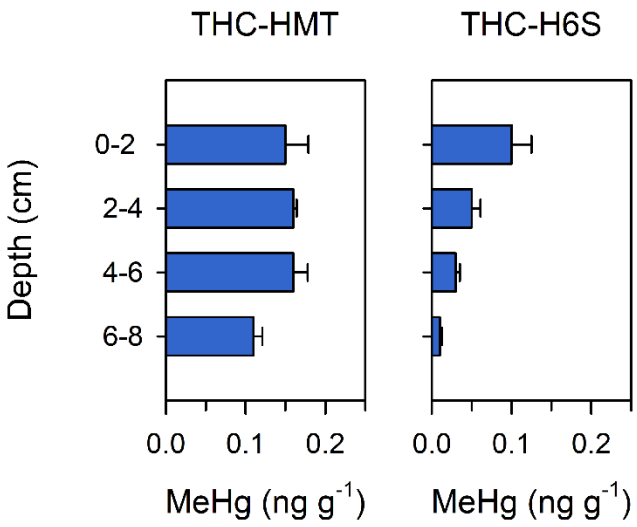

Fig. 2.5 Concentration of sorbed MeHg in biochar samples versus depth after termination of humidity cell experiments using input derived from source columns HMT and H6S. Error bars show the results of the first standard deviation of duplicate extractions at each depth.

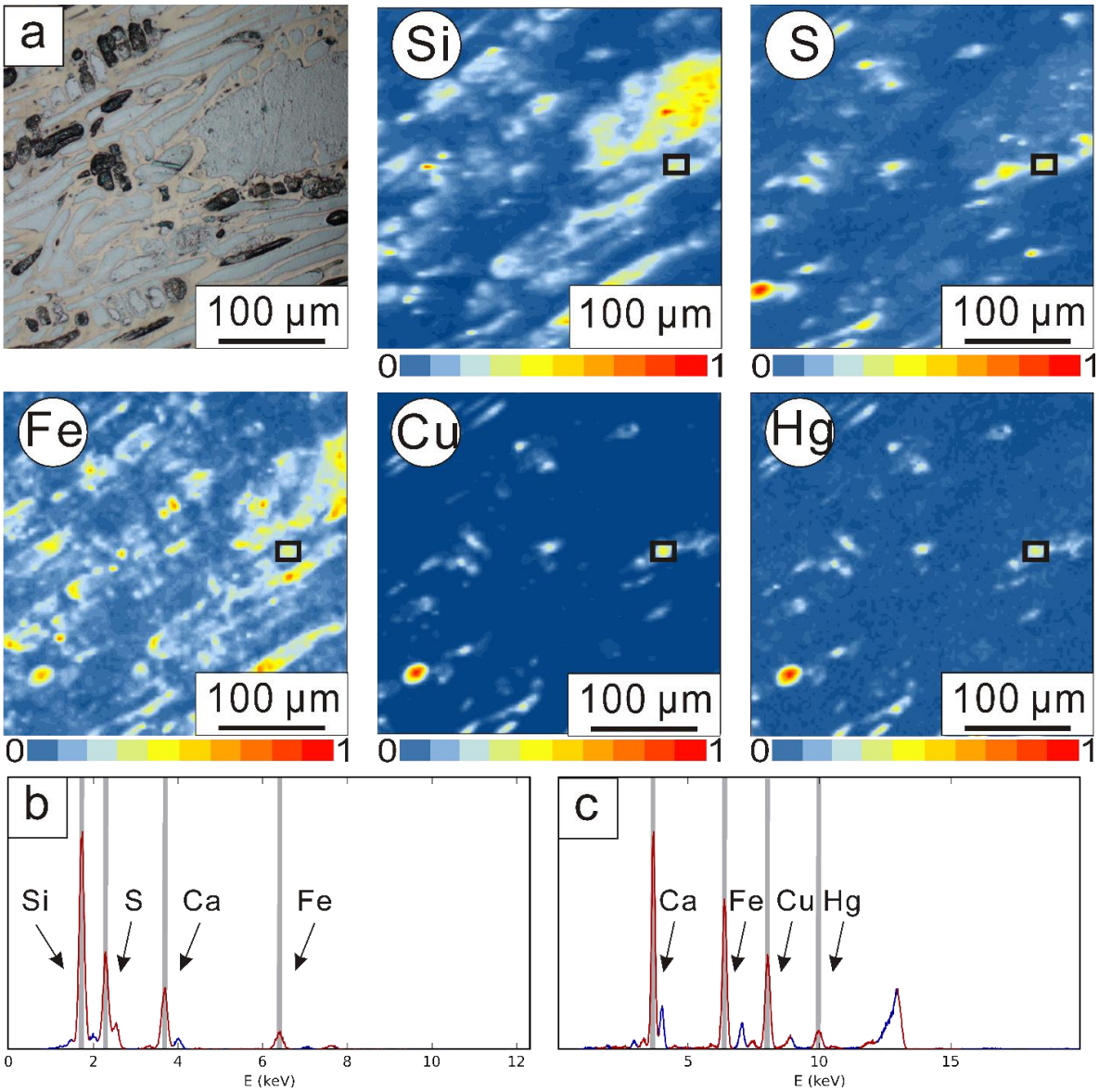

Fig. 2.6 Transmitted light microscope image and normalized µ-XRF maps for Si, S, Fe, Cu, and Hg (a) obtained from the hardwood biochar collected from 0-2 cm of treatment column THC-HMT, and the corresponding XRF spectra obtained from the location denoted by (□) for lighter elements (b) and heavier elements (c).

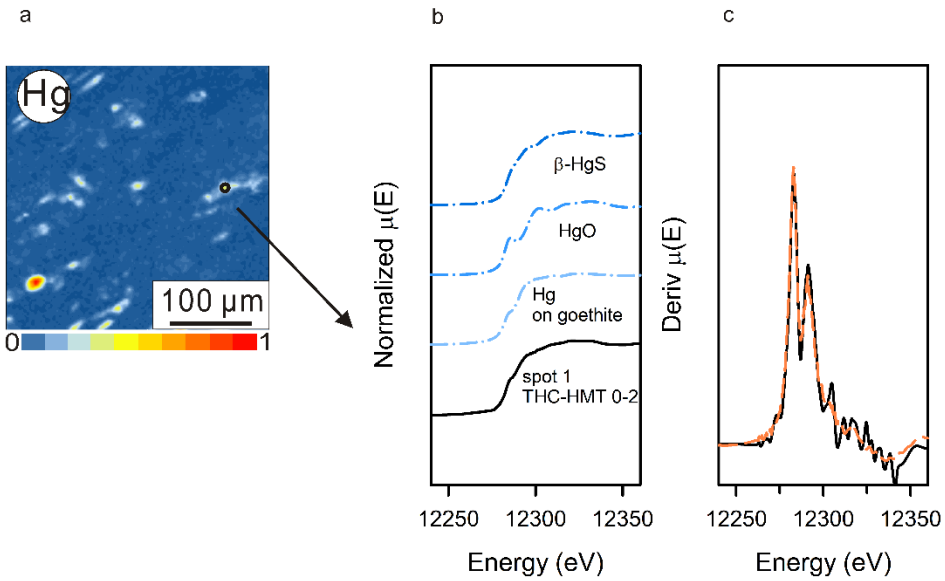

Fig. 2.7 Hg L_{III}-edge µ-XANES analyses for biochar collected at depths 0-2 cm in THC-HMT. a. µ-XRF map for Hg showing selected area for collecting µ-XANES. b. Normalized Hg LIII-edge µ-XANES (black solid line) and reference compounds (blue dash-dot line). c. best-fit (orange dashed line) (NSS = 0.02) in derivative using the three reference compounds.

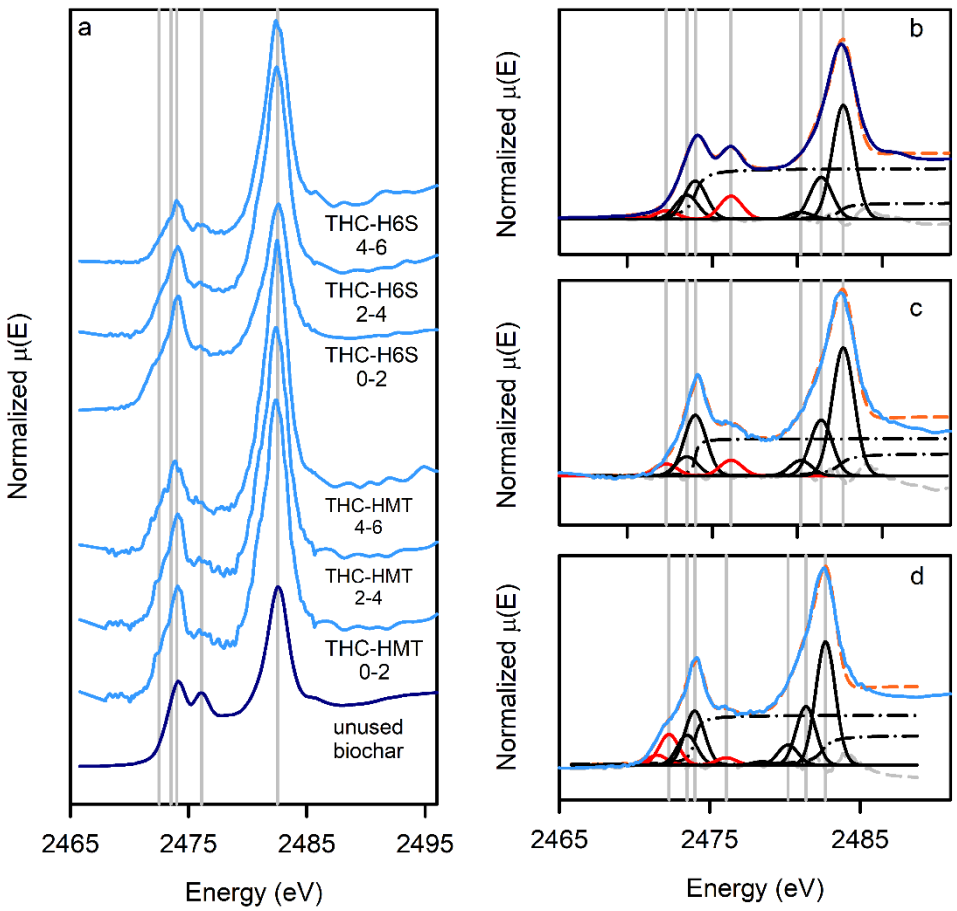

Fig. 2.8 Sulfur K-edge spectra (a) for the unused biochar and biochar after treatment at the different depths (in cm) from treatment columns THC-HMT and THC-H6S. Examples showing Gaussian peak fittings (orange dashed line) between 2466 and 2489 eV for fresh hardwood biochar (b, NSS = 6.5×10^{-3}), and biochar collected from 0-2 cm in THC-HMT (c, NSS = 3.9×10^{-3}) and THC-H6S (d, NSS = 2.8×10^{-3}). Two optimized arctangent steps (black dash-dot line) were used to simulate reduced sulfur groups at 2474 eV and oxidized sulfur groups at 2482.5 eV. The grey solid lines indicated white line positions for sulfide minerals (2470.4 eV, 2472.3 eV), exocyclic sulfide (2473.5 eV), heterocyclic S (2474 eV), sulfoxide (2476.1 eV), sulfone (2480.2 eV), sulfonate (2481.4 eV), and sulfate (2482.7 eV).

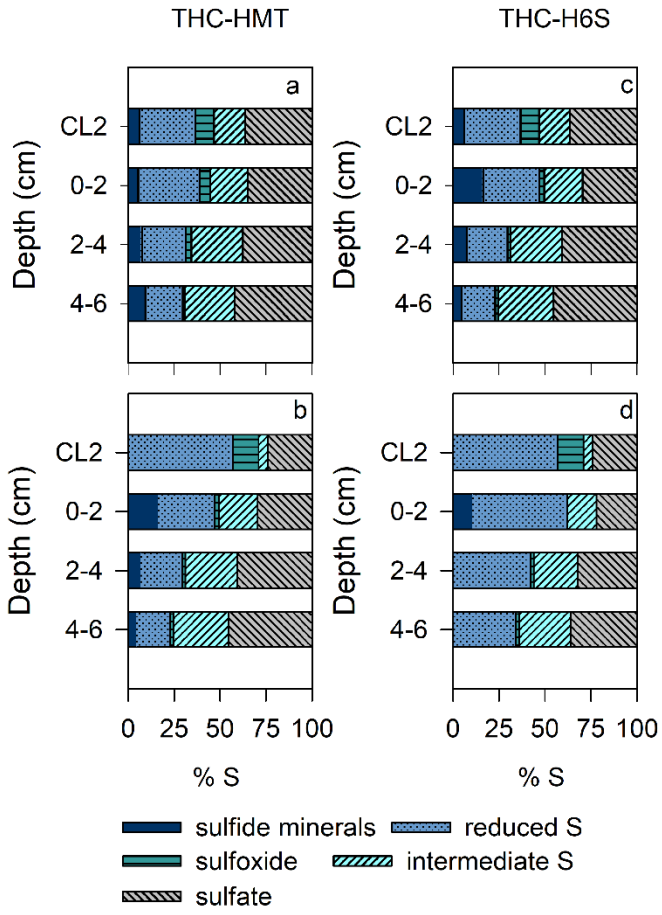

Fig. 2.9 Results of quantified S K-edge XANES using Gaussian peak fitting (a, c) and linear combination fitting (b, d) for the unused biochar and the biochar collected from treatment columns THC-HMT and THC-H6S.

Table 2.1 Mean chemical compositions of effluents released from source columns (HMT and H6S) and treatment columns (THC-HMT, THC-H6S) over 100 weeks. Value represents mean +/- variance.

Parameter	HMT	THC-HMT	H6S	THC-H6S
pH	5.59 +/- 0.99	7.79 +/- 0.58	7.81 +/- 0.20	8.01 +/- 0.41
Eh, mV	539 +/- 87	470 +/- 78	427 +/- 42	424 +/- 74
Alkalinity, mg L^{-1} (as $CaCO_3$)	5 +/- 4	63 +/- 45	89.83 +/- 43.19	116 +/- 38
Dissolved organic carbon, mg L^{-1}	5.31 +/- 1.47	2.89 +/- 0.66	2.912 +/- 0.468	3.99 +/- 2.09
Lactate, mg L^{-1}	< 0.06	< 0.06	< 0.03	< 0.06
Acetate, mg L^{-1}	< 0.6	< 0.2	< 0.08	< 0.3
Propionate, mg L^{-1}	< 0.07	<0.07	< 0.07	< 0.07
Formate, mg L^{-1}	< 0.06	<0.06	< 0.03	< 0.06
0.45-µm filtered THg, ng L^{-1}	3,180 +/- 1,510	541 +/- 227	472 +/- 79.1	151 +/- 75
unfiltered THg, ng L^{-1}	27,000 +/- 11,400	7,700 +/- 861	11,200 +/- 11,400	538 +/- 241
F^-, mg L^{-1}	0.02 +/- 0.01	0.05 +/- 0.11	0.08 +/- 0.01	0.10 +/- 0.01
Cl^-, mg L^{-1}	0.26 +/- 0.26	1.25 +/- 1.36	5.70 +/- 0.68	6.70 +/- 1.0
NO_2^-, mg L^{-1}	< 0.09	0.70 +/- 1.34	< 0.09	< 2
Br^-, mg L^{-1}	< 0.4	1.02 +/- 1.42	< 0.4	< 0.4
NO_3^-, mg L^{-1}	4.83 +/- 3.11	4.83 +/- 2.65	4.01 +/- 2.23	1.40 +/- 0.60
SO_4^{2-}, mg L^{-1}	2.48 +/- 0.35	5.54 +/- 1.62	7.87 +/- 1.54	10.3 +/- 2.40
Na, mg L^{-1}	2.93 +/- 1.76	0.19 +/- 0.19	4.20 +/- 0.51	3.52 +/- 1.09
Mg, mg L^{-1}	1.25 +/- 0.38	1.75 +/- 0.89	4.66 +/- 0.86	7.40 +/- 0.75
Al, µg L^{-1}	44.3 +/- 20.0	18.3 +/- 25.3	2.75 +/- 0.59	13.8 +/- 11.6
Si, mg L^{-1}	3.20 +/- 0.81	2.82 +/- 0.59	9.66 +/- 0.55	6.63 +/- 1.08
Ca, mg L^{-1}	9.63 +/- 2.64	5.42 +/- 12.6	58.0 +/- 1.61	37.5 +/- 5.4
K, mg L^{-1}	1.68 +/- 0.98	14.8 +/- 30.2	1.95 +/- 0.46	20.8 +/- 34.1
MeHg, ng L^{-1}	1.62 +/- 1.76	0.38 +/- 0.23	0.28 +/- 0.16	0.11 +/- 0.02

Table 2.2 Mean total Hg retained on biochar obtained from the differences of unfiltered Hg in effluent from source and treatment columns and normalized to mass of biochar in treatment columns.

Reactive Material in Humidity Cells	THC-HMT	THC-H6S
Hg loaded on biochar (μg g^{-1})	7.96	2.38
Cumulative Hg eluted (μg g^{-1})	1.52	0.09
Hg retained on biochar (μg g^{-1})	6.44	2.29
Percent Hg retained on biochar	81.3%	96.2%

Chapter 3 Use of hardwood and sulfurized-hardwood biochars as amendments to floodplain soil from South River, VA, USA: Impacts of drying-rewetting on Hg removal

This chapter has been submitted to

Wang, A.O., Ptacek, C.J., Blowes, D.W., Finfrock, Y. Z., Paktunc, D., Mack, E.E., 2019. Use of hardwood and sulfurized-hardwood biochars as amendments to floodplain soil from South River, VA, USA: Impacts of drying-rewetting on Hg removal. Accepted for publication in Science of the Total Environment

Summary

Periodic flooding and drying conditions in floodplains affect the mobility and bioavailability of Hg in aquatic sediments and surrounding soils. Sulfurized materials have been recently proposed as Hg sorbents due to their high affinity to bind Hg, while sulfurizing organic matter may enhance methylmercury (MeHg) production, offsetting the beneficial aspects of these materials. This study evaluated hardwood biochar (OAK) and sulfurized-hardwood biochar (MOAK) as soil amendments for controlling Hg release in a contaminated floodplain soil under conditions representative of periodic flooding and drying in microcosm experiments in three stages: (1) wet biochar amended-systems with river water in an anoxic environment up to 200 d; (2) dry selected reaction vessels in an oxic environment for 90 d; (3) rewet such vessels with river water in an anoxic environment for 90 d. In Stage 1, greater Hg removal (17-98% for unfiltered total Hg (THg) and 47-99% for 0.45-μm THg) and lower MeHg concentration (<20 ng L^{-1}) were observed in MOAK-amended systems (10%MOAKs). In Stage 3, release of Hg in 10%MOAKs was eight-fold lower than in soil controls (SedCTRs), while increases in aqueous (up to 21 ng L^{-1}) and soil (up to 88 ng g^{-1})

MeHg concentrations were observed. The increases in MeHg corresponded to elevated aqueous concentrations of Mn, Fe, SO_4^{2-}, and HS^- in Stage 3. Results of S K-edge X-ray absorption near edge structure (XANES) analysis suggest oxidation of S in Stage 2 and increases in polysulfur in Stage 3. Results of pyrosequencing analysis indicate sulfate-reducing bacteria (SRB) became abundant in Stage 3 in 10%MOAKs. The shifts in biogeochemical conditions in 10%MOAKs in Stage 3 may increase the bioavailability of Hg to methylating bacteria. The results suggest limited impacts on Hg removal during drying and rewetting, while changes in biogeochemical conditions may affect MeHg production in sulfurized biochar-amended systems.

3.1 Introduction

Mercury (Hg) contamination related to industrial activities is a worldwide occurrence (Kocman et al., 2013). Hg is transported through air, water bodies, and accumulates in surrounding soils and sediments, and is a potential long-term source of contamination through sediment resuspension, soil erosion, and flooding events (Carter, 1977; Gibson et al., 2015; Kockman et al., 2013; Mucci et al., 2015; Poulin et al., 2016; Singer et al., 2016).

Inorganic Hg species are transformed into methylmercury (MeHg) by anaerobic bacteria, including sulfate-reducing bacteria (SRB), iron-reducing bacteria (FeRB), methanogens, and fermenters (Fleming et al., 2006; Gilmour et al., 2013a; Hu et al., 2013; Jonsson et al., 2012; Yu et al., 2012). MeHg production not only depends on microbial activity but also bioavailability of Hg species (Hsu-Kim et al., 2013; Liu et al., 2019). MeHg is a major

concern for human health because it is a neurotoxin and accumulates through the aquatic food chain (Mergler et al., 2007).

Frequent drying and flooding events induce changes in geochemical conditions in floodplain environments. During drying stages, oxidation of S, Fe, Mn, and N occurs to form SO_4^{2-}, Fe(III) and Mn(IV) oxides, and NO_3^-, respectively. The newly formed Fe(III) and Mn(IV) oxides are potent sorbents for heavy metals (Borch et al., 2010). During extended flooding, floodplain soil becomes anoxic after O_2 is consumed through microbial aerobic respiration. Microorganisms utilize NO_3^-, Mn(IV) and Fe (III) (oxy)hydroxides, and SO_4^{2-} as terminal electron acceptors for organic carbon oxidation coupled with NO_3^-, Mn(IV)-, Fe(III), SO_4^{2-}-reduction and methanogenesis. Remobilization of Hg in anoxic conditions has been associated with reductive dissolution of Hg-bearing Fe oxides (Mucci et al., 2015), binding to particulate soil organic matter, reductive dissolution of metacinnabar (β-HgS) to $Hg(0)_{aq}$ (Poulin et al., 2016), and release of Hg-bearing nanoparticles (Hofacker et al., 2013). Iovieno and Bååth (2008) observed a rapid increase in bacterial growth (within 7 h) after rewetting air-dried soil, and relatively high MeHg production potential is proposed to occur in floodplains during long inundation events (Singer et al., 2016).

Traditional soil remediation techniques include excavation, stabilization, immobilization, vitrification, thermal desorption, soil washing, electro-remediation, and phytoremediation (Akcil et al., 2015; Dermont et al., 2008; Mulligan et al., 2001; Wang et al., 2004; Wang et al, 2012). However, these techniques either require high operational costs or disturb the natural systems, and therefore these techniques may be difficult to apply in large-scale contaminated sites. For example, physically excavating may remobilize Hg through sediment

resuspension (Gibson et al., 2015; Wang et al., 2004). Soil washing can potentially alter soil properties using strong chemicals, and release of these chemicals to the environment can lead to unintended consequences (Dermont et al., 2008). *In situ* stabilization has recently become more widely utilized due to its potential for lowering costs and limiting disturbance to natural systems (Ghosh, 2011; Wang et al., 2019).

Biochars, with a relatively large surface areas and abundance of functional groups, are increasingly proposed as reactive materials for in situ Hg stabilization (Bekers et al., 2019; Desrochers, 2013; Fellin, 2016; Gilmour et al., 2018; Paulson, 2014; Peterson et al., 2017; Ting et al., 2018; Wang et al., 2019). Laboratory column studies revealed that such applications decrease Hg release and suppress MeHg production under saturated-flow conditions (Desrochers, 2013; Fellin, 2016; Paulson, 2014; Peterson et al., 2017) as well as under flooding and drainage conditions (Wang et al., 2019). In floodplains where extended inundation occurs, biochars are proposed as in situ capping materials to control Hg release as well as MeHg production (Bekers et al., 2019; Gilmour et al., 2013b; 2018; Gomez-Eyles et al., 2013; Liu et al., 2017, 2018b; Xing et al., 2019; Zhang et al., 2018). Variable Hg removal and MeHg production are observed in these studies, which are likely to be related to different raw materials used in the production of biochars.

Sulfurized materials, with a relative high affinity for Hg, have been proposed as Hg adsorbents for vapour phase (Feng et al., 2006), aqueous solutions (Asasian and Kaghazchi, 2012; Huang et al., 2019; Liu et al., 2018b; Park et al., 2019), and in sediment, as a reactive capping mat (Ting et al., 2018), and as amendments in Hg-contaminated sediment (Fellin, 2016; O'Connor et al., 2018; Ting et al., 2018). Most sulfurization processes are conducted at

high temperature with corrosive chemicals (Feng et al., 2006; Graydon et al., 2009; O'Connor et al., 2018; Ting et al., 2018). Current research interests focus on using more environmentally friendly compounds, such as disulfide solution, a US FDA approved flavor additive (Asasian and Kaghazchi, 2012), or lime sulfur solution, a US EPA approved insecticide and fungicide (Liu et al., 2018b). In previous studies on lime sulfur-modified biochar, more than 99.5% Hg removal was achieved from spiked simulated groundwater (Liu et al., 2018b) and >80% when the biochar was used as a soil amendment under saturated-flow conditions (Fellin, 2016). These high rates of Hg removal suggest sulfurized biochar may be effective in controlling Hg in floodplain soils.

Most studies on Hg removal using sulfurized materials in spiked solution and sediments were reacted for relatively short contact times (up to 72 h for aqueous solutions and 5 d for spiked sediments) (Asasian and Kaghazchi, 2012; Liu et al., 2018b; O`Connor et al., 2018; Pap et al., 2018; Park et al., 2019). The long-term impacts of applying sulfurized biochar in natural sediment or soil have not been extensively studied. Ting et al. (2018) observed a lower Hg removal rate in spiked sediments using sulfurized activated carbon than unmodified activated carbon, likely related to release of nanoparticulate HgS through dissolution of S functionalities. Adding an organic carbon amendment to soil may also alter the microbial community structure (Christensen et al., 2018). Periodic drying and rewetting in floodplains may further alter microbial community structure (Fierer et al., 2003). Increases in Hg methylation with sulfurized organic matter have been recently documented (Drott et al., 2013; Graham et al., 2017; Jay et al., 2000; Liem-Nguyen et al., 2017; Poulin et al., 2017). Liu et al. (2018b) observed oxidation of sulfurized biochar after being exposed to air for 60

d, but Hg removal and MeHg production associated with oxidation by-products of sulfurized biochar in soil during periodic flooding and drainage is unclear. As such, there is a need to evaluate the performance of sulfurized materials before applying at the field-scale.

This study evaluated long-term Hg removal and MeHg production using hardwood (OAK) and sulfurized-hardwood biochars (MOAK) under repeated wetting and drying conditions. Geochemical measurements and solid phase analyses were conducted to provide insights into the long-term effectiveness of *in situ* Hg stabilization in floodplains using hardwood and sulfurized-hardwood biochars.

3.2 Experimental Details

3.2.1 Study Site

Hg contamination in the South River watershed is related to the use of $HgSO_4$ as a catalyst for acetate fiber production from 1929 to the 1950s by a textile plant in Waynesboro, VA, USA. Elevated Hg was found downstream of the historical release site in river water, surrounding sediments and soil, shallow groundwater and fish tissues 20 years since the use of $HgSO_4$ had ended (Carter, 1977; Lazareva et al., 2019). Bank erosion is one of the primary factors contributing to Hg release in the South River (Eggleston, 2009; Rhoades et al., 2009).

3.2.2 Materials

Floodplain soil was collected 36.5 km downstream of the textile plant in 3.7-L high-density polyethylene bottles and shipped to the University of Waterloo and stored at 4 °C. The floodplain soil was air-dried for 3 d and sieved to <2 mm to remove large pebbles, plant roots, and organic debris, then homogenized and stored in 1-L high density polyethylene

wide-mouth bottles. South River water (SRW) was collected 4.8 km upstream of the textile plant and shipped to the University of Waterloo on ice and stored in dark conditions at temperatures <4 °C.

Hardwood biochar (OAK), prepared from oak and maple hardwood at 700 °C, was obtained from Cowboy Charcoal LLC (Brentwood, TN, USA). OAK was sieved to between 0.5 to 2 mm and washed in ultrapure water. Sulfurized-hardwood biochar (MOAK) was prepared by immersing 20 g of rinsed and sieved OAK in 0.4% lime sulfur solution (Green Earth Sure-Gro IP Inc.) for 7 d in a 3.5% H_2/balance with N_2 vinyl anaerobic chamber (Coy Laboratory Products, Inc.) following the procedure described by Liu et al. (2018b). After 7 d, the supernatant was decanted, and the sulfurized biochar (MOAK) was rinsed six times with ultrapure water before drying in the anaerobic chamber.

3.2.3 Experimental design

Microcosm experiments were conducted in three stages to represent periodic flooding, drying, and reflooding in the South River floodplain (Table 3.1). Stage 1 included submerging 20 g air-dried floodplain soil with and without 2 g biochar in 250-mL individual reaction vessels with 240 mL SRW to minimize headspace. Reaction vessels were equilibrated in anoxic environments for 7d up to 200 d (denoted as wet). Floodplain soil and biochar mixtures were equilibrated in an anaerobic chamber for 24 h before adding SRW. Controls included ultrapure water controls and SRW controls (SRWCTRs) at 7, 90, and 200 d. Triplicate microcosm experiments were conducted for 7, 90, and 200 d, and an additional duplicate experiment was conducted at a randomly selected reaction interval. A total of 48

reaction vessels were assembled in a random order within a 2-week period to minimize the effect of changes in floodplain soil and river water composition. At the end of each reaction time interval, aqueous and solid samples were collected for further analyses, except solid residues in two of triplicate reactors at 7, 90, and 200 d. In Stage 2 (denoted as dry), these solid residues were air-dried for 90 d under natural light conditions in their original reaction vessels. In Stage 3 (denoted as rewet), the air-dried solid residues were rewet with 240 mL SRW in an anaerobic chamber and equilibrated for an additional 90 d. After 90 d, aqueous and solid samples were collected. All reactors in Stages 1 and 3 were homogenized every 2 d by gently inverting 10 times by hand.

3.2.4 Sample collection

Aqueous samples were collected in anaerobic chamber for pH, Eh, alkalinity as $CaCO_3$ (alk), concentrations of $CH_{4(aq)}$, total sulfide, total Hg (THg), MeHg, major and trace cations, inorganic and organic anions, dissolved organic carbon (DOC), NH_3-N, and PO_4^{3-}. Samples for, total sulfide, cations, anions, DOC, NH_3-N, PO_4^{3-}, and MeHg were passed through 0.45-µm filter membranes, and samples for THg were passed through different filter sizes, including unfiltered (unf), 0.45-µm, 0.2-µm, and 0.1-µm. Further details of sampling methodology for aqueous samples are provided in supporting information (Text B 1). After collecting aqueous samples, solid residuals were collected in 20-mL VWR® TraceClean® vials. Samples for polymerase chain reaction sequencing analysis were collected in autoclaved 50-mL centrifuge tubes. All solid samples were stored <−20 °C prior to analysis.

3.2.5 Analytical methods

Total C, H, N, and O were determined using a combustion method at 950 °C (ASTM, 2008), with ash content determined at 550 °C to minimize thermal degradation of the mineral phase (Bachmann et al., 2016). Major and trace metals were determined using a heated strong acid digestion with HNO_3 and HCl modified from US EPA Method 200.2 (Martin et al., 1994) and analyzed using inductively coupled plasma-mass spectrometry (ICP-MS). Concentrations of Hg in biochars prior to utilization as amendments were analyzed using cold vapour atomic fluorescence spectroscopy (CVAFS) (US EPA, 2002). Total Kjeldahl N was determined by digesting the biochar in H_2SO_4 with $CuSO_4$ and K_2SO_4 as catalysts, followed by colorimetric analysis at 660 nm.

pH, Eh, and alkalinity were determined immediately after collection. pH was determined on unf samples using a combination Ross electrode (Orion model 8156, Thermo Scientific) and calibrated with three-point (7.00, 4.01, and 10.01). Eh was determined on unf samples using a combination platinum Ag/AgCl electrode (Orion 9678, Thermo Scientific. The Eh probes were checked against ZoBell`s (Nordstrom, 1977) and Light`s solutions (Light, 1972). All Eh values were corrected to the standard H_2 electrode. Alkalinity was determined by titrating samples passing 0.45-µm filter membranes with a digital titrator using 0.16N H_2SO_4 and bromocresol-green methyl red as an indicator (Hach Method 8203).

Concentrations of dissolved $CH_{4(aq)}$ were determined using a headspace method (Kampbell and Vandegrift, 1998) on a gas chromatography (GC). Concentrations of total sulfide were determined using the methylene blue method reported as S^{2-} (Hach Method 8131) and converted to HS^- in this study the reflect the predominant species in at the pH ranges

determined in the microcosm experiments (Richard and Luther III, 2007). Concentrations of major cations were determined using inductively coupled plasma optical emission spectrometry (ICP-OES), and concentrations of trace elements were determined using ICP-MS. Concentrations of inorganic anions and organic acids were determined using ion chromatography. Concentrations of DOC were determined using a wet oxidation method following US EPA Method 415.3 (US EPA, 2009). Concentrations of NH_3-N were determined using the salicylate method (Hach Method 10023). Concentrations of reactive phosphorus (PO_4^{3-}) were determined using the ascorbic acid method (Hach Method 8048). Concentrations of THg (unf, 0.45-µm, 0.2-µm, and 0.1-µm fractions) were determined using CVAFS following US EPA Method 1631 Revision E (US EPA, 2002) with an instrument method detection limit (n = 16) of 0.16±0.07 ng L^{-1}. The relative percent difference (%RSD) for duplicate analyses (n = 19) was 2.5±2.4%. Recoveries for matrix spikes (n = 8) and standard reference material (NIST 1641e, Hg in water) were 95-115% and 101-112%, respectively. Detailed information for instrumentation used for analytical methods is provided in supporting information (Text B 2).

Concentrations of aqueous and solid MeHg were determined following US EPA Method 1630 (US EPA, 2001). Freeze-dried solid samples were digested in 25% (w/w) KOH-MeOH solution prior to analysis. Instrument detection limit for MeHg was <0.08 ng L^{-1}, matrix spike recovery was 77.5-98%, and recoveries of quality controls were 86-94%.

Total S concentrations in solid residues were determined by infrared absorption spectroscopy following combustion using a LECO resistance furnace analyzer.

3.2.6 Synchrotron-based spectroscopy analyses

3.2.6.1 High-energy resolution fluorescence detection X-ray absorption spectroscopy (HERFD-XAS)

HERFD-XAS analysis of floodplain soil at the Hg Lα fluorescence emission line was conducted at CLS@APS, Sector 20 ID line, Advanced Photon Source (APS; Argonne National Laboratory, Lemont, IL, USA). The HERFD-XAS experiment was conducted using Rowland geometry with one bent Si (111) crystal analyzer with a radius of 0.5 m, and a PILATUS 100K pixel detector at 77 K modified from Manceau et al. (2015). A focus beam size measuring 300×500 μm^2 was used. A He path was installed between samples and the crystal analyzer to minimize air absorption ~~in air~~. The floodplain soil sample was homogenized before packing in polytetrafluoroethylene holders sealed in Kapton® tape. Five scans at five different locations were collected and merged prior to data analysis.

Hg reference compounds included mineral specimens of cinnabar (α-HgS) and corderoite ($Hg_3S_2Cl_2$) (Excalibur Mineral Corp., Peekskill, NY, USA) as well as reagent-grade mercury compounds HgO, $HgCl_2$, and $HgSO_4$ (Sigma-Aldrich, Oakville, ON, Canada). Synthesized metacinnabar (β-HgS) and Hg sorbed on soil organic matter (Hg_SOM) were prepared according to Manceau et al. (2015). Synthesized β-HgS were prepared by mixing $Hg(NO_3)_2 \cdot H_2O$ (Sigma-Aldrich, Oakville, ON, Canada) with L-cystine (Sigma-Aldrich, Oakville, ON, Canada) and heated at 20 °C/h from 60 to 160 °C, then held at 160 °C for 48 h before gradually cooled to 40 °C at 15 °C/h. Hg associated with soil organic matter was prepared by adding Hg as $Hg(NO_3)_2 \cdot H_2O$ in an Elliott Soil humic acid suspension (International Humic Substances Society) at pH 6 for 15 hours and then filtered and dried.

Mercury bound to thiol compounds, $Hg(HCys)_2$ were prepared by adding $Hg(NO_3)_2 \cdot H_2O$ in L-Cysteine solutions, and aqueous complexes of two-coordinated $[Hg(HCys)_2]^{2-}$ and four-coordinated $[Hg(HCys)_4]^{6-}$ complexes were prepared with molar ratios of L-Cysteine and Hg(II) as 2.2 and 15, respectively in alkaline conditions following the description by Jalilehvand et al. (2006). Hg sorbed on Fe oxides were prepared according to Kim et al. (2004).

3.2.6.2 S K-edge X-ray absorption near edge structure (XANES)

S K-edge XANES for solid samples were collected at Beamline 9-BM at the APS in fluorescence mode. Solid samples were freeze-dried and stored in an anaerobic chamber prior to S K-edge XANES measurements. Solid samples were ground and smeared as thin films on conductive double-sided tape, and a He chamber was used between samples and fluorescence detector to minimize absorption during spectra collection. An extra 10%MOAKs sample from Stage 3 was prepared and analyzed as a duplicate. Five scans were collected for each sample and merged in μ(E) prior to quantitative analysis. S K-edge XANES spectra were calibrated to the white line position for $CaSO_4 \cdot 2H_2O$ at 2482.7 eV.

3.2.6.3 Spectral analysis

Data processing was performed using ATHENA (Ravel and Newville, 2005). Linear combination fitting for HERFD-XAS at the Hg Lα emission line was conducted following the "combo method" of Manceau et al., 2012. Reference compounds were first applied with unconstrained weights, and negative weighted components was eliminated in an ascending order. Then, a maximum of three components was used to determine the best-fit.

S K-edge XANES spectra were decomposed into 11 Gaussian peaks representing sulfide minerals (2470.4, 2471.5, and 2472.5 eV), elemental sulfur (or polysulfur) (2472.7 eV), exocyclic S (2473.5 eV), heterocyclic S (2474.2 eV), sulfoxide (2476.1 eV), sulfite (2478.5 eV), sulfone (2480.2 eV), sulfonate (2481.4 eV), and sulfate (2482.7 eV) using two arctangent steps representing reduced S (2474 eV) and oxidized S (2483.8 eV) between 2466 and 2489 eV following Manceau and Nagy (2012). Diluted L-cysteine (Sigma Aldrich) and $CaSO_4 \cdot 2H_2O$ (2%) were first decomposed with peak positions and widths unconstrained. The determined shift in whiteline position (0.15 eV) and peak width for L-cysteine were applied to reduced S species (sulfide minerals, exocyclic S, heterocyclic S, and sulfoxide), and the peak width for $CaSO_4 \cdot 2H_2O$ was applied to intermediate and oxidized S species (sulfite, sulfone, and sulfonate and sulfate). Then, the 11 Gaussian peaks were used to decompose S K-edge XANES spectra for solid collected in soil controls (SedCTRs) and biochar-amended systems (10%OAKs and 10%MOAKs) with constrained peak positions and widths and unconstrained peak heights. Gaussian peaks with negative height values were eliminated from fitting in an ascending order. A generic scaling factor determined by Manceau and Nagy (2012) was used to overcome changes in absorption cross-section as oxidation status increases and to quantify fractions of S species in the solids. Goodness-of-fit was evaluated by excluding components weighted <10% to assess whether their exclusion significantly affected fitting results. Exclusions that resulted in insignificant changes to the goodness-of-fit were no longer considered. Pyrosequencing Analysis

DNA purification for PCR analysis was completed for soil amendments stored <0.5 year after being frozen at −20 °C following manufacturer protocols given in the Powder Soil®

DNA Isolation Kit (Mo Bio Laboratories) in a Clean-Ceil^{TM} Fan Filter Module (Microzone). Purified DNA was shipped frozen to MR DNA Laboratory (Shallowater, TX, USA) for pyrosequencing analysis using primer 515/806 targeting bacteria and archaea. Details about polymerase chain reaction, sequencing, and data analysis are summarized in supporting information (Text B 3).

3.2.7 Statistical analysis

The effects of amending floodplain soil with OAK and MOAK and of drying-rewetting were evaluated using an unbalanced two-way ANOVA with a 95% confidence interval. Pearson product moment correlation coefficients (r) were calculated to determine correlations between measured parameters.

3.3 Results and Discussion

3.3.1 Composition of floodplain soil and biochar

The floodplain soil used in this study is rich in Al (6700 µg g^{-1}), Fe (24 000 µg g^{-1}), and organic matter (14 800 µg g^{-1}), and low S (159 µg g^{-1}) (Table B 1). Concentrations of Hg in the floodplain soil (55 µg g^{-1}) exceed the screening level for residential soil (23 µg g^{-1}) (US EPA, 2019). The floodplain soil is fine grained and classified as silt according to the USDA soil texture system (Soil Survey Divison Staff, 1993). The best-fit of linear combination fitting (NSS=4.17×10^{-3}) for HERFD-XAS spectra at the Hg Lα emission line for the floodplain soil reveal that Hg is mainly associated with soil organic matter (57%), with almost equal fractions of metacinnabar (β-HgS) (27%) and Hg bound to organic thiol complexes ($[Hg(HCys)_2]^{2-}$ (18%) (Fig. B 1). The linear combination fitting was also

conducted with/without the aqueous Hg-thiol complexes. The excluding $[Hg(HCys)_2]^{2-}$ resulted in limited changes in fitting quality (NSS=4.30×10^{-3}). Therefore, the two-coordinated $[Hg(HCys)_2]^{2-}$ aqueous species was excluded. Hg in the floodplain soil is mainly present as Hg associated with soil organic matter (58%) and β-HgS (42%). XRD analysis of the sediment indicates crystalline phases that mainly consist of silicate minerals, including quartz (SiO_2) and Mg/Fe/Al silicates (e.g., vermiculite ($Mg_3Si_4O_{10}(OH)_2$) and biotite $K(Mg, Fe^{+2})_3(Al, Fe^{+3})Si_3O_{10}(OH,F)_2$).

The hardwood biochar (OAK) is highly aromatic (H/C = 0.02) and mainly contains C (~90%) with relatively low concentrations of major and trace elements (Table 3.2). A previous study reported hydroxyl, quinone, and aliphatic are the three most abundant functional groups on the biochar (Liu et al., 2015). OAK has a low S content (<0.16%), and the S K-edge XANES analysis indicates S on OAK is mainly associated oxidized S (inorganic SO_4^{2-} and ester SO_4^{2-}) (47%), followed by heterocyclic S (19%), intermediate S (17%)and sulfoxide (15%),with minimal elemental S (or polysulfur) (2%) (Fig. 3.1).

Sulfurization of OAK resulted in up to a nine-fold increase in S and a two-fold increase in Ca (Table 3.2). Sulfurized-hardwood biochar (MOAK) contains similar major and trace elements as OAK (Table 3.2). S K-edge XANES analysis indicates the sulfurization process shifted S species toward polysulfur (57%) and heterocyclic S (19%) with minimal sulfide minerals, intermediate sulfate, and oxidized S (<10%) (Fig. 3.1).

3.3.2 Aqueous chemical concentrations in Stages 1 and 3

3.3.2.1 Stage 1: Initially wet under anoxic conditions

3.3.2.1.1 General chemical compositions

Concentrations of DOC, acetate, and HS^- increased and Eh, alkalinity (as $CaCO_3$), and concentrations of SO_4^{2-} decreased in SRW controls (SRWCTR) over 200 d (Fig. 3.2). Other parameters, including pH and concentrations of $CH_{4(aq)}$ (<0.1 mg L^{-1}), THg (<20 ng L^{-1}), MeHg (<0.3 ng L^{-1}), NO_3^- (<0.1 mg L^{-1}), NH_3-N (<0.2 mg L^{-1}), and PO_4^{3-} (<0.4 mg L^{-1}), remained relatively unchanged over 200 d. The increases in DOC and acetate in SRWCTRs are likely associated with the breakdown of particulate organic matter in the river water. The decreases in Eh and SO_4^{2-} coupled with increases in HS^- indicate sulfate reducing conditions were established in Stage 1 (Eq. 3.1):

$$2(CH_2O)_x(NH_3)_y(H_3PO_4)_z + xSO_4^{2-} \rightarrow 2xHCO_3^- + xHS^- + 2yNH_3 + 2zH_3PO_4 \quad \text{Eq. 3.1}$$

Eh and concentrations of DOC, acetate, NO_3^-, and SO_4^{2-} in the soil controls (SedCTRs) were similar to SRWCTRs (Fig. 3.1), suggesting DOC, NO_3^- and SO_4^{2-} in the systems mainly reflect the composition of SRW. Increases in alkalinity and concentrations of Mn, Fe, $CH_{4(aq)}$, NH_3-N, and PO_4^{3-} coupled with lower pH and HS^- concentrations were observed (Fig. 3.1; Fig. B 2). The minimal NO_3^- and increases in concentrations of Mn, Fe, and $CH_{4(aq)}$ coupled with lower pH and increases in alkalinity, NH_3-N, and PO_4^{3-} indicate organic matter oxidation in SedCTRs is likely associated with denitrification, Mn and Fe reduction, and methanogenesis reactions (Eqs. 3.2-5):

$$5(CH_2O)_x(NH_3)_y(H_3PO_4)_z + 4xNO_3^- \rightarrow 5xHCO_3^- + 2xN_2 + 2xH_2O + xH^+ + 5yNH_3 + 5zH_3PO_4 \quad \text{Eq. 3.2}$$

$$(CH_2O)_x(NH_3)_y(H_3PO_4)_z + 2xMnO_2 + 3xH^+ \rightarrow xHCO_3^- + 2xMn^{2+} + 2H_2O + yNH_3 + zH_3PO_4 \quad \text{Eq. 3.3}$$

$$(CH_2O)_x(NH_3)_y(H_3PO_4)_z + 4xFe(OH)_3 + 7xH^+ \rightarrow xHCO_3^- + 4xFe^{2+} + 10H_2O + yNH_3 + zH_3PO_4 \quad \text{Eq. 3.4}$$

$$(CH_2O)_x(NH_3)_y(H_3PO_4)_z + xH_2O + \rightarrow xHCO_3^- + xCH_4 + yNH_3 + zH_3PO_4 \quad \text{Eq. 3.5}$$

The lower concentrations of HS^- (<5 μg L^{-1}) in SedCTRs than in SRWCTRs indicate the formation of FeS, and the peak at 30 d (127 μg L^{-1}) is likely associated with buildup of HS^- with a slow release of Mn and Fe early in the experiment (Waybrant et al., 2002).

Applying biochars to the floodplain soil slightly altered river water composition (Fig. 3.2; Fig. B 2). Parameters associated with organic matter oxidation (e.g., pH, Eh, alkalinity, and concentrations of DOC, NH_3-N, and PO_4^{3-}) in biochar-amended systems were similar to those in SedCTR (Fig. 3.2; Fig. B 2), indicating organic matter oxidation is mainly derived from organic matter in the floodplain soil instead of from biochar.

In 10%OAKs, river water compositions were similar to SedCTRs except for an elevated SO_4^{2-} at 200 d and higher concentrations of $CH_{4(aq)}$. This elevated SO_4^{2-} is likely related to continuous release of SO_4^{2-} derived from oxidized S species on OAK (Fig. 3.1), which is consistent with a previous study on OAK controls (OAK+SRW) and OAK-amended systems (Liu et al., 2018a). The elevated SO_4^{2-} is similar to SRWCTRs at 200 d, indicating that variability of SO_4^{2-} in SRW may contribute to this elevated concentration. Increased concentrations of $CH_{4(aq)}$ suggest applying OAK promotes methanogenesis.

In 10%MOAKs, elevated concentrations of acetate, Fe, Mn, SO_4^{2-}, HS^-, and $CH_{4(aq)}$ were observed (Fig. 3.2). Concentrations of acetate were elevated at 7 d, and gradually decreased

to <0.4 mg L^{-1} at 120 d. Concentrations of Mn and Fe rapidly increased to 10- and >32-fold higher than the SedCTRs at 30 d before slowly decreasing to concentrations similar to SedCTRs at 200 d. The elevated Mn and Fe in 10%MOAKs are not likely derived from MOAK due to similar Mn and Fe content in OAK and MOAK (Table 3.2). A peak in SO_4^{2-} concentration (18 mg L^{-1}) was observed at 120 d, likely associated with variability of SO_4^{2-} in the river water and not derived from the release of oxidized S in MOAK (due to the relatively low oxidized S content as indicated in the S K-edge XANES analysis; Fig. 3.1). Concentrations of HS^- were elevated (~300 µg L^{-1}) at 7 d and then declined to <5 µg L^{-1}. Concentrations of $CH_{4(aq)}$ were five-fold higher than the concentration in SedCTRs. The elevated concentrations of acetate, Mn, Fe, HS^-, and $CH_{4(aq)}$ indicate organic matter oxidation (Eqs. 3.1-5) is more prone to occur in MOAK-amended systems.

3.3.2.1.2 Total Hg removal and MeHg production

Release of both unf and 0.45-µm THg from SedCTRs increased prior to 120 d and fluctuated within 10% thereafter (Fig. 3.3). Concentrations of unf THg increased from 10,800 to 71,700 ng L^{-1}, and concentrations of 0.45-µm THg increased from 1140 to 51,400 ng L^{-1}. Release of Hg from SedCTRs shifted from predominantly particulate forms (unf) to colloidal forms (e.g., 0.45-µm, 0.2-µm, and 0.1-µm fractions) as incubation time increased (Fig. B 3). Releases of unf ($r = 0.64$) and 0.45-µm THg ($r = 0.82$) were positively correlated with DOC concentration. This positive correlation is consistent with the majority of Hg release being associated with Hg bound to soil organic matter (Fig. B 1).

Application of biochar, especially MOAK, to the floodplain soil significantly lowered concentrations of both unf and 0.45-µm THg ($p<0.01$) (Fig. 3.3). Greater removal of unf and

0.45-μm THg were observed after 120 d when Hg derived from the floodplain soil is mainly associated with colloidal forms (Fig. B 3). In 10%OAKs, removal of unf THg was between 53 and 68% after 120 d; the removal of 0.45-μm THg was between 7 and 82% over 200 d. In a previous study, limited removal of Hg was observed in OAK-amended systems when applied at a 5% dry weight ratio in Hg-contaminated river bank sediment (Liu et al., 2018a). The greater Hg removal observed in this study suggests that the enhanced Hg stabilization is due to the higher biochar to solid ratio. In 10%MOAKs, the removal of unf THg was between 16-98% over 200 d. Concentrations of 0.45-μm THg were <600 ng L^{-1}, representing 47-99% Hg removal over the duration of the experiment.

A previous study on the use of OAK for stabilizing Hg derived from riverbank sediment and floodplain soil suggests the predominant Hg removal mechanisms include both stabilization of Hg-bearing particulates with the porous structure of the biochar and complexation with O-containing functionalities on the biochar (Wang et al., 2019). Liu et al. (2019a) suggest the mechanisms of Hg removal using biochar in long-term anoxic environments may involve transforming less stable Hg forms (dissolved, colloidal) into more stable Hg-S on biochar. Polysulfur, the predominant S on MOAK (Fig. 1), may contribute to the enhanced Hg removal through formation of HgS with the polysulfur structure as suggested by Liu et al. (2018b). Kim and Luthy (2011) observed formation of Hg-S-DOM complexes on a polysulfide-rubber polymer. Kim et al. (2012) later suggest the mechanism of Hg removal using polysulfide-rubber-coated activated carbon involves both surface and intra-particle migration. In contrast to the better Hg removal rate observed in 10%MOAKs, Ting et al. (2018) observed a lower Hg removal rate for sulfurized activated carbon due to

release of nanoparticulate HgS. The inconsistency of Hg removal rates may be due to different reagents used in the sulfurization process.

Applying OAK and MOAK to the floodplain soil lowered concentrations of MeHg in SRW (Fig. 3.3). Concentrations of MeHg in SedCTRs were <60 ng L^{-1}. Applying OAK and MOAK to floodplain soil reduced the concentration of aqueous MeHg by up to 60%. Concentrations of MeHg in 10%OAK were similar to a previous study in which OAK was used to stabilize Hg from another South River sediment (Liu et al., 2018a). Concentrations of MeHg in 10%MOAK were similar to those in vertical-flow microcosm experiments conducted with spiked sediments and sulfurized materials over 80 d (Ting et al., 2018).

3.3.2.2 Stages 2-3: Drying and rewetting

After drying selected reaction vessels under oxic conditions for 90 d (Stage 2), the reaction vessels were rewet under anoxic conditions for 90 d (Stage 3) to evaluate potential impacts of drying and rewetting on biochar-amended systems. Results of average aqueous concentrations in replicates after rewetting were compared to the initially wet conditions to explain changes in geochemical conditions during drying and rewetting.

3.3.2.2.1 General geochemical properties

In Stage 3, minimal changes in the concentrations of NO_3^- (<0.2 mg L^{-1}), NH_3-N, PO_4^{3-}, and $CH_{4(aq)}$ were noted, but large variations in other aqueous parameters associated with organic matter oxidation (e.g., pH, Eh, and concentrations of DOC, acetate, Mn, Fe, SO_4^{2-}, and HS^-) were observed (Fig. 3.4; Fig. B 4). Substantial increases in concentrations of DOC, Mn, and Fe were observed in systems reacted for 7 d in Stage 1, while concentrations of Mn and Fe

were close to those reacted for 90 d in Stage 1. Concentrations of DOC in Stage 3 were six- to eight-fold higher than in Stage 1. In addition to increases in concentrations of DOC, Mn and Fe, elevated SO_4^{2-} (up to 113 mg L^{-1}) and HS^- (up to 107 µg L^{-1}) were observed in 10%MOAKs, indicating the development of more strongly sulfidogenic conditions than for SedCTRs and 10%OAKs.

3.3.2.2.2 THg and MeHg

Release of Hg in SedCTRs and 10%OAKs increased in systems reacted for 7 d in Stage 1, where Hg release in 10%MOAKs was limited (Fig. 3.5a). Concentrations of unf and 0.45-µm THg in SedCTRs in Stage 3 were up to three- and >200-fold higher than in Stage 1, respectively. Concentrations of unf and 0.45-µm THg in 10%OAKs in Stage 3 were two-fold higher than in Stage 1, respectively. The relatively higher concentrations of unf and 0.45-µm THg in SedCTRs and 10%OAKs were associated with increases in DOC in Stage 3 (Fig. 3.4), suggesting Hg in SedCTRs and 10%OAKs remobilized as a result of enhanced organic matter decomposition after the drying-rewetting process. In 10%MOAKs, concentrations of unf THg were eight-fold and 50-fold lower than in corresponding systems in Stage 1 and in SedCTRs in Stage 3, respectively. Concentrations of 0.45-µm THg were close to the concentrations in Stage 1. The relatively low concentrations of unf and 0.45-µm THg in 10%MOAKs suggest that Hg retained in MOAK-amended systems is less extensively remobilized by the drying-rewetting process.

Limited changes in MeHg production were observed in SedCTRs and 10%OAKs, whereas increases in MeHg were observed in 10%MOAKs compared toStage 1 (Fig. 3.5a). Concentrations of MeHg in SedCTRs and 10%OAKs were <5 ng L^{-1}, and concentrations of

MeHg in 10%MOAKs increased up to 10-fold to 21 ng L^{-1}. The increased MeHg in 10%MOAK is associated with elevated concentrations of Mn, Fe, SO_4^{2-}, and HS^- (Fig. 3.4).

3.3.3 Solid-phases analyses

Selected solid samples in Stages 1, 2, and 3 were collected and analyzed to evaluate transformations in solid phases after drying (Stage 2) and rewetting (Stage 3). Solid-phase analyses included solid MeHg content, total S content, S K-edge X-ray absorption near edge structure (XANES), and 16s rRNA sequencing.

3.3.3.1 MeHg in solid

Solid samples in reaction vessels reacted for 200 d in Stage 1 and after rewetting were collected and analyzed for MeHg. In Stage 1, solid MeHg content in biochar-amended systems (25-36 ng g^{-1}) was similar to SedCTRs (23 ng g^{-1}). After drying and rewetting, solid MeHg content in SedCTRs and 10%OAKs decreased by 83%, whereas solid MeHg content in 10%MOAKs (up to 88 ng g^{-1}) increased up to two-fold (Fig 5b).

The increases in both aqueous and solid MeHg in 10%MOAK suggest an increase in MeHg production. Biochars contain strong adsorption sites for MeHg, which can decrease as dissolved organic matter increases in anoxic sediments (Gomez-Eyles et al., 2013; Schwartz et al., 2019). If changes in MeHg sorption-desorption equilibrium had occurred due to enhanced DOC production after drying and rewetting, increases in aqueous MeHg coupled with decreases in solid MeHg should have been observed. The increases in both aqueous and solid MeHg (Fig. 3.5 ab) coupled with enhanced DOC production (Fig. 3.4) in 10%MOAKs

indicate enhanced MeHg production, inhibited degradation or loss rather than changes in MeHg sorption-desorption equilibrium (Gilmour et al., 2018).

3.3.4 Solid-phase S transformation in Stages 1-3

Solid samples in systems reacted for 200 d in Stage 1 and in their corresponding systems in Stages 2 and 3 were analyzed for total S content. Solid samples form SedCTR and 10%OAK contained similar S content, and MOAK addition to floodplain soil increased S content by three-fold in Stage 1 (Fig. B 5). Drying-rewetting resulted in limited changes in total S content (Fig. B 5).

Solid samples collected from the same systems as total S content were analyzed for S K-edge XANES. Results of Gaussian peak fitting on duplicate S K-edge XANES indicate minimal differences (<5%) in fractions of sulfide minerals, reduced S, and oxidized S and moderate differences (<10%) in fractions of polysulfur and intermediate S. The differences between duplicate analysis are within analytical error.

Results of S K-edge XANES analysis for SedCTRs and 10%OAKs samples reveal similar S forms in Stage 1 and limited changes after Stages 2-3 (Fig. 3.6ab; Figs. B 6-7). S in SedCTRs reacted for 200 d in Stage 1 is mainly associated with oxidized S (~48%), intermediate S (sulfoxide, sulfite, sulfonate, and sulfone) (~30%), oxidized S (inorganic sulfate and ester sulfate) (~30%), reduced S (heterocyclic S) (~10%), elemental (or polysulfide) (~10%), and minimal sulfide minerals (<5%).

Results of S K-edge XANES analysis for 10%MOAKs indicates shifts toward elemental S (or polysulfur) in Stage 1 and transformation of S in Stages 2-3 (Fig. 3.6; Fig. B 8). In Stage

1, S in 10%MOAKs is mainly associated with elemental S (or polysulfur) (~30%), followed by oxidized S (inorganic and ester sulfate) (~22%), intermediate S (sulfite, sulfone, and sulfonate) (~22%), sulfide minerals (~14%), and reduced S (exocyclic S) (~12%). The shifts toward elemental S (polysulfur) and reduced S are likely associated with the sulfurization process in MOAK (Fig. 3.1). The higher fraction of sulfide minerals in 10%MOAKs is likely related to formation of HgS and other sulfide minerals through bacterial sulfate reduction reactions. In Stage 2, minimal sulfide minerals coupled with an increase in oxidized S (52%), indicating sulfide oxidation during drying according to:

$$MS + O_2 \rightarrow SO_4^{2-} + M^{2+} \quad \text{Eq. 3.6}$$

Liu et al. (2018b) observed increases in oxidized S after storing MOAK in an oxic environment for 60 d. The increase in oxidized S coupled with a decrease in polysulfur (~12%) may also be associated with oxidation of elemental (or polysulfur) in MOAK. In Stage 3, increases in polysulfur (~44%) and sulfide minerals (4%) and decreases in oxidized S (27%) were observed. The increases in sulfide minerals and decreases in oxidized S may be related to sulfate reduction (Eq. 3.1). Polysulfur, a major intermediate species of sulfide oxidation, forms through a wide range of abiotic and biotic pathways (Findlay, 2016). Yao and Miller (1996) observed formation of polysulfur as an initial product of sulfide oxidation coupled to Fe(III) and Mn(IV) reduction. The increases in fractions of polysulfur in solid materials might release dissolved polysulfide (S_x^{2-}) to solution, where it associates with organic matter to form sulfurized organic matter (Graham et al., 2017; Gun et al., 2000). The formation of sulfurized organic matter can lead to increases in net MeHg production through

either formation of highly bioavailable Hg-S-DOM complexes or inhibition of nanoparticulate β-HgS aggregation (Graham et al., 2017).

3.3.5 Microbial communities

Solid materials in systems reacted for 7, 90, and 200 d in Stage1 and their corresponding systems in Stages 2 and 3 were collected for 16s rRNA sequencing analysis. After denoising the pyrosequencing data, an effective sequencing reads for the air-dried floodplain soil was 62 029±10 470, with 2481±293 operational taxonomic units (OTUs) detected (>97% percent homology). The effective sequencing reads for samples collected in SedCTRs, 10%OAKs, and 10%MOAKs was 83 880±20 916 per sample. Effective sequencing reads for biochar-amended systems in Stage 1 are similar to SedCTRs. Significantly ($p = 0.005$) higher effective sequencing reads per sample (98 271±13 178) were observed in solid samples collected in Stage 3 than in Stage 1 (75 137±19 104). The mean number of OTUs for solid materials in SedCTRs, 10%OAKs, and 10%MOAKs was 1982±335 (>97% percent homology). OTUs for solid materials collected in 10%MOAKs reacted for 90 and 200 d in Stage 1 (2556±188) were significantly higher ($p<0.005$) than OTUs in other reactors in Stages 1 (1909±244) and 3 (1799±138). The results of duplicate samples were within 20% relative standard difference.

The air-dried floodplain soil was highly heterogeneous due to the relatively large differences in the results of pyrosequencing (Fig. 3.7ab). The air-dried floodplain soil had abundant Proteobacteria (22-34%), Acidobacteria (16-32%), Bacteroidetes (3-20%), Actindobacteria (1-15%), Gemmatimonadetes (1-8%), and Chloroflexi (3-8%).

In Stage 1, similar microbial communities with <10% differences were observed in SedCTRs and 10%OAKs, whereas greater changes in microbial communities were observed in 10%MOAKs (Fig. 3.7a). In SedCTRs and 10%OAKs, Proteobacteria, Bacteroidetes, and Firmicutes were the three most abundant communities at early time points in Stage 1 (Fig. 3.7a). In 10%MOAKs, Proteobacteria, Bacteroidetes, and Firmicutes were the three most abundant communities after 7 d. Shifts toward Bacteroidetes were observed in 10%MOAKs at 200 d, where Bacteroidetes (26%), Proteobacteria (25%), and Euryarchaeota (16%) became the most three abundant communities. At genera taxonomic ranking, microbial community in SedCTRs and 10%OAKs shifted from rhizosphere bacteria (e.g., *Massilia*) and nitrogen-fixing bacteria (e.g., *Herbaspirillum*) toward FeRB (e.g., *Prolixibacter*, *Geothrix*, *Geobacter*) and fermenters (e.g., *Pelobacter*) as incubation time increased. In 10%MOAKs, microbial community shifted from FeRB (e.g., *Geobacter*) toward methylotrophic bacteria (e.g., *Methylobacillus*), fermenters (e.g., *Anaerophage*, *Alkaliflexus*), and methanogens (e.g., *Methanobacterium*) attributed to the shifts toward Bacteroidetes and Euryarchaeota (Fig. 3.7b).

Redox-active biochars function as electron shuttles between FeRB and Fe(III) oxides and promote dissimilatory Fe(III)-reduction (Kappler et al., 2014; Klüfoel et al., 2014). Biochars with more redox-active properties also promote methane production by facilitating direct interspecies electron transfers between FeRB and methanogens (Yuan et al., 2018). The higher abundance of FeRB and methanogens (Fig. 3.7ab) as well as elevated concentrations of Mn, Fe and $CH_{4(aq)}$ (Fig .2) in 10%MOAKs indicate MOAK may be more redox-active than OAK. Polysulfur as the predominant S phases in MOAK (Fig. 3.1) stimulates Fe(III)

reduction and methanogenesis (Flynn et al., 2014 Thermodynamic calculations suggest FeRB favour mediating elemental S reduction than Fe(III) reduction at alkaline pH (7-8) and further reduce Fe(III) oxides through abiotic reduction (Flynn et al., 2014; Kiene et al., 1986).

In Stage 3, Proteobacteria and Bacteroidetes were the most abundant phyla in soil and biochar-amended systems, and changes in other soil communities were observed (Fig. 3.7a). Euryarchaeota, mostly containing methanogens, became abundant (3-9%) in SedCTRs and 10%OAKs reacted for 200 d in Stage 1. Nitrospirae, including mainly nitrifiers (e.g., *Nitrospira*), became more abundant in 10%MOAKs (~5-16%) whereas this bacterial community remained in relatively low abundance (<1%) in SedCTRs and 10%OAKs (Fig. 3.7a).

In Stage 1, applying OAK and MOAK increased the relative abundance of predicted Hg methylators and drying and rewetting may shift methylating communities (Fig. 3.8). The relative abundance of identified genera containing predicted Hg methylators was <20% in the air-dried floodplain soil before the experiment. Higher relative abundances of genera containing predicted Hg methylators were observed in biochar-amended systems (13-21%) than in SedCTRs (<1%). FeRB (e.g., *Geobacter*) and fermenters (e.g., *Pelobacter*) accounted for the most abundant genera containing predicted Hg methylators in Stage 1. Although higher abundances of methylators were observed in biochar-amended systems, MeHg in biochar-amended systems was similar to SedCTR (Fig. 3.3; Fig 5b). This inconsistency between relative abundances of methylators and MeHg is likely related to the presence of less bioavailable Hg species in the biochar-amended systems.

In Stage 3, relative abundances of genera containing predicted Hg methylator in SedCTRs and 10%OAKs increased, whereas shifts toward SRB (e.g., *Desulfomicrobium* and *Desulfobulbus*) occurred in 10%MOAKs (Fig. 3.8). The increases in the relative abundances of genera containing potential methylators in SedCTRs and 10%OAKs are likely related to the observed increases in DOC and acetate available to microorganisms as an energy source (Fig. 3.4). *Desulfobulbus* bacteria mediate S/polysulfur disproportionation to form both HS^- and SO_4^{2-} (Eq. 3.7) and reduction of Mn(IV)(Eq. 3.8) in anoxic sediments (Böttcher et al., 2001; Fuseler and Cypionka, 1995; Lovley and Phillips, 1994):

$$8.5S^0 + 8H_2O \rightarrow 5HS^- + 1.5\,H_2S + 2SO_4^{2-} + 8H^+ \quad \text{Eq. 3.7}$$

$$S^0 + 3MnO_2 + 4H^+ \rightarrow SO_4^{2-} + 3Mn^{2+} + 2H_2O \quad \text{Eq. 3.8}$$

The shifts in predicted Hg methylators toward SRB corresponded to elevated concentrations of Fe, SO_4^{2-}, HS^-, and MeHg observed in 10%MOAKs in Stage 3, which likely promoted conditions favourable for MeHg production (Figs. 3.4-5). Elemental S disproportionation (Eqs. 3.7-8) by SRB produced elevated concentrations of SO_4^{2-}, HS^-, Mn, and Fe, potentially affecting Hg methylation. SO_4^{2-} provides terminal electron accepters that further stimulate SRB growth (Gilmour et al., 1992). Concentrations of sulfide in aqueous solutions control the bioavailability of Hg by forming neutrally charged Hg-S species (Benoit et al., 1999). DOC further enhances Hg bioavailability by inhibiting aggregation of neutrally charged nanoparticulate Hg-S species (Graham et al., 2012). The increases in polysulfur after Stage 3 in 10%MOAKs (Fig. 3.6; Fig. B 8) may promote formation of sulfurized organic

matter, which forms highly bioavailable Hg-thiol-DOM aqueous complexes under conditions that are supersaturated with respect to β-HgS (Graham et al., 2017).

3.4 Environmental Implications

The effectiveness of biochar amendment with MOAK is strongly dependant on the conditions where the biochar was applied. Under conditions where soil remained saturated for a relatively long time (days to months), MOAK effectively controlled the release of Hg from sediment without significantly promoting MeHg production. The drying-rewetting process enhanced microbial activity and shifted microbial composition. After drying-rewetting the 10%MOAKs, Mn(IV) and Fe(III) reduction occurred with the production of $SO_4^{2-,}$ and HS^-, which were associated with microbially mediated elemental (or polysulfur) S disproportionation. The changes in aqueous composition and shifts in microbial composition may favour MeHg production by changing Hg-S-DOM equilibrium (Graham et al., 2017; Liem-Nguyen et al., 2017; Poulin et al., 2017).

The applied biochar to solid ratio (10% wt.) was higher than typical biochar loading rates (1~5%) used as sediment amendments in other studies (Liu et al., 2017, 2018a; Gilmour et al., 2018; Zhang et al., 2018). Abujabhah et al. (2016) observed increases in soil pH, moisture content and exchangeable cations, and decreases in microbial biomass in 10% wt. biochar amended sandy loam soil compared to lower application rates (0, 2.5, 5%). Soil physical, chemical and biological properties may differ at lower biochar to solid ratios, which may affect the efficacy of *in situ* Hg stabilization. Therefore, detailed investigations

regarding the hydrogeological and biogeochemical conditions should be completed before applying sulfurized biochar amendments at the field-scale.

Table 3.1 Experimental set-up including reaction time in Stage 1(wet) and reactors selected for Stages 2 (dry) and 3 (rewet).

Reaction time (d)	Soil controls (SedCTR)	10% dry wt. MOAK (10%MOAKs)	10% dry wt. OAK (10%OAKs)	Ultrapure water control	SRW control (SRWCTRs)
7	a[1*], b[2*], c[3]	a*, b*, c	a*, b*, c	a	a
30	a	a, b	a		
60	a, b	a	a, b		
90	a*, b*, c	a*, b*, c	a*, b*, c	a	a
120	a	a	a		
160	a	a	a		
200	a*, b*, c	a*, b*, c	a*, b*, c	a	a

[1] Replicate experiment 1

[*] Reactors used for Stages 2-3

[2] Replicate experiment 2

[3] Replicate experiment 3

Table 3.2 Physical characteristics and elemental composition of hardwood biochar (OAK) and sulfurized-hardwood biochar (MOAK). Surface area and C, H, O, N, and ash content were not remeasured after sulfurization.

	OAK	MOAK
Surface area, $m^2\ g^{-1}$	65	-
Ash content % (550 °C)	3.1	-
C, %	89.5	-
Volatile C, %	16.0	-
H, %	1.57	-
O, %	4.08	-
N, %	0.26	-
Total Kjeldahl N, %	0.22	-
S, %	0.16	0.55±0.24
Al, mg kg^{-1}	77	<50
Ag, mg kg^{-1}	<0.10	<0.10
As, mg kg^{-1}	<0.10	<0.10
B, mg kg^{-1}	<5.0	<5.0
Ba, mg kg^{-1}	30.4	28.0
Be, mg kg^{-1}	<0.10	<0.10
Bi, mg kg^{-1}	<0.20	<0.20
Ca, mg kg^{-1}	3880	5050
Cd, mg kg^{-1}	<0.020	<0.02
Co, mg kg^{-1}	<0.10	<0.10
Cr, mg kg^{-1}	<0.50	0.65
Cu, mg kg^{-1}	1.71	1.02
Fe, mg kg^{-1}	106	63
Hg, mg kg^{-1}	0.02	0.04
K, mg kg^{-1}	1340	1430
Mg, mg kg^{-1}	299	261
Mn, mg kg^{-1}	54.1	71.7
Mo, mg kg^{-1}	<0.10	<0.10
Na, mg kg^{-1}	<50	<50
Ni, mg kg^{-1}	0.93	2.66
P, mg kg^{-1}	94	54
Pb, mg kg^{-1}	0.84	0.65
Sb, mg kg^{-1}	<0.10	<0.10
Sn, mg kg^{-1}	<1.0	<1.0
Sr, mg kg^{-1}	14.1	15.8
Ti, mg kg^{-1}	1.6	<1.9
U, mg kg^{-1}	<0.050	<0.050
Zn, mg kg^{-1}	9.1	7.3

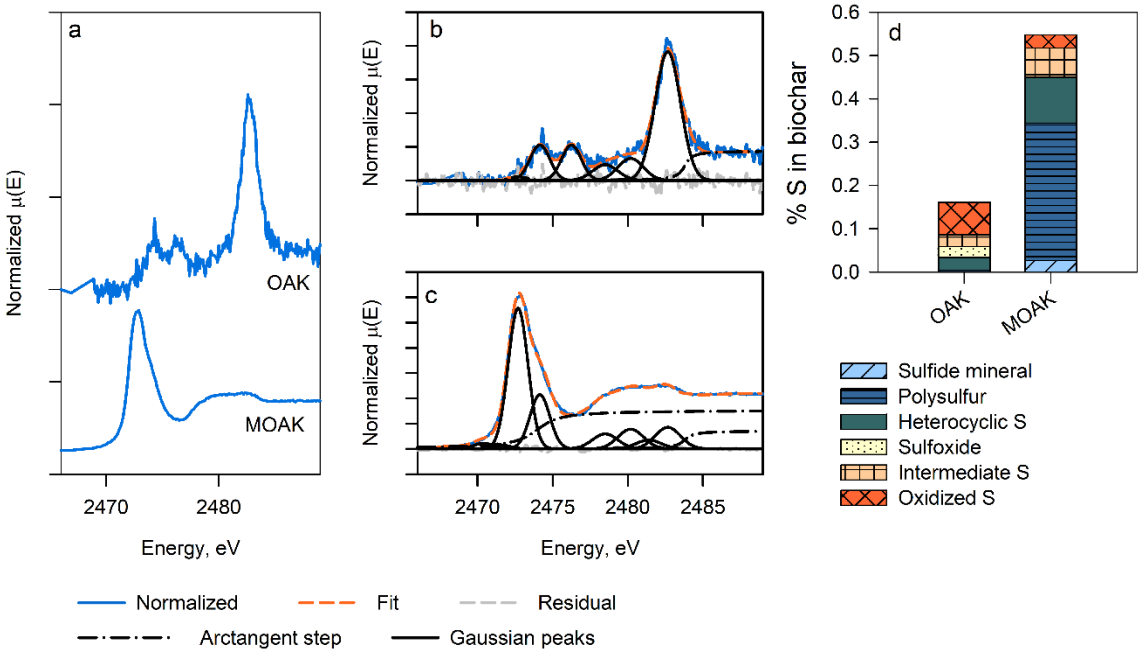

Fig. 3.1 S K-edge X-ray absorption near edge structure (XANES) spectroscopy for hardwood (OAK) and sulfurized-hardwood biochar (MOAK). Measured spectra (a) (blue solid line) and best-fit (orange dash line) using Gaussian peak fitting for OAK (NSS=1.47×10^{-2}) (b) and MOAK (NSS=4.75×10^{-4}) (c). Distribution of S based on S K-edge XANES data corrected with total S in biochar (d).

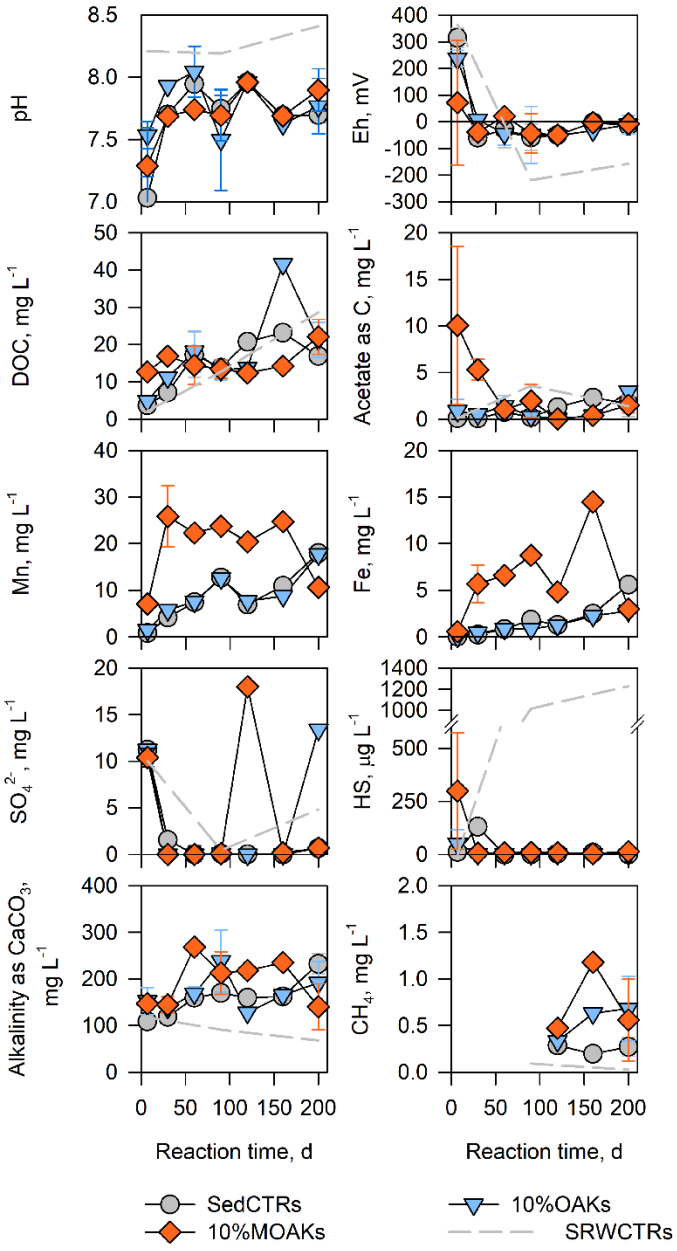

Fig. 3.2 pH, Eh, alkalinity, and concentrations of dissolved organic carbon (DOC), acetate, Mn, Fe, SO_4^{2-}, HS^-, and $CH_{4(aq)}$ in South River water controls (SRWCTRs) (grey dashed line), soil controls (SedCTRs) (grey circles), OAK- (10%OAKs) (blue triangles) and MOAK-amended systems (10%MOAKs) (orange diamonds). Error bars indicate standard deviation of results obtained from replicate experiments.

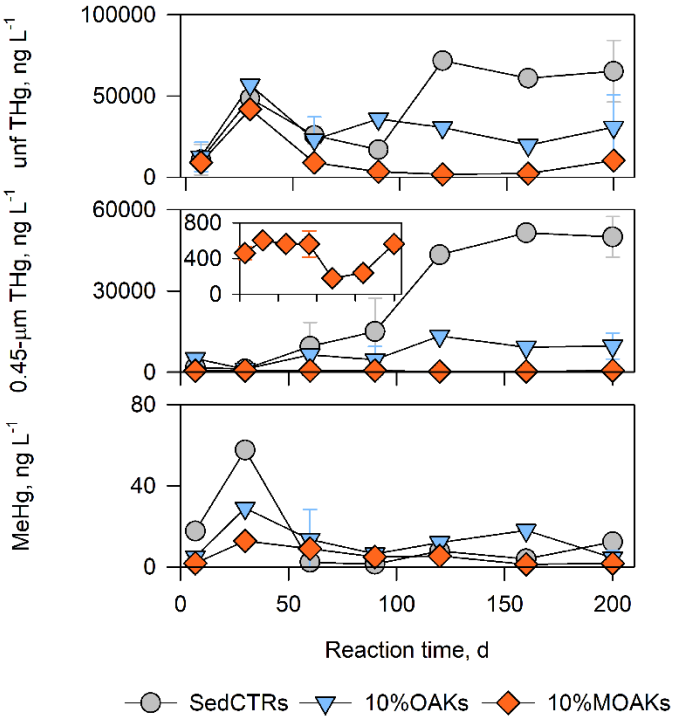

Fig. 3.3 Concentrations of unfiltered (unf) and 0.45-µm THg and MeHg in soil controls (SedCTRs) and systems amended with 10% dry wt. hardwood biochar (10%OAKs) and sulfurized-hardwood biochar (10%MOAKs). Error bars represent standard deviation of the mean for replicate experiments. The inset x-axis represents the same time scale as the large plots.

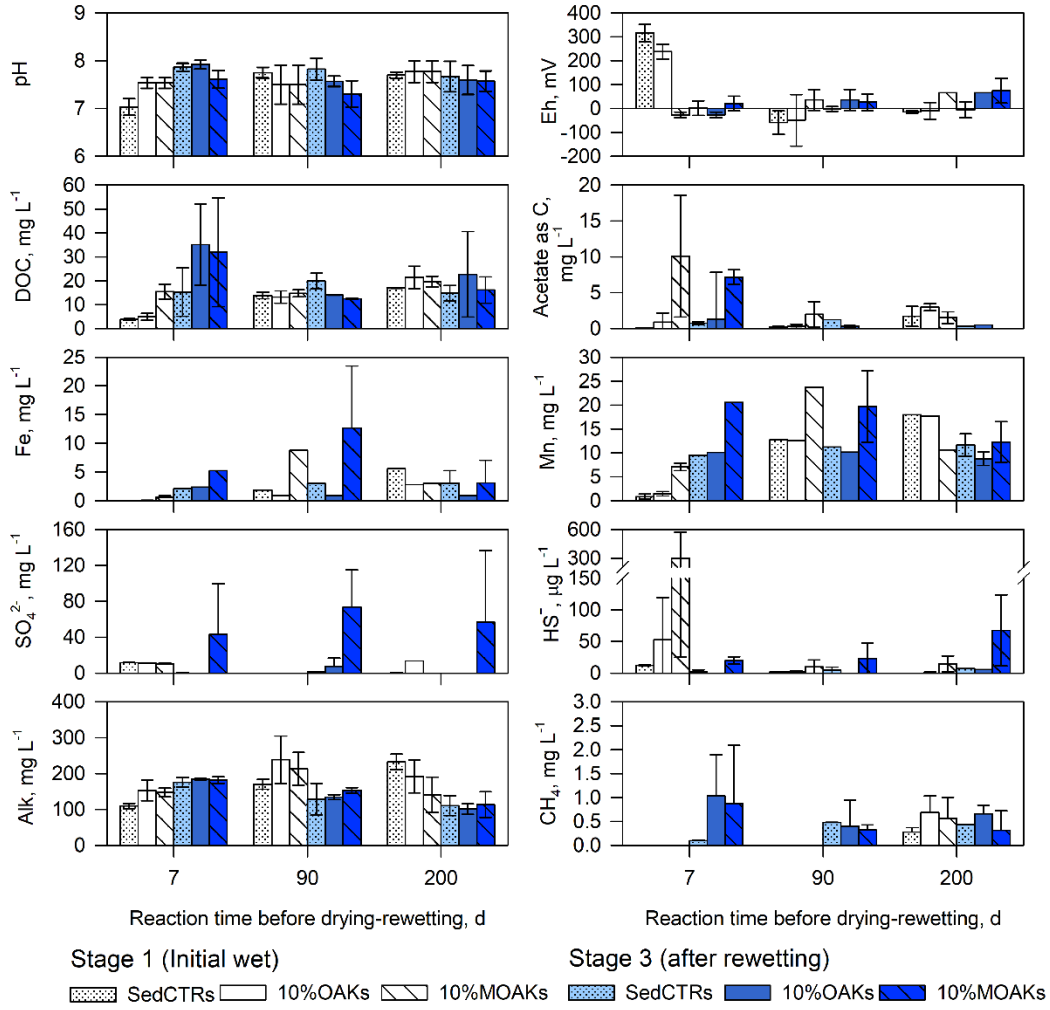

Fig. 3.4 pH, Eh, alkalinity, and concentrations of DOC, acetate, Mn, Fe, SO_4^{2-}, HS^-, and $CH_{4(aq)}$ in systems reacted for 7, 90, and 200 d in Stages 1 and their corresponding systems in Stage 3. $CH_{4(aq)}$ for samples reacted for 7 and 90 d in Stage 1 were not collected and analyzed. Error bars indicate standard deviation of the mean for replicate experiments.

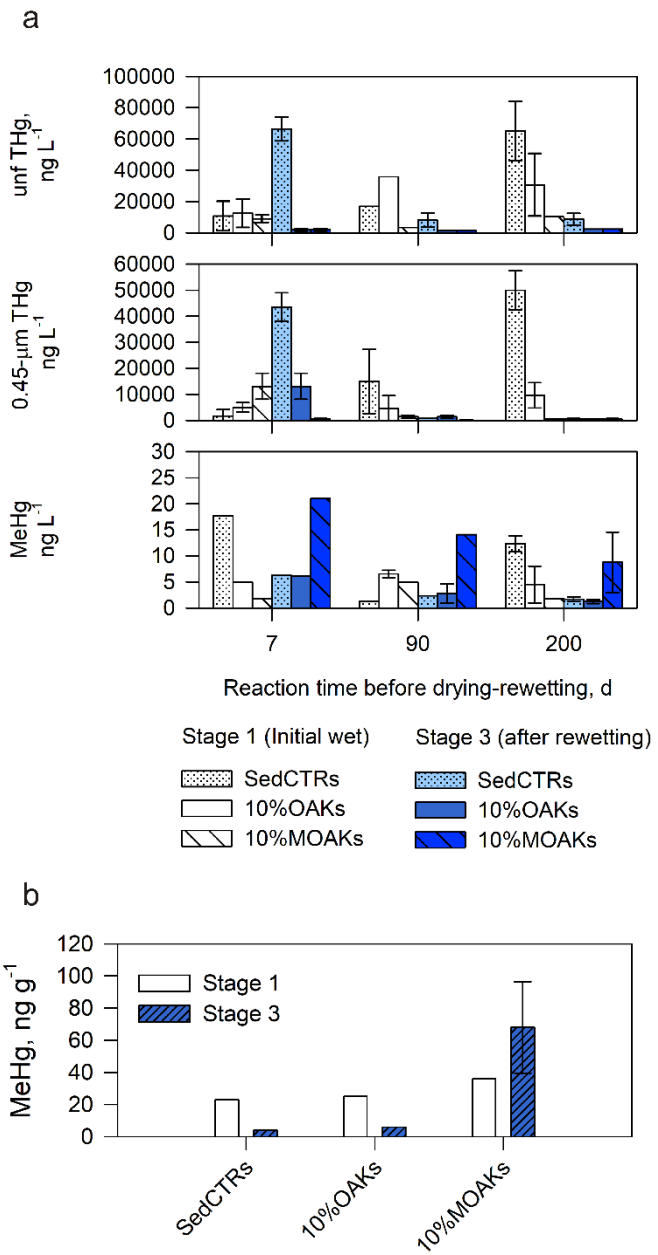

Fig. 3.5 Concentrations of Hg and MeHg in systems after drying and rewetting (Stage 3) compare to the initial wet conditions (Stage 1). Aqueous THg (unf and 0.45-µm) and MeHg in systems reacted for 7, 90, and 200 d in Stage 1 and their corresponding systems in Stage 3 (a). Solid MeHg content in systems reacted for 200 d in Stages 1 and their corresponding systems in Stage 3 (b). Error bars represent standard deviation from the mean for replicate experiments.

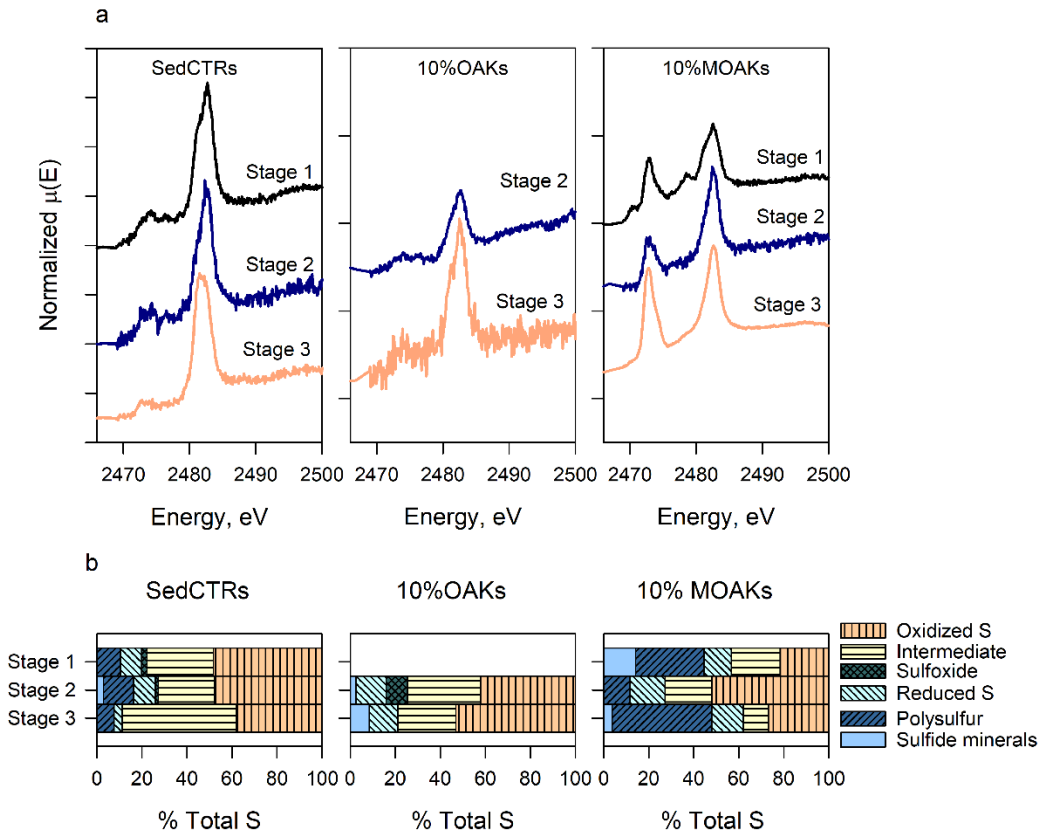

Fig. 3.6 Results of S K-edge XANES analysis for solid materials collected in systems reacted for 200 d in Stage 1 and their corresponding systems in Stages 2 and 3 for SedCTRs, 10%OAKs, and 10%MOAKs. Normalized S K-edge XANES spectra (a) and fractions of S species obtained from Gaussian peak fitting (NSS<3.06×10^{-2}) (b). S K-edge XANES spectra for the 10%OAKs at 200 d in Stage 1 were noisy, so the normalized spectra were excluded.

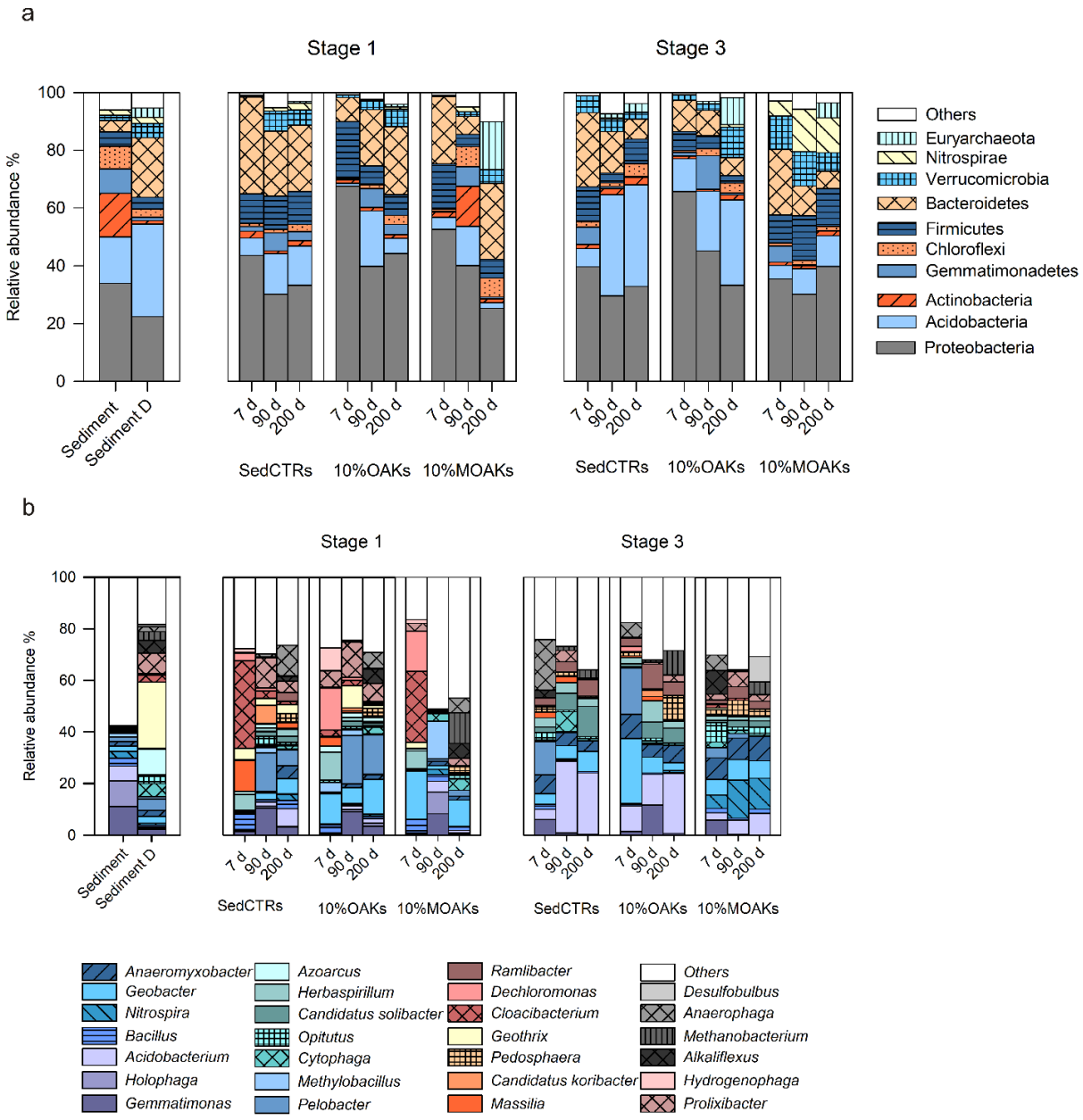

Fig. 3.7 Results of 16s rRNA sequencing showing relative abundance of predominant phyla (a) and genera (b) (>5%) for air-dried floodplain soil and duplicate (Sediment and Sediment D), solid materials in systems reacted for 7, 90 , and 200 d in Stage 1 and their corresponding samples in Stage 3 for soil controls (SedCTRs), 10%OAKs and 10%MOAKs.

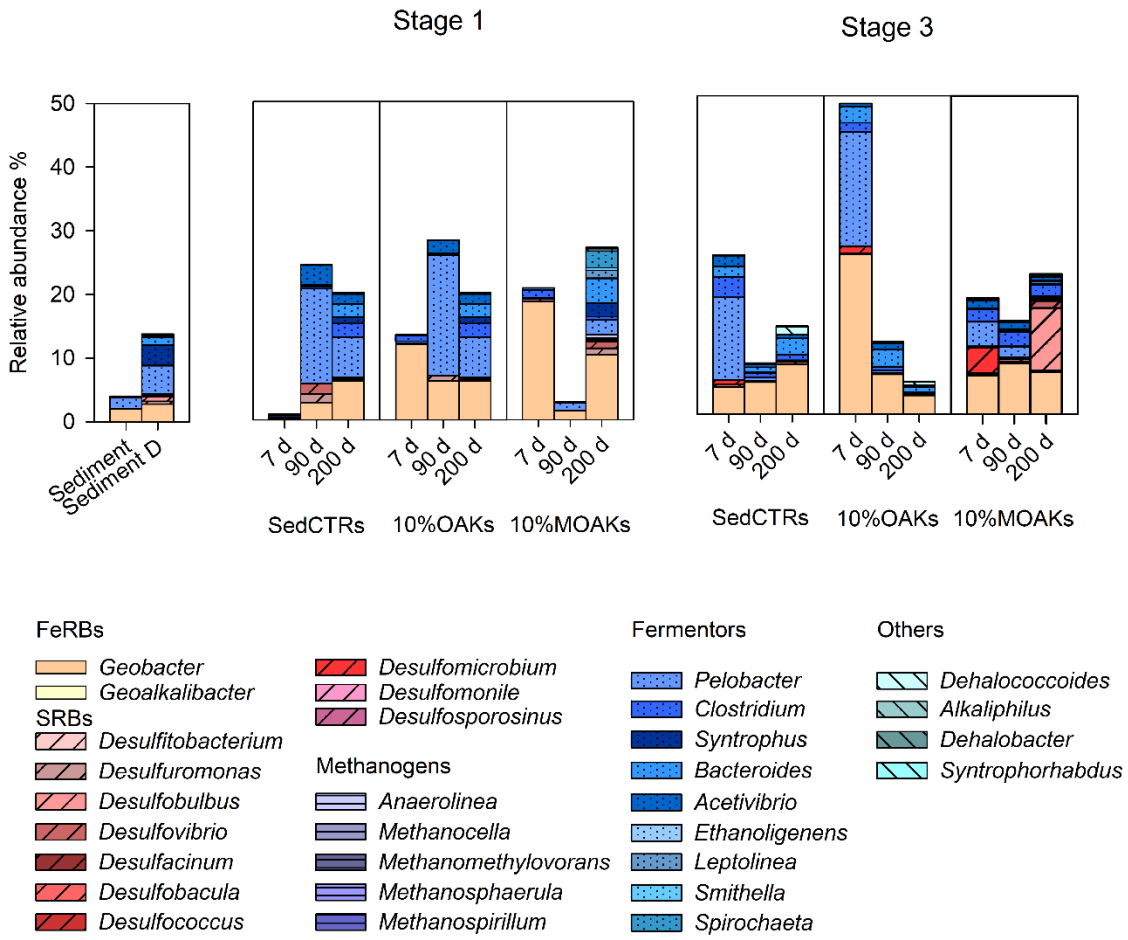

Fig. 3.8 Results of 16s rRNA sequencing showing identified genera containing predicted Hg methylators according to the online database organized by Oak Ridge National Laboratory (ORNL, http://www.esd.ornl.gov/programs/rsfa/data.shtml) for air-dried floodplain soil and duplicate (Sediment and Sediment D), solid materials in systems reacted for 7, 90, and 200 d in Stage 1 and their corresponding samples in Stage 3 for SedCTRs, 10%OAKs and 10%MOAKs.

Chapter 4 Application of biochar prepared from ethanol refinery by products for Hg stabilization in floodplain soil: Impacts of drying and rewetting

Summary

This study evaluated three biochars derived from bioenergy by-products — manure-based anaerobic digestate (DIG), distillers' grains (DIS), and a mixture thereof (75G25S) — as amendments to stabilize Hg in contaminated floodplain soil under long-term water-saturated conditions (up to 200 d) and under cyclic drying and rewetting. Greater total Hg (THg) removal (72 to nearly 100%) and limited MeHg production (<65 ng L^{-1}) were observed in digestate-based biochar-amended systems under initial saturated conditions. Drying and rewetting resulted in limited release of THg. Slight increases in aqueous MeHg occurred in digestate-based biochar-amended systems, while solid MeHg concentrations decreased 50% compared to those prior to drying and rewetting. Changes in Fe and S chemistry as well as microbial communities during drying and rewetting were observed, potentially affecting MeHg production. Biochars derived from anaerobic digestion by-products may be effective as amendments to control Hg release and minimize MeHg production in floodplain soils.

4.1 Introduction

Mercury (Hg) contamination related to various industrial activities has been documented worldwide (Kocman et al., 2013). Terrestrial Hg poses a risk of legacy contamination at the catchment scale by entering freshwater systems through soil erosion, sediment resuspension, and flooding events (Carter, 1977; Gibson et al., 2015; Kocman et al., 2013; Mucci et al., 2015; Poulin et al., 2016). Hg is transformed into methylmercury (MeHg), a more toxic

neurotoxin that accumulates through the food chain, mainly by microbially-driven processes (Hsu-Kim et al., 2013). Sulfate-reducing bacteria (SRB), iron-reducing bacteria (FeRB), methanogens, and fermentative bacteria all contain members that can stimulate Hg methylation (Compeau and Bartha, 1985; Fleming et al., 2006; Gilmour et al., 2013; Hu et al., 2013; Liu et al., 2017, 2018; Paulson et al., 2016). Hg methylation processes mainly depend on the microbial activity of methylating bacteria and the bioavailability of Hg species (Hsu-Kim et al., 2013), the latter of which may be affected by changes in concentrations of dissolved organic carbon (DOC), SO_4^{2-}, and HS^- (Graham et al., 2012; Hsu-Kim et al., 2013; Poulin et al., 2017).

Biochars, prepared from organic raw materials, have been proposed as reactive materials for *in situ* Hg stabilization. Biochars can be used as passive reactive mats under environmentally relevant conditions, such as saturated flowing (Fellin, 2016; Paulson, 2014) and flooding/drainage conditions (Wang et al., 2019). Biochars can also be used as soil amendments in areas where extensive flooding may occur (Beckers et al., 2019; Chapter 3; Gilmour et al., 2018, Liu et al., 2017, 2018). The effectiveness of Hg stabilization using biochars depends on the type of raw materials used to produce the biochar as well as environmental conditions. In studies where hardwood biochar was used as a permeable reactive mat to intercept discharge waters, effective removal of Hg without promotion of MeHg production was observed (Wang et al., 2019; Paulson, 2014). In studies where biochars were applied as soil amendments, the removal of Hg was more variable; the use of hardwood biochar was less effective than manure-based and switchgrass biochars, and the

addition of pine dust biochar resulted in a smaller reduction of MeHg than activated carbon (Gilmour et al., 2018; Liu et al., 2017, 2018).

Periodic flooding and drying in floodplains can alter the geochemical and microbial conditions that control Hg mobility and bioavailability. Drying and rewetting may enhance DOC production and carbon mineralization (Iovieno and Bååth, 2008). Drying and rewetting may also affect Fe and Mn chemistry, which are terminal electron acceptors for microbial activity contributing to MeHg production, and also potential sinks for heavy metals (Borch et al., 2010; Fleming et al., 2006; Gilmour et al., 2013; Poulin et al., 2016). For example, release of Hg may occur through reductive dissolution of Fe oxides and the associated release of particulate soil organic matter (Mucci et al., 2015; Poulin et al., 2016). Substantial Hg release corresponding to elevated DOC has also been observed in biochar-amended systems under dynamic redox conditions (Chapter 3; Beckers et al., 2019). In addition, drying and rewetting can stress microbial communities, leading to shifts in community composition and changes in microbial respiration (Chapter 3; Fierer et al., 2003; Iovieno and Bååth, 2008; Yu et al., 2014). Changes in microbial activity may also control Hg methylation (Marvin-DiPasquale et al., 2014), as iincreases in MeHg coupled with shifts toward SRB have been observed in sulfurized-biochar-amended systems after a drying and rewetting event (Chapter 3).

Recent interest in using biochars derived from bioenergy by-products has grown due to their potential in terms of sustainable resource management. Biochars derived from manure-based anaerobic digestion have been highly effective for removing heavy metals (e.g., Pb^{2+}, Cu^{2+}, Ni^{2+}, Cd^{2+}) from aqueous solution (Inyang et al., 2012; Ni et al., 2019). Distillers'

grains have been evaluated as a soil amendment, but enhanced As mobility has been observed (Jia et al., 2012). Using such biochars for Hg stabilization as soil amendments under conditions representative of periodic flooding and drying in floodplain has not been widely evaluated.

This study focused on utilizing biochars derived from bioenergy by-products as soil amendments for *in situ* Hg stabilization under periodic flooding and drying typical of conditions occurring in floodplain settings. Chapter 3 (2019b) describes the use of hardwood and sulfurized biochar as amendments to floodplain soil under such conditions. The current study complements this previous work by evaluating alternative materials for *in situ* Hg stabilization using the same biochar to solid ratio. Geochemical measurements, solid-phase characterization, and pyrosequencing were conducted to provide insights into Hg removal mechanisms, factors contributing to MeHg production, and impacts of drying and rewetting in biochar-amended systems.

4.2 Materials and Methods

4.2.1 Materials

Hg-contaminated floodplain soil was collected 36.5 km downstream of a legacy contaminated site on the South River in Waynesboro, VA, USA. Floodplain soil was air-dried for 3 d and sieved to <2 mm before use in the experiments. South River water (SRW) was collected 4.8 km upstream of the historical release site.

Three biochars—100% anaerobic digestate (DIG), 100% distillers' grains (DIS), and a mixture composed of DIG and DIS at a ratio of 3:1 (75G25S)—were prepared at Cornell

University (Ithaca, NY) using feedstocks produced by an advanced bioenergy (Coaltec Energy, Carterville IL, USA). DIG was prepared using a digestate mixture containing beef cattle manure and thin stillage extracted from an ethanol refinery and separating the liquid from solids. DIS was separated from the ethanol refinery without removing oils. 75G25S was prepared by mixing 75% anaerobic digestate and 25% distillers' grains prior to pyrolysis.

4.2.2 Experimental setup

Microcosm experiments were conducted by mixing Hg-contaminated floodplain soil and biochars at a ratio of 10:1 at three stages representing dynamic flooding-drying-flooding conditions as previously described (Table C 1) (Chapter 3). Each reaction vessel contained 20 g of air-dried floodplain soil, with or without 2 g of biochar, in a 250-mL wide-mouth amber bottle. Amber bottles were cleaned with 10% HCl and rinsed with ultrapure water before use. Stage 1 included equilibrating 240 mL of SRW in an anaerobic chamber with 3.5% H_2/balance N_2 (Coy Laboratory Products, Inc.) for up to 200 d. Replicate experiments were conducted at 7, 90, and 200 d and at randomly selected reaction times for soil control (SedCTR) and 10% anaerobic digestate biochar (10%DIG)-, 10% distillers' grains biochar (10%DIS)-, and mixed biochar (10%75G25S)-amended systems. Controls included SRW control (SRWCTRs) and ultrapure water control (WatCTRs) as previously described (Chapter 3). Experiments with a total of 62 reaction vessels were conducted over a 2-week period in random order to minimize changes in floodplain soil and SRW. At the end of each reaction time, aqueous and solid samples were collected for further analyses, with the exception of solid residues in two of three replicates at 7, 90, and 200 d. Stage 2 included drying these residues in their reaction vessels under an oxic environment for 90 d under

natural light conditions. Stage 3 included rewetting the reaction vessels with 240 mL of SRW in an anaerobic chamber for 90 d. All reaction vessels in Stages 1 and 3 were mixed every 2 to 3 d by gentle inversion.

4.2.3 Sample collection

Aqueous samples were collected for pH, Eh, alkalinity, cations, anions, DOC, $CH_{4(aq)}$, NH_3-N, PO_4^{3-}, total Hg (THg) passing different filter sizes (unfiltered (unf), 0.45-µm, 0.2-µm, 0.1-µm), and MeHg analyses. Solid samples were collected and stored below −20 °C before solid MeHg, S K-edge X-ray absorption near edge structure (XANES), and 16s rRNA polymerase chain reaction analyses. Details about sample collection have been previously described (Chapter 3; Chapter 4).

4.2.4 Analytical methods

4.2.4.1 Aqueous samples

Concentrations of THg passing different filter membranes (unf, 0.45, 0.2, 0.1 µm) were determined using automated cold vapour atomic fluorescence spectroscopy (CVAFS, Tekran® 2600, Tekran Instruments Corp, Scarborough, ON, Canada) following US EPA Method 1631 Revision E (US EPA, 2002). The instrument method detection limit (n = 16) was 0.16±0.07 ng L^{-1}. Relative standard deviation (%RSD) for duplicate analyses (n = 33) was 0.1 to 14%. Recoveries for matrix-spike samples (n = 13) were 95 to 115%. Recoveries for standard reference material (NIST 1641e, Hg in water) (n = 16) were 101 to 112%.

Concentrations of MeHg were determined at the Biotron Experimental Climate Change Research Centre (University of Western Ontario, London, ON, Canada) following US EPA

Method 1630 (US EPA, 2001). The instrument detection limit was <0.08 ng L^{-1}. Matrix spike recoveries were 77.5 to 98%. Relative percent differences for matrix spikes were <15%. Recoveries for quality controls were 86 to 94%.

Other aqueous parameters, including pH, Eh, alkalinity, concentrations of DOC, organic acids, total sulfide (S^{2-}), nitrogen ammonia (NH_3-N), reactive phosphorus (PO_4^{3-}), $CH_{4(aq)}$, trace elements, and major cations and anions, were determined as previously described (Chapter 3). Details for analytical methods for these aqueous parameters are provided in the supporting information. Concentrations of total sulfide are reported as concentrations of HS^- (Text C 1).

4.2.4.2 Biochar characterization

C, H, N, and O contents were determined using a combustion method (>950 °C) modified from ASTM D5373-16 (ASTM, 2008) by ALS Environmental (Tucson, AZ, USA). Ash content was determined at 550 °C to minimize the thermal degradation of minerals (Bachmann et al., 2016). S content was determined using a method modified from ASTM D4239-11 (ASTM, 2012). Major and trace elements were digested with heated HNO_3 and HCl modified from US EPA method 200.2 (Martin et al., 1994). Concentrations of major and trace elements in the biochars were analyzed using inductively coupled plasma-mass spectrometry (ICP-MS). Concentrations of Hg in the biochars were analyzed using cold vapour atomic fluorescence spectroscopy following US EPA method 1631 E (US EPA, 2002). Total Kjeldahl N was determined by digesting biochar samples in H_2SO_4 with $CuSO_4$ and K_2SO_4 as catalysts at ALS Environmental (Saskatoon, SK, Canada). The biochar

samples were characterized using Fourier-transform infrared (FTIR) spectroscopy (Tensor 27 FT-IR, Bruker) at the University of Waterloo (Waterloo, ON, Canada).

4.2.4.3 Solid-phase analyses

Solid concentrations of MeHg in SedCTR and biochar-amended systems were determined by digesting freeze-dried materials with 25% (w/w) KOH-MeOH solution and analyzing following US EPA Method 1630 (US EPA, 2001) at the Biotron Experimental Climate Change Research Centre.

S K-edge XANES spectra for biochars and solid materials in batch systems wetted for 200 d in Stage 1 and their corresponding systems in Stages 2 and 3 were collected at Beamline 9-BM at the Advanced Photon Source (APS), Argonne National Laboratory (Lemont, IL, USA) using fluorescence mode. Reference compounds including L-cystine (Sigma Aldrich) and $CaSO_4 \cdot 2H_2O$ were ground and diluted to 2% with graphene. Solid samples were ground and smeared as thin films on conductive double-sided tape, and a He chamber was used to minimize X-ray absorption. Five scans were collected and merged in μ(E) prior to spectral analysis. S K-edge XANES spectra were calibrated to the white line position for $CaSO_4 \cdot 2H_2O$ at 2482.7 eV.

Data processing for S K-edge XANES spectra was performed using ATHENA software (Ravel and Newville, 2005). S K-edge XANES spectra were decomposed into Gaussian peaks with two arctangent steps representing reduced S (2474 eV) and oxidized S (2483.8 eV) between 2466 and 2489 eV as described previously (Chapter 3) following Manceau and Nagy (2012). Diluted L-cysteine and $CaSO_4 \cdot 2H_2O$ were first decomposed with

unconstrained white line positions and peak widths. Shifts in white line positions (0.15 eV) and the peak width (0.658) for L-cysteine were applied to Gaussian peaks representing sulfide minerals (2470.6, 2471.7, 2472.5 eV), elemental S (or polysulfur) (2472.7 eV), exocyclic S (2473.5 eV), heterocyclic S (2474.3 eV), and sulfoxide (2476.3 eV). The peak width (0.848) for $CaSO_4 \cdot 2H_2O$ was used to constrain peak widths for Gaussian peaks representing sulfite (2478.5 eV), sulfone (2480.2 eV), sulfonate (2481.4 eV), and sulfate (2482.7 eV). Then, S K-edge XANES spectra for solid materials collected from the microcosm experiment were decomposed into these 11 Gaussian peaks with constrained peak positions and peak widths. Peaks with negative peak heights were eliminated in an ascending order. Results of the Gaussian peak fitting analysis were used to quantify fractions of each representative S fraction by using a generic equation accounting for changes in absorption cross-section with increases in S oxidation status as suggested by Manceau and Nagy (2012). Fitting quality was determined using a normalized-square sum (NSS). . Goodness-of fit was evaluated by eliminating components weighted <10% in an ascending order, and exclusions resulted in insignificant changes in fitting quality were not considered.

DNA purification for 16s rRNA pyrosequencing analysis was completed for solid materials in biochar-amended systems in a Clean-Ceil^{TM} Fan Filter Module (Microzone) following the manufacturer's protocols (Powder Soil® DNA Isolation Kit, MO BIO Laboratories). Purified DNA was shipped frozen to MR DNA Laboratory (Shallowater, TX, USA) for pyrosequencing analysis using primer 515/806F targeting bacteria and archaea. Sequencing was performed on an Ion Torrent PGM following the manufacturer's guidelines, and sequencing data were analyzed using an in-house analysis pipeline (MR DNA,

Shallowater, TX). Details for pyrosequencing reaction and data analysis are provided in the supporting information (Text C 2). Identified genera containing predicted Hg methylators were compared to the Oak Ridge National Laboratory database (ORNL, 2016).

4.2.5 Geochemical calculations

Calculations of saturation indices and Hg speciation were conducted with PhreeqcI (Parkhurst and Appelo, 1999) using the MINTEQA2 database (Allison et al., 1991). The MINTEQA2 database was modified by Liu et al. (2019b) to include thermodynamic constants for organic complexes. Thermodynamic constants for Hg-S-DOM and MeHg-S-DOM reported by Drott et al. (2013), Graham et al. (2017), and Liem-Nguyen et al. (2017) were added to the previously modified MINTEQA2 database (Table. C 2).

4.2.6 Statistical analysis

Statistical analysis was performed at a 95% confidence level. Effects of drying and wetting and biochar addition on river water composition, solid MeHg content, and microbial taxonomic communities were determined using two-way ANOVA. Dunn's multiple comparison test was used to further compare parameters in biochar-amended systems and soil controls if the ANOVA suggested significant differences. Correlation analysis on concentrations of MeHg and measured parameters was conducted using Pearson's correlation coefficient (r) to identify factors that potentially influence MeHg production.

4.3 Results

4.3.1 Overview of sediment and river water

The floodplain soil is rich in Al, Fe, and organic matter with elevated concentrations of Hg. The Hg in the floodplain soil is mainly associated with Hg bound to soil organic matter, and metacinnabar (β-HgS). SRW has a neutral to slightly alkaline pH, elevated concentrations of SO_4^{2-} (up to 20 mg L^{-1}), and minimal concentrations of $CH_{4(aq)}$, NH_4^+, PO_4^{3-}, THg, and MeHg. The chemical compositions of the floodplain soil and SRW were previously described (Chapter 3).

4.3.2 Overview of biochar

Biochars prepared from anaerobic digestate (DIG and 75G25S) have similar surface areas and elemental composition compared to the biochar prepared from distillers' grains (DIS) (Table 4.1). DIG and 75G25S, with relatively large surface area and high ash content, are composed of C, O, elevated amounts of nutrients (N, P, K, S, Ca, and Mg), and trace amount of metals. S content in DIG and 75G25S is between 0.33 and 0.75%. DIS, with minimal surface area and relatively low ash content, is mainly composed of C, N, and O with a limited amount of nutrients, trace elements, and S. S content in DIS is <0.11%. FTIR spectra for DIG show two strong vibration stretches (3257 and 1024 cm^{-1}) and two weak vibration stretches (874 and 602 cm^{-1}); minimal vibration stretches are observed for DIS (Fig. C 1). S K-edge XANES analysis indicates different S species in digestate-based biochars and DIS (Fig. C 2). S in DIG and 75G25S is mainly associated with elemental or polysulfur S (~40%), oxidized S (21-28%), and reduced S (e.g., heterocyclic S and exocyclic S) (~20%), while S in DIS is

mainly associated with heterocyclic S (57%) and sulfoxide (13%) and to a limited extent with other S functional groups (<10%).

4.3.3 Aqueous concentrations under initial wetting conditions

4.3.3.1 THg and MeHg

Greater Hg removal was observed in the batches containing 10%DIG and 10%75G25S than 10%DIS (Fig. 4.1). Hg removal increased as reaction time increased with limited removal observed after 7 d. In 10%DIG, concentrations of unf THg were between 2320 and 15,500 ng L^{-1}, representing 72-93% removal of Hg. Concentrations of 0.45-µm THg were between 102 and 643 ng L^{-1}, representing 75 to nearly 100% Hg removal. In 10%DIS, limited removal of unf THg was observed over 200 d, and removal of 0.45-µm THg was minimal before 90 d and 51-76% thereafter.

Concentrations of MeHg in 10%DIG and 10%75G25S were similar to SedCTR over 200 d (<60 ng L^{-1}), while elevated concentrations of MeHg were observed in 10%DIS (Fig. 4.1). Concentrations of MeHg peaked at 30 d and stabilized over 200 d. The highest peak concentration was in 10%DIS and more than four-fold higher than in SedCTR.

4.3.3.2 General geochemical parameters, carbon source, and nutrients

Biochar addition resulted in limited changes in pH, Eh, alkalinity, and concentrations of NO_3^-, DOC, acetate, and major cations, but notably affected concentrations of Mn, Fe, SO_4^{2-}, HS^-, $CH_{4(aq)}$, and PO_4^{3-} (Fig. 4.2; Fig. C 3). Higher concentrations of SO_4^{2-}, HS^-, and PO_4^{3-} were observed in 10%DIG and 10%75G25S than in SedCTR while concentrations of Mn and Fe were 50-80% lower. Concentrations of SO_4^{2-} were up to 30 mg L^{-1} in 10%DIG over 200 d,

while SO_4^{2-} was depleted after 60 d in other systems. Concentrations of HS^- peaked after 30 d in all biochar-amended systems, and peak concentrations (630-720 µg L^{-1}) were more than five-fold higher than in SedCTR. Concentrations of PO_4^{3-} were up to two-fold greater than in SedCTR. In 10%DIS, river water chemistry was similar to SedCTR except for $CH_{4(aq)}$, which was up to seven-fold higher.

4.3.4 Aqueous concentrations after drying and rewetting

4.3.4.1 THg and MeHg

After drying selected sediment and biochar mixtures for 90 d and then rewetting with SRW for 90 d, limited release of Hg was observed in biochar-amended systems, while slight increases in MeHg concentrations were observed in systems amended with digestate-based biochars (Fig. 4.3). Concentrations of THg (unf and 0.45-µm) in 10%DIG and 10%75G25S systems were up to 99% lower than in SedCTR; in 10%DIS systems, the concentrations were up to 79% lower (Fig. 4.3). Concentrations of MeHg in systems amended with digestate-based biochars (8-12 ng L^{-1}) were three- to seven-fold higher than in Stage 1, and up to 10-fold higher than in SedCTR in Stage 3.

4.3.4.2 Aqueous parameters

Increases in concentrations of DOC, acetate, Mn, Fe, SO_4^{2-}, and HS^- in digestate-based biochar amended systems were observed in Stage 3, especially in 10%DIG (Fig. 4.4; Fig. C 4). Reaction time before drying and rewetting slightly affected river water composition, and the most pronounced changes (DOC, acetate, Mn, and Fe) occurred in systems at the early sampling time (7 d) in Stage 1. Elevated concentrations of DOC and acetate were observed in

10%DIG reacted for 7d in Stage 1. Concentrations of DOC (up to 109 mg L^{-1}) were up to 20- and seven-fold higher than corresponding systems in Stage 1 and SedCTR in Stage 3, respectively. Concentrations of acetate (up to 72 mg L^{-1}) were more than 100-fold higher than corresponding systems in Stage 1 and SedCTR in Stage 3. Increases in concentrations of Mn (4.3-11 mg L^{-1}) and Fe (0.8-2.9 mg L^{-1}) were observed in 10%DIG reacted for 7 d in Stage 1, which were up to 14- and 30-fold higher than corresponding systems in Stage 1, respectively. However, these observed Mn and Fe concentrations were similar to SedCTR in Stage 3. Concentrations of SO_4^{2-} (13-45 mg L^{-1}) remained elevated in 10%DIG systems, which were up to 58-fold higher than corresponding systems in Stage 1 and SedCTR in Stage 3. Concentrations of HS^- (up to 639 µg L^{-1}) in systems amended with digestate-based biochars were up to 16-fold higher than corresponding systems in Stage 1, which were significantly higher ($p<0.05$) than SedCTR.

4.3.5 Solid-phase characterizations

4.3.5.1 Solid MeHg content

Solid materials in systems reacted for 200 d in Stage 1 and their corresponding systems in Stage 3 were collected and analyzed for solid MeHg content (Fig. C 5). In Stage 1, biochar additions insignificantly affected solid MeHg content (23-34 ng g^{-1}). Solid MeHg contents in Stage 3 were 50% lower ($p = 0.005$) than in Stage 1.

4.3.5.2 S

Solid materials in systems reacted for 200 d in Stage 1 and their corresponding systems in Stages 2 and 3 were collected for total S content and S K-edge XANES analysis. In Stage 1,

S content in 10%DIG systems was 40% higher than in SedCTR systems. In Stages 2 and 3, S content did not significantly change in any system (Fig. C 6).

Shifts in S in solid materials collected in biochar-amended systems reacted for 200 d in Stage 1 and their corresponding systems in Stages 2 (drying) and 3 (rewetting) were observed (Fig. 4.5; Fig. C 7-9). In Stage 1, S K-edge XANES spectra for 10%DIG and 10%75G25S systems contained two peaks in the reduced S (2472 eV) and oxidized S (2482.7 eV) regions, while spectra for solid materials collected from 10%DIS systems in Stage 1 showed one pronounced peak in the intermediate and oxidized S region (2482.7 eV) (Fig. 4.5a; Figs. C 7a, 9a). Gaussian peak fitting for these spectra suggest S in 10%DIG is mainly associated with polysulfur (34%), oxidized S (22%), and reduced S (exocyclic and heterocyclic S) (23%) (Fig. C 7a); S in 10%75G25S is mainly associated with sulfide minerals (49%), oxidized S (20%), and reduced S (exocyclic S) (19%) (Fig. C 9a); S in 10%DIS is mainly associated with intermediate S (56%), oxidized S (27%), and polysulfur (14%) (Fig. 4.5b; Fig. C 8a). In Stage 2, increases in fractions of oxidized S (29-40%) were observed in the biochar-amended systems, while decreases in fractions of sulfide minerals (10%75G25S) and polysulfur (10%DIG and 10%DIS) were observed (Fig. 4.5; Figs. C 7b, 8b, and 9b). In Stage 3, shifts toward the sulfide region (2470-2472 eV) were observed in solid materials collected from biochar-amended systems, and Gaussian peak fitting analysis suggests increases in fractions of sulfide minerals and decreases in fractions of oxidized S (Fig. 4.5; Figs. C 7c, 8c and 9c).

4.3.6 Microbial community

Solid samples collected in systems reacted for 7, 90, and 200 d in Stage 1 and their corresponding systems in Stage 3 were selected for 16s rRNA pyrosequencing. After denoising sequencing data, effective sequencing reads for soil control and biochar-amended systems was 88 632±19 073 per sample, with 1,866±188 detected operational taxonomic units (OTUs). Application of biochar to floodplain soil did not significantly affect the effective sequencing reads ($p = 0.94$) and OTUs ($p = 0.12$). Effective sequencing reads in Stage 3 (100 412±14 018) were significantly ($p = 0.003$) higher than in Stage 1 (77 833±16 820). No significant differences for OTUs were observed between Stages 1 and 3.

Shifts in microbial composition in phyla taxonomic rankings were observed with biochar addition in Stages 1 and 3 (Fig. 4.6a). In Stage 1, applying biochar resulted in shifts in microbial composition toward Bacteroidetes and Firmicutes. Euryarchaeota, primarily containing methanogens, became more abundant as incubation time increased. In Stage 3, Nitrospirae, containing nitrifiers, became more abundant in 10%DIG and 10%75G25S. Acidobacteria became more abundant in 10%DIS.

Fe-reducing bacteria (FeRB), sulfate-reducing bacteria (SRB), and fermentative bacteria were the predominant genera containing predicted Hg methylators in biochar-amended systems in Stage 1, and limited changes in microbial structure containing predicted Hg methylators were observed in Stage 3 (Fig. 4.6b). In Stage 1, SRB were more abundant in 10%DIG and 10%75G25S systems. In Stage 3, increases in the relative abundance of FeRB

were observed in systems reacted for 7 d in Stage 1. The highest abundance (19%) of FeRB was observed in 10%DIG systems.

4.4 Discussion

4.4.1 Mechanisms of Hg removal under initial wet conditions

Multiple processes may contribute to greater Hg removal using digestate-based biochars. Oxygen-containing functional groups and hydrophilic surface properties may contribute to Hg removal (Liu et al., 2016; Xu et al., 2016). Greater O/C molar ratios for DIG and 75G25S (0.15 to 0. 2) compared to DIS (0.03) indicate digestate-based biochars have abundant oxygen-containing functional groups. Strong vibration stretches observed for DIG can be assigned to H-bound hydroxyl (-OH) groups (3257 cm^{-1}) and symmetric C-O stretches (1024 cm^{-1}) (Keiluweti and Nico, 2010). Formation of Hg-S on biochar is likely the predominant mechanism controlling Hg in biochar-amended systems under anoxic conditions (Liu et al., 2019a). Polysulfur and reduced S functionalities on DIG and 75G25S, as determined from S K-edge XANES analyses, may promote the formation of Hg-S complexes (Fig. C 2). Physically filtering Hg-bearing particulates by the porous biochar structure may also occur in biochar-amended systems, as suggested by Wang et al. (2019).

FeS is a strong scavenger for Hg through coprecipitation and complexation (Han et al., 2014). PhreeqcI calculations indicate FeS is near saturation in 10%DIG and 10%75G25S systems at early times before becoming undersaturated (Fig. C 10). The near saturation with respect to FeS is likely due to the production of HS^- and generation of reduced Fe (Fig. 4.2). Dissolved Hg(II) and Hg bound to organic thiol ($Hg(SR)_2$) react with FeS to form β-HgS

(Skyllberg and Drott, 2010), which lower the release of Hg derived from the floodplain soil. Oxygen-containing functional groups in biochars are redox active, providing similar electron transfer capacities as humic substances (Klüpfel et al., 2014). Biochars stimulate microbial Fe(III) reduction by acting as electron shuttles, first reducing redox-active sites on biochars and then transferring electrons to Fe(III) minerals (Kappler et al., 2014). Digestate-based biochars with more oxygen-containing functionalities (Fig. C 1) are more redox active than DIS, and thus stimulate microbial Fe (III) reduction to form FeS under anaerobic conditions.

4.4.2 MeHg production under initial wet conditions

Concentrations of MeHg in biochar-amended systems were positively correlated ($r > 0.88$) with concentrations of HS^-. This observation is consistent with Benoit et al. (1999), in that MeHg production in sulfidic pore water is associated with elevated concentrations HS^-. PhreeqcI calculations suggest aqueous Hg-S species (e.g., HgS_2H^-) were the predominant species in the biochar-amended systems, and the peak HgS_2H^- concentration corresponded to peak aqueous MeHg at 30 d (Fig. C 11). HgS_2H^- forms through reactions of metacinnabar (β-HgS) and HS^-(Eq. 4.1) and dissolution of neutrally charged $Hg(SH)_2^0$ species (Eq. 4.2) (Drott et al., 2013), which are available for passive uptake by Hg methylating bacteria (Graham et al., 2012; Hsu-Kim et al., 2013).

$$HgS_{(s)} + HS^- = HgS_2H^- \qquad \text{Log K= -4.3±0.1} \qquad \text{Eq. 4.1}$$

$$Hg(SH)_2^0 = HgS_2H^- + H^+ \qquad \text{Log K = -6.6±0.1} \qquad \text{Eq. 4.2}$$

The size and structural order of β-HgS in systems supersaturated with respect to β-HgS depends on the concentration of HS^- and aromaticity of dissolved organic matter (Graham et al., 2012; Slowry 2010). In anoxic systems, the high aromaticity of organic matter with

relatively low concentrations of HS^- leads to the formation of disordered nanoparticulate β-HgS that is highly bioavailable (Poulin et al., 2017). The aromaticity of dissolved organic matter in this study was not measured, but Liu et al. (2018) observed elevated aromaticity in biochar-amended systems before 100 d. The elevated MeHg in 10%DIS at 30 d (Fig. 4.1) may result from formation of poorly ordered nanoparticulate β-HgS as indicated by the elevated concentrations of unf THg and low concentrations of HS^- (Fig. 4.2).

Solid MeHg content in systems amended with digestate-based biochars were up to two-fold higher than in SedCTR (Fig. C 5). Solid MeHg content is positively correlated ($r = 0.93$) with fractions of Hg bound to thiol functional groups on dissolved organic matter (e.g., $HgDOMS^+$). Polysulfur identified on DIG and 75G25S (Fig. 4.5; Fig. C 2) may lead to organic matter sulfurization, because polysulfur is one of the primary sources contributing to organic matter sulfurization (Werne et al., 2008). Hg bound to sulfurized organic matter enhances Hg bioavailability in a similar pathway as Hg bound to low-molecular weight thiols due to active transport by Hg methylating bacteria (Graham et al., 2017; Schaefer and Morel, 2009). Elevated nutrient content in systems amended with digestate-based biochars may further increase microbial activity and promote MeHg production, as suggested by Liem-Nguyen et al. (2016).

4.4.3 Impacts of drying and rewetting in biochar-amended systems

Reaction time prior to drying and rewetting potentially affects the release of DOC and increase in concentrations of Fe in biochar-amended systems (Fig. 4.4). Elevated concentrations of DOC are likely related to the release of residual labile organic matter,

which is consistent with increases in DOC in manure/anaerobic-digestate-amended systems after a dry-rewet cycle (Schouten et al., 2012). Elevated concentrations of Fe in systems at earlier reaction time (7 d) coupled with increases in the relative abundance of FeRB (e.g., Geobacter) (Fig. 4.6) indicate conditions favourable for microbially driven Fe(III) reduction. Similar increases in Mn and Fe were observed in hardwood- and sulfurized-biochar-amended systems after drying and rewetting (Chapter 3).

Drying and rewetting resulted in changes in S chemistry in the biochar-amended systems. After drying, the decreased fractions of sulfide minerals and polysulfur with the increased oxidized S in solid collected from biochar-amended systems (Fig. 4.5; Figs. C 7-9) indicate oxidation of sulfide minerals and polysulfur. After rewetting, the increased fractions of sulfide minerals and the decreased oxidized S (Fig. 4.5; Figs. C 7-9) reflect the occurrence of SO_4^{2-} reduction and sulfide mineral formation. Polysulfur forms as a by-product for sulfide oxidation in anoxic sediments through either abiotic or biotic pathways mediated by sulfur oxidizing bacteria (Findlay, 2016). With the limited abundance of sulfur oxidizing bacteria in 10%DIS after rewetting (Fig. C 8c), the increased fraction of polysulfur is likely related to abiotic oxidation of sulfides in solid materials and aqueous solutions.

The elevated concentrations of SO_4^{2-} and HS^- in 10%DIG and 10%75G25S systems likely reflect net reactions of dissimilatory SO_4^{2-} reduction, microbially driven S disproportionation as well as continuous release of oxidized S from the biochar. The increased relative abundances of sulfate-reducing bacteria (SRB) indicate the stimulation of dissimilatory SO_4^{2-} reduction. The co-existence of SO_4^{2-} and HS^- in biochar-amended systems after drying and rewetting is also likely related to microbially driven S disproportionation as previously

observed (Chapter 3). SRB (e.g., *Desulfovibrio, Desulfobulbus*) in systems amended with digestate-based biochars in Stage 3 (Fig. 4.6) may stimulate S disproportionation to form both SO_4^{2-} and HS^- (Eqs. 4.3-4) (Fuseler and Cypionka, 1995; Jørgensen, 1990). Oxidized S on digestate-based biochars (Fig. C 2) may account for the elevated aqueous SO_4^{2-} in 10%DIG and 10%75G25S systems, consistent with elevated SO_4^{2-} in manure-based-biochar systems (Liu et al., 2015, 2018). For systems with less reaction time (7 and 90 d) prior to drying, concentrations of SO_4^{2-} remained elevated under initial wetting conditions, and the elevated concentrations in Stage 3 also are likely related to the net effects of dissimilatory SO_4^{2-} reduction, S disproportion, and the release of residual oxidized S functionalities on the biochar. For systems with a longer reaction time (200 d) in Stage 1, SO_4^{2-} was depleted in Stage 1 and then became elevated in Stage 3 (Fig. 4.4). The increases in SO_4^{2-} in such systems may be related to the release of newly formed oxidized S during drying. For such systems, the limited abundance of SRB observed (Fig. 4.6) indicates factors other than SO_4^{2-} stimulate microbial SO_4^{2-} reduction.

$$S_2O_3{}^{2-} + H_2 \rightarrow SO_4{}^{2-} + HS^- + H^+ \quad \text{Eq. 4.3}$$

$$8.5S^0 + 8H_2O \rightarrow 5HS^- + 1.5\,H_2S + 2SO_4^{2-} + 8H^+ \quad \text{Eq. 4.4}$$

Hg in biochar-amended systems was resistant to changes in geochemical conditions after drying and rewetting, especially for systems amended with digestate-based biochars (Fig. 4.3). Hg in the floodplain soil, as previously described (Chapter 3), is mainly associated with Hg bound to soil organic matter and metacinnabar (β-HgS). The release of Hg in SedCTR associated with the release of DOC after drying and rewetting was observed (Chapter 3). Although elevated concentrations of DOC occurred in 10%DIG reacted for 7 d in Stage 1,

concentrations of THg (unf and 0.45-µm) were >89% lower than in SedCTR. The relatively low concentrations of THg suggest Hg was maintained in more stable forms in biochar-amended systems than in SedCTR.

Changes in geochemical conditions and shifts in the microbial community after drying and rewetting may affect net MeHg production (Fig. 4.3; Fig. C 5). FeRB and SRB are known to mediate Hg methylation in anoxic sediments (Fleming et al., 2006; Gilmour et al., 2013a). The increased aqueous MeHg in 10%DIG reacted for 7 d in Stage 1 is associated with the increased concentrations of DOC, acetate, Fe, SO_4^{2-} and HS^- (Fig. 4.4) as well as the increased relative abundances of the potential Hg methylators FeRB and SRB (Fig. 4.6). The increased DOC and acetate are available for FeRB and SRB to utilize as electron donors for growth and to stimulate Fe(III) and SO_4^{2-} reduction to form Fe(II) and HS^-. Therefore, the increased aqueous MeHg after drying and rewetting is likely related to enhanced microbial-driven Fe(III) and SO_4^{2-} reduction. For systems reacted for 200 d in Stage 1, the decreased solid MeHg content in Stage 3 (Fig. C 5) indicates conditions favourable for either inhibition of MeHg production or demethylation reactions. The lower MeHg contents in 10%DIG and 10%DIS in Stage 3 corresponded to limited concentrations of DOC and acetate as well as decreased relative abundances of FeRB and SRB (Fig. 4.6). In 10%75G25S, the relative abundances of FeRB did not change significantly, and the relative abundances of SRB increased compared to in Stage 1 (Fig. 4.6). Concentrations of SO_4^{2-} and HS^- in 10%75G25S remained elevated with limited concentration of Fe (Fig. 4.4). The low MeHg concentrations in 10%75G25S are not as clearly related to biological activity. The decreased solid MeHg concentration (Fig. C 5) concurrent with increasing SO_4^{2-} concentrations (Fig. 4.4) is

inconsistent with the previous results with respect to increased MeHg in sulfurized-hardwood-biochar-amended systems after drying and rewetting (Chapter 3). However, Bailey et al. (2017) observed a similar inverse relation between porewater and solid MeHg in sulfate-impacted lake sediments with elevated HS^- and low Fe. Therefore, systems amended with biochars prepared from anaerobic digestate and distillers' grains may have the potential for inhibiting MeHg production, and MeHg production is less likely affected during drying and rewetting events.

Long-term drying and rewetting of floodplain soils may further affect microbial activity as well as MeHg production. The frequency of wet-dry-wet cycles, duration of moist periods, and substrates present at end of each wet-dry-wet cycle may influence cumulative microbial respiration (Yu et al., 2014). Iovieno and Bååth (2008) observed variable microbial growth rates at different times after rewetting dried sediment. Long-term impacts of dynamic drying and rewetting on Hg removal in floodplains may need to be further evaluated before conducting large-scale field applications.

4.5 Environmental Implications

The results of this study indicate digestate-based biochars can decrease Hg release in floodplain soils under anoxic conditions as well as after drying and rewetting conditions without substantially promoting MeHg production. Application of biochars derived from anaerobic digestion may increase reactive phosphorus during long periods (months) of flooding. Digestate-based biochars may not be suitable for direct application in freshwater systems due to the elevated nutrient concentrations, however, it may be beneficial if used in

floodplains to provide nutrients for plant growth. Reaction time prior to drying and rewetting events may influence the evolution of geochemical and microbial reactions. Biochar produced from a mixture of anaerobic digestate and distillers' grains may provide comparable Hg stabilization in floodplain soil to biochar produced from anaerobic digestion without introducing elevated SO_4^{2-}.

Table 4.1 Properties for biochar prepared from ethanol refinery by-products including 100% anaerobic digestate (DIG), 100% distillers' grains (DIS), and 75% anaerobic digestate + 25% distillers' grains (75G25S).

	DIG	DIS	75G25S
Surface area, $m^2 g^{-1}$	53.2	<0.5	24.2
H, %	0.65	0.75	0.59
C, %	42.7	78.9	52.8
N, %	2.02	7.29	3.36
Total Kieldahl N, %	1.84	6.23	3.08
O, %	11.8	3.22	10.4
S, %	0.75	<0.11	0.33
Ash content, % (550 °C)	53.7	9.7	41.1
Volatile matter, %	10.6	12.4	11.2
P, $mg\ kg^{-1}$	53 500	2180	40 100
K, $mg\ kg^{-1}$	11 300	1360	9870
Na, $mg\ kg^{-1}$	4130	733	3660
Mg, $mg\ kg^{-1}$	11 600	1050	12 700
Mn, $mg\ kg^{-1}$	766	12.2	496
Ca, $mg\ kg^{-1}$	94 000	553	65 300
Fe, $mg\ kg^{-1}$	4430	1080	3210
Al, $mg\ kg^{-1}$	4650	106	2830
Cu, $mg\ kg^{-1}$	191	1.93	90.8
Hg, $mg\ kg^{-1}$	<0.0050	0.0175	0.019
Zn, $mg\ kg^{-1}$	3240	30.7	1930

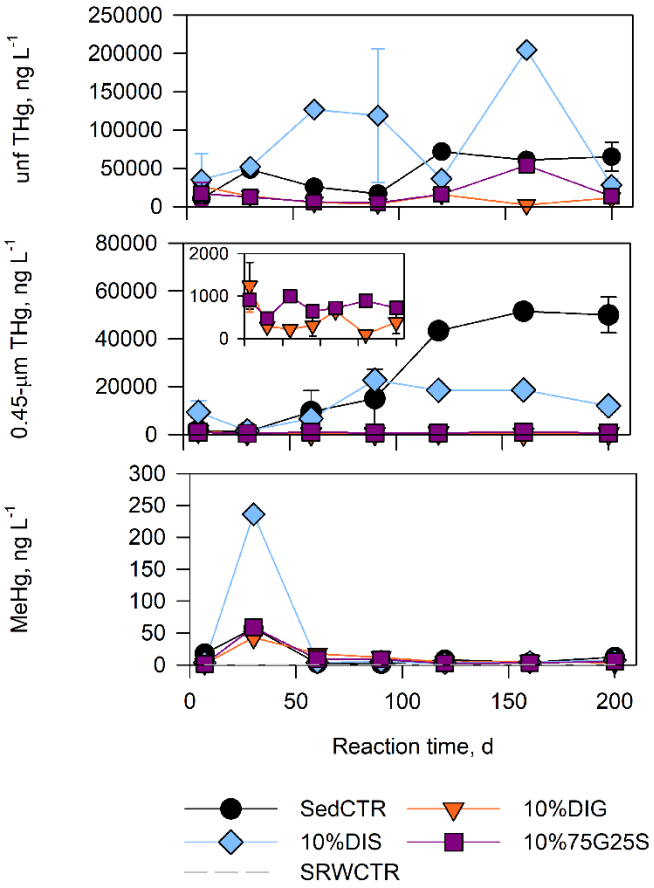

Fig. 4.1 Concentrations of unf THg, 0.45-µm THg, and MeHg in Stage 1. Error bars represent the standard deviation from replicate experiments. Inset plot for 0.45-µm THg has the same time scale as large plot. Results for soil control (SedCTR) are from Chapter 3.

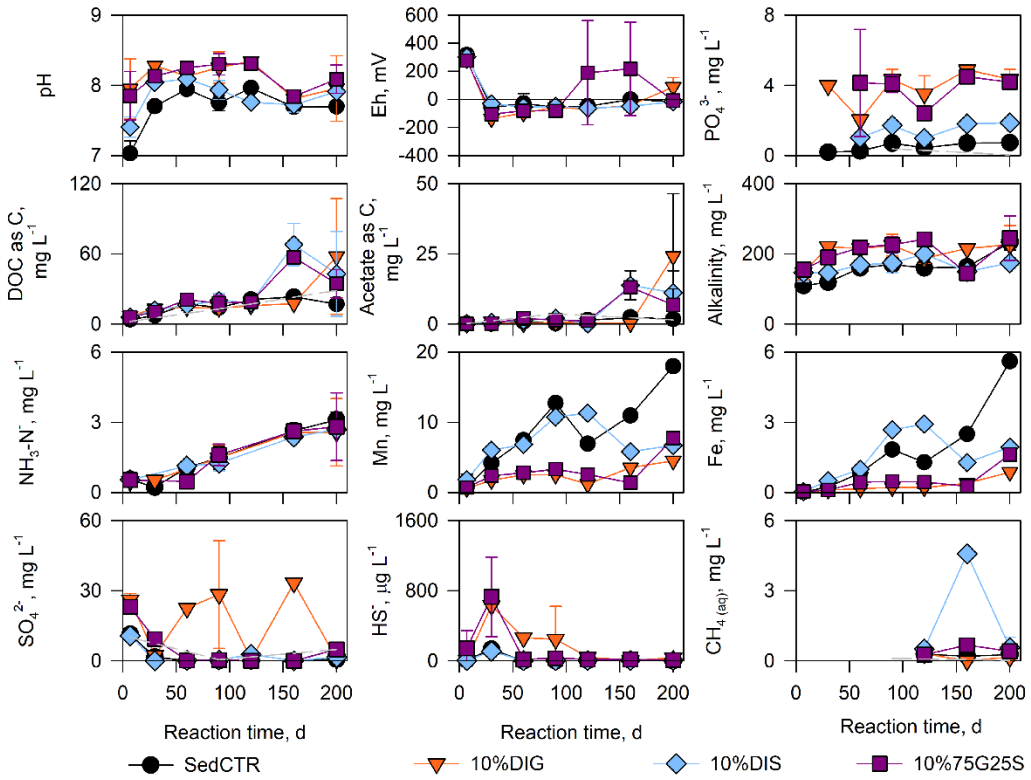

Fig. 4.2 pH, Eh, alkalinity, and concentrations of DOC, acetate, Mn, Fe, SO_4^{2-}, HS^-, and $CH_{4\,(aq)}$ in biochar-amended systems in Stage 1 compared to soil controls (SedCTR). Error bars represent the standard deviation from replicate experiments. Results of soil control are from Chapter 3.

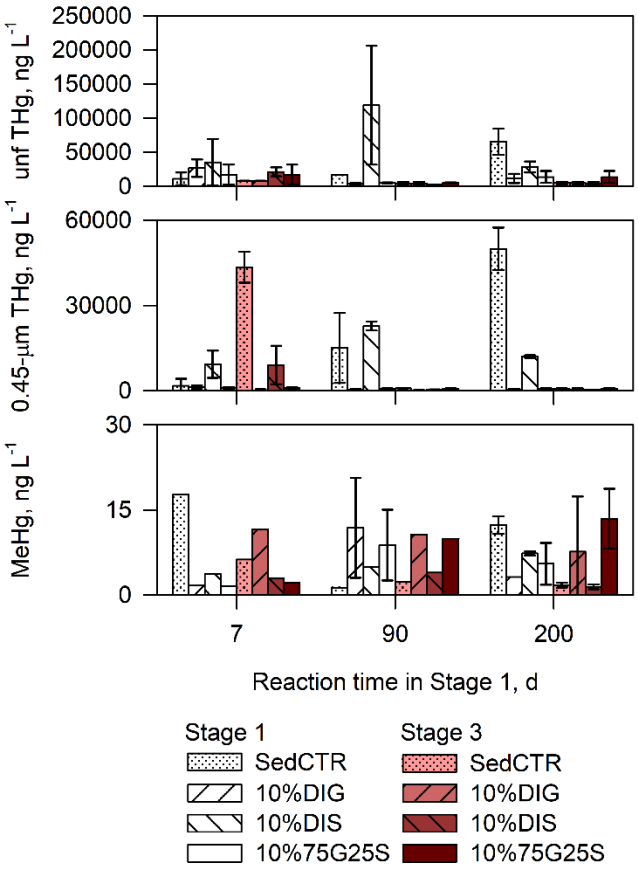

Fig. 4.3 Concentrations of unf THg, 0.45-µm THg, and MeHg in biochar-amended systems in Stage 3 (red) compared to their corresponding systems in Stage 1 (white). Error bars represent the standard deviation from replicate experiments. Results for soil controls (SedCTRs) are from Chapter 3.

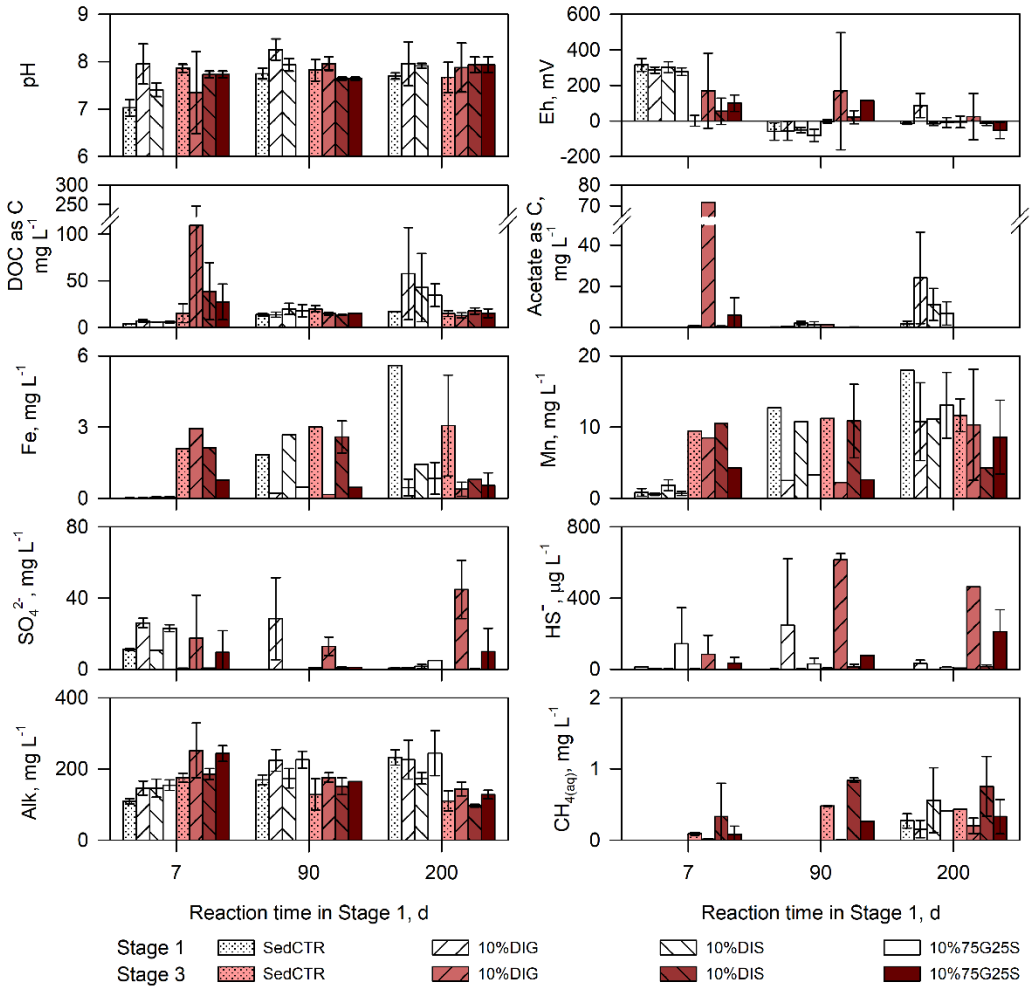

Fig. 4.4 pH, Eh, alkalinity, and concentrations of DOC as C, acetate as C, Mn, Fe, SO_4^{2-}, HS^-, and $CH_{4(aq)}$ in biochar-amended systems in Stage 3 (red) compared to their corresponding systems in Stage 1 (white). Concentrations of $CH_{4(aq)}$ in systems reacted for 7 or 90 d in Stage 1 were not collected and analyzed. Error bars represent the standard deviation from replicate experiments. Results for soil controls (SedCTR) are from Chapter 3.

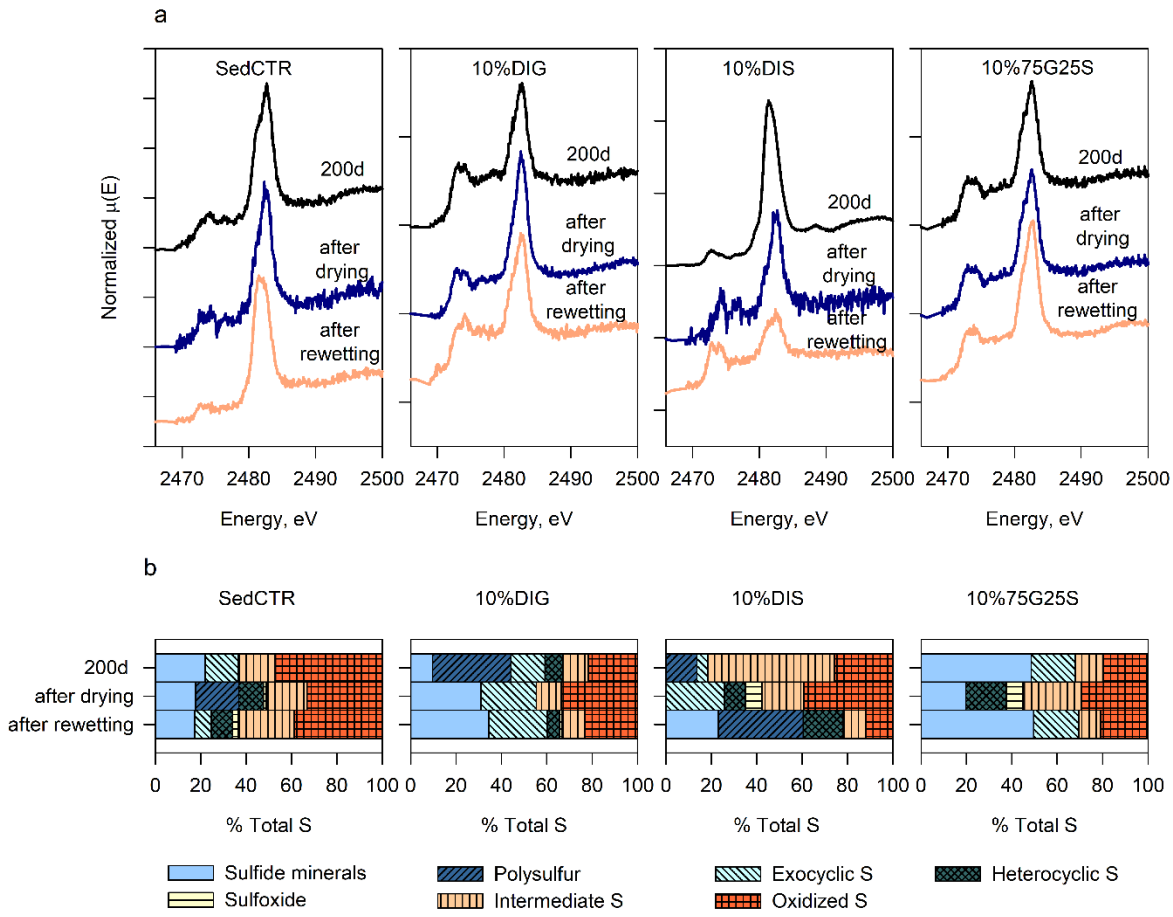

Fig. 4.5 Measured S K-edge XANES spectra (a) and fractions of S forms obtained Gaussian peak analysis (NSS<2.74×10^{-2}) (b) for solid materials collected in systems reacted for 200 d in Stage 1 and their corresponding systems in Stages 2 (drying for 90 d) and 3 (rewetted for 90 d). Spectra for the soil control are from Chapter 3.

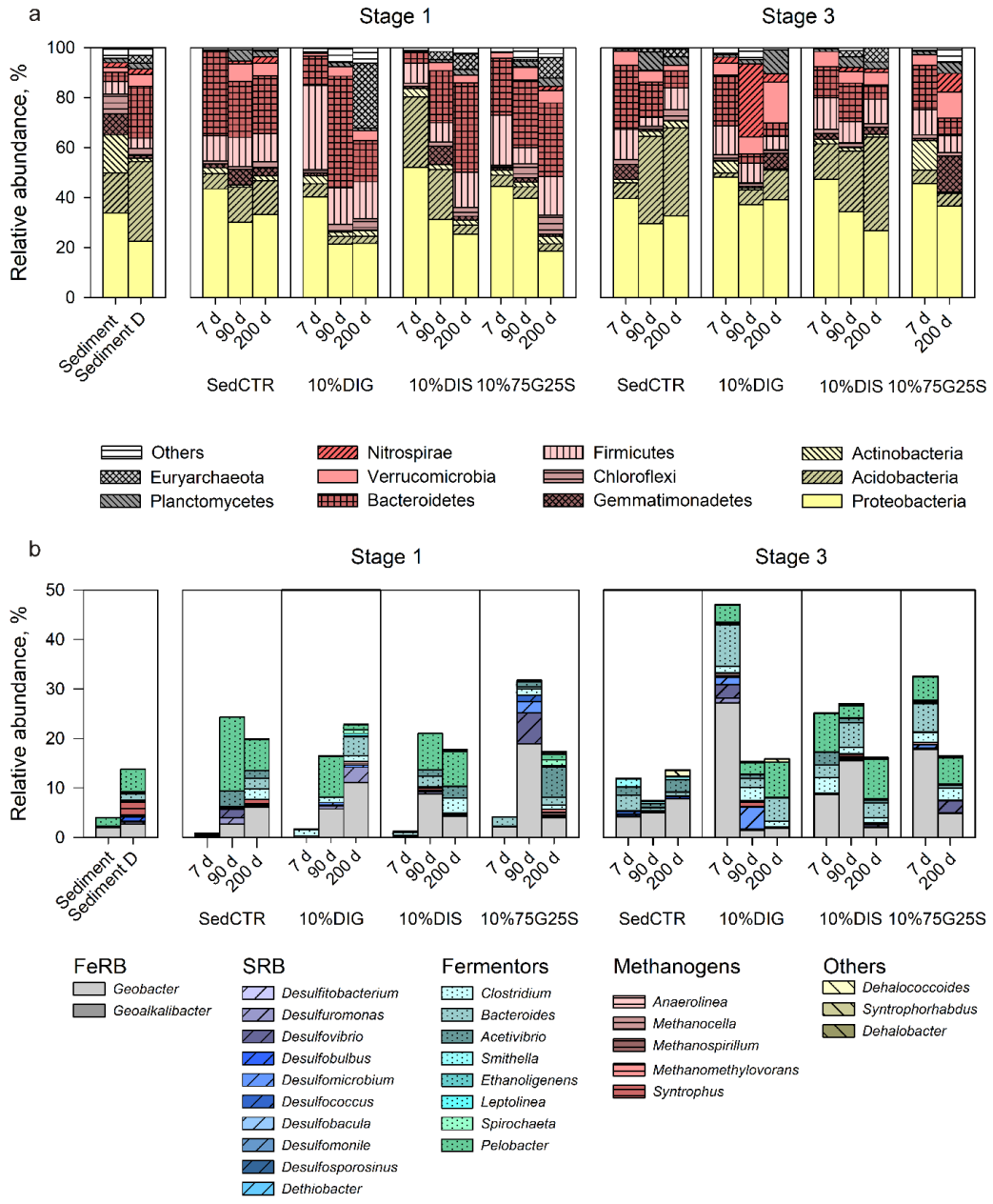

Fig. 4.6 Results of 16s rRNA sequencing showing the microbial structure in predominant phyla (>5%) (a) and predicted Hg methylators (b). Results for air-dried sediment (sediment and sediment D) and soil controls (SedCTR) are from Chapter 3.

Chapter 5 Impact of multiple drying and rewetting events on biochar amendments for Hg stabilization in floodplain soil from South River, VA

Summary

Biochar prepared from anaerobic digestate (DIG, a product of bio-fuel production) and sulfurized-hardwood biochar (MOAK) are potential amendment materials for *in situ* Hg stabilization in soils. Drying and rewetting as a result of flooding/precipitation and drainage events in floodplains can induce redox oscillations that may affect the effectiveness of Hg removal using these materials. This study evaluated continuously repeated drying and rewetting events on DIG- and MOAK-amended systems using a modified humidity cell protocol. The ten sequential cycles each consisted of a wetting stage, followed by leaching and drying stages. An early flush (before the 4th wetting and drying cycle) characterized by elevated concentrations of filter-passing (0.45-µm) total Hg (THg), DOC, and Mn was observed. Concentrations of 0.45-µm THg were up to five-fold higher in the biochar-amended systems than in the soil control during this early flush. Thereafter, limited decreases (up to 57%) in 0.45-µm THg and greater decreases in unfiltered THg (up to 93%) were observed in both biochar-amended systems. MeHg concentrations in the soil control and the DIG-amended system were <0.3 ng L^{-1}, while MeHg was present in concentrations up to 158 ng L^{-1} in the MOAK-amended system. THg and MeHg showed strong correlations with DOC ($r>0.95$) and Mn ($r>0.98$). Initial release of elevated concentrations of SO_4^{2-} were observed in the DIG-amended system. As the number of wetting and drying cycles increased, oxidation of MOAK led to decreases in pH and alkalinity as well as increases in concentrations of SO_4^{2-} (up to 796 mg L^{-1}) and Ca (up to 215 mg L^{-1}), whereas oxidation of

DIG was not observed. Results of S K-edge X-ray absorption near edge structure (XANES) analysis suggest polysulfur is the predominant S phase in both MOAK- and DIG-amended systems. Changes in S chemistry were observed in the MOAK-amended systems as the number of wetting and drying cycles increased. Results of 16s rRNA pyrosequencing indicate community shifts toward sulfur-oxidizing bacteria occurred in the MOAK-amended system, whereas the community in the DIG-amended system was similar to the soil control. The different responses to the repeated wetting and drying events in these two biochar-amended systems are likely related to differences in elemental compositions and species of S on biochar. Repeated wetting and drying as a result of flooding/precipitation and drainage events alters biogeochemical conditions affecting microbial activities in biochar amended systems. The impacts of drying and rewetting are recommended to consider before designing large field-scale applications.

5.1 Introduction

Mercury (Hg) contamination in freshwater systems has been documented worldwide (Kocman et al., 2013, 2017). Disposal of Hg-contaminated products from industrial activities (the second largest source after small-scale gold mining) has led to a legacy of elevated Hg in numerous watersheds (Kocman et al., 2017). At many legacy contaminated sites, riverbank erosion is the predominant transport mechanism causing large-scale dispersal of Hg that can continue decades after phasing out Hg usage (Eggleston, 2009; Flanders et al., 2010; Horvat et al., 1999). Hg entrained in floodplain soils and sediments is mainly associated with nanoparticulate metacinnabar (β-HgS), thiol groups in soil organic matter, and poorly crystalline and amorphous Mn and/or Fe oxyhydroxides and clay minerals, which can be

remobilized during flooding events (Lazareva et al., 2019; Manceau et al., 2015; Poulin et al., 2016).

During flooding events, Hg has a great potential for forming methylmercury (MeHg) (Poulin et al., 2016; Singer et al., 2016), a neurotoxin that accumulates through the food web (Jackson et al., 2011; Mergler et al., 2007). Under these conditions, water displaces O_2 in pore spaces, generating anoxic conditions that stimulate Hg methylation through biouptake of inorganic Hg species by anaerobic microbes (Fleming et al., 2006; Gilmour et al., 2013a; Hamelin et al., 2011; Hsu-Kim et al., 2013). Lazareva et al. (2019) observed elevated concentrations of MeHg in floodplain soils associated with elevated concentrations of poorly crystalline and amorphous Fe and/or Mn oxyhydroxides, suggesting active Fe and Mn cycling may play a strong role in controlling methylation reactions in floodplain soils. Correlations between concentrations of MeHg and both Fe and Mn have also been observed in lake water as a result of changing redox conditions (Dent et al., 2014). Singer et al. (2016) noted that MeHg production hotspots are mostly associated with areas with a high flood frequency compared to areas with a low flood frequency. A MeHg-based model showed MeHg biomagnification factors are higher in floodplains than in adjacent rivers (Newman et al., 2011), suggesting the need to apply remediation activities in floodplains in a manner that limits methylation reactions.

Conventional soil remediation approaches (e.g., soil washing, physical extraction, containment, thermal extraction, vitrification; Mulligan et al., 2001) can be costly to apply to large contaminated floodplains. Recent alternative management strategies for Hg-contaminated sediments and soils have focused on the application of *in situ* amendments with

green materials that sequester Hg in the solid phase and concurrently minimize methylation without disturbing the natural system. Carbonaceous materials, including activated carbon and biochars, have been evaluated as sediment capping materials and amendments under fully-saturated stagnant anoxic conditions (Beckers et al., 2019; Chapters 3 and 4; Desrochers, 2013; Gilmour et al., 2013b, 2018; Liu et al., 2017, 2018a, 2019a; O'Connor et al., 2018) and saturated-flow conditions (Ting et al., 2018).

Differences in biochar properties can lead to different Hg removal outcomes. Limited decreases in concentrations of THg and MeHg have been observed in systems amended with biochars prepared from pine cone, oak and maple, pine dust, switchgrass, and manure (Beckers et al., 2019; Chapter 3, Gilmour et al 2013b, Gilmour et al, 2019; Liu et al, 2017, 2018 a), whereas the additions of sulfurized materials and biochar prepared from anaerobic digestate to Hg-contaminated sediments and soils substantially decreases Hg concentrations with limited formation of MeHg under anoxic conditions (Chapters 3 and 4, O'Connor et al., 2018). In previous studies, a sulfurized biochar prepared with lime sulfur solution, an EPA approved fungicide and insecticide, was evaluated as a reactive material for Hg removal (Felin, 2016; Liu et al., 2018 b). A column study reveals greater Hg stabilization in systems amended with 5% sulfurized-hardwood biochar (MOAK) compared to hardwood biochar under saturated-flow conditions (Fellin, 2016). Laboratory microcosm experiments demonstrate a nearly 100% decrease in Hg concentrations in systems amended with 10% dry wgt. MOAK and biochar prepared from anerobic digestate (DIG) with minimum net MeHg production under anoxic conditions for up to 200 d (Chapters 3 and 4). These studies suggest

that MOAK and DIG are potentially effective reactive materials for use as soil amendments in floodplains.

Changes in hydrological and biogeochemical conditions during precipitation/flooding and drainage events can alter soil organic matter oxidation (Chow et al., 2006; Fierer et al., 2002; Rezanezhad et al., 2014), microbial structure (Fierer et al., 2003), cycling of Fe, Mn, and S (Borch et al., 2010; Rezanezhad et al., 2014), and, in turn, indirectly influence Hg transport and methylation reactions in floodplain settings (Frohne et al., 2012; Poulin et al., 2016). A single drying and rewetting event has a limited impact on Hg release and MeHg production in DIG-amended systems but may induce shifts in microbial structure and favour MeHg production in MOAK-amended systems (Chapters 3 and 4). However, the impacts of ongoing repeated wetting and drying events, which occur in floodplain settings, with these biochars are unclear.

Ongoing repeated drying and rewetting results in different cumulative microbial respiration and microbial activity than a single drying and rewetting event. Cumulative microbial respiration after each wetting and drying cycle is dependent on end products from the previous cycle (Yu et al., 2014). Microbial respiration may rapidly increase during the first few drying and rewetting events after extended drought conditions and then slows with further wetting and drying cycles (Fierer and Schimel, 2002). Therefore, a single drying and rewetting event as previously evaluated for DIG- and MOAK-amended systems (Chapters 3 and 4) may not fully represent responses under conditions of repeated drying and rewetting.

The humidity cell test method is a standardized laboratory weathering protocol that enhances the release of reaction products from a known mass of mine waste rock and ores (ASTM, 2012). The standardized protocol includes weekly drying and wetting cycles providing oxidative conditions with three days dry air, three days water-saturated air, followed by a leach with water. The protocol has been applied to mine tailings and waste rock to evaluate contaminant release in response to oxidative conditions (Ardau et al., 2009; Langman et al., 2015a,b; Maest and Nordstrom, 2017). A modified protocol has been applied to evaluate hardwood biochar as a reactive mat for Hg removal under cyclical flooding and drainage conditions (Wang et al., 2019). Although information obtained from the humidity cell test may not directly predict leachate concentrations under field conditions, the results can reflect field-scale major geochemical and microbial processes (Ardau et al., 2009; Maest and Nordstrom, 2017). Integrated models incorporating detailed temporal variables (e.g., temperature fluctuations and water infiltrations parameters) and developed from laboratory humidity cell experiments can provide a reasonable agreement between laboratory and field measurements that capture major weathering processes, which can be used for geochemical evaluations under realistic multi-year field conditions(Wilson et al., 2018). Therefore, results obtained from humidity cell tests can provide more realist information in terms of conditions exposed to redox oscillations than from batch-scale experiments.

This study evaluated DIG and MOAK as potential candidate amendments for *in situ* Hg stabilization in floodplain soils subjected to multiple drying and rewetting conditions using the same biochar to solid ratio as previously described (Chapters 3 and 4). A modified procedure from the standard humidity cell protocol representing dynamic flooding and

drainage was applied over ten wetting and drying cycles. Each cycle featured wetting, leaching, and drying stages. Geochemical analyses and solid-phase characterization were conducted to provide information related to the application of DIG and MOAK as soil amendments in floodplains`

5.2 Study Site

Soils were collected from the floodplain of the 608 km^2 South River watershed, located in the Shenandoah Valley, VA, USA. The floodplain is occupied by pastures and agricultural fields, together with forest and open space (URS, 2018). At a historical release site, $HgSO_4$ was used as a catalyst for fabric production and discharged into the river near Waynesboro, VA from 1929 to 1950. As early as the 1970s, elevated concentrations of Hg were reported in the downstream river water, surrounding soil, and fish tissues (Carter, 1977). Hg persists today and has been observed throughout the floodplain with variable concentrations more than 40 km downstream of the textile plant (Eggleston, 2009; Flanders et al., 2010; Lazareva et al., 2019; URS, 2018). Hg is concentrated in surface soil and subsoil (<200 cm) along the river edge close to the textile plant (<8 km) (Lazareva et al., 2019; URS, 2018). One of the highest reported Hg concentrations (1200 mg kg^{-1}) was observed 5.6 km downstream of the textile plant and 3 m in from the river edge (Lazareva et al., 2019). Moving downstream from the textile plant, Hg persists in surface soils (<40 cm) 40 km downstream within the 100-year floodplain, with analyzed Hg concentrations (N=508) ranging from 0.01 to 71 µg g^{-1}(URS, 2018). Elevated concentrations of MeHg have also been observed in fish tissue, amphibians, and birds up to 137 km downstream of the textile plant (Bergeron et al., 2011; Carter, 1977;

Jackson et al., 2011). Greater MeHg biomagnification factors are observed within the floodplain than in the South River (Newman et al., 2011).

5.3 Materials and Methods

5.3.1 Materials

Floodplain soil was collected 36.5 km downstream of the textile plant in three 3.7-L high-density polyethylene bottles, shipped to the University of Waterloo with icepacks, and stored at <4 °C under dark conditions. The floodplain soil was homogenized, air dried, and sieved to <2 mm before conducting the experiment. South River water (SRW) was collected seasonally 4.8 km upstream of the textile plant and shipped to the University of Waterloo on ice. SRW was also stored at <4 °C under dark conditions.

Anaerobic digestate (DIG) biochar were prepared at Cornell University (Ithaca, NY) using feedstocks produced by an advanced bioenergy (Coaltec Energy, Carterville IL, USA). The digestate grains contained a mixture of beef cattle manure, captured in a clean catch manure system, and thin stillage extracted from the ethanol refinery. After digestion, solids were separated from liquids and dried. Sulfurized-hardwood biochar (MOAK) was prepared by immersing an oak biochar (~700 °C, Cowboy Charcoal Co LLC, Bretwood, TN) in a 0.4% CaS_x solution using garden-grade lime sulfur (Green Earth Sure-Gro IP Inc.) in a 3.5% H_2/balance N_2 vinyl anaerobic chamber (Coy Laboratory Products, Inc.) for 7 d and rinsing with ultrapure water as previously described (Chapter 3; Liu et al., 2018b).

5.3.2 Experimental design

A modified humidity cell protocol was applied using three acrylic columns with dimensions of 7.6 cm (height) × 23 cm (internal diameter). Each column consisted of customized ports: one leachate port below the bottom; one solid collection port, two pore water collection ports in opposing directions, and a soil moisture sensor (EC-5, Decagon Device, Pullman, WA) installed 2.5 cm above the bottom; two stagnant water collection ports in opposing directions 5.5 cm above the bottom; and one influent port and two air release ports on the top (Fig. 5.1). The pore water collection ports were connected to micro-Rhizon samplers with a 5-cm porous length and 0.15-μm pore size (Rhizon MOM, Rhizosphere Research Products B.V. Wageningen, Netherlands). The stagnant water collection ports were connected to 10-cm polytetrafluoroethylene tubes (3.2 mm OD × 1.6 mm ID) with multiple holes drilled at random intervals. The experiment included one soil control (HCSed) and two amended systems with 10% biochar by dry weight: one DIG-amended soil system (HCDIG) and one MOAK-amended soil system (HCMOAK). Each column was started with 0.5 cm silica sand on the bottom to which floodplain soil with or without biochar was added to a final height of 5 cm above the column bottom. Biochars were mixed and homogenized with the floodplain soil every 100 g increment to an approximately total solid mass of 1200 g.

Each humidity cell column was subjected to ten subsequent wetting and drying cycles. During the wetting periods, 1000 mL SRW were added through the influent port and allowed to stagnate in each column with both the influent port and the air-release port closed. At the end of each wetting period, stagnant water (85.9±16.3 mL for HCSed, 80.6±21.5 mL for HCDIG, and a limited volume for HCMOAK) was collected through the stagnant water

collection port before the leaching began. During the leaching periods, SRW was drained through the solid matrix by gravity with the air release port opened. A 125-mL amber-glass bottle pre-filled with Ar (99.999%) was connected to the leachate collection port. An aliquot of initial leachate was collected within 30 min after the leaching began, and the remaining aliquots were collected within 24 h. During drying periods, solid materials were dried with the top lid left open and covered with a NITEX cloth. Pore water was collected 48 h after the drying periods began. The leaching and drying periods during the 1st wetting and drying cycle were 7 d, after which they were increased to 14 d to generate lower moisture contents.

5.3.3 Sample collection

Aqueous samples of the stagnant water and leachate were collected for determination of pH, Eh, alkalinity, and concentrations of total Hg (THg) (unfiltered (unf), 0.45- and 0.2-µm), methylmercury (MeHg), inorganic anions, organic acids, major and trace elements, NH_3-N, PO_4^{3-}, dissolved organic carbon (DOC), S^{2-}, and $CH_{4(aq)}$. The stagnant water and leachate were collected using 20-mL polypropylene/polyethylene sterile Luer Lock syringes (Norm-Ject, Thermo Fisher Scientific) passing through 32-mm diameter syringe filters with 0.45-µm Supor® membranes (Acrodisc®, VWR) except for pH, Eh, and unf and 0.2-µm THg. Pore water samples were collected for THg, MeHg, inorganic anions, organic acids, and major and trace elements in 9-mL plastic vacuum tubes with no preservative (VACUTTE®, Greiner-Bio-One International GmbH). All aqueous samples were preserved and determined as described previously (Chapters 3 and 4; Wang et al., 2019). Details about analytical information and QA/QC are summarized in the supporting information (see Text D1).

Solid samples at the end of the 1st and 4th cycles were collected from the solid port and the volume removed replaced with silica sand. At the end of the 10th cycle, solid materials in each column were separated into 2-cm intervals from the air/solid interface (0-2 cm) to the bottom (2-4 cm). Four separate samples were collected from each interval, generating a total of eight samples for each column. Solid samples were collected for total S content, S K-edge X-ray absorption near edge structure (XANES) spectroscopy, and 16s rRNA pyrosequencing analyses. Solid samples for total S and XANES analysis were collected in 20-mL glass vials (VWR®, TraceClean®, avantor™) and for 16s rRNA were collected in autoclaved 50-mL plastic centrifuge tubes. All solid samples were stored at −20 °C prior to analyses.

5.3.4 Total S content

Total S content in solid samples collected at end the of 4th and 10th wetting and drying cycles was analyzed by combustion using a resistance furnace analyzer (ELTRA® CS-2000, ELTRA GmbH).

5.3.5 S K-edge XANES

S K-edge XANES spectroscopy was performed for solid materials collected from the 4th cycle at beamline 9-BM at the Advanced Photon Source, Argonne National Laboratory (Lemont, IL, USA). S K-edge XANES spectra were collected using fluorescence mode with a beam size measuring 1000μm×1000 μm. Solid samples were ground and smeared as thin films on conductive double-sided tape, then mounted in a He chamber during the experiment. S K-edge XANES spectra were calibrated to the white line position for gypsum ($CaSO_4$•$2H_2O$) at 2482.7 eV. Reference compounds included diluted L-cysteine and gypsum

(2%). Three spectra were collected for reference compounds, and five spectra were collected for each sample and merged in μ(E) prior to normalization and data analysis.

S K-edge XANES spectral analysis was performed using the ATHENA package (Ravel and Newville, 2005) by decomposing normalized spectra into several Gaussian peaks between 2466 and 2489 eV representing different S species, following Manceau and Nagy (2012) and summarized previously (Chapters 3 and 4; Wang et al., 2019). A total of 11 Gaussian peaks representing sulfide minerals (2470.4, 2471.5, 2472.45 eV), elemental sulfur (or polysulfur) (2472.7 eV), exocyclic S (2473.5 eV), heterocyclic S (2474.15 eV), sulfoxide (2476.25 eV), sulfite (2478.5 eV), sulfone (2480.2 eV), sulfonate (2481.4 eV), and oxidized S (inorganic sulfate or ester sulfate) (2482.7 eV) as well as two arctangent steps representing reduced S species (2474 eV) and oxidized S species (2482.5 eV) were used with unconstrained peak heights and constrained peak widths. . Peak widths for reduced S components (sulfide minerals, polysulfur, exocyclic S and heterocyclic S) were constrained at 0.658 according to the peak width for the diluted L-cysteine, and peak widths for intermediate S and oxidized S were constrained at 0.848 according to the peak width for the diluted gypsum. Components with negative peak heights were eliminated in an ascending order. The areas under each Gaussian peak were normalized to the area under the elemental S peak (2472 eV) to overcome the proportional peak area increases with increases in vacancies in 3p transitions of S species (Waldo et al., 1991) using a generic equation suggested by Manceau and Nagy (2012). . The fitting quality was assessed using a normalized-sum square (NSS). Goodness-of fit was evaluated by eliminating components with <10% weight, and exclusions insignificantly affecting the fitting quality were not considered..

5.3.6 Pyrosequencing analysis

Solid samples collected at the end of the 4^{th} and 10^{th} cycles were analyzed for 16s rRNA sequencing. DNA purification for such solid samples was conducted using the Power Soil® DNA Isolation Kit (Mo Bio Laboratories) following the manufacturer's protocols in a Clean-Ceil™ Fan Filter Module (Microzone). Purified DNA samples were shipped frozen to MR DNA Laboratory (Shallowater, TX, USA) for the analysis using primer 515/806 targeting bacteria and archaea. Details about polymerase chain reaction, sequencing procedures, and data analysis are summarized in the supporting information (see Text D 2).

5.3.7 Statistical analysis

Correlations between the measured parameters were determined using Pearson's correlation coefficient (r) at a 95% confidence interval ($p<0.05$). One-way ANOVA was used to evaluate the impact of the biochar amendments on total S content and microbial effective sequence reads at a 95% confidence interval. Dunnett's test was used to compare results from the biochar-amended systems to the soil control.

5.4 Results and Discussion

5.4.1 Overview of sediment, river water, and biochar

The floodplain soil is fine grained with elevated Fe (24 000 μg g^{-1}) and organic matter (14 800 μg g^{-1}), moderate Al (6700 μg g^{-1}), Ca (1500 μg g^{-1}), Mn (1500 μg g^{-1}), and Mg (1100 μg g^{-1}), and limited S (159 μg g^{-1}) concentrations. Vermiculite ($Mg_3Si_4O_{10}(OH)_2$), biotite $K(Mg, Fe^{+2})_3(Al, Fe^{+3})Si_3O_{10}(OH,F)_2$, and quartz ($SiO_2$) are the predominant crystalline mineral phases. Hg (55 μg g^{-1}) in the floodplain soil is mainly associated with Hg bound to

soil organic matter and metacinnabar (β-HgS). Further details about the floodplain soil are described previously (Chapters 3 and 4). SRW has a slightly alkaline pH, measurable Na, Mg, Ca, K, Cl, NO_3^-, and SO_4^{2-} concentrations, and minimal NH_3-N, PO_4^{3-}, THg, and MeHg concentrations (Table 5.1). DIG and MOAK have similar surface areas and solid phase S concentrations. DIG has elevated ash content and concentrations of both nutrients (e.g., N, P) and other major elements (e.g., Ca, K, Mg, Fe, and Zn) (Table 5.2). MOAK is mainly composed of C (90%) with moderate concentrations of major elements (e.g., Ca and K) (Table 5.2). Previous S K-edge XANES analysis suggests DIG and MOAK contain similar fractions of polysulfur (47-60%), reduced S (exocyclic S and heterocyclic S) (15-19%), sulfide minerals (15%), and intermediate S (7%), and DIG also contains moderate fractions of oxidized S (11%) compared to MOAK (2%) (Chapters 3 and 4) (Fig. D 1).

5.4.2 Volumetric water content (VMC)

The mean volumetric water content (θ) in HCSed during the wetting and drying periods was 0.4 and 0.15, respectively (Fig. 5.2). Before the 2nd cycle, limited changes in θ were observed between the wetting periods, indicating the drying period (<7 d) was not sufficient to achieve a low moisture content. After increasing the time between wetting periods to 14 d, the θ values observed during the drying periods ranged between 0.08 and 0.16. Slightly higher θ values were observed in HCDIG and HCMOAK during the wetting periods (between 0.45 and 0.60) and the drying periods (between 0.11 and 0.28). The slightly higher θ values during the wetting periods are likely related to a higher pore volume derived from the relatively high internal porosities of the biochars as indicated by their relatively large measured surface areas (Table 5.2). The slightly increased water content in biochar-amended systems is

consistent with increased moisture content observed in a soil system amended with the same biochar to solid ratio, which can increase microbial activities (Reddy et al., 2015). During the leaching periods, θ values decreased at different rates in HCSed, HCDIG, and HCMOAK. Specifically, θ values decreased at a higher rate in HCDIG but at a lower rate in HCMOAK compared to HCSed. The different drying behaviors observed in the biochar-amended systems are likely associated with different internal porous structures for DIG and MOAK. The different leaching rate in these biochar-amended systems reflect changes in hydraulic conductivity and permeability with the additions of biochar in soils (Reddy et al., 2015).

5.4.3 Aqueous parameters

5.4.3.1 THg and MeHg

An early flush of THg (<0.45-µm) was observed in pore water and leachate from HCSed and the biochar-amended systems, and the pore water concentrations were consistent with leaching concentrations passing 0.2-µm filter membranes (Table D1) except for an elevated initial concentration in HCMOAK. In HCSed, concentrations of 0.45-µm THg was initially 752 ng L^{-1}, then decreased and stabilized between 63 and 115 ng L^{-1} (Fig. 5.3a). The initial concentrations of 0.45-µm THg in leachate from HCDIG and HCMOAK were up to 3550 ng L^{-1}. The initial concentrations of Hg in pore water in HCMOAK (28 400 ng L^{-1}) were eight-fold higher than in the leachate. After the early flush, concentrations of 0.45-µm THg (between 116 and143 ng L^{-1}) in HCDIG were similar to HCSed, while a much smaller release of 0.45-µm THg (49-95 ng L^{-1}) was observed in HCMOAK. Concentrations of 0.45-µm THg in stagnant water from HCSed remained <100 ng L^{-1} for the duration of the experiment, while higher concentrations were observed in the biochar-amended systems

during the early flush. The initial concentrations of 0.45-µm THg in stagnant water from HCDIG (433 ng L^{-1}) and HCMOAK (2110 ng L^{-1}) were seven- and 33-fold higher than HCSed, respectively. The early flush has also been observed in other mining projects evaluated using humidity cell tests (Maest et al., 2017). The early flush may represent release of Hg associated with pre-existing oxidation products.

Although after the early flush, concentrations of 0.45-µm THg in the leachate from the biochar-amended systems are similar to HCSed, concentrations of unf THg continued to decline (Fig. 5.3a). Concentrations of unf THg in leachate from HCSed were between 2060 and 47 800 ng L^{-1}, and a peak was observed at the 4th cycle after the release of 0.45-µm THg stabilized. Concentrations of unf THg in leachate from HCDIG and HCMOAK systems decreased as wetting and drying continued. Concentrations of unf THg in leachate from HCDIG decreased from 7110 to 1970 ng L^{-1}, representing a minimal to 90% decrease. Concentrations of unf THg in leachate from HCMOAK rapidly decreased from 32 000 ng L^{-1} before the early flush and stabilized below 1000 ng L^{-1} thereafter, representing a 24 to 93% decrease. The variable concentrations of unf THg in HCSed are consistent with the large variations in unf THg observed in South River sediments collected at different locations in a previous humidity cell experiment (Wang et al., 2019). After the early flush, Hg release in HCSed shifted from colloidal particles (<0.45-µm) to mostly particulate-bound (>0.45-µm), increasing from 68% to greater than 97% of unf THg. In the biochar-amended systems, the greater release of unf THg during the early flush may result from the release of Hg associated with smaller biochar particles. After the early flush, the greater decreases in unf THg in the biochar-amended systems indicate biochars as soil amendments stabilize particulate-bound

Hg better than colloidal or dissolved Hg under the experimental conditions. The limited stabilization of colloidal or dissolved fractions (<0.45-µm) is likely related to the relatively high leaching rate (>0.02 mL h^{-1}), which may not provide sufficient time to allow precipitation/ adsorption reactions within the biochars.

5.4.3.2 Minimal concentrations of MeHg were observed in leachate and pore water from HCSed and HCDIG (<0.3 ng L-1) over the duration of the experiment, while elevated initial concentrations of MeHg were observed in leachate and pore water collected from HCMOAK (Fig. 5.3a). Concentrations of MeHg in leachate and pore water collected from HCMOAK were initially 15 and 158 ng L-1, respectively, then decreased to 0.6 ng L-1 within the 2nd cycle and remained <0.1 ng L-1 thereafter. The relatively low concentrations of MeHg in HCSed and HCDIG are similar to those reported in a previous study that used a hardwood biochar as a reactive mat to stabilize Hg release in South River sediments from different locations under flooding and drainage conditions (Wang et al., 2019). The elevated leachate and pore water MeHg in HCMOAK is striking as MeHg production in natural environments occurs under anaerobic conditions (Gilmour et al., 2013a), and lower MeHg fluxes are usually observed in aerobic conditions compared to anaerobic conditions (Duvil et al., 2018). The elevated MeHg in leachate collected from HCMOAK during the early flush is three-fold higher than the peak concentrations observed under saturated flow conditions (Fellin, 2016), and similar to long-term anaerobic conditions (Wang et al., 2019). The elevated pore water

concentrations are similar to other biochar-amended studies for stabilizing Hg-contaminated riverbank sediments under anoxic conditions for 400 d (Liu et al., 2017, 2018a).

5.4.3.3 Eh, DOC, and Mn

Increases in Eh were observed during the early flush when concentrations of DOC and Mn decreased as the number of wetting and drying cycles increased (Fig. D 2). Stagnant water had a slightly higher Eh and lower DOC than leachate. Eh in leachate from HCSed varied between 377 and 430 mV, indicating aerated conditions. Eh in leachate from HCDIG and HCMOAK was initially lower (328 mV for HCDIG; 280 mV for HCMOAK) and then increased to nearly 400 mV as the number of cycles continued, indicating shifts from moderately anaerobic to aerobic conditions in the biochar-amended systems. Concentrations of DOC in leachate from the HCSed and HCMOAK systems decreased from 24 mg L^{-1}, and then fluctuated between 5 and 10 mg L^{-1}. Concentrations of DOC in leachate from HCDIG fluctuated between 14 and 18 mg L^{-1} except for a low value of 7 mg L^{-1} at the 8^{th} cycle. Similar to DOC, elevated initial concentrations of Mn were observed in leachate from the HCSed (1.7 mg L^{-1}) and HCMOAK (25 mg L^{-1}) systems that then decreased to below 0.1 mg L^{-1}. Concentrations of Mn in leachate from HCSed stabilized by the 2^{nd} cycle. Concentrations of Mn in HCMOAK stabilized by the 5^{th} cycle. In contrast, concentrations of Mn in HCDIG were below 0.5 mg L^{-1} throughout the experiment.

The increases in Eh coupled with decreases in concentrations of DOC and Mn indicate favourable conditions in HCSed for reductive dissolution of Mn(IV) during the early flush that became less favourable at later times (Stumm and Morgan,1996; Husson, 2013). Fierer

and Schimel (2002) suggest the release of DOC after a wetting and drying cycle could be related to the release of labile organic substrates as a result of biomass turnover. With repeated wetting and drying cycles, the solids likely become more aerated. Less labile organic matter and changes in microbial composition may lead to decreases in DOC (Fierer and Schimel, 2002). Loss of Mn may occur through co-precipitation with Fe oxides during continuous aeration (Dent et al.,2014).

Addition of biochars in the floodplain soil further affects Eh as well as concentrations of DOC and Mn. Biochars can act as electron shuttles to transfer electrons between bacteria and terminal electron accepters (e.g., Fe (III) minerals) (Kappler et al., 2014). Therefore, the lower Eh observed in HCDIG and HCMOAK at early time points may be due to enhanced electron transfer with the addition of biochars. The relatively higher DOC concentrations in HCDIG are consistent with enhanced soil organic matter release after a rewetting event in anaerobic digestate-amended systems (Chapter 4; Schouten et al., 2012), which is likely related to the continuous release of labile organic matter as wetting and drying cycles continued. Enhanced dissimilatory reduction of Mn(IV) was observed in MOAK-amended systems under long-term anaerobic conditions (Chapter 3). The elevated initial aqueous Mn concentrations in HCMOAK are almost the same as under fully-saturated and anoxic conditions at 30 d (Eh=−39±28 mV) (Chapter 3). Although the Eh was moderately reducing (300 mV) in HCMOAK leachates, more reducing conditions may occur within the pore spaces. Therefore, the elevated initial concentrations of aqueous Mn in the HCMOAK system are likely associated with the reductive dissolution of Mn oxides.

5.4.3.4 Release of Hg and MeHg associated with DOC and Mn dynamics

The release of THg (0.45-µm) is positively correlated with concentrations of DOC ($r>0.989$, $p<0.05$) and Mn ($r>0.953$, $p<0.05$), especially in HCSed and HCMOAK (Fig. 5.3b-c). Remobilization of Hg associated with soil organic matter has been reported in flooded floodplain soil (Chapter 3; Poulin et al., 2016) and in biochar-amended systems after drying and rewetting events (Chapters 3 and 4). In addition to positive correlations between THg and Mn, the elevated Mn in HCMOAK corresponds to elevated MeHg ($r=0.979$, $p<0.05$) (Fig. 5.3d). Strong correlations between Hg or MeHg and Mn have been observed in river water and shallow groundwater at the South River site (Lazareva et al., 2019) and an anoxic lake (Dent et al., 2014).

5.4.3.5 pH, alkalinity, Ca, and SO_4^{2-}

The addition of DIG and MOAK affected pH, alkalinity, and concentrations of Ca and SO_4^{2-} (Fig. 5.4). Specifically, the addition of DIG led to slightly higher pH (7.75±0.11) and alkalinity (145±35 mg L^{-1}) values. Concentrations of SO_4^{2-} in HCDIG decreased from 369 to 95 mg L^{-1} over the course of the experiment, indicating the release of oxidized S fractions from DIG (Fig. D 1). The addition of MOAK lowered the pH by 1.2 units and alkalinity by 90%, coupled with increases in Ca and SO_4^{2-} until peak concentrations of 215 and 796 mg L^{-1}, respectively, occurred at the 5th cycle. pH and alkalinity then stabilized, and concentrations of Ca and SO_4^{2-} decreased.

5.4.3.6 Other major elements (K and Cl) and nutrients (NH_3-N, NO_3^-, and PO_4^{3-})

Addition of DIG and MOAK resulted in changes in N chemistry, and the release of PO_4^{3-}, K, and Cl was also observed for HCDIG (Fig. D 3-4). Decreases in NH_3-N coupled with

increases NO_3^- concentrations were observed in HCSed and HCDIG before the early flush. After the early flush, NH_3-N was <0.1 mg L^{-1} while NO_3^- plateaued as the systems became more aerated. The stabilized concentrations of NO_3^- in HCDIG were 50% lower than in HCSed, suggesting addition of DIG may suppress nitrification. Unlike HCSed and HCDIG, concentrations of NH_3-N in HCMOAK peaked at the 2nd cycle (2.2 mg L^{-1}) and then slowly decreased to 0.5 mg L^{-1}, while concentrations of NO_3^- were <1 mg L^{-1}. Addition of DIG resulted in increases in concentrations of PO_4^{3-} over the experimental duration. Initial releases of elevated K (105 mg L^{-1}) and Cl (108 mg L^{-1}) were observed in HCDIG.

5.4.4 Solid-phases analysis

5.4.4.1 S in solid

Solid materials collected at the end of the 4th and 10th cycles were analyzed for total S content in solid (Fig. 5.5a-d). Addition of DIG and MOAK led to significant increases (α=0.05, p=0.00001) in total S in solid materials, with the highest total S observed in HCMOAK (Fig. 5.5a). The total S contents of solid samples collected from each system at different depths at the end of 10th cycle were not significantly different in soil control and biochar-amended systems. As wetting and drying cycles increased, insignificant changes in S content were observed in HCDIG (α=0.05, p=0.63), while S content in HCSed and HCMOAK decreased significantly (α=0.05, p<0.0001) by 23 and 37%, respectively (Fig. 5.5b-d).

5.4.4.2 S K-edge XANES

S K-edge XANES analysis of solid material collected at end of the 4th cycle demonstrates different S species for solid materials in HCSed, HCDIG, and HCMOAK (Fig. 5.5e-g). S K-

edge XANES spectra for solid materials collected from HCSed contain one pronounced peak in the oxidized S region (2482 eV) (Fig. 5.5e). S K-edge XANES spectra for solid materials collected from HCDIG and HCMOAK contain pronounced peaks in the reduced S region (2470 eV) as well as in the oxidized S region (2482 eV) (Fig. 5.5e and f).

Gaussian peak fitting analysis suggests the addition of DIG or MOAK to the floodplain soil shifts intermediate S toward polysulfur, reduced S, and sulfide minerals in solid materials, while fractions of oxidized S remain relatively unchanged (Figs. 5.5e-h). Results of Gaussian peak fitting for solid materials collected in HCSed suggest S is mainly associated with intermediate S (61%), oxidized S phases (30%), and limited other S fractions (<10%) (Figs. 5.5e and h). Addition of DIG and MOAK to the floodplain soil increased fractions of polysulfur (26-35%) and reduced S (exocyclic S and heterocyclic S) (12-15%) (Figs. 5.5f-h).

5.4.4.3 Microbial community

After denoising pyrosequencing data, the number of effective sequencing reads was 126,126±13,040 per sample, with 1042±38 detected operational taxonomic units (OTUs) (>97% percent homology). The effective sequencing reads per sample (α=0.05, p=0.51) and detected OTUs did not change significantly (α=0.05, p=0.68) during the experiment. Application of DIG and MOAK as soil amendments resulted in minor changes in both effective sequencing reads (α=0.05, p=0.16) and OTUs (α=0.05, p=0.17).

Shifts in microbial community at the phyla and genera taxonomic levels were observed as the number of wetting and drying cycles increased (Fig. 5.6ab). Proteobacteria were the predominant microbial community as the number of cycles increased (Fig. 5.6a). Decreases

in the relative abundances of *Bacillus* and *Sporosarcina* members accounted for the decreases in Firmicutes. Other than the decreases in Firmicutes, addition of DIG or MOAK led to limited changes in microbial communities at the phyla taxonomic level.

At lower taxonomic levels, such as the genera level, shifts in the microbial community increased over time (Fig. 5.6b). For example, bacteria that are more resistant to arid/semi-arid environments (e.g., *Gemmatimonas* and *Ramlibacter*) became more abundant in the biochar-amended systems. These shifts in taxonomic structure in soils are consistent with other observations after drying and rewetting events (Sun et al., 2018). As wetting and drying cycles increased, the microbial communities in HCSed and HCDIG were similar, while more distinct changes were observed in HCMOAK. For example, nitrogen fixing bacteria (e.g., *Azoarcus*), sulfur oxidizing bacteria (SOB) (e.g., *Thiobacillus*), and acid tolerant bacteria (e.g., *Candidatus Koribacter*) were abundant in solid materials collected at the end of the 4^{th} cycle in HCMOAK; at the end of the 10^{th} cycle, the relative abundances of *Thiobacillus* dropped while the relative abundances of methylotrophs (e.g., *Methylotenera* and *Methylophilus*) increased.

SOB communities can utilize NO_3^- as an electron accepter in the presence of elemental S (Germida and Janzen, 1993; Okabe et al., 2005). The abundance of SOB coupled with lower concentrations of NO_3^- in HCMOAK than in HCSed and HCDIG (Fig. D 3) suggests NO_3^- in HCMOAK was utilized by microorganisms for growth. The increases in the relative abundances of *Thiobacillus* species in solid materials collected in HCMOAK at the end of the 4^{th} cycle are consistent with increases in *Thiobacillus* species in soils amended with elemental S (Yang et al., 2008). Members of *Thiobacillus* are the most important microbes

mediating biotic elemental S oxidation in soils. The abundance of *Thiobacillus* coupled with low pH, alkalinity, and peak SO_4^{2-} (Fig. 5.4) in HCMOAK suggests the activity of these microorganisms is responsible for the slightly acidic conditions generated in HCMOAK during the early flush. Germida and Janzen (1993) state oxidation of elemental S depends on physicochemical properties of soil and amended S that are available for microbes. Although increases in fractions of polysulfur (or elemental S) were observed in solid materials collected from HCDIG and HCMOAK (Fig. 5.5e-h), polysulfur is likely more available to support microbial growth in HCMOAK than in HCDIG.

The increases in concentrations of Ca from HCMOAK (Fig. 5.4) during the early flush are likely related to the oxidation of polysulfur in MOAK. Increases in Ca concentrations under acid-generating conditions are mostly associated with the dissolution of carbonate minerals that buffer acidic pH water and maintain near neutral (6-8) pH conditions (Johnson et al., 2000; Jurjovec et al., 2002). Decreases in biochar pore volume have been reported in other studies using sulfurizing carbonaceous materials, likely due to the trapping of polysulfide solution in the porous structure after sulfurization (Asasian and Kaghazchi, 2012; O'Connor et al., 2018). Asasian and Kaghazchi (2012) state that the trapped solution is difficult to eliminate even after rinsing several times with distilled water. Oxidation of polysulfide solution trapped in the biochar porous structure during sulfurization processes may also lead to increases in concentrations of Ca in leachate from HCMOAK.

After the 4th cycle, decreases in the abundance of *Thiobacillus* may indicate a decline in SOB activity (Fig. 5.4). The decreases in the relative abundance are consistent with the decline in *Thiobacillus* population after eight weeks of elemental S application in a shallow

soil (Yang et al., 2010), which is likely related to a decrease in bacterial growth with SO_4^{2-} concentrations greater than 100 mM (Suzuki et al., 1999). The elevated concentrations of SO_4^{2-} released in HCDIG early in the experiment may have inhibited the growth of SOB, and therefore limited polysulfur from DIG for SOB growth.

5.5 Conclusions

Although additions of biochars to floodplain soils decreased the release of Hg especially in particulate forms, repeated drying and rewetting can affect the efficacy of Hg stabilization. Enhanced release of THg and MeHg associated with the release of DOC and reductive dissolution of Mn(IV) can occur in biochar-amended systems during an early flush. Although the early flush was only observed once under the experimental condition, the enhanced release can recur on a seasonal basis as results of changes in hydrogeological and meteorological conditions (Maest and Nordstrom, 2017). For example, the enhanced release can occur during heavy rainfall events after a long-term drought. After the early flush, additions of MOAK to floodplain soil resulted in lower Hg release in colloidal or dissolved fractions (<0.45-µm) as well as particulate (>0.45-µm) fractions compared to the additions of DIG. For conditions where the efficacy of washing contaminated soil is more important than changes in microbial processes, MOAK is likely a better candidate than DIG.

Addition of different biochars to floodplain soils may result in different environmental consequences. The addition of DIG, with elevated major element and nutrient content, may release elevated concentrations of K^+, Cl^- and SO_4^{2-} to aqueous phases at early times. Elevated SO_4^{2-} concentrations of solutes can inhibit the growth of sulfur-oxidizing bacteria

communities, thus limiting the oxidation of S functionalities in the biochar. Addition of DIG can increase nutrients that may become available for plants. Addition of MOAK, with elevated fractions of polysulfur and limited other major and trace elements, has the potential to stimulate growth of sulfur-oxidizing bacteria and promote microbially-driven oxidization of polysulfur as the system becomes aerated during repeated drying and rewetting.

Results of this study suggest redox oscillations caused by repeated drying and rewetting as well as biochar compositions can affect outcomes for remediation activities in field applications. Assessment of local and regional environmental conditions and characterizations of biochars are recommended before implementing field-scale remediation projects.

Table 5.1 Chemical composition of South River water (SRW) showing mean values and standard deviation from the mean.

Parameter	Value[#]
pH	7.60±0.14
Eh, mV	342±31
Alkalinity, as $CaCO_3$ mg L^{-1}	169
Cl, mg L^{-1}	15.0±9.20
NO_3^-, mg L^{-1}	2.67±2.21
SO_4^{2-}, mg L^{-1}	15.7±4.86
Na, mg L^{-1}	5.84±0.08
Mg, mg L^{-1}	11.2±0.56
K, mg L^{-1}	2.20±0.06
Ca, mg L^{-1}	29.6±1.19
DOC, mg L^{-1}	1.4±0.1
MeHg, ng L^{-1}	0.02
NH_3-N, mg L^{-1}	0.01
PO_4^{3-}, mg L^{-1}	0.03
THg, ng L^{-1}	2.50±1.35

Table 5.2 Physical characteristics and major elemental composition of biochar prepared from anaerobic digestate (DIG) and sulfurized hardwood biochar (MOAK). Surface area, C, H, O, N, and ash content for MOAK were measured prior to sulfurizing the hardwood biochar. Values for DIG and MOAK are from Chapters 3 and 4.

	DIG	MOAK
Surface area, m^2/g	53.2	65
H, %	0.65	1.57
C, %	42.7	89.5
N, %	2.02	0.26
Total Kjeldahl nitrogen, %	1.84	0.22
O, %	11.8	4.08
S, %	0.75	0.54±0.24
Ash content % (550 °C)	53.7	3.1
Volatile component	10.6	15.9
Al, mg kg^{-1}	4650	77
Ca, mg kg^{-1}	94 000	3880
Cu, mg kg^{-1}	191	1.71
Fe, mg kg^{-1}	4430	106
Hg, mg kg^{-1}	<0.0050	0.02
K, mg kg^{-1}	11 300	1340
Mg, mg kg^{-1}	11 600	299
Mn, mg kg^{-1}	766	54.1
Na, mg kg^{-1}	4130	<50
P, mg kg^{-1}	53 500	94
Zn, mg kg^{-1}	3240	9.1

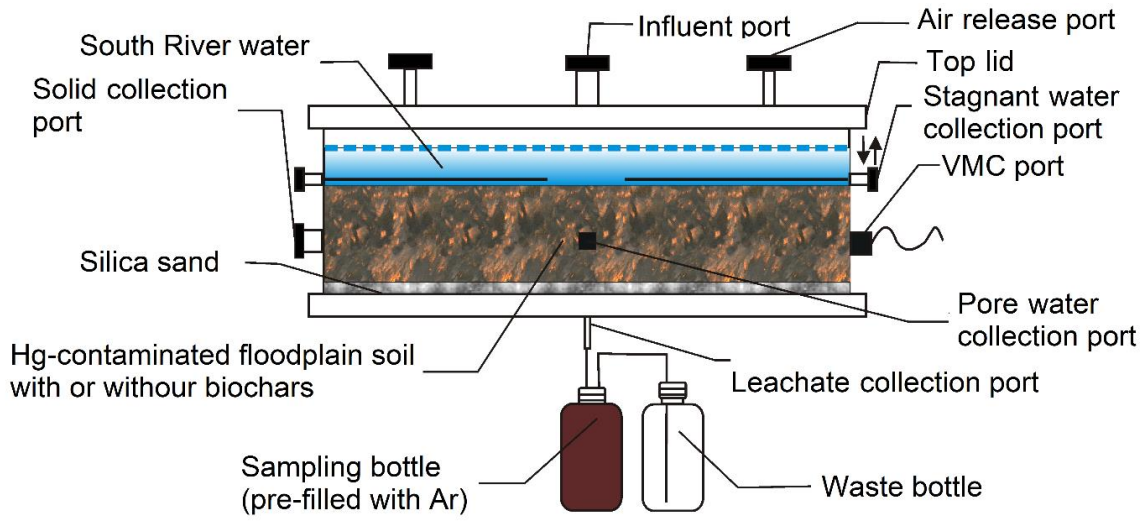

Fig. 5.1 Schematic diagram showing experimental design for modified humidity cell experiment.

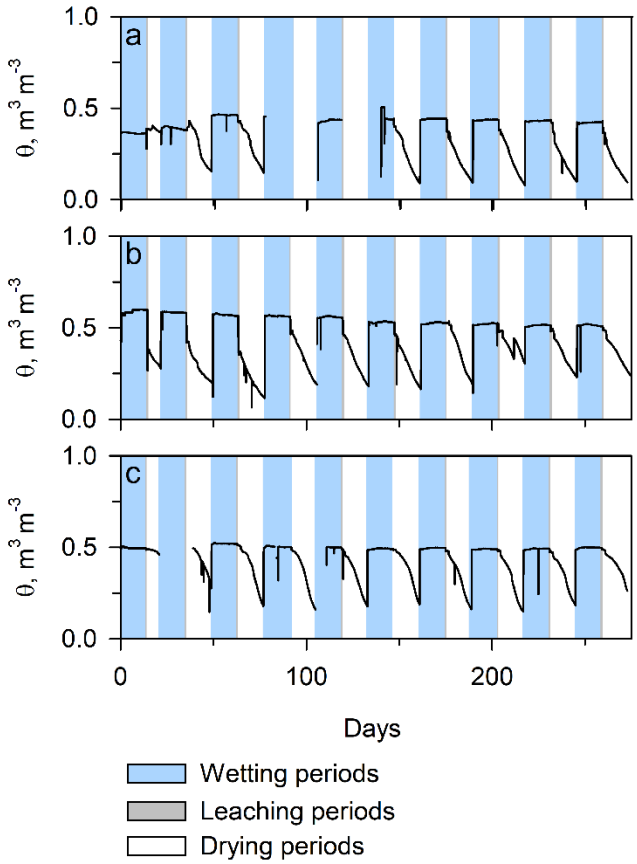

Fig. 5.2 Volumetric water content (θ) measured by soil moisture content sensors installed in soil control (HCSed), DIG- (HCDIG), and MOAK-amended systems (HCMOAK) over the course of the experiment. The data gaps represent times when the installed soil moisture content sensors lost connection with the data logger.

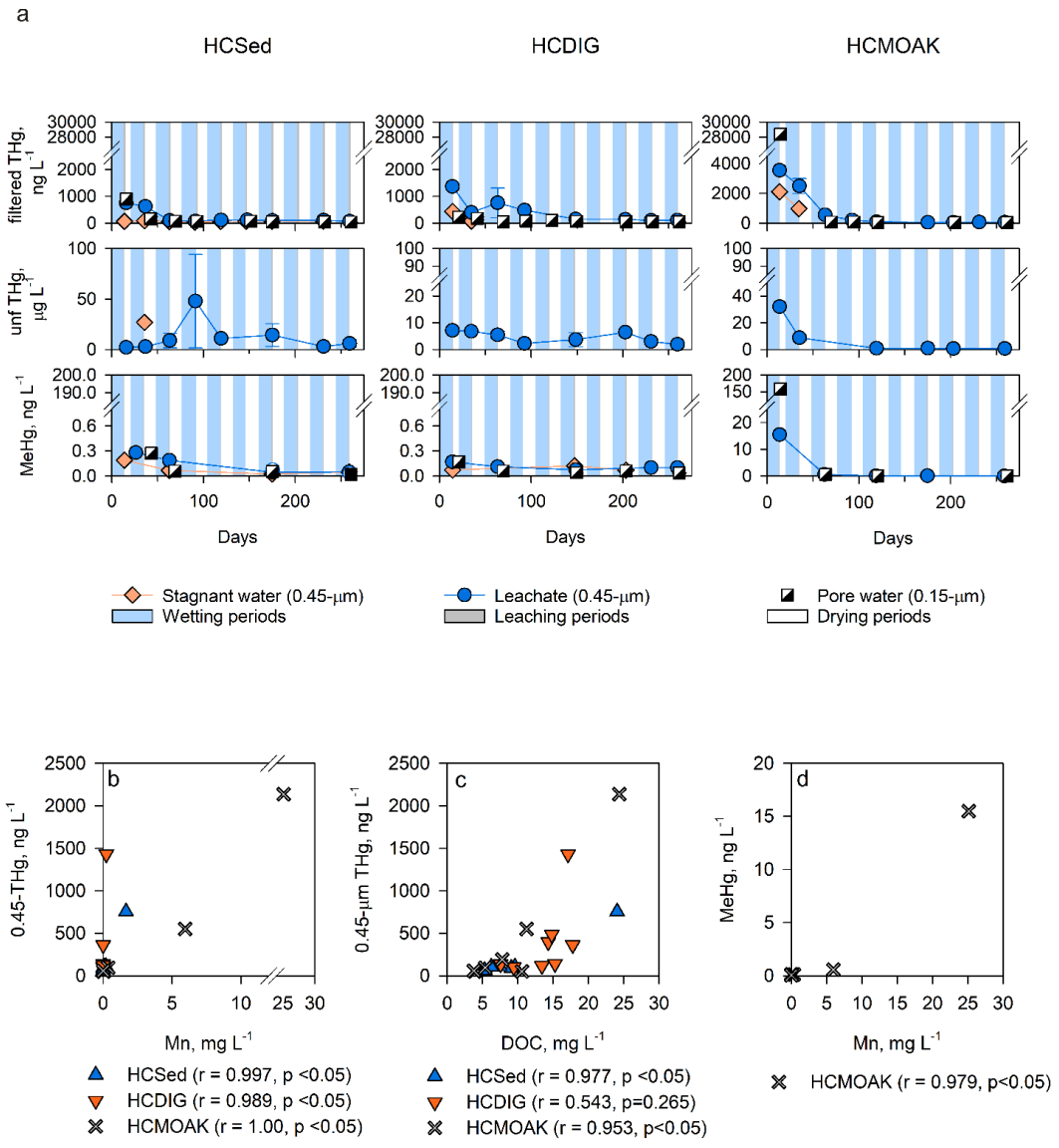

Fig. 5.3 Concentrations of filtered and unfiltered (unf) total Hg (THg) and MeHg (a) and correlation analysis (b-d) for soil control (HCSed), DIG- (HCDIG), and MOAK-amended systems (HCMOAK) with respect to wetting and drying cycles. Correlation analysis for 0.45-µm THg with Mn (n=6) (b), DOC (n=6) (c), and MeHg with Mn for HCMOAK (n=5) (d). Error bars for leachate represent standard deviation for leachates collected within 24 h after leaching; the exception is error bars for unfiltered THg, which represent the minimum and maximum concentrations due to the relatively large variation. Error bars for pore water represent standard deviations for concentrations obtained from two pore water collection ports on each humidity cell. Error bars for MeHg are smaller than the symbol size.

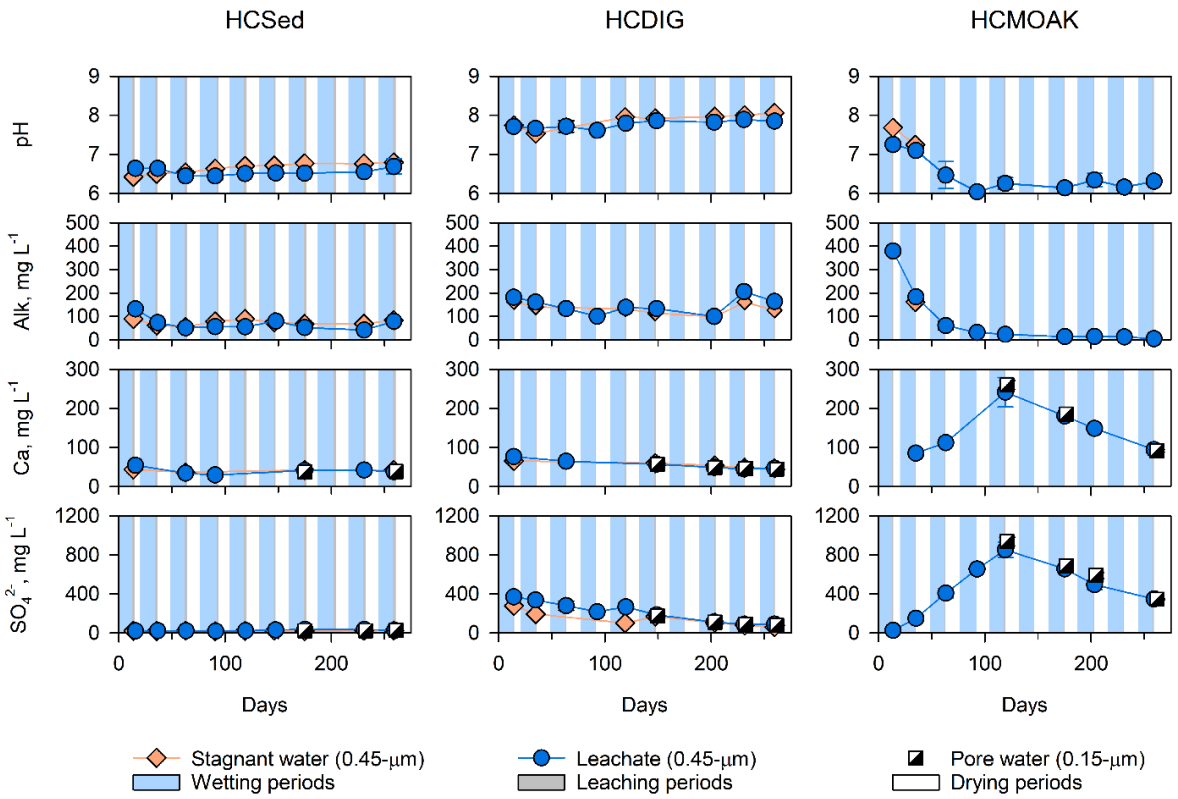

Fig. 5.4 pH, alkalinity as $CaCO_3$ mg L^{-1} (Alk), and concentrations of Ca and SO_4^{2-} for soil control (HCSed), DIG- (HCDIG), and MOAK-amended systems (HCMOAK) with respect to wetting and drying cycles. Error bars for leachates represent the standard deviation of leachate collected within 24 h during leaching periods. Error bars for pore water represent the standard deviation of samples collected from two pore water collection ports on each humidity cell.

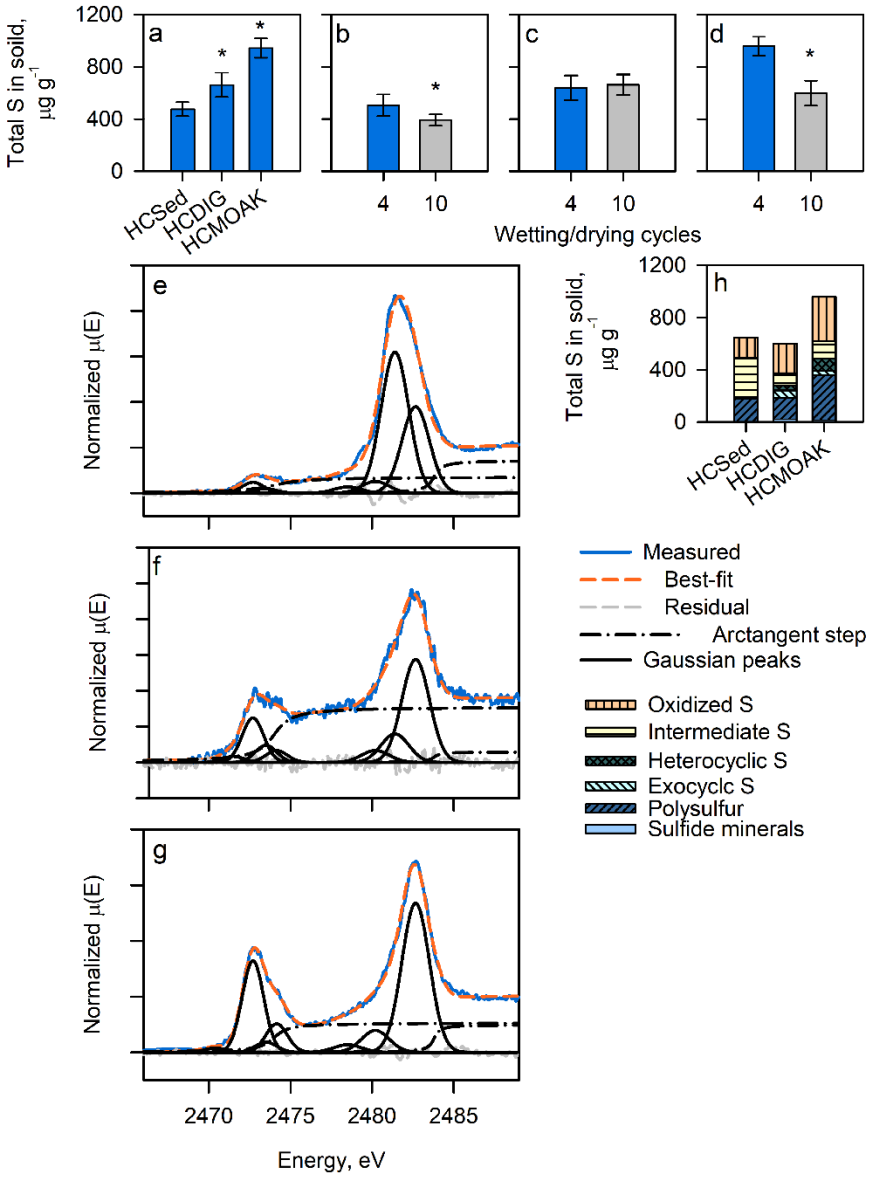

Fig. 5.5 Total S content and S K-edge X-ray absorption near edge structure (XANES) analysis for solid materials collected from soil control (HCSed), DIG- (HCDIG), and MOAK-amended systems (HCMOAK). Total S content for solid materials collected at the end of the 4th (a) as well as at 4th and 10th wetting and drying cycle for soil control (HCSed) (b), DIG- (HCDIG) (c) and MOAK-amended systems (HCMOAK) (d). Gaussian peak fitting analysis for S K-edge XANES in solid materials collected at the end of the 4th wetting and drying cycle in HCSed (e, NSS=3.21×10^{-3}), HCDIG (f, NSS=3.99×10^{-3}), and HCMOAK (g, NSS=1.21×10^{-3}). Fractions of S in solid materials obtained from Gaussian peak fitting analysis (h). Asterisks (∗) denote significant differences ($p<0.01$) at a 95% confidence interval. Error bars represent the standard deviation from the mean.

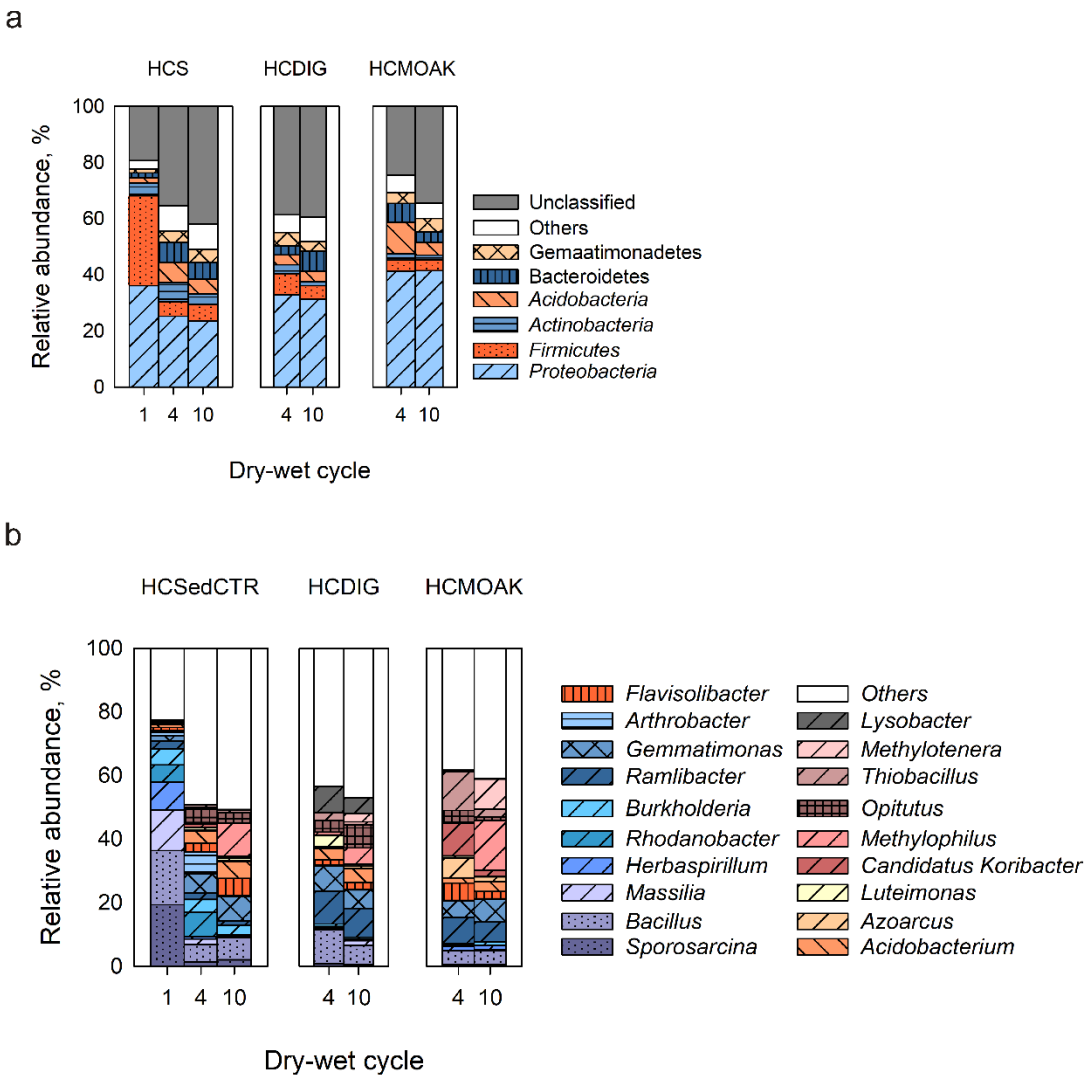

Fig. 5.6 Results of 16s rRNA pyrosequencing for solid samples collected over the course of the experiment showing predominant phyla (>5%) (a) and genera (>5%) (b) taxonomic microbial compositions.

Chapter 6 Conclusions

6.1 Summary of Research

Remediation of Hg contaminated sites in riverine settings is complex due to the dynamic nature of river geomorphology, water levels, and geochemical conditions that affect the release, transport and bioavailability of Hg. Biochar has been proposed for use as a reactive media in bank stabilization capping mats (Desrochers, 2013; Paulson, 2014; Ting et al., 2018) and as soil amendments (Fellin, 2016; Gilmour et al., 2013b, 2018; Liu et al., 2017, 2018a, 2019; O'Connor et al., 2018) under fully-saturated conditions. Hg stabilization using biochars in settings exposed to flooding and drying has not been widely evaluated. In this thesis, a set of complementary laboratory experiments was conducted using five selected biochars for application as reactive capping mats and soil amendments under variably saturated conditions relevant to riverine environments (e.g., long-term flooding and drainage, long-term fully-saturated, drying and rewetting, long-term drying and rewetting). The five biochars tested included hardwood biochar (OAK), sulfurized-hardwood biochar (MOAK), biochar prepared from 100% anaerobic digestate (DIG), 100% distillers` grains (DIS), and a mixture of 75% anaerobic digestate and 25% distillers` grains (75G25S).

Chapter 2 evaluated OAK as a reactive material for encapsulation in geotextile materials installed along riverbanks for bank stabilization under long-term flooding and drainage conditions using a weekly-cyclic experiment for 100 weeks (Wang et al., 2019). Treatment systems containing 50% v/v OAK and non-reactive quartz sand retained more than 80% Hg with minimal MeHg production in both aqueous and solid phases. Retaining dissolved and particulate Hg in the biochar porous structure and forming complexes with functionalities on

the biochar are the predominant mechanisms contributing to Hg removal. Results of this chapter suggest OAK is a promising material for embedment in geotextile layers for bank stabilization, and the effectiveness of Hg removal is expected to be minimally impacted by changes in stream level and groundwater/surface water interactions.

Chapter 3 evaluated OAK and MOAK as soil amendments in floodplain soil under anoxic conditions as well as impacts of drying and rewetting on the biochar-amended systems. In contrast to limited Hg removal in the OAK-amended systems, a 99% reduction in Hg release and limited MeHg production were observed in the MOAK-amended systems relative to the soil controls. Drying and rewetting enhanced the mobilization of Hg in the OAK-amended systems, likely due to the complexation with dissolved organic carbon (DOC). In the MOAK-amended systems, shifts in microbial community compositions and changes in S chemistry during drying and rewetting likely contributed to increases in aqueous and solid MeHg. Results of this chapter suggest MOAK enhanced Hg removal under anoxic conditions, and changes in biogeochemical conditions as a result of drying and rewetting may influence MeHg production.

Chapter 4 evaluated DIG, DIS, and 75G25S as alternative soil amendments in floodplains under anoxic conditions and impacts of drying and rewetting on their effectiveness following the same experimental design as in the previous chapter. Addition of digestate-based biochars (DIG and 75G25S) in floodplain soil under anoxic conditions substantially decreased the release of Hg (up to a 99% reduction) without promoting MeHg production compared to the soil controls, while addition of DIS resulted in limited Hg removal and increased aqueous MeHg concentrations. Drying and rewetting had limited impacts on Hg

release and MeHg production in these biochar-amended systems. Results of this chapter suggest digestate-based biochars may be applied as sediment capping materials under anoxic or occasionally drying and rewetting conditions.

Chapter 5 further evaluated MOAK and DIG as soil amendments under repeated wetting and drying conditions using dynamic column experiments for a total of ten wetting and drying cycles. Limited decrease in Hg release (<60%) was observed in the biochar-amended systems under the experimental conditions, likely related to the relatively low release of Hg from the floodplain soil under oxic conditions and the rapid rate of drainage from the solid matrix. An early flush of Hg and MeHg in the MOAK-amended system was positively correlated with the aqueous concentrations of DOC and Mn. In the DIG-amended system, minimal production of MeHg was observed, and the release of Hg during the early flush was positively correlated with concentrations of DOC. Shifts in microbial community structure toward sulfur-oxidizing bacteria were observed in the MOAK-amended system, which may stimulate oxidation of polysulfur in MOAK to form elevated SO_4^{2-} and decrease pH. In the DIG-amended system, sulfur-oxidizing bacteria were not as abundant as in the MOAK-amended system. The initial release of elevated SO_4^{2-} in the DIG-amended system can inhibit growth of sulfur-oxidizing bacteria as well as oxidation of S in DIG. Results of this chapter demonstrate that MOAK is more susceptible to changes in biogeochemical conditions, and addition of DIG did not increase MeHg concentrations or alter microbial structure under repeated drying and rewetting conditions.

6.2 Contributions and Environmental Implications

Results of this research complement studies on Hg removal using biochars by evaluating different conditions relevant to riverine environments (Table 6.1). Results of this thesis suggest biochars may be effective reactive materials for stabilizing Hg at the field-scale, provided careful consideration is given to the application methods, environmental conditions, biochar properties, and forms of Hg in contaminated sediments.

Most studies evaluating Hg removal using biochars start with batch experiments to obtain sorption isotherms using input solutions spiked with Hg salts (Gomez-Eyles et al., 2013; Huang et al., 2019; Liu et al., 2016; Peterson et al., 2017; Park et al., 2019). These experiments provide an initial indication of the Hg removal capacity of different biochars. However, the higher removal capacity of the investigated biochars in Hg salt spiked do not fully incorporate the impacts of DOC. Lower sorption of Hg/MeHg on activated carbon has been observed in simulated oxic solution containing organic matter than Hg salts (e.g., $HgCl_2$, or $Hg(NO_3)_2$) spiked solution (Johs et al., 2019; Schwartz et al., 2019). When biochars are proposed as reactive materials embedded in geotextile installed along riverbanks for bank stabilization, these types of experimental approaches may provide initial screening results on the sorption capacity of the investigated biochars. For example, OAK was previously demonstrated to have a large Hg removal capacity (>99%) in $HgCl_2$ spiked solutions (Liu et al., 2016, 2018b). Similar removal (>80%) was observed when OAK was evaluated as a reactive material for stabilizing Hg derived from contaminated sediments in fully-saturated column experiments (Desrochers, 2013; Paulson, 2014) and under flooding and drainage conditions (Wang et al., 2019). The similar Hg removal rate is likely related to

limited DOC in leachate derived from Hg-contaminated sediments in these experiments (Wang et al., 2019).

When biochars are directly amended in riverbank sediments or floodplain soils, soil organic matter further lowers the effectiveness of Hg removal by forming Hg-S-DOM complexes or decreasing the rate of formation of β-HgS (Schwartz et al., 2019). For example, although OAK has been demonstrated previously to have a large Hg removal capacity (Liu et al., 2016), limited removal was observed when OAK was used as a soil amendment in anoxic sediments (Chapter 3; Liu et al., 2018a). MOAK has been demonstrated previously to remove more than 99% Hg in $HgCl_2$ spiked simulated groundwater (Liu et al., 2018b), but a lower rate of Hg removal was observed when MOAK was evaluated as a soil amendment under saturated-flow conditions (>74%) (Fellin, 2016) and anoxic conditions (47-99%)(Chapter 3). Therefore, isothermal sorption studies with Hg added as inorganic salts may not fully capture the complexities of Hg forms in natural environments, overestimating Hg removal when biochars are applied as soil amendments.

Drying and rewetting in riverine environments induces oscillations in biogeochemical conditions, which further influence the efficacy of *in situ* Hg stabilization using biochars. For example, remobilization of Hg associated with DOC occurs in the OAK-amended systems after drying and rewetting (Chapter 3). In the MOAK-amended systems, remobilization of Hg associated with DOC was limited, but increases in MeHg were observed in both aqueous and solid phases (Chapter 3). Increases in Mn, Fe, SO_4^{2-} and HS^- concentrations associated with microbially-driven disproportionation of polysulfur on MOAK and changes in S chemistry in MOAK-amended systems during drying and rewetting may generate conditions

favourable for MeHg production (Benoit et al., 1999; Chiasson-Gould et al., 2014; Graham et al., 2012, 2017; Jonsson et al., 2017; Liem-Nguyen et al., 2016). Repeated drying and rewetting events in floodplains further alter biogeochemical conditions in the MOAK-amended system which influence the release of Hg and MeHg. Increases in MeHg concentrations have been reported with fluctuations of Mn concentrations (Dent et al., 2014; Lazareva et al., 2019). Repeated drying and rewetting in floodplains may promote microbial oxidation of S on MOAK (Chapter 5).

Variations in biochar properties may lead to different geochemical responses. Amendment with digestate-based biochars (DIG and 75G25S) containing abundant nutrient elements, O-containing functional groups and elevated S content reduced Hg release in floodplain soil by 99% without increasing MeHg in aqueous and solid phases (Chapter 4). Drying and rewetting of these biochar-amended systems resulted in limited impacts on Hg release, MeHg production as well as shifts in microbial structure (Chapter 4). Under multiple wetting and drying events, oxidation of polysulfur on DIG was not observed although MOAK and DIG contained similar S contents, likely caused by the initial release of SO_4^{2-} inhibiting the growth of sulfur oxidizing bacteria (Chapter 5; Suzuki et al., 1999). Elevated reactive P was observed in the digestate-biochar amended systems under anoxic conditions, after drying and rewetting, and under repeated wetting and drying conditions.(Chapters 4 and 5). In freshwater systems, the bioavailability of P from the biochar-amended systems to phytoplankton community may need to be addressed first. Addition of biochars prepared from distillers` grains, with limited O-containing functional groups, enhanced Hg release in

particulate forms and raised aqueous MeHg concentrations (Chapter 4), likely related to formation of highly bioavailable nanoparticulate metacinnabar (β-HgS) (Poulin et al., 2017).

Different environmental conditions result in release of Hg associated with different predominant fractions, which further affect the efficacy of Hg stabilization in biochar-amended systems. Under fully-saturated conditions, greater decreases in Hg release in both particulate-bound (>0.45 μm) and colloidal (<0.45 μm) fractions in biochar-amended systems were observed when Hg was mainly associated with colloidal fractions (Chapters 3 and 4). Hg is entrained within the biochar porous structure and forms complexes with functionalities on the biochar (Liu et al., 2017, 2018a, 2019a). Under repeated wetting and drying as well as rapid drainage conditions, Hg was mainly associated with particulate fractions (Chapter 5). Greater decrease in the release of particulate fractions (>0.45 μm) occurred with limited decreases in colloidal fractions, likely due to the rapid drainage rates that retain a lesser amount of Hg associated with smaller fractions in the biochar porous structure than particulate fractions.

Results of this thesis suggest that the extent of Hg removal using biochars in riverine environments is dependent on application methods, environmental conditions and biochar properties (Table 6.1; Fig. 6.1). If biochars are applied as a reactive capping mat, materials with high removal capacity, such as OAK, may be used. If biochars are applied as soil amendments, environmental conditions and biochars properties require consideration Biochars with abundant functional groups (e.g., MOAK, DIG, and 75G25S) may be used under conditions that remain fully-saturated and anoxic. Sulfurizing biochars may enhance Hg removal, but the sulfurizing processes may shift surface functionalities toward more

redox-active moieties available for microbial growth. Biochars prepared from anaerobic digestate are more resistant to changes in redox conditions than sulfurized biochars. Fast drainage rates as well as frequent redox oscillations in floodplains may limit Hg removal and generate unintended environmental consequences.

6.3 Research Limitations

Although all laboratory-scale experiments were carefully designed to mimic relevant conditions in riverine environments, these experiments may not fully represent field conditions due to seasonal fluctuations in hydrological, biogeochemical, and climatic conditions. For example, frequency and duration of drying and rewetting vary depending on the season. Changes in frequency and duration of drying and rewetting lead to changes in microbial cumulative respiration and activity (Yu et al., 2014), which may indirectly affect microbially-driven processes. The early flush observed in the biochar-amended systems under repeated drying and rewetting conditions (Chapter 5) may recur in the field during a heavy rain after a long period of drought. More extreme weather conditions are expected to occur as a result of climate change, which may further influence the effectiveness of Hg removal using biochars in the field.

This research focused on the impacts of environmental conditions, other factors may affect the long-term kinetic reactions, such as biochar particle size and biochar to solid ratio, are not evaluated. Changes in biochar particle size and biochar to solid ratio affect geotechnical properties of soil (Reddy et al. ,2015). Release of fine biochar particles may occur during an early flush, resulting in increase in biochar particle size and decreases in biochar to solid ratio

in amended systems. Long-term biochar stability needs to be considered together with changes in environmental conditions.

This research focused on sediments collected at a few locations along the South River. Previous studies showed that variations in sediment properties (e.g., organic content, Fe and Mn oxides, predominant Hg phases and microbial communities) affect the associated Hg release and MeHg production (Lazareva et al., 2019; Poulin et al., 2016; Schwartz et al., 2019). Implementing remediation operations in the South River or other Hg contaminated systems will require careful characterization of local soils and sediments to maximize control of Hg release and bioavailability.

6.4 Future Directions

Both MOAK, DIG, and 75G25S showed greater Hg removal than OAK under anoxic conditions (Chapters 3 and 4), but their potential use as reactive capping materials were not evaluated. Future studies are recommended to evaluate DIG or MOAK as reactive capping materials under saturated-flow conditions as well as flooding and drainage conditions.

Mid-scale pilot studies may assist in evaluation of the effectiveness of Hg stabilization using selected biochars under local environments and impacts of seasonal fluctuations. Although, data obtained from this thesis might not be directly applied in the field, experimental designs can provide initial information on geochemical and microbial evaluations of the additions of biochar in field conditions. Biochars may be sandwiched between geotextiles that intercept flow paths or installed along riverbanks. Biochars may be directly applied as soil amendments in floodplains depending on the environmental

conditions. Results obtained from pilot studies should be compared to the results obtained from laboratory-scale systems to evaluate whether laboratory-scale experiments are good predictors of field-scale behavior.

Large-scale applications require careful planning to incorporate sediment characteristics, biochar properties, and local environments. Local sediments may be characterized by grain size, elemental compositions and mineralogy. Synchrotron-based techniques such as HERFD-XAS provide insights regarding predominant Hg phases in local sediments. Biochar properties control the effectiveness of Hg removal and their environmental consequences. Biochars that are redox-sensitive should not be applied in environments that are exposed to frequent redox oscillations. Biochars with elevated nutrients may not be suitable for freshwater systems or any systems that are sensitive to nutrient release.

Other biochars with different raw materials may result in different environmental consequences. Sulfurizing hardwood biochar after pyrolysis enhanced Hg removal, but polysulfur on the biochar is available for microbially-driven S oxidation. Sulfurizing biochar prior to pyrolysis may stabilize S-containing groups in the biochar structure (Huang et al., 2019). Future studies on sulfurizing biochar prior to pyrolysis may be useful for evaluating alternative reactive materials.

Table 6.1 Application of biochars for *in situ* Hg stabilization under different conditions showing 0.45-µm THg removal, peak aqueous MeHg concentrations, and measured solid MeHg content.

Biochar		OAK		MOAK		DIS		DIG		75G25S	
Description		Hardwood biochar		Sulfurized-hardwood biochar		100% Distillers` Grains		100% Digestate		75% Digestate +25% Distillers`	
		THg removal	MeHg	THg removal	MeHg	THg removal	MeHg	THg removal	MeHg	THg removal	MeHg
Batch experiment	Spiked ultrapure water	☺ [1]	NA		NA	NA	NA	NA	NA	NA	NA
	Spiked simulated groundwater	☺ [1]	NA	☺ [2]	NA	NA	NA	NA	NA	NA	NA
Reactive capping mat	Saturated-flow	☺ [1]			NA	NA	NA	NA	NA	NA	NA
	Flooding and drainage	☺ [2]			NA	NA	NA	NA	NA	NA	NA
Soil amendments	Saturated-flow	☹ [5]	☺ [5]	☺ [5]	☺	NA	NA	NA	NA	NA	NA
	Saturated and anoxic (up to 200d)	☹ [6] 😐 [7]	☺ [6] ☺ [7]	☺% [7]	☺ [7]	😐 [8]	☹ [8]	☺ [8]	☺ [8]	☺ [8]	☺ [8]
	Drying for 90d and rewetting for 90d		↓ [7]	↓ [7]	↑ [7]	↓	↓	↓	↓	↓	↓
	Long-term drying and rewetting	NA	NA	😐 [9]	☹ [9]	NA	NA	☹ [9]	☺ [9]	NA	NA

Notes:
The highest THg removal over experimental durations:
☺ >80%; 😐 20-79%; ☹ <20%
MeHg production:
☺ similar to control; ☹ higher than control
NA: Not applicable
Drying and rewetting compared to initial conditions:
↑ increases; ↓ decreases; ─ limited changes

References:
[1] Liu et al. (2016)
[2] Liu et al. (2018a)
[3] Paulson (2014)
[4] Wang et al. (2019)
[5] Fellin (2016)
[6] Liu et al. (2018b)
[7] Chapter 3
[8] Chapter 4
[9] Chapter 5

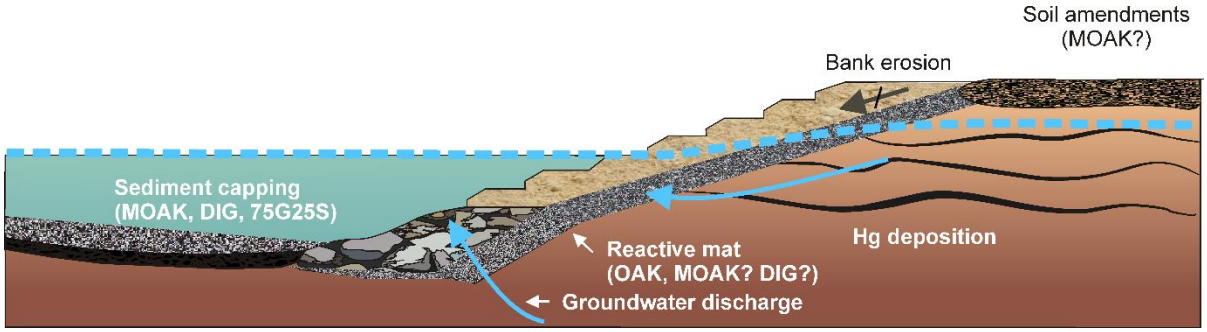

Fig. 6.1 Proposed biochar applications according to results obtained from the evaluated experimental conditions. Question marks (?) represent further studies are recommended before field installations.

References

Abujablah, I., Doyle, R., Bowman, J.P., 2016. The effect of biochar loading rates on soil fertility, soil biomass, potential nitrification, and soil community metabolic profiels in three different soils. J. Soil. Sediment. 18(1), 148-158. doi: https://doi.org/10.1007/s11368-017-1733-1

Adler Miserendino, R., Guimarães, J.R.D., Schudel, G., Ghosh, S., Godoy, J.M., Silbergeld, E.K., Lees, P.S.J., Bergquist, B.A., 2018. Mercury Pollution in Amapá, Brazil: Mercury Amalgamation in Artisanal and Small-Scale Gold Mining or Land-Cover and Land-Use Changes? ACS Earth Sp. Chem. 2, 441–450. doi:10.1021/acsearthspacechem.7b00089

Akar, T., Tunali, S., 2006. Biosorption characteristics of Aspergillus flavus biomass for removal of Pb(II) and Cu(II) ions from an aqueous solution. Bioresour. Technol. 97, 1780–1787. doi:10.1016/j.biortech.2005.09.009

Akcil, A., Erust, C., Ozdemiroglu, S., Fonti, V., Beolchini, F., 2014. A review of approaches and techniques used in aquatic contaminated sediments: Metal removal and stabilization by chemical and biotechnological processes. J. Clean. Prod. 86, 24–36. doi:10.1016/j.jclepro.2014.08.009

Al, T.A., Leybourne, M.I., Maprani, A.C., MacQuarrie, K.T., Dalziel, J.A., Fox, D., Yeats, P.A., 2006. Effects of acid-sulfate weathering and cyanide-containing gold tailings on the transport and fate of mercury and other metals in Gossan Creek: Murray Brook mine, New Brunswick, Canada. Appl. Geochemistry 21, 1969–1985. doi:10.1016/j.apgeochem.2006.08.013

Allison, J.D., Brown, D.S., Novo-Gradac, K.J., 1991. MINTEQA2/PRO-DEFA2: A Geochemical Assessment Model for Environmental Systems. Version 3.0 User`s Manual. Washington, D.C.

Alpers, C.N., Hunerlach, M.P., May, J.T., Hothem, R.L., Taylor, H.E., Antweiler, R.C., De Wild, J.F., and Lawler, D.A., 2005. Geochemical characterization of water, sediment, and biota affected by mercury contamination and acidic drainage from historical gold mining, Greenhorn Creek, Nevada County, California, 1999-2001: U.S. Geological Survey Scientific Investigations Report 2004-5251, 278 p. Retrieved on June 16, 2019 at https://pubs.usgs.gov/sir/2004-5251/.

APHA, 2005. Standard Method for Examination of Water and Waste Water, 21st ed.

Ardau, C., Blowes, D.W., Ptacek, C.J., 2009. Comparison of laboratory testing protocols to field observations of the weathering of sulfide-bearing mine tailings. J. Geochemical Explor. 100, 182–191. doi:10.1016/j.gexplo.2008.06.005

Asasian, N., Kaghazchi, T., 2012. Comparison of dimethyl disulfide and carbon disulfide in sulfurization of activated carbons for producing mercury adsorbents. Ind. Eng. Chem. Res. 51, 12046–12057. doi:10.1021/ie3001474

ASTM, 2008. D5373-16 Standard Test Methods for Instrumental Determination of Carbon, Hydrogen, and Nitrogen in Laboratory Samples of Coal 1–11. doi:10.1520/D5373-16.2

ASTM, 2012. Standard D5744-12: Standard Test Method for Laboratory Weathering of Solid Materials Using a Humidity Cell, 1–19. doi:10.1520/D5744-12.2

Babiarz, C., Hoffmann, S., Wieben, A., Hurley, J., Andren, A., Shafer, M., Armstrong, D., 2012. Watershed and discharge influences on the phase distribution and tributary loading of total mercury and methylmercury into Lake Superior. Environ. Pollut. 161, 299–310. doi:10.1016/j.envpol.2011.09.026

Bachmann, H.J., Bucheli, T.D., Dieguez-Alonso, A., Fabbri, D., Knicker, H., Schmidt, H.P., Ulbricht, A., Becker, R., Buscaroli, A., Buerge, D., Cross, A., Dickinson, D., Enders, A., Esteves, V.I., Evangelou, M.W.H., Fellet, G., Friedrich, K., Gasco Guerrero, G., Glaser, B., Hanke, U.M., Hanley, K., Hilber, I., Kalderis, D., Leifeld, J., Masek, O., Mumme, J., Carmona, M.P., Calvelo Pereira, R., Rees, F., Rombolà, A.G., De La Rosa, J.M., Sakrabani, R., Sohi, S., Soja, G., Valagussa, M., Verheijen, F., Zehetner, F., 2016. Toward the standardization of biochar analysis: The COST action TD1107 interlaboratory comparison. J. Agric. Food Chem. 64, 513–527. doi:10.1021/acs.jafc.5b05055

Bailey, L.T., Mitchell, C.P.J., Engstrom, D.R., Berndt, M.E., Coleman Wasik, J.K., Johnson, N.W., 2017. Influence of porewater sulfide on methylmercury production and partitioning in sulfate-impacted lake sediments. Sci. Total Environ. 580, 1197–1204. doi:10.1016/j.scitotenv.2016.12.078

Beckers, F., Awad, Y.M., Beiyuan, J., Abrigata, J., Mothes, S., Tsang, D.C.W., OK, Y.S., Rinklebe, J., 2019. Impact of biochar on mobilization, methylation, and ethylation of mercury under dynamic redox conditions in a contaminated floodplain soil. Environ.Int. 127, 276-290 doi:10.1016/j.envint.2019.03.040

Benoit, J.M., Gilmour, C.C., Mason, R.P., Heyes, A., 1999. Sufide controls on bioavailability to methylating bacteria in sediment pore waters. Environ. Sci. Technol. 33, 951–957

Benoit, J.M., Gilmour, C.C., Mason, R.P., 2001. The influence of sulfide on solid phase mercury bioavailability for methylation by pure cultures of. Environ. Sci. Technol. 35, 127–132. doi:10.1021/es001415n

Benson, D.A., Karsch-Mizrachi, I., Lipman, D.J., Ostell, J., Sayers, E.W., 2009. GenBank. Nucleic Acids Res. 37, D26–D31. doi:10.1093/nar/gkn723

Bergeron, C., Hopkins, W.A., Todd, B.D., Hepner, M.J., Unrine, J.M., 2011. Interactive effects of maternal and dietary mercury exposure have latent and lethal consequences for amphibian larvae. Environ. Sci. Technol. 45(8), 3781-3787. doi : 10.1021/es104210a

Bloom, N.S., Preus, E., Katon, J., Hiltner, M., 2003. Selective extractions to assess the biogeochemically relevant fractionation of inorganic mercury in sediments and soils. Anal. Chim. Acta 479, 233–248. doi:10.1016/S0003-2670(02)01550-7

Borch, T., Kretzschmar, R., Kappler, A., Van Cappellen, P., Ginder-Vogel, M., Voegelin, A., Campbell, K., 2010. Biogeochemical redox processes and their impact on contaminant dynamics. Environ. Sci. Technol. 44, 15–23. doi: 10.1021/es9026248

Böttcher, M.E., Thamdrup, B., Vennemann, T.W., 2001. Oxygen and sulfur isotope fractionation during anaerobic bacterial disproportionation of elemental sulfur. Geochim. Cosmochim. Acta 65, 1601–1609. doi:10.1016/S0016-7037(00)00628-1

Bravo, A.G., Peura, S., Buck, M., Ahmed, O., Mateos-Rivera, A., Ortega, S.H., Schaefer, J.K., Bouchet, S., Tolu, J., Björn, E., Bertilsson, S., 2018. Methanogens and iron-reducing bacteria: the overlooked members of mercury-methylating microbial

ommunities in boreal lakes. Appl. Environ. Microbiol. 84, 1–16. doi:10.1128/AEM.01774-18
Brooks, S.C., Southworth, G.R., 2011. History of mercury use and environmental contamination at the Oak Ridge Y-12 Plant. Environ. Pollut. 159, 219-228. doi: 10.1016/j.envpol.2010.09.009
Bundschuh, M., Zubrod, J.P., Seitz, F., Newman, M.C., 2015. Effects of two sorbents applied to mercury-contaminated river sediments on bioaccumulation in and detrital proceccing by Hyalella Azteca. J. Soil. Sediments. 15, 1265-1274. doi: 10.1007/s11368-015-1100-z
Calligaris, M., 2004. Structure and bonding in metal sulfoxide complexes: An update. Coord. Chem. Rev. 248, 351–375. doi:10.1016/j.ccr.2004.02.005
Calligaris, M., Carugo, O., 1996. Structure and bonding in metal sulfoxide complexes. Coord. Chem. Rev. 153, 83–154. doi: 10.1016/0010-8545(95)01193-5
Carter, L.J., 1977. Chemical plants leave unexpected legacy for two Virginia rivers. Science 198, 1015–1020. doi:10.1126/science.198.4321.1015
Cheah, S., Malone, S.C., Feik, C.J., 2014. Speciation of sulfur in biochar produced from pyrolysis and gasification of oak and corn stover. Environ. Sci. Technol. 48, 8474–8480. doi:10.1021/es500073r
Christensen, G.A., Somenahally, A.C., Moberly, J.G., Miller, C.M., King, A.J., Gilmour, C.C., Brown, S.D., Podar, M., Brandt, C.C., Brooks, S.C., Palumbo, A. V., Wall, J.D., Elias, D.A., 2018. Carbon amendments alter microbial community structure and net mercury methylation potential in sediments. Appl. Environ. Microbiol. 84, 1–14. doi:10.1128/AEM.01049-17
Compeau, G.C., Bartha, R., 1985. Sulfate-reducing bacteria: Principal methylators of mercury in anoxic estuarine sediment. Appl. Environ. Microbiol. 50, 498–502.
Cooke, C.A., Balcom, P.H., Biester, H., Wolfe, A.P., 2009. Over three millennia of mercury pollution in the Peruvian Andes. Proc. Natl. Acad. Sci. 106, 8830–8834. doi:10.1073/PNAS.0900517106
Cristol, D.A., Brasso, R.L., Condon, A.M., Fovargue, R.E., Friedman, S.L., Hallinger, K.K., Monroe, A.P., White, A.E., 2008. The movement of aquatic mercury through terrestrial food webs. Science. 320 (5874), 335. doi: 10.1126/science.1154082
Dent, S.R., Beutel, M.W., Gantzer, P., Moore, B.C., 2014. Response of methylmercury, total mercury, iron and manganese to oxygenation of an anoxic hypolimnion in North Twin lake, Washington. Lake Reserv. Manag. 30, 119–130. doi:10.1080/10402381.2014.898350
Dermont, G., Bergeron, M., Mercier, G., 2008. Metal-contaminated soils : Remediation practices and treatment technologies. Pr. Period. Hazard. Toxic Radioact. Waste Manag. 12, 188–209. doi:10.1061/(ASCE)1090-025X(2008)12:3(188)
DeSantis, T.Z., Hugenholtz, P., Larsen, N., Rojas, M., Brodie, E.L., Keller, K., Huber, T., Dalevi, D., Hu, P., Andersen, G.L., 2006. Greengenes, a chimera-checked 16S rRNA gene database and workbench compatible with ARB. Appl. Environ. Microbiol. 72, 5069–5072. doi:10.1128/AEM.03006-05
Desrochers, K.A.N, 2013. Geochemical characterization and assessment of stabilization mechanisms for mercury contaminated riverbank sediments from the South River,

Virginia (USA). MSc Thesis, Earth Sciences, University of Waterloo, Waterloo, ON, Canada.
Desrochers, K.A.N., Paulson, K.M.A., Ptacek, C.J., Blowes, D.W., Gould, W.D., 2015. Effect of electron donor to sulfate ratio on mercury methylation in floodplain sediments under saturated flow conditions. Geomicrobiol. J. 32, 924–933. doi:10.1080/01490451.2015.1035818
Drott, A., Björn, E., Bouchet, S., Skyllberg, U., 2013. Refining thermodynamic constants for mercury(II)-sulfides in equilibrium with metacinnabar at sub-micromolar aqueous sulfide concentrations. Environ. Sci. Technol. 47, 4197–4203. doi:10.1021/es304824n
Duvil, R., Beutel, M.W., Fuhrmann, B., Seelos, M., 2018. Effect of oxygen, nitrate and aluminum addition on methylmercury efflux from mine-impacted reservoir sediment. Water Res. 144, 740–751. doi:10.1016/j.watres.2018.07.071
Eggleston, J., 2009. Mercury loads in the South River and simulation of mercury total maximum daily loads (TMDLs) for the South River, South Fork Shenandoah River, and Shenandoah River: Shenandoah Valley, Virginia Scientific Investigations Report 2009 – 5076, Virginia and Department of Environmental Quality U.S. Environmental Protection Agency.
Fellin, S., 2016. Mercury stabilization in contaminated sediment by co-blending with solid-phase reactive media. MSc Thesis, Earth Sciences, University of Waterloo, Waterloo, ON, Canada.
Feng, W., Borguet, E., Vidic, R.D., 2006. Sulfurization of a carbon surface for vapor phase mercury removal – II: Sulfur forms and mercury uptake. Carbon. 44, 2998–3004. doi:10.1016/J.CARBON.2006.05.053
Fierer, N., Schimel, J.P., 2002. Effects of drying-rewetting frequency on soil carbon and nitrogen transformations. Soil Biol. Biochem. 34, 777–787. doi:10.1016/S0038-0717(02)00007-X
Fierer, N., Schimel, J.P., Holden, P.A., 2003. Influence of drying-rewetting frequency on soil bacterial community strucutre. Microb. Ecol. 45, 63-71. doi: 10.1007/s00248-002-1007-2
Findlay, A.J., 2016. Microbial impact on polysulfide dynamics in the environment. FEMS Microbiol. Lett. 363, 1–12. doi:10.1093/femsle/fnw103
Fitzgerald, W.F., Lamborg, C.H., 2013. Geochemistry of Mercury in the Environment, 11th ed, Treatise on Geochemistry: Second Edition. Elsevier Ltd. doi:10.1016/B978-0-08-095975-7.00904-9
Flanders, J.R., Turner, R.R., Morrison, T., Jensen, R., Pizzuto, J.E., Skalak, K., Stahl, R., 2010. Distribution, behavior, and transport of inorganic and methylmercury in a high gradient stream. Appl. Geochem. 25, 1756–1769. doi:10.1016/j.apgeochem.2010.09.004
Fleming, E.J., Mack, E.E., Green, P.G., Nelson, D.C., 2006. Mercury methylation from unexpected sources: Molybdate-inhibited freshwater sediments and an iron-reducing bacterium. Appl. Environ. Microbiol. 72, 457–464. doi:10.1128/AEM.72.1.457-464.2006
Flynn, T.M., O`Loughlin, E.J., Mishra, B., Dichristina, T.J., Kemner, K.M., 2014. Sulfur-mediated electron shuttling during bacteria iron reduction. Science. 344 (6187), 1039-

1043. doi:10.1126/science.1252066
Fuseler, K., Cypionka, H., 1995. Elemental sulfur as an intermediate of sulfide oxidation with oxygen by Desulfobulbus propionicus. Arch. Microbiol. 164, 104–109. doi:10.1007/s002030050241
Germida, J.J., Janzen, H.H., 1993. Factors affecting the oxidation of elemental sulfur in soils. Fertil. Res. 35, 101–114. doi:10.1007/BF00750224
Ghosh, U., 2011. In-situ sorbent amendments: A new direction in contaminated sediment management. Environ. Sci. Technol. 45, 1163-1168. doi: 10.1021/es102694h
Gibson, B.D., Ptacek, C.J., Lindsay, M.B.J., Blowes, D.W., 2011. Examining mechanisms of groundwater Hg(II) treatment by reactive materials: An EXAFS study. Environ. Sci. Technol. 45, 10415–10421. doi:10.1021/es202253h
Gibson, B.D., Ptacek, C.J., Blowes, D.W., Daugherty, S.D., 2015. Sediment resuspension under variable geochemical conditions and implications for contaminant release. J. Soils Sediments. 15, 1644-1656. doi:10.1007/s11368-015-1106-6
Gilmour, C.C., Henry, E.A., Mitchell, R., 1992. Sulfate stimulation of mercury methylation in freshwater sediments. Environ. Sci. Technol. 26, 2281–2287. doi:10.1021/es00035a029
Gilmour, C.C., Podar, M., Bullock, A.L., Graham, A.M., Brown, S.D., Somenahally, A.C., Johs, A., Hurt, R.A., Bailey, K.L., Elias, D.A., 2013a. Mercury methylation by novel microorganisms from new environments. Environ. Sci. Technol. 47, 11810–11820. doi:10.1021/es403075t
Gilmour, C.C., Riedel, G.S., Riedel, G., Kwon, S., Landis, R., Brown, S.S., Menzie, C.A., Ghosh, U., 2013b. Activated carbon mitigates mercury and methylmercury bioavailability in contaminated sediments. Environ. Sci. Technol. 47, 13001–13010. doi:10.1021/es4021074
Gilmour, C.C., Bell, T., Soren A., Riedel, G., Kopec, D., Bodaly, D., Ghosh, U., 2018. Activated carbon thin-layer placement as an *in situ* mercury remediation tool in a Penobscot River salt marsh. Sci. Total. Environ. 621, 839-848. doi:10.1016/j.scitotenv.2017.11.050
Gomez-Eyles, J.L., Yupanqui, C., Beckingham, B., Riedel, G., Gilmour, C., Ghosh, U., 2013. Evaluation of biochars and activated carbons for in situ remediation of sediments impacted with organics, mercury, and methylmercury. Environ. Sci. Technol. 47, 13721-13729. doi : 10.1021/es403712q
Graham, A.M., Aiken, G.R., Gilmour, C.C., 2012. Dissolved organic matter enhances microbial mercury methylation under sulfidic conditions. Environ. Sci. Technol. 46, 2715–2723. doi:10.1021/es203658f
Graham, A.M., Cameron-Burr, K.T., Hajic, H.A., Lee, C., Msekela, D., Gilmour, C.C., 2017. Sulfurization of dissolved organic matter increases Hg-sulfide-dissolved organic matter bioavailability to a Hg-methylating bacterium. Environ. Sci. Technol. 51, 9080–9088. doi:10.1021/acs.est.7b02781
Gray, J.E., Hines, M.E., Higueras, P.L., Adatto, I., Lasorsa, B.K., 2004. Mercury speciation and microbial transformations in mine wastes, stream sediments, and surface waters t the Almadén mining district, Spain. Environ. Sci. Technol. 38, 4285-4292. doi :

10.1021/es040359d
Graydon, J.W., Zhang, X., Kirk, D.W., Jia, C.Q., 2009. Sorption and stability of mercury on activated carbon for emission control. J. Hazard. Mater. 168, 978–982. doi:10.1016/J.JHAZMAT.2009.02.118
Guedron, S., Cossa, D., Grimaldi, M., Charlet, L., 2011. Methylmercury in tailings ponds of Amazonian gold mines (French Guiana): Field observations and an experimental flocculation method for in situ remediation. Appl. Geochemistry 26, 222–229. doi:10.1016/j.apgeochem.2010.11.022
Gun, J., Goifman, A., Shkrob, I., Kamyshny, A., Ginzburg, B., Hadas, O., Dor, I., Modestov, A.D., Lev, O., 2000. Formation of polysulfides in an oxygen rich freshwater lake and their role in the production of volatile sulfur compounds in aquatic systems. Environ. Sci. Technol. 34, 4741–4746. doi:10.1021/es991389x
Hamelin, S., Amyot, M., Barkay, T., Wang, Y., Planas, D., 2011. Methanogens: Principla methylators of mercury in Lake Periphyton. Environ. Sci. Technol. 45(18), 7693-7700. doi: 10.1021/es2010072
Han, D. suk., Orillano, M., Khodary, A., Duan, Y., Batchelor, B., Abdel-Wahab, A., 2014. Reactive iron sulfide (FeS)-supported ultrafiltration for removal of mercury (Hg(II)) from water. Water Res. 53, 310–321. doi:10.1016/j.watres.2014.01.033
Harahuc, L., Lizama, H.M., Suzuki, I., 2000. Selective inhibition of the oxidation of ferrous iron or sulfur in Thiobacillus ferrooxidans. Appl. Environ. Microbiol. 66, 1031–1037. doi:10.1128/AEM.66.3.1031-1037.2000
Hempel, M., Thoeming, J., 1999. Remediation Techniques for Hg-Contaminated Sites, in: Ebinghaus, R., Turner, R.R., de Lacerda, L.D., Vasiliev, O., Salomons, W. (Eds.), Mercury Contaminated Sites: Characterization, Risk Assessment and Remediation. Springer, Berlin Heidelberg, pp. 113–130.
Hesterberg, D., Chou, J.W., Hutchison, K.J., Sayers, D.E., 2001. Bonding of Hg(II) to reduced organic sulfur in humic acid as affected by S/Hg ratio. Environ. Sci. Technol. 35, 2741–2745. doi:10.1021/es001960o
Hofacker, A.F., Voegelin, A., Kaegi, R., Kretzschmar, R., 2013. Mercury mobilization in a flooded soil by incorporation into metallic copper and metal sulfide nanoparticles. Environ. Sci. Technol. 47, 7739–7746. doi:10.1021/es4010976
Horowitz, H.M., Jacob, D.J., Amos, H.M., Streets, D.G., Sunderland, E.M., 2014. Historical mercury releases from commercial products: global environmental implications. Environ. Sci. Technol. 48, 10242–50. doi:10.1021/es501337j
Horvat, M., Covelli, S., Faganeli, J., Logar, M., Mandié., Rajar, R., Sirca, A., Zagar, D., 1999. Mercury in contaminated coastal environments; a case study: the Gulf of Trieste. Sci. Total. Environ. 237-238, 1999, 43-56. doi.org/10.1016/S0048-9697(99)00123-0
Hsu-Kim, H., Kucharzyk, K.H., Zhang, T., Deshusses, M.A., 2013. Mechanisms regulating mercury bioavailability for methylating microorganisms in the aquatic environment: A critical review. Environ. Sci. Technol. 47, 2441–2456. doi:10.1021/es304370g
Hu, H.Y., Lin, H., Zheng, W., Tomanicek, S.J., Johs, A., Feng, X.B., Elias, D.A., Liang, L.Y., Gu, B.H., 2013. Oxidation and methylation of dissolved elemental mercury by anaerobic bacteria. Nat. Geosci. 6, 751–754. doi:10.1038/ngeo1894

Huang, S., Liang, Q., Geng, J., Luo, H., Wei, Q., 2019. Sulfurized biochar prepared by simplified technic with superior adsorption property towards aqueous Hg(II) and adsorption mechanisms. Mater. Chem. Phys. 121919. doi: 10.1016/j.matchemphys.2019.121919

Husson, O., 2013. Redox potential (Eh) and pH as drivers of soil/plant/microorganism systems: A transdisciplinary overview pointing to integrative opportunities for agronomy. Plant Soil 362, 389–417. doi:10.1007/s11104-012-1429-7

Inyang, M., Gao, B., Yao, Y., Xue, Y., Zimmerman, A.R., Pullammanappallil, P., Cao, X., 2012. Removal of heavy metals from aqueous solution by biochars derived from anaerobically digested biomass. Bioresour. Technol. 110, 50–56. doi:10.1016/j.biortech.2012.01.072

Iovieno, P., Bååth, E., 2008. Effect of drying and rewetting on bacterial growth rates in soil. FEMS Microbiol. Ecol. 65, 400–407. doi:10.1111/j.1574-6941.2008.00524.x

Ippolito, J.A., Strawn, D.G., Scheckel, K.G., Novak, J.M., Ahmedna, M., Niandou, M.A.S., 2012. Macroscopic and molecular investigations of copper sorption by a steam-activated biochar. J. Environ. Qual. 41, 1150. doi:10.2134/jeq2011.0113

Jackson, A., Evers, D., Folsom, S.B., Condon, A.M., Diener, J., Goodrick, L.F., McGann, A.J., Schmerfeld, J., Cristol, D., 2011. Mercury exposure in terrestrial birds far downstream of an historical point source. Environ. Pollut. 159, 3302-3308. doi : 10.1016/j.envpol.2011.08.046

Jalilehvand, F., Leung, B.O., Izadifard, M., Damian, E., 2006. Mercury(II) cysteine complexes in alkaline aqueous solution. Inorg. Chem. 45, 66–73. doi:10.1021/ic0508932

Jay, J.A., Morel, F.M.M., Hemond, H.F., 2000. Mercury speciation in the presence of polysulfides. Environ. Sci. Technol. 34, 2196–2200. doi:10.1021/es9911115

Jia, Y., Huang, H., Sun, G.X., Zhao, F.J., Zhu, Y.G., 2012. Pathways and relative contributions to arsenic volatilization from rice plants and paddy soil. Environ. Sci. Technol. 46, 8090–8096. doi:10.1021/es300499a

Johnson, N.W., Reible, D.D., Katz, L.E., 2010. Biogeochemical changes and mercury methylation beneath an in-situ sediment cap. Environ. Sci. Technol. 44, 7280–7286. doi:10.1021/es100161p

Johnson, R.H., Blowes, D.W., Robertson, W.D., Jambor, J.L., 2000. The hydrogeochemistry of the Nickel Rim mine tailings impoundment, Sudbury, Ontario. J. Contam. Hydrol. 41, 49–80. doi:10.1016/S0169-7722(99)00068-6

Johs, A., Eller, V.A., Mehlhorn, T.L., Brooks, S.C., Harper, D.P., Mayes, M.A., Pierce, E.M., Peterson, M.J., 2019. Dissolved organic matter reduces the effectiveness of sorbents for mercury removal. Sci. Total Environ. 690, 410-416. doi: 10.1016/j.scitotenv.2019.07.001

Jonsson, S., Skyllberg, U., Nilsson, M.B., Westlund, P., Shchukarev, A., Lundberg, E., Bjo, E., 2012. Mercury methylation rates for geochemically relevant Hg^{II} species in sediment. Environ. Sci. Technol. 46, 11653–11659. doi: 10.1021/es3015327

Jørgensen, B.B., 1990. The sulfur cycle of freshwater sediments: Role of thiosulfate. Limnol. Oceanogr. 35, 1329–1342. doi: 10.4319/lo.1990.35.6.1329

Jurjovec, J., Ptacek, C.J., Blowes, D.W., 2002. Acid neutralization mechanisms and metal release in mine tailings: A laboratory column experiment. Geochim. Cosmochim. Acta 66, 1511–1523. doi:10.1016/S0016-7037(01)00874-2

Kampbell, D.H., Vandegrift, S.A., 1998. Analysis of dissolved methane, ethane, and ethylene in ground water by a standard gas chromatographic technique. J. Chromatogr. Sci. 36, 253–256. doi:doi:10.1063/1.555654

Kappler, A., Wuestner, M.L., Ruecher, A., Harter, J., Halama, M., Behrens, S., 2014. Biochar as an electron shuttle between bacteria and Fe(III) minerals. Environ. Sci. Tech. Let. 1, 339-344. doi. 10.1021/ez5002209

Keiluweit, M., Nico, P., 2010. Dynamic molecular structure of plant biomass-derived black carbon (biochar). Environ. Sci. Technol. 44, 1247–1253. doi:10.1021/es9031419

Kiene, R.P., Oremland, R.S., Catena, A., Miller, L.G., Capone, D.G., 1986. Metabolism of reduced methylated sulfur compounds in anaerobic sediments and by a pure culture of an estuarine methanogen. Appl. Environ. Microbiol. 52, 1037–1045.

Kim, C.S., Brown, G.E., Rytuba, J.J., 2000. Characterization and speciation of mercury-bearing mine wastes using X-ray absorption spectroscopy. Sci. Total Environ. 261, 157–168. doi :10.1016/S0048-9697(00)00640-9

Kim, C.S., Bloom, N.S., Rytuba, J.J., Brown, G.E., 2003. Mercury speciation by X-ray absorption fine structure spectroscopy and sequential chemical extractions: A comparison of speciation methods. Environ. Sci. Technol. 37, 5102–5108. doi:10.1021/es0341485

Kim, C.S., Rytuba, J.J., Brown, G.E., 2004. EXAFS study of mercury(II) sorption to Fe- and Al-(hydr)oxides: I. Effects of pH. J. Colloid Interface Sci. 271, 1–15. doi:10.1016/S0021-9797(03)00330-8

Kim, E.A., Luthy, R.G., 2011. Partitioning of dissolved organic matter-bound mercury between a hydrophobic surface and polysulfide-rubber polymer. Water Res. 45, 5441–5448. doi:10.1016/j.watres.2011.08.003

Kim, E.A., Masue-Slowey, Y., Fendorf, S., Luthy, R.G., 2012. Intra-particle migration of mercury in granular polysulfide-rubber-coated activated carbon (PSR-AC). Chemosphere 86, 648–654. doi:10.1016/j.chemosphere.2011.11.012

Klüpfel, L., Keiluweit, M., Kleber, M., Sander, M. 2014. Redox properties of plant biomass-derived black carbon (biochar). Environ. Sci. Technol. 48, 5601-5611. doi: 10.1021/es500906d

Kocman, D., Horvat, M., Pirrone, N., Cinnirella, S., 2013. Contribution of contaminated sites to the global mercury budget. Environ. Res. 125, 160–170. doi:10.1016/j.envres.2012.12.011

Kocman, D., Wilson, S., Amos, H., Telmer, K., Steenhuisen, F., Sunderland, E., Mason, R., Outridge, P., Horvat, M., 2017. Toward an Assessment of the Global Inventory of Present-Day Mercury Releases to Freshwater Environments. Int. J. Environ. Res. Public Health 14, 138. doi:10.3390/ijerph14020138

Krabbenhoft, D., Sunderland, E.M., 2013. Global change and mercury. Science. 341 (6153), 1457-1458. doi: 10.1126/science.1242838

Langman, J.B., Blowes, D.W., Sinclair, S.A., Krentz, A., Amos, R.T., Smith, L.J.D., Pham,

H.N., Sego, D.C., Smith, L., 2015a. Early evolution of weathering and sulfide depletion of a low-sulfur, granitic, waste rock in an Arctic climate: A laboratory and field site comparison. J. Geochemical Explor. 156, 61–71. doi:10.1016/j.gexplo.2015.05.004

Langman, J.B., Blowes, D.W., Veeramani, H., Wilson, D., Smith, L., Sego, D.C., Paktunc, D., 2015b. The mineral and aqueous phase evolution of sulfur and nickel with weathering of pyrrhotite in a low sulfide, granitic waste rock. Chem. Geol. 401, 169–179. doi:10.1016/j.chemgeo.2015.02.024

Lazareva, O., Sparks, D.L., Landis, R., Ptacek, C.J., Ma, J. 2019. Investigation of legacy industrial mercury in floodplain soils: South River, Virginia, USA. Environ. Earth. Sci. 8, 246. doi:10.1007/s12665-019-8253-9

Li, Y., Li, H., Yu, Y., Zhao, J., Wang, Y., Hu, C., Li, H., Wang, G., Li, Y., Gao, Y., 2018. Thiosulfate amendment reduces mercury accumulation in rice (Oryza Sativa L.). Plant. Soil. 430 (1-2), 413-422. doi: 10.1007/s11104-018-3726-2

Liem-Nguyen, V., Skyllberg, U., Björn, E., 2017. Thermodynamic modeling of the solubility and chemical speciation of mercury and methylmercury driven by organic thiols and micromolar sulfide concentrations in boreal wetland soils. Environ. Sci. Technol. 51, 3678–3686. doi:10.1021/acs.est.6b04622

Light, T.S., 1972. Standard solution for redox potential measurements. Anal. Chem. 44, 1038–1039. doi:10.1021/ac60314a021

Liu, J., Wang, J., Ning, Y., Yang, S., Wang, P., Shaheen, S., Feng, X., Rinklebe, J., 2019. Methylmercury production in a paddy soil and its uptake by rice plants as affected by different geochemical mercury pools. Environ. Int. 129, 461-469. doi: 10.1016/j.envint.2019.04.068

Liu, P., Ptacek, C.J., Blowes, D.W., Berti, W.R., Landis, R.C., 2015. Aqueous leaching of organic acids and dissolved organic carbon from various biochars prepared at different temperatures. J. Environ. Qual. 44, 684–695. doi:10.2134/jeq2014.08.0341

Liu, P., Ptacek, C.J., Blowes, D.W., Landis, R.C., 2016. Mechanisms of mercury removal by biochars produced from different feedstocks determined using X-ray absorption spectroscopy. J. Hazard. Mater. 308, 233–242. doi:10.1016/j.jhazmat.2016.01.007

Liu, P., Ptacek, C.J., Blowes, D.W., Finfrock, Y.Z., Gordon, R.A., 2017. Stabilization of mercury in sediment by using biochars under reducing conditions. J. Hazard. Mater. 325, 120–128. doi:10.1016/j.jhazmat.2016.11.033

Liu, P., Ptacek, C.J., Blowes, D.W., Gould, W.D. 2018a. Control of mercury and methylmercury in contaminated sediments using biochar: A long-term microcosm study. Appl. Geochem. 92, 30-44. doi: 10.1016/j.apgeochem.2018.02.004

Liu, P., Ptacek, C.J., Elena, K.M.A., Blowes, D.W., Gould, D.W., Finfrock, Y.Z., Wang, A.O., Landis, R.C., 2018b. Evaluation of mercury stabilization mechanisms by sulfurized biochars determined using X-ray absorption spectroscopy. J. Hazard. Mater. 347, 114–122. doi:10.1016/j.jhazmat.2017.12.051

Liu, P., Ptacek, C., Blowes, D., Finfrock, Y., 2019a. Mercury distribution and speciation in biochar particles reacted with contaminated sediment up to 1030 days: A synchrotron-based study. Sci. Total Environ. 662, 915–922. doi:10.1016/j.scitotenv.2019.01.148

Liu, P., Ptacek, C.J., Blowes, D.W. 2019b. Mercury complexation with dissolved organic

matter released from thirty six types of biochar. Bull. Environ. Contam. Toxicol. 103 (1), 175-180. doi: 10.1007/s00128-018-2397-2
Lovley, D.R., 2013. Dissimilatory Fe(III)- and Mn(IV)-Reducing Prokaryotes, in: Rosenberg, E., Delong, E.F., Lory, S., Stackebrandt, E., Thompson, F. (Eds.), The Prokaryotes. Springer, Berlin, Heidelberg, pp. 287–308. doi:https://doi.org/10.1007/978-3-642-30141-4_69
Lovley, D.R., Phillips, E.J.P., 1994. Novel processes for anaerobic sulfate production from elemental sulfur by sulfate-reducing bacteria. Appl. Environ. Microbiol. 60, 2394–2399.
Lowry, G. V., Shaw, S., Kim, C.S., Rytuba, J.J., Brown, G.E., 2004. Macroscopic and microscopic observations of particle-facilitated mercury transport from New Idria and Sulphur Bank mercury mine tailings. Environ. Sci. Technol. 38, 5101–5111. doi:10.1021/es034636c
Maest, A., Nordstrom, D.K., 2017. A geochemical examination of humidity cell tests. Appl. Geochem. 81, 109-131. doi: .1016/j.apgeochem.2017.03.016
Manceau, A., Marcus, M.A., Grangeon, S., 2012. Determination of Mn valence states in mixed-valent manganates by XANES spectroscopy. Am. Mineral. 97, 816–827. doi:10.2138/am.2012.3903
Manceau, A., Nagy, K.L., 2012. Quantitative analysis of sulfur functional groups in natural organic matter by XANES spectroscopy. Geochim. Cosmochim. Acta 99, 206–223. doi:10.1016/j.gca.2012.09.033
Manceau, A., Lemouchi, C., Enescu, M., Gaillot, A., Lanson, M., Magin, V., Glatzel, P., Poulin, B.A., Ryan, J.N., Aiken, G.R., Gautier-Luneau, I., Nagy, K., 2015. Formation of mercury sulfide from Hg(II)-thiolate complex in natural organic matter. Environ. Sci. Technol. 49 (16), 9787-9796. doi: 10.1021/acs.est.5b02522
Marvin-DiPasquale, M., Windham-Myers, L., Agee, J.L., Kakouros, E., Kieu, L.H., Fleck, J.A., Alpers, C.N., Stricker, C.A., 2014. Methylmercury production in sediment from agricultural and non-agricultural wetlands in the Yolo Bypass, California, USA. Sci. Total Environ. 484, 288–299. doi:10.1016/j.scitotenv.2013.09.098
Mergler, D., Anderson, H.A., Chan, L.H.M., Mahaffey, K.R., Murray, M., Sakamoto, M., Stern, A.H., 2007. Methylmercury exposure and health effects in humans: A worldwide concern. AMBIO A J. Hum. Environ. 36, 3–11. doi:10.1579/0044-7447(2007)36[3:MEAHEI]2.0.CO;2
Montgomery, D.C., 2012. Simple comparative experiments, in: Design and Analysis of Experiments. John Wiley & Sons, Inc., Hoboken, NJ, pp. 25–59.
Mosher, J.J., Vishnivetskaya, T.A., Elias, D.A., Podar, M., Brooks, S.C., Brown, S.D., Brandt, C.C., Palumbo, A. V., 2012. Characterization of the Deltaproteobacteria in contaminated and uncontaminated stream sediments and identification of potential mercury methylators. Aquat. Microb. Ecol. 66, 271–282. doi:10.3354/ame01563
Morway, E.D., Thodal, C.E., Marvin-Dipasquale, M., 2017. Long-term trends of surface-water mercury and methylmercury concentrations downstream of historic mining within the Carson River watershed. Eviron. Pollut. 229, 1006-1018. doi:10.1016/j.envpol.2017.07.090
Mucci, A., Bernier, G., Guignard, C., 2015. Mercury remobilization in Saguenay Fjord

(Quebec, Canada) sediments: Insights following a mass-flow event and its capping efficiency. Appl. Geochem. 54, 13–26. doi:10.1016/j.apgeochem.2014.12.008
Mulligan, C.N., Yong, R.N., Gibbs, B.F., 2001. An evaluation of technologies for the heavy metal remediation of dredged sediments. J. Hazard. Mater. 85, 145–163. doi:10.1016/S0304-3894(01)00226-6
Neff, M.R., Bhavsar, S.P., Arhonditsis, G.B., Fletcher, R., Jackson, D. a., 2012. Long-term changes in fish mercury levels in the historically impacted English-Wabigoon River system (Canada). J. Environ. Monit. 14, 2327. doi:10.1039/c2em30324h
Newman, M.C., Xu, Xiaoyu., Condon, A., Liang, L., 2011. Floodplain methylmercury biomagnification factor higher than of the continuous river (South River, Virginia USA). Environ. Pollut. 159 (10), 2840-2844. doi: 10.1016/j.envpol.2011.04.045
Ni, B.J., Huang, Q.S., Wang, C., Ni, T.Y., Sun, J., Wei, W., 2019. Competitive adsorption of heavy metals in aqueous solution onto biochar derived from anaerobically digested sludge. Chemosphere 219, 351–357. doi:10.1016/j.chemosphere.2018.12.053
Nordstrom, D.K., 1977. Thermochemical redox equilibria of ZoBell's solution. Geochim. Cosmochim. Acta 41, 1835–1841. doi:10.1016/0016-7037(77)90215-0
O'Connor, D., Peng, T., Li, G., Wang, S., Duan, L., Mulder, J., Cornelissen, G., Cheng, Z., Yang, S., Hou, D., 2018. Sulfur-modified rice husk biochar: A green method for the remediation of mercury contaminated soil. Sci. Total Environ. 621, 819–826. doi:10.1016/j.scitotenv.2017.11.213
Okabe, S., Ito, T., Sugita, K., Satoh, H., 2005. Succession of internal sulfur cycles and sulfur-oxidizing bacterial communities in microaerophilic wastewater biofilms. Appl. Environ. Microbiol. 71, 2520–2529. doi:10.1128/AEM.71.5.2520-2529.2005
ORNL, Predicted methylators (2016). https://www.esd.ornl.gov/programs/rsfa/data/PredictedMethylators/PredictedMethylators_20160420.pdf. (Accessed 8 April 2019)
Pap, S., Bezanovic, V., Radonic, J., Babic, A., Saric, S., Adamovic, D., Turk Sekulic, M., 2018. Synthesis of highly-efficient functionalized biochars from fruit industry waste biomass for the removal of chromium and lead. J. Mol. Liq. 268, 315–325. doi:10.1016/j.molliq.2018.07.072
Park, J.-H., Wang, J.J., Zhou, B., Mikhael, J.E.R., DeLaune, R.D., 2019. Removing mercury from aqueous solution using sulfurized biochar and associated mechanisms. Environ. Pollut. 244, 627–635. doi:10.1016/j.envpol.2018.10.069
Parkhurst, D.L., Appelo, C., 1999. User`s Guide to PHREEQC (Version 2): A Computer Program for Speciation, Batch-reaction, One-dimensional Transport, and Inverse Geochemical Calculations. US Department of the Interior and US Geological Survey, Denver, CO, USA.
Paulson, K.M.A., 2014. Methylmercury production in riverbank sediments of the South River, Virginia (USA) and assessment of biochar as a mercury treatment option. MSc Thesis, Earth Sciences, University of Waterloo, Waterloo, ON, Canada.
Paulson, K.M.A., Ptacek, C.J., Blowes, D.W., Gould, W.D., Ma, J., Landis, R.C., Dyer, J.A., 2016. Role of organic carbon sources and sulfate in controlling net methylmercury production in riverbank sediments of the South River, VA (USA). Geomicrobiology J.

0, 1–14. doi:10.1080/01490451.2016.1247483
Persson, I., Eriksson, L., Lindqvist-Reis, P., Persson, P., Sandstrom, M., 2008. An EXAFS spectroscopic, large-angle X-ray scattering, and crystallographic study of hexahydrated, dimethyl sulfoxide and pyridine 1-oxide hexasolvated mercury(II) ions. Chem. Eur. J. 14, 6687–6696. doi:10.1002/chem.200800225
Peterson, M.J., Mayes, M.A., Brooks, S.C., Mathews, T.J., Johs, A., Goñes Rodriguez, L., DeRolph, C., Pierce, E., Watson, D.B., Muller, K.A., Olsen, T., Lowe, K., McManamay, R., Smith, J., Morris, J., Jones, M., 2017. Mercury Remediation Technology Development for Lower East Fork Poplar Creek - FY 2017 Progress Report. Oak Ridge National Laboratory, ORNL/TM-2017/480. doi:10.2172/1255676
Pizzuto, J., 2012. Predicting the accumulation of mercury-contaminated sediment on riverbanks-An analytical approach. Water Resour. Res. 48, 1–13. doi:10.1029/2012WR011906
Poulin, B.A., Aiken, G.R., Nagy, K.L., Manceau, A., Krabbenhoft, D.P., Ryan, J.N., 2016. Mercury transformation and release differs with depth and time in a contaminated riparian soil during simulated flooding. Geochim. Cosmochim. Acta 176, 118–138. doi:10.1016/j.gca.2015.12.024
Poulin, B.A., Gerbig, C.A., Kim, C.S., Stegemeier, J.P., Ryan, J.N., Aiken, G.R., 2017. Effects of sulfide concentration and dissolved organic matter characteristics on the structure of nanocolloidal metacinnabar. Environ. Sci. Technol. 51, 13133–13142. doi:10.1021/acs.est.7b02687
Prietzel, J., Thieme, J., Neuhäusler, U., Susini, J., Kögel-Knabner, I., 2003. Speciation of sulphur in soils and soil particles by X-ray spectromicroscopy. Eur. J. Soil Sci. 54, 423–433. doi:10.1046/j.1365-2389.2003.00543.x
Ravel, B., Newville, M., 2005. ATHENA, ARTEMIS, HEPHAESTUS: Data analysis for X-ray absorption spectroscopy using IFEFFIT. J. Synchrotron Radiat. 12, 537–541. doi:10.1107/S0909049505012719
Ravichandran, M., 2004. Interactions between mercury and dissolved organic matter - A review. Chemosphere 55, 319–331. doi:10.1016/j.chemosphere.2003.11.011
Reardon, J., Foreman, J.A., Searcy, R.L., 1966. New reactants for the colorimetric determination of ammonia. Clin. Chim. Acta 14, 403–405. doi: 10.1016/0009-8981(66)90120-3
Reddy, K., Yaghoubi, P., Yukselen-Aksoy, Y. 2015. Effects of biochar amendment on geotechnical properties of landfill cover soil. Waste Manage. Res. 33(6), 524-532. Doi: 10.1177/0734242X15580192
Rezanezhad, F., Couture, R.M., Kovac, R., O'Connel, D., Van Cappellen, P., 2014. Water table flucuations and soil biogeochemistry: An experimental approach using an automated soil column systems. J. Hydrol. 509, 242-256. doi: 10.1016/j.jhydrol.2013.11.036
Rhoades, E.L., O'Neal, M. a., Pizzuto, J.E., 2009. Quantifying bank erosion on the South River from 1937 to 2005, and its importance in assessing Hg contamination. Appl. Geogr. 29, 125–134. doi:10.1016/j.apgeog.2008.08.005
Rimondi, V., Bardelli, F., Benvenuti, M., Costagliola, P., Gray, J.E., Lattanzi, P., 2014.

Mercury speciation in the Mt. Amiata mining district (Italy): Interplay between urban activities and mercury contamination. Chem. Geol. 380, 110–118. doi:10.1016/j.chemgeo.2014.04.023

Sanford, R.A., Cole, J.R., Tiedje, J.M., 2002. Characterization and description of *Anaeromyxobacter* dehalogenans gen. nov., sp. nov., an aryl-halorespiring facultative anaerobic myxobacterium. Appl. Environ. Microbiol. 68, 893–900. doi:10.1128/AEM.68.2.893

Santoro, A., Terzano, R., Blo, G., Fiore, S., Mangold, S., Ruggiero, P., 2010. Mercury speciation in the colloidal fraction of a soil polluted by a chlor-alkali plant: A case study in the South of Italy. J. Synchrotron Radiat. 17, 187–192. doi:10.1107/S0909049510002001

Sayers, E.W., Barrett, T., Benson, D.A., Bryant, S.H., Canese, K., Chetvernin., V., Church, D.M., Dicuccio, M., Edgar, R., Federhen, S., Feolo, M., Geer, L.Y., Helmberg, W., Kapustin, Y., Landsman, D., Lipman, D.J., Madden, T.L., Maglott, D.R., Miller, V., Mizrachi, I., Ostell, J., Pruitt, K.D., Schuler, G.D., Sequeira, E., Sherry, S.T., Shumway, M., Sirotkin, K., Souvorov, A., Starchenko, G., Tatusova, T.A., Wagner, L., Yaschenko, E., Ye, J., 2009. Database resources of the National Center for Biotechnology Information. Nucleic Acids Res. 37, 5–15. doi:10.1093/nar/gkn741

Schaefer, J.K., Morel, F.M.M.M., 2009. High methylation rates of mercury bound to cysteine by Geobacter sulfurreducens. Nat. Geosci. 2, 123–126. doi:10.1038/ngeo412

Schippers, A., Sand, W., 1999. Bacterial leaching of metal sulfides proceeds by two indirect mechanisms via thiosulfate or via polysulfides and sulfur. Appl. Environ. Microbiol. 65, 319–321.

Schouten, S., van Groenigen, J.W., Oenema, O., Cayuela, M.L., 2012. "Bioenergy from cattle manure? Implications of anaerobic digestion and subsequent pyrolysis for carbon and nitrogen dynamics in soil." GCB Bioenergy 4, 751–760. doi:10.1111/j.1757-1707.2012.01163.x

Schwartz, G.E., Sanders, J.P., Mcburney, A.M., Brown, S.S., Ghosh, U., Gilmout, C.C., 2019. Impact of dissolved organic matter on mercury and methylmercury sorption to activated carbon in soils: implications for remediation. Environ. Sci.: Process Impacts, 2019, 21, 485-496. doi:10.1039/c8em00469b

Sela-Adler, M., Ronen, Z., Herut, B., Antler, G., Vigderovich, H., Exkert, W., Sivan, O., 2017. Co-existence of methanogenesis and sulfate reduction with common sustrates in sulfate-rich estuarine sediments. Front. Microbiol. 8, 1–11. doi:10.3389/fmicb.2017.00766

Singer, M.B., Harrison, L.R., Donovan, P. M., Blue, J.D., Marvin-DiPasquale, M., 2016. Hydrologic indicators of hot spot and hot moments of mercury methylation potential along river corridors. Sci. Total. Environ. 568, 691-711. doi:10.1016/j.scitotenv.2016.03.005

Skyllberg, U., Bloom, P.R., Qian, J., Lin, C.M., Bleam, W.F., 2006. Complexation of mercury(II) in soil organic matter: EXAFS evidence for linear two-coordination with reduced sulfur groups. Environ. Sci. Technol. 40, 4174–4180. doi:10.1021/es0600577

Skyllberg, U., Drott, A., 2010. Competition between disordered iron sulfide and natural

organic matter associated thiols for mercury (II)-An EXAFS study. Environ. Sci. Technol. 44, 1254-1259. doi: 10.1021/es902091w
Slowey, A.J., 2010. Rate of formation and dissolution of mercury sulfide nanoparticles: The dual role of natural organic matter. Geochim. Cosmochim. Acta 74, 4693–4708. doi:10.1016/j.gca.2010.05.012
Soil Survey Division Staff., 1993.Soil Survey Manual. U.S. Govt. Printing Office. Retrieved 25 September 2018.
Streets, D.G., Horowitz, H.M., Jacob, D.J., Lu, Z., Levin, L., Ter Schure, A.F.H., Sunderland, E.M., 2017. Total mercury released to the environment by human activities. Environ. Sci. Technol. 51, 5969–5977. doi:10.1021/acs.est.7b00451
Stumm, W., Morgan, J.J., 1996. Aquatic Chemistry, Chemical Equilibria and Rates Waters. 3rd Edition, John Wiley & Sons, Inc., New York.
Sun, D., Bi, Q., Li, K., Zhu, J., Zhang, Q., Jin, C., Lu, L., Lin, X., 2018. Effect of soil drying intensity during an experimental drying-rewetting event on nutrient transformation and microbial community composition. Pedosphere 28, 644–655. doi:10.1016/S1002-0160(17)60450-8
Suzuki, I., Lee, D., Mackay, B., Harahuc, L., Oh, J.K., 1999. Effect of various ions, pH, and osmotic pressure on oxidation of elemental sulfur by Thiobacillus thiooxidans. Appl. Environ. Microbiol. 65, 5163–5168.
Takaoka, S., Fujino, T., Hotta, N., Ueda, K., Hanada, M., Tajiri, M., Inoue, Y., 2014. Signs and symptoms of methylmercury contamination in a First Nations community in Northwestern Ontario, Canada. Sci. Total Environ. 468–469, 950–957. doi:10.1016/j.scitotenv.2013.09.015
Terzano, R., Santoro, A., Spagnuolo, M., Vekemans, B., Medici, L., Janssens, K., Göttlicher, J., Denecke, M.A., Mangold, S., 2010. Solving mercury (Hg) speciation in soil samples by synchrotron X-ray microspectroscopic techniques. Environ. Pollut. 158, 2702–2709. doi:10.1016/j.envpol.2010.04.016
Ting, Y., Chen, C., Ch'ng, B.-L., Wang, Y.-L., Hsi, H.-C., 2018. Using raw and sulfur-impregnated activated carbon as active cap for leaching inhibition of mercury and methylmercury from contaminated sediment. J. Hazard. Mater. 354, 116–124. doi:10.1016/J.JHAZMAT.2018.04.074
Turner, R.R., Southworth, G.R., 1999. Mercury-Contaminated Industrial and Mining Sites in North America: an Overview with Selected Case Studies, in: Ebinghaus, R., Turner, R.R., de Lacerda, L.D., Vasiliev, O., Salomons, W. (Eds.), Mercury Contaminated Sites: Characterization, Risk Assessment and Remediation. Springer, Berlin,Germany, pp. 89–113.
Uchimiya, M., Bannon, D.I., Wartelle, L.H., 2012. Retention of heavy metals by carboxyl functional groups of biochars in small arms range soil. J. Agric. Food Chem. 60, 1798–1809. doi: 10.1021/jf2047898
URS, 2018. Final Report: Ecological Study of the South River and a Segment of the South Fork Shenandoah River, Virginia.
US EPA, 1994. Method 200.2: Sample Preparation Procedure for Spectrochemical Determination of Total Recoverable Elements.

US EPA, 2001. Method 1630: Methyl mercury in water by distillation, aqueous ethylation, purge and trap, and CVAFS. EPA-821-R-01-020.
US EPA, 2002. Method 1631, Revision E: Mercury in water by oxidation, purge and trap, and cold vapor atomic fluorescence spectrometry. EPA-821-R-02-019 38.
US EPA, 2009. Method 415.3, Revision 1.2: Determination of total organic carbon and specific UV absorbance at 254 nm in source water and drinking water. EPA/600/R-09/122.
US EPA, 2019. Regional screening levels (RSL)-generic table. Retrieved at https://www.epa.gov/risk/regional-screening-levels-rsls-generic-tables on Oct 29, 2019.
Waldo, G.S., Carlson, R.M.K., Moldowan, J.M., Peters, K.E., Penner-hahn, J.E., 1991. Sulfur speciation in heavy petroleums: Information from X-ray absorption near-edge structure. Geochim. Cosmochim. Acta 55, 801–814. doi:10.1016/0016-7037(91)90343-4.
Wang, A.O., Ptacek, C.J., Blowes, D.W., Gibson, B.D., Landis, R.C., Dyer, J.A., Ma, J., 2019. Application of hardwood biochar to stabilize mercury derived from contaminated floodplain soil and river bank sediments as a reactive mat in fluvial systems. Sci. Total Environ. 652, 549–561. doi:10.1016/J.SCITOTENV.2018.10.213
Wang, J., Feng, X., Anderson, C.W.N., Xing, Y., Shang, Li., 2012. Remediation of mercury contaminated sites – A review. J. Hazard. Mater. 221-222, 1-18. Doi: 10.1016/j.jhazmat.2012.04.035
Wang, J., Xing, Y., Xie, Y., Meng, Y., Xia, J., Feng, X., 2019. The use of calcium carbonate-enriched clay minerals and diammonium phosphate as novel immobilization agents for mercury remediation: Spectral investigations and field applications. Sci. Total. Environ. 646, 1615-1623. doi: 10.1016/j.scitotenv.2018.07.225
Wang, Q., Garrity, G.M., Tiedje, J.M., Cole, J.R., 2007. Naïve Bayesian classifier for rapid assignment of rRNA sequences into the new bacterial taxonomy. Appl. Environ. Microbiol. 73, 5261–5267. doi:10.1128/AEM.00062-07
Waybrant, K.R., Ptacek, C.J., Blowes, D.W., 2002. Treatment of mine drainage using permeable reactive barriers: Column experiments. Environ. Sci. Technol. 36, 1349–1356. doi:10.1021/es010751g
Werne, J.P., Lyons, T.W., Hollander, D.J., Schouten, S., Hopmans, E.C., Sinninghe Damsté, J.S., 2008. Investigating pathways of diagenetic organic matter sulfurization using compound-specific sulfur isotope analysis. Geochim. Cosmochim. Acta 72, 3489–3502. doi:10.1016/j.gca.2008.04.033
Wilson, D., Amos, R.T., Blowes, D.W., Langman, J.B., Smith, L., Sego, D.C., 2018. Diavik waste rock project: Scale-up of a reactive transport model for temperature and sulfide-content dependent geochemical evolution of waste rock. Appl. Geochem. 96, 177-190. doi: 10.1016/j.apgeochem.2018.07.001
Xing, Y., Wang, J., Xia, J., Liu, Z., Zhang, Y., Du, Y., Wei, W., 2019. A pilot study on using biochars as sustainable amendments to inhibit rice uptake of Hg from a historically polluted soil in a Karst region of China. Ecotox. Environ. Safe. 170, 18-24. doi: 10.1016/j.ecoenv.2018.11.111
Xu, X., Schierz, A., Xu, N., Cao, X., 2016. Comparison of the characteristics and

mechanisms of Hg(II) sorption by biochars and activated carbon. J. Colloid Interface Sci. 463, 55–60. doi:10.1016/j.jcis.2015.10.003

Yang, Z., Haneklaus, S., Singh, B.R., Schnug, E., 2008. Effect of repeated applications of elemental sulfur on microbial population, sulfate concentration, and pH in soils. Commun. Soil Sci. Plant Anal. 39, 124–140. doi:10.1080/00103620701759079

Yang, Z.H., Stöven, K., Haneklaus, S., Singh, B.R., Schnug, E., 2010. Elemental sulfur oxidation by Thiobacillus spp. and aerobic heterotrophic sulfur-oxidizing bacteria. Pedosphere 20, 71–79. doi:10.1016/S1002-0160(09)60284-8

Yao, W., Miller, F.J., 1996. Oxidation of hydrogen sulfide by hydrous Fe(III) oxides in seawater. Mar. Chem. 52, 1–16. doi: 10.1016/0304-4203(95)00072-0

Yu, R.-Q., Flanders, J.R., Mack, E.E., Turner, R., Mirza, M.B., Barkay, T., 2012. Contribution of coexisting sulfate and iron reducing bacteria to methylmercury production in freshwater river sediments. Environ. Sci. Technol. 46, 2684–2691. doi: 10.1021/es2033718

Yu, Z., Wang, G., Marschner, P., 2014. Drying and rewetting – Effect of frequency of cycles and length of moist period on soil respiration and microbial biomass. Eur. J. Soil Biol. 62, 132–137. doi:10.1016/J.EJSOBI.2014.03.007

Zhang, Y., Liu, Y., Lei, P., Wang, Y., Zhong, H., 2018. Biochar and nitrate reduce risk of methylmercury in soils under straw amendment. Sci. Total. Environ. 619-620, 384-390. doi: 10.1016/j.scitotenv.2017.11.106

Zhou, X., Fornara, D., Ikenaga, M., Akagi, I., Zhang, R., Jia, Z., 2016. The resilience of microbial community under drying and rewetting cycles of three forest soils. Front. Microbiol. 7, 1–12. doi:10.3389/fmicb.2016.01101

Appendix A

Supporting Information for Chapter 2

Table A 1 Physicochemical properties of riverbank sediment (SR6) and floodplain soil (MOTO), including concentrations of Hg, and main elements (Al, Ca, Fe, K, Mg, Mn, C) and grain size analysis.

	SR6	MOTO
Description	Riverbank sediment	Floodplain soil
Relative km to historical contaminated site	0.16 km	2.56 km
Hg, µg g^{-1}	280	77
Al, µg g^{-1}	5400	3800
Ca, µg g^{-1}	4100	1600
Fe, µg g^{-1}	16 000	14,000
K, µg g^{-1}	820	920
Mg, µg g^{-1}	930	760
Mn, µg g^{-1}	300	290
C, µg g^{-1}	22 800	15 300
TOC, µg g^{-1}	18 400	24 800
S, µg g^{-1}	400	330
Sand, %	28	26
Silt, %	66	68
Clay, %	7	6

Table A 2 QAQC for THg analysis including 0.45-µm filtered THg, unfiltered THg, and matrix spike. The table contained the number of samples for QAQC, averaged relative standard deviation (% R.S.D), and the averaged relative percent difference (% R.P.D) for 0.45-µm filtered and unfiltered THg.

Samples	0.45-µm THg			unfiltered THg			Matrix Spike	
	NO. Samples	% R.S.D	% R.P.D	NO. Samples	% R.S.D	% R.P.D	NO. Samples	% Recovery
THC-HMT	3	8.27	15.0	4.0	7.57	13.27	8	102
THC-H6S	4	4.62	5.95	7	11.3	21	7	104
HMT	7	19.9	28.9	7	10.4	12.3	3	108
H6S	7	10.2	14.7	7	2.02	2.01	4	108
Average		10.7	16.1		7.82	12.1		106

Table A 3 Chemical information for selected reference compounds including oxidation states, CAS number, chemical structure/formula, and whiteline positions obtained from S K-edge XANES spectra at the Canadian Light Source (Saskatoon, SK).

Compounds	Group	Oxidation state	CAS number/ Origin	Chemical formula	Structural formula	Max Peak eV (Whiteline position)
Pyrrhotite	Inorganic sulfide			$Fe_{1-x}S$		2470.4
Cinnabar	Inorganic sulfide	-2	23333-45-1	α-HgS		2471.2
Pentlandite	Inorganic sulfide			$(Fe, Ni)_{9\pm x}S_8$		2471.8
Pyrite	Inorganic sulfide	-1		FeS_2		2472.4
Marcasite	Inorganic sulfide	-1		FeS_2		2472.4
Metacinnabar	Inorganic sulfide	-2	23333-45-1	β-HgS		2472.2
Sulfur	Elemental sulfur	0		S_8		2472.7
Dibenzyl-disulfide	Exocyclic S	+0.2	150-60-7	$C_{14}H_{14}S_2$	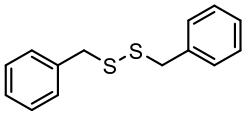	2473.4
L-cysteine	Exocyclic S	+0.5	52-90-4	$C_3H_7NO_2S$	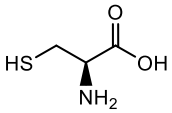	2473.6
Dibenzo-thiophene	Heterocyclic S	+1	132-65-0	$C_{12}H_8S$	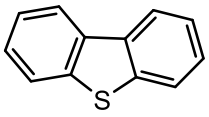	2474.0
Tetramethylene sulfoxide	Sulfoxide	+2	1600-44-8	C_4H_8OS	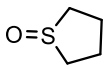	2476.1
Sodium sulfite	Sulfite	+4	7757-83-7	Na_2SO_3		2478.5
Butyl sulfone	Sulfone	+4	598-04-9	$C_8H_{18}O_2S$	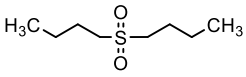	2480.2
Sodium methane sulfonate	Sulfonate	+5	2386-57-4	CH_3NaO_3S	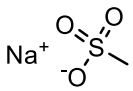	2481.4
Mercury sulfate	Inorganic sulfate	+6	7783-35-9	$HgSO_4$		2483
Ferrous sulfate	Inorganic sulfate	+6	7720-78-7	$FeSO_4$		2482.8
Nickle sulfate	Inorganic sulfate	+6	7786-81-4	$NiSO_4$		2482.9
Potassium sulfate	Inorganic sulfate	+6	7778-80-5	K_2SO_4		2482.2
Gypsum	Inorganic sulfate	+6		$CaSO_4 \cdot 2H_2O$		2482.7

Table A 4 Whiteline positions and scaling factors selected sulfur group.

Sulfur Group	Whiteline position eV	Scaling Factor
Sulfide minerals (pyrrohotite)	2470.4	0.708
Sulfide minerals (cinnabar, pentlandite)	2471.5	0.767
Sulfide minerals (metacinnabar, pyrite)	2472.3	0.809
Exocyclic S	2473.5±0.1	0.873
Heterocyclic S	2474.0	0.899
Sulfoxide	2476.1	1.011
Sulfite	2478.5	1.138
Sulfone	2480.2	1.229
Sulfonate	2481.4	1.292
Sulfate	2482.7±0.3	1.361

Table A 5 Gaussian peak fitting (GPF) and linear combination fitting (LCF) (NSS <0.006) for S K-edge XANES spectra for the biochar collected from different depths in treatment columns THC-HMT and THC-H6S at the end of the experiment.

Sample		pyrrohotite	cinnabar, pentlandite	metacinnabar pyrite	exocyclic S	heterocyclic S	sulfoxide	sulfone	sulfonate	sulfate
		2470.4 eV	2471.5 eV	2472.3 eV	2473.5 eV	2474 eV	2476.1 eV	2480.2 eV	2481.4 eV	2482.7 eV
Unused biochar	GPF	1%	0%	5%	12%	18%	10%	2%	14%	36%
	LCF				28%	29%	14%		5%	24%
THC-HMT 0-2	GPF	0%	0%	5%	8%	25%	6%	5%	16%	35%
	LCF				18%	42%	1%	0%	11%	28%
THC-HMT 2-4	GPF	0%	0%	8%	12%	12%	3%	6%	22%	38%
	LCF	0%	0%	0%	22%	23%	3%	0%	22%	30%
THC-HMT 4-6	GPF	0%	0%	9%	10%	11%	1%	5%	22%	42%
	LCF				25%	14%	0%	0%	23%	36%
THC-H6S 0-2	GPF	0%	4%	12%	11%	20%	2%	5%	15%	30%
	LCF				21%	30%	0%	0%	16%	22%
THC-H6S 2-4	GPF	0%	0%	7%	11%	11%	1%	6%	22%	41%
	LCF				22%	20%	2%	0%	24%	32%
THC-H6S 4-6	GPF	0%	0%	5%	10%	8%	2%	6%	24%	45%
	LCF				16%	18%	2%	0%	28%	36%

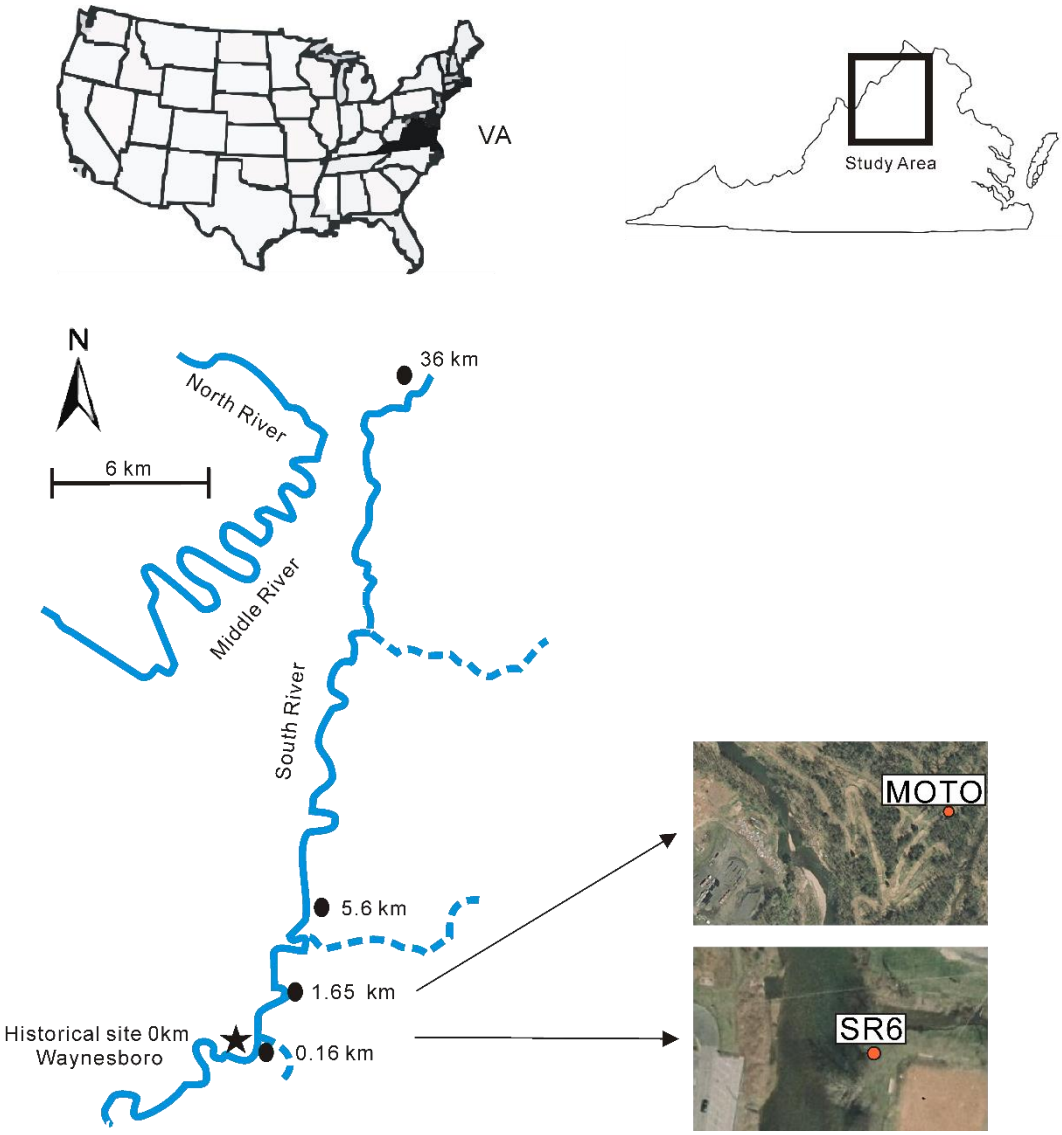

Fig. A 1 Maps showing the sampling location for river bank sediments (SR6) and floodplain soils (MOTO). SR6 was collected near the surface at 0.16 km from the historical disposal site, and MOTO was collected in the centre of a cut-off floodplain at 1.65 km from the historical disposal site.

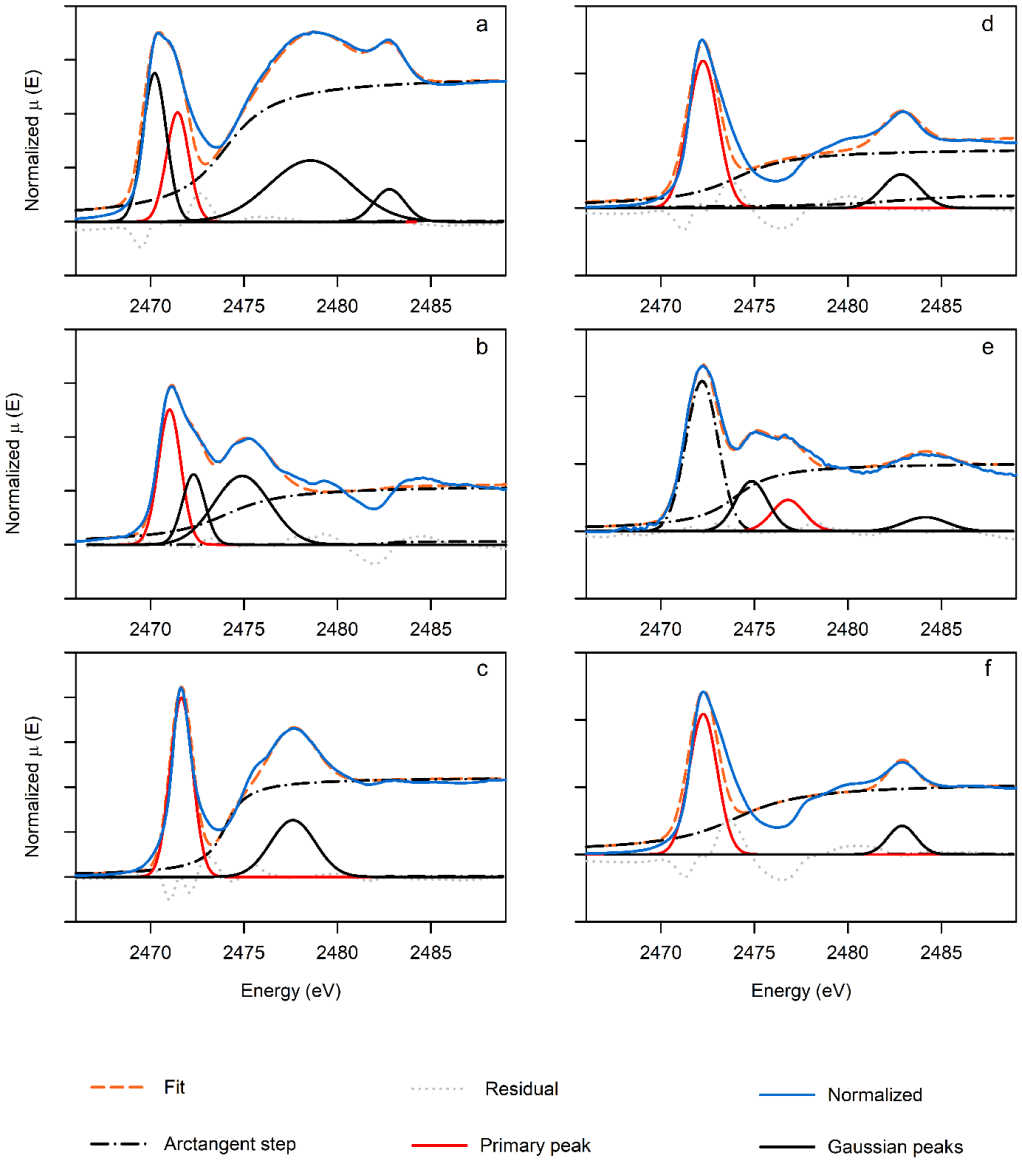

Fig. A 2 Decomposing S K-edge XANES spectra between 2466 and 2489 eV into several Gaussian peaks for sulfide minerals (NSS <0.03), including pyrrhotite (a), cinnabar (b), pentlandite (c), marcasite (d), metacinnabar (e), and pyrite (f).

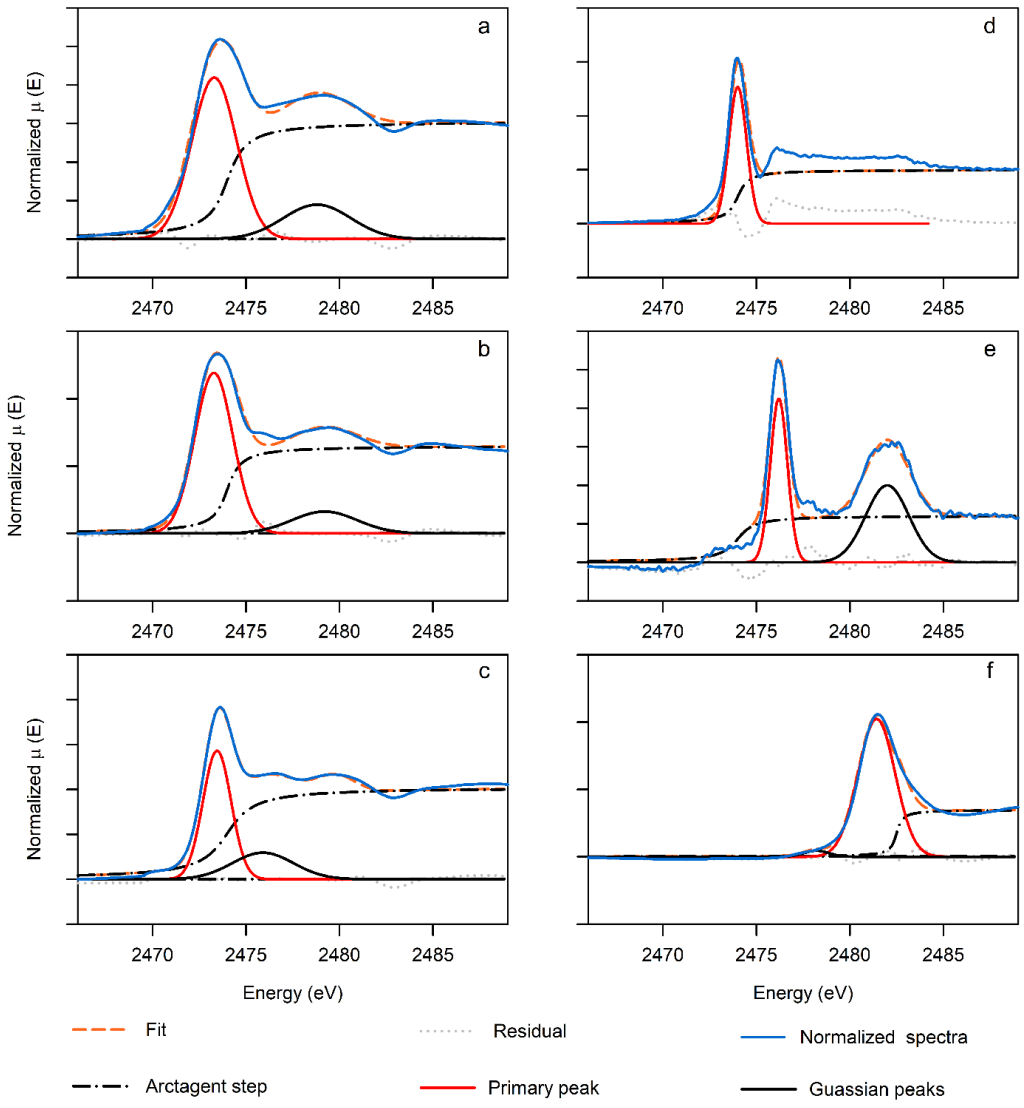

Fig. A 3 Decomposing S K-edge XANES spectra between 2466 and 2489 eV for reduced organic sulfur reference compounds (NSS <0.03), including L-cysteine (a), dibenzyl disulfide (b), and dibenzyl thiofide (c), dibenzo thiophene (d), tetramethylene sulfoxide (e), and butylsulfone (f).

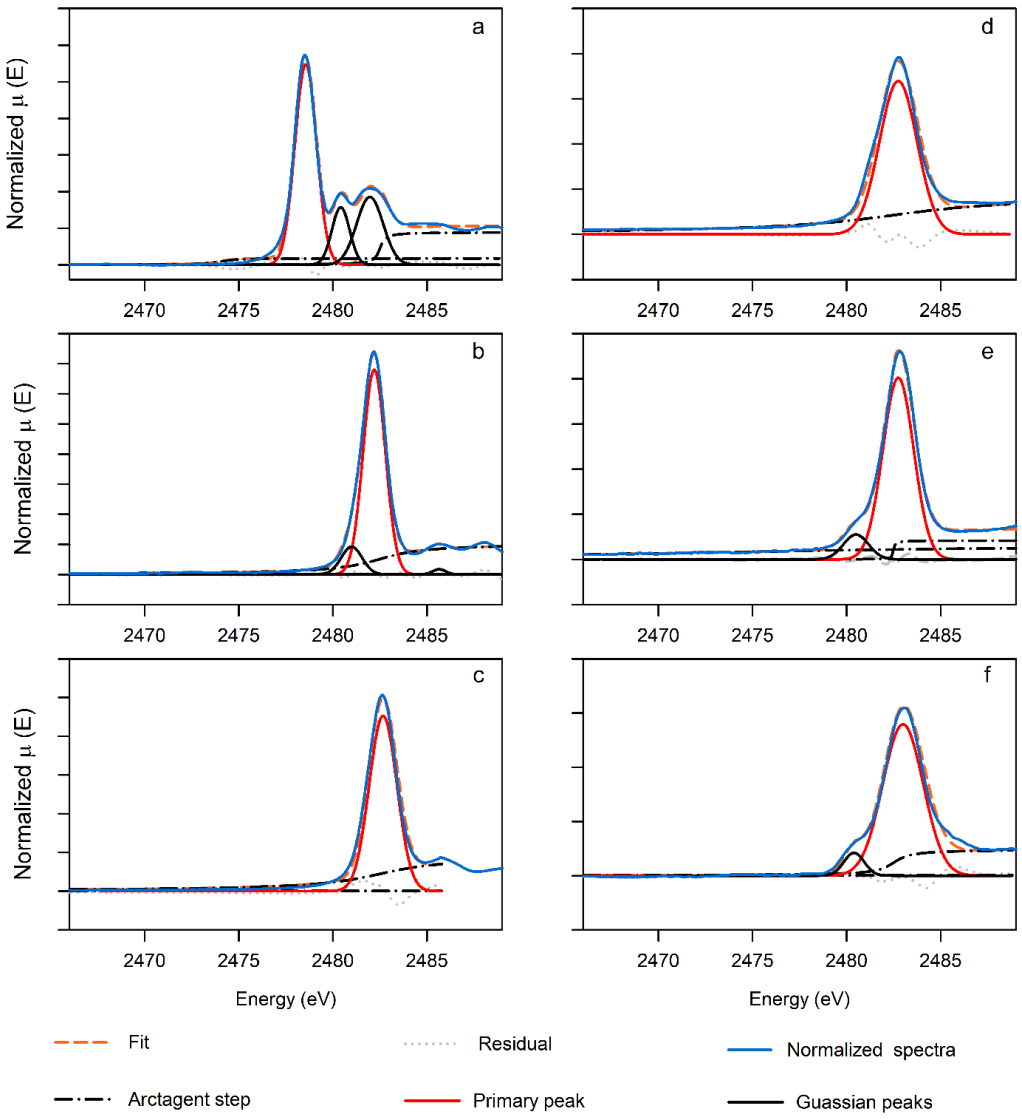

Fig. A 4 Decomposing S K-edge XANES spectra between 2466 eV and 2489 eV for intermediate and oxidized inorganic reference compounds (NSS <0.006), including sodium sulfite (a), potassium sulfate (b), gypsum (c), ferrous sulfate (d), nickel sulfate (e), and mercury sulfate (f).

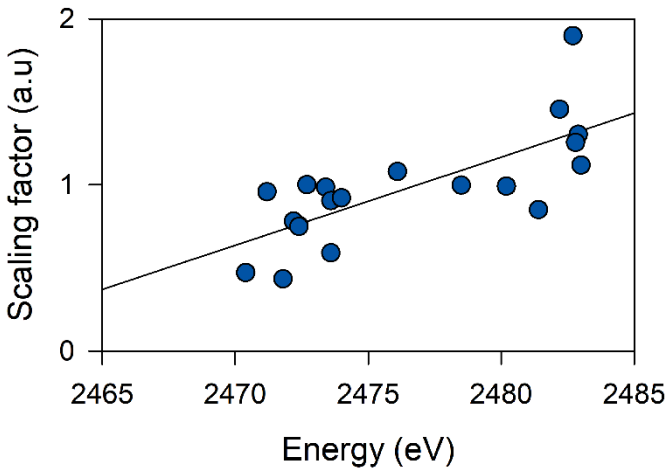

Fig. A 5 Scaling factor used to quantify S functionalities from Gaussian peak fitting. Scaling factors were plotted by normalizing area under whiteline positions for reference compounds to that for elemental S at 2472.7 eV.

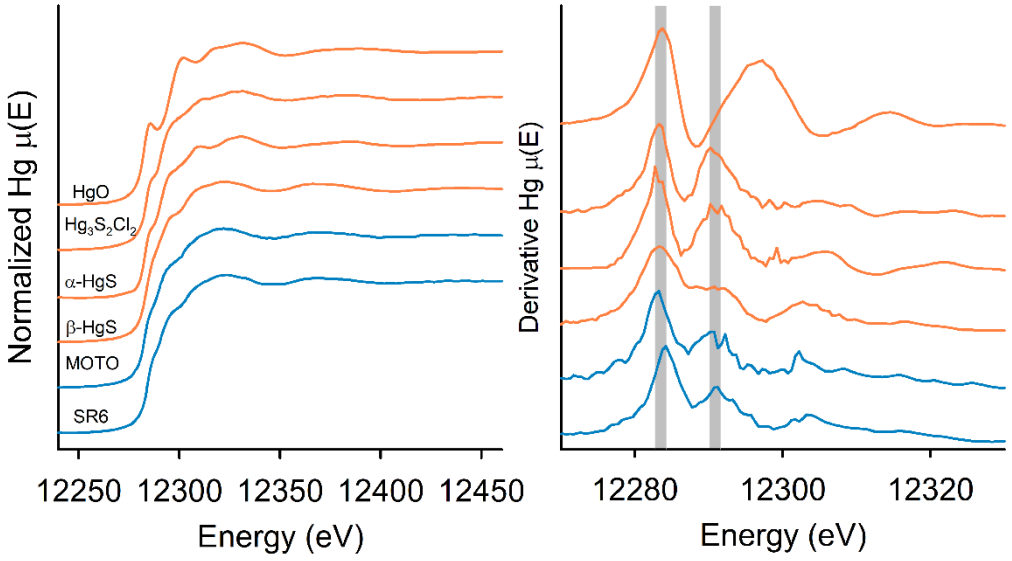

Fig. A 6 Hg L_{III}-edge XANES spectra for selected riverbank sediment (SR6) and floodplain soil (MOTO) collected along the South River, Virginia, USA.

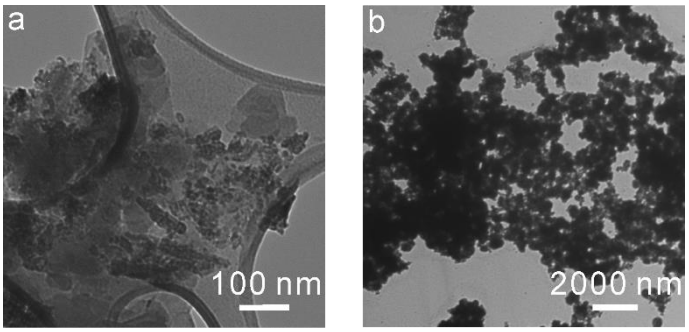

Fig. A 7 Selected transmission electron microscope (TEM) images collected at 60 kV for particles in leachate derived from HMT (a) and H6S (b).

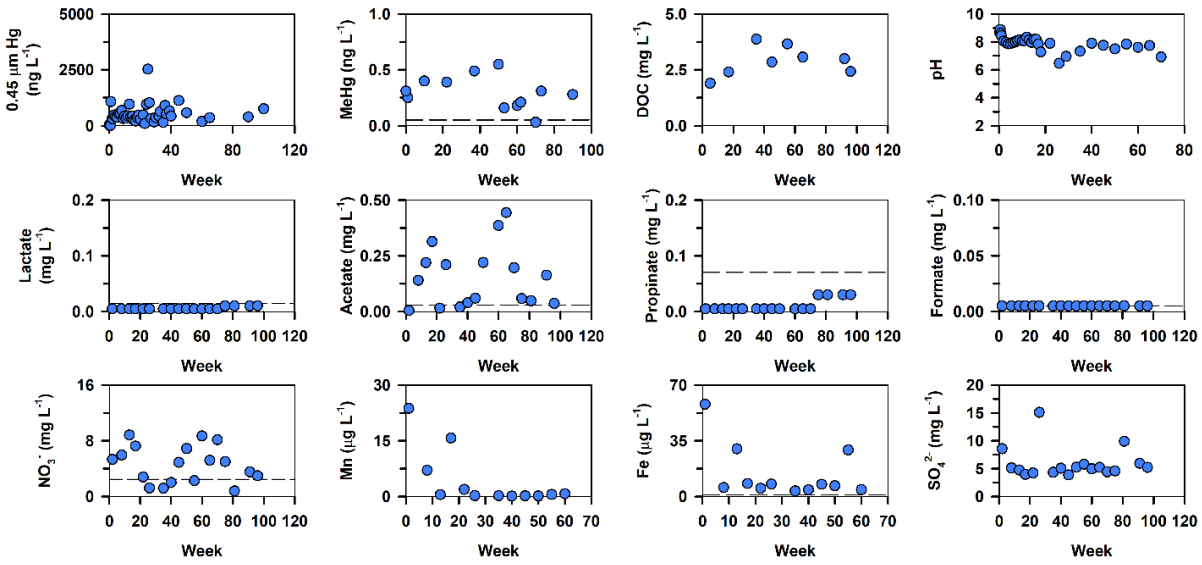

Fig. A 8 Temporal changes in chemical composition of effluent collected from hardwood biochar loaded with leachates from HMT (THC-HMT).

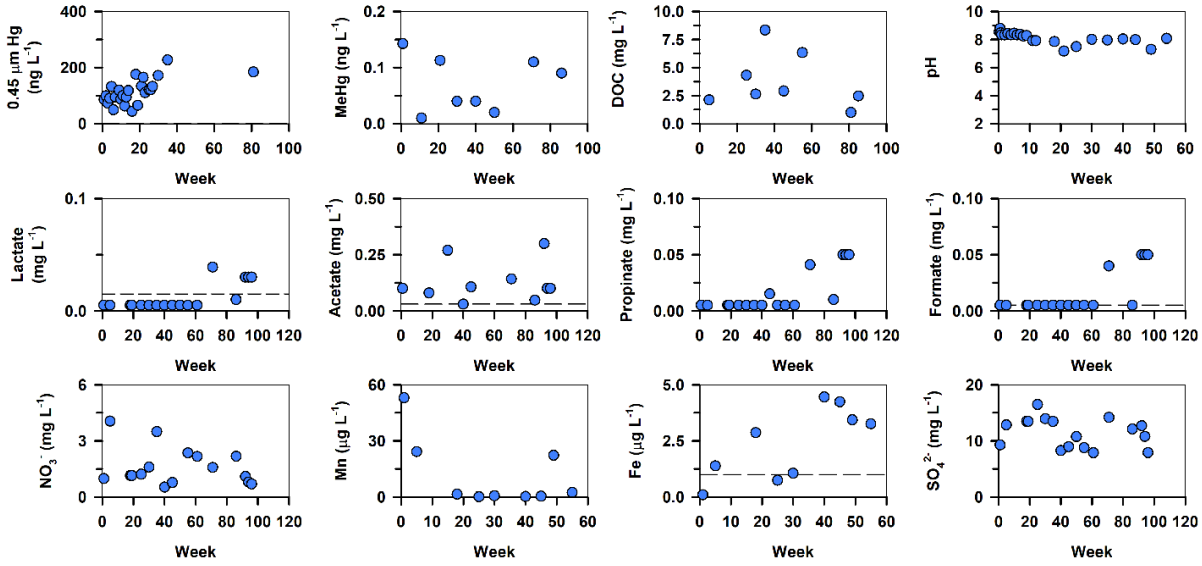

Fig. A 9 Temporal changes in chemical composition of effluent collected from hardwood biochar treatment loaded with leachates collected from H6S (THC-H6S).

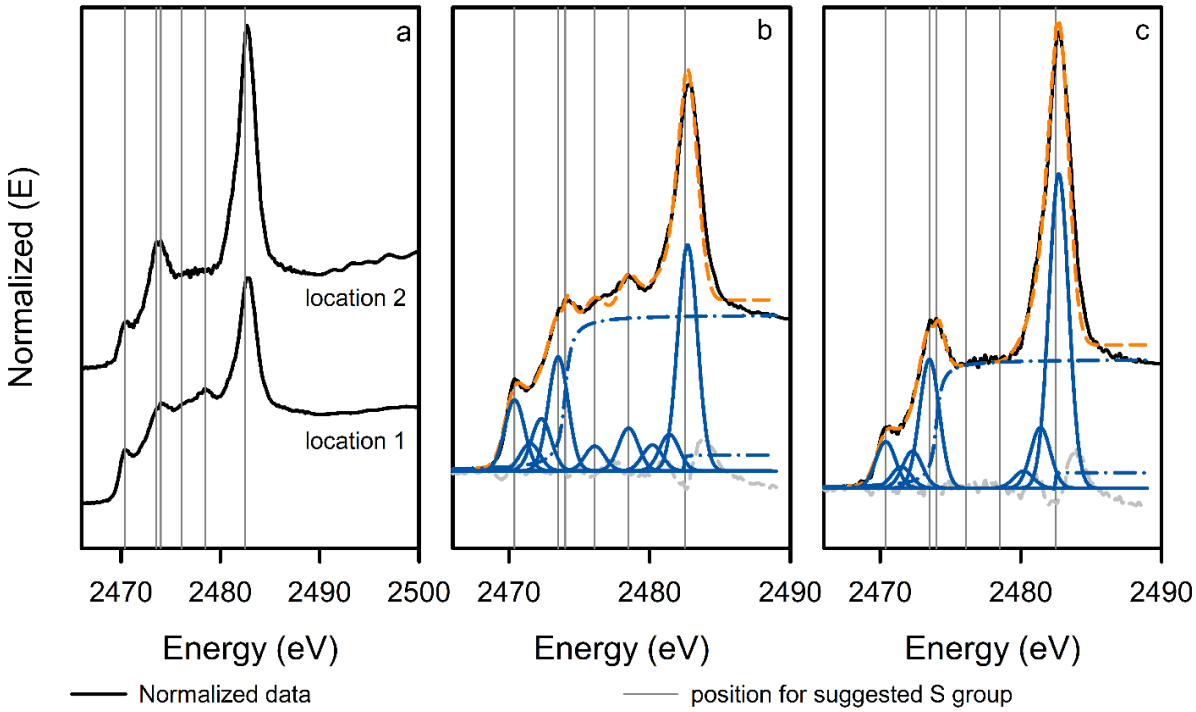

Fig. A 10 Normalized S K-edge μ-XANES (black solid line) spectra for the biochar sample THC-HMT 0-2 (NSS $<3.5\times10^{-3}$) at separate locations (a) and modeled spectra (orange medium dashed line) by decomposing spectra into several Gaussian peaks (blue solid line) for location 1 (b) and location 2 (c). Location 1 was from an area where only μ-XRF maps were collected, and location 2 was close to the area where μ-XANES were collected across Hg L_{III}-edge. Two optimized arctangent steps (blue dash-dot line) were used to simulate reduced sulfur groups at 2474 eV and oxidized sulfur groups at 2482.5 eV. The grey solid lines indicate whiteline positions for sulfide (2470.4 eV, 2472.3 eV), exocyclic sulfide (2473.5 eV), heterocyclic S (2474 eV), sulfoxide (2476.1 eV), and sulfate (2482.7 eV).

Appendix B

Supporting Information for Chapter 3

Experimental Details

Text B 1: Collections of aqueous samples

Aqueous samples were collected using 20-mL polypropylene/ polyethylene sterile Luer Lock syringes (Norm-Ject, Thermo Fisher Scientific). Samples for $CH_{4(aq)}$ (at 120, 160, and 200 d) were collected using gas-tight 30-mL glass syringes (BD Multifit™ Syringes, BD Bioscience). Samples for $CH_{4(aq)}$ were immediately sealed with a two-way polycarbonate stopcock (Cole Parmer Canada Inc.) before storage under water at <4 °C for a maximum of 7 d. Samples for total sulfides were collected passing through 0.45-µm Supor® syringe filters (32-mm in diameter, Acrodisc®, VWR) in gas-tight glass syringes and sealed with three-way polycarbonate stopcocks. The collected total sulfide samples were analyzed within 24 h. Samples for cations, DOC THg, and MeHg were preserved <pH 2 and stored < 4 °C before analysis. Samples for anions, NH_3-N, and PO_4^{3-} were not preserved. Samples for anions were kept frozen before analysis, and samples for NH_3-N and PO_4^{3-} were analyzed within 24 h.

Text B 2: Analytical method

Concentrations of dissolved $CH_{4(aq)}$ were determined on gas chromatography (GC) (7890B, Agilent). Concentrations of major cations were determined using ICP-OES (iCAP 6000, Thermo Scientific). Concentrations of trace elements were determined using ICP-MS (X Series 2, Thermo Scientific). Concentrations of inorganic anions and organic acids were determined using ion chromatography (Dionex™, ICS-5000+ DC, Thermo Fisher Scientific).

Concentrations of DOC were determined on a TOC analyzer (Aurora 1030W TOC analyzer, OI Analytical, College Station, TX, USA). Concentrations of THg (unf, 0.45-µm, 0.2-µm, and 0.1-µm fractions) were determined using CVAFS (Tekran® 2600, Tekran Instruments Corp.).

Text B 3: Pyrosequencing analysis

The 16S rRNA gene V4 variable region PCR primers 515/806 for soil control and biochar-amended systems were conducted by MR DNA Laboratory (Shallowater, TX, USA) in a single-step 30 cycle PCR using a HotStarTaq Plus Master Mix Kit (Qiagen, USA). The reaction conditions were 94 °C for 3 mins, 28 cycles (5 cycles used on PCR products) at 94 °C for 3 s, 53 °C for 40 s, and 72 for 1 min, followed by a final elongation step at 72 °C for 5 min. Sequencing was performed on a Ion Torrent PGM following the manufacturer's guidelines, and sequencing data were analyzed using an in-house analysis pipeline (MR DNA, Shallowater, TX). Sequences were denoised by depleting barcodes and primers and removing sequence data with <150 bp, with ambiguous base calls, and with homopolymer runs exceeding 6 bp. Operational taxonomic units (OTUs) were generated by defining clusters at 97% similarity using a basic local alignment search tool (BLAST) against a curated database derived from Green Gennes (DeSantis et al., 2006), RDP (Wang et al., 2007), and NCBI (Benson et al., 2009; Sayers et al., 2009).

Table and Figures

Table B 1. Elemental composition and grain size classification according to the USDA soil texture classification (Soil Survey Divison Staff, 1993) for floodplain soil collected 36.5 km downstream from the historical release site near South River, VA, USA.

Parameter	Concentration
Hg, µg g^{-1}	57
Al, µg g^{-1}	6700
As, µg g^{-1}	4.4
Ba, µg g^{-1}	140
Ca, µg g^{-1}	1500
Cu, µg g^{-1}	130
Fe, µg g^{-1}	24 000
K, µg g^{-1}	780
Mg, µg g^{-1}	1100
Mn, µg g^{-1}	1500
Na, µg g^{-1}	29
Ni, µg g^{-1}	22
Pb, µg g^{-1}	27
Ti, µg g^{-1}	70
V, µg g^{-1}	20
Zn, µg g^{-1}	100
C, µg g^{-1}	19 090
TOC, µg g^{-1}	14 800
S, µg g^{-1}	159
Sand, %	10.3
Silt, %	80.4
Clay, %	9.3

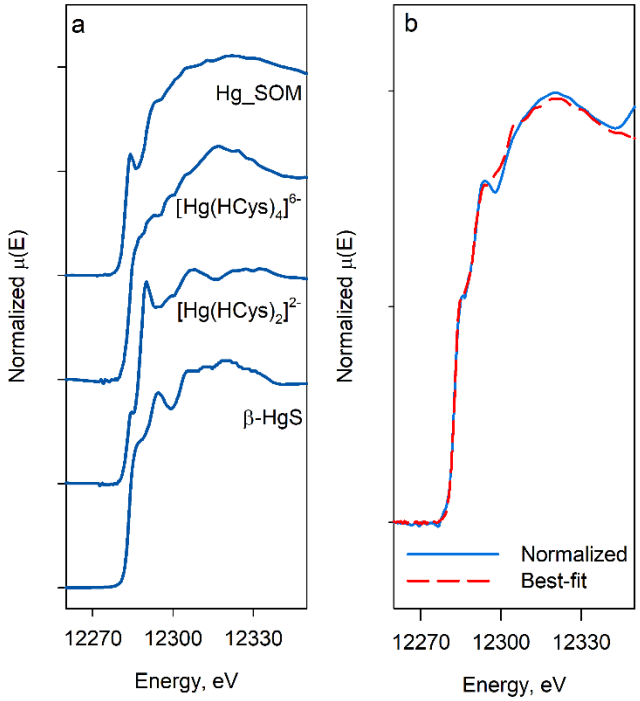

Fig. B 1 High energy resolution fluorescence detection X-ray absorption spectroscopy (HERFD-XAS) at Hg Lα fluorescence emission line for selected references compounds used in linear combination fitting analysis (a) and best-fit showing normalized (blue solid line) and the best-fit (red dashed line) between 12263.6 eV to 12243.6 eV for the floodplain soil collected 36.5 km downstream from the historical release site in South River, VA (b). Selected reference compounds include metacinnabar (β-HgS), two-coordinated $[Hg(HCys)_2]^{2-}$ complexes, four-coordinated $[Hg(HCys)_4]^{6-}$ complexes, and Hg sorbed on soil organic matter.

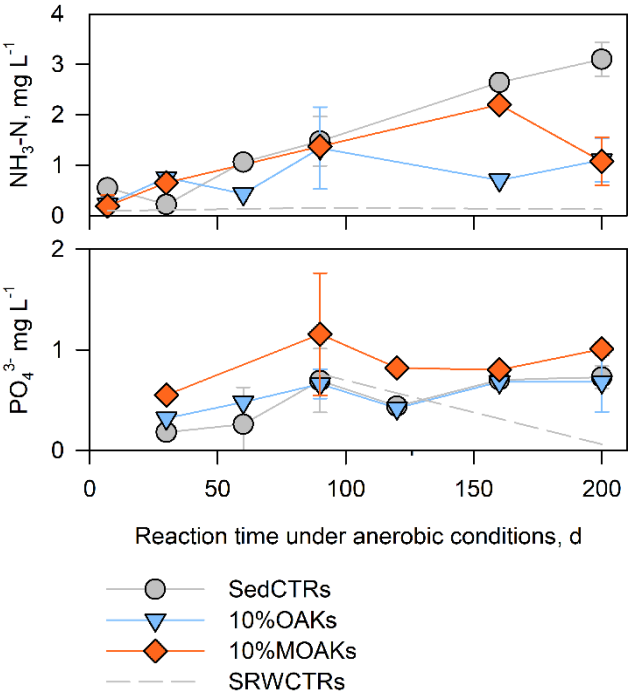

Fig. B 2 Concentrations of NH_3-N and PO_4^{3-} for soil controls (SedCTR), OAK-(10%OAKs) and MOAK-amended systems (10%MOAKs), and river water controls (SRWCTRs) in Stage 1.

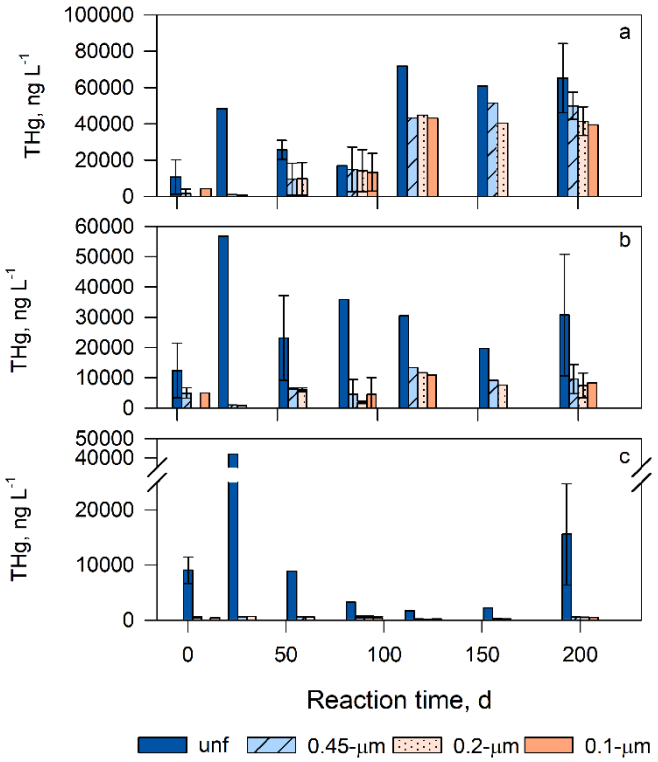

Fig. B 3 Concentrations of Hg passing different filter sizes for soil controls (a), OAK-amended (b), and MOAK-amended (c) systems in Stage 1. Note the axis break in (c) to highlight the low concentrations of filtered Hg.

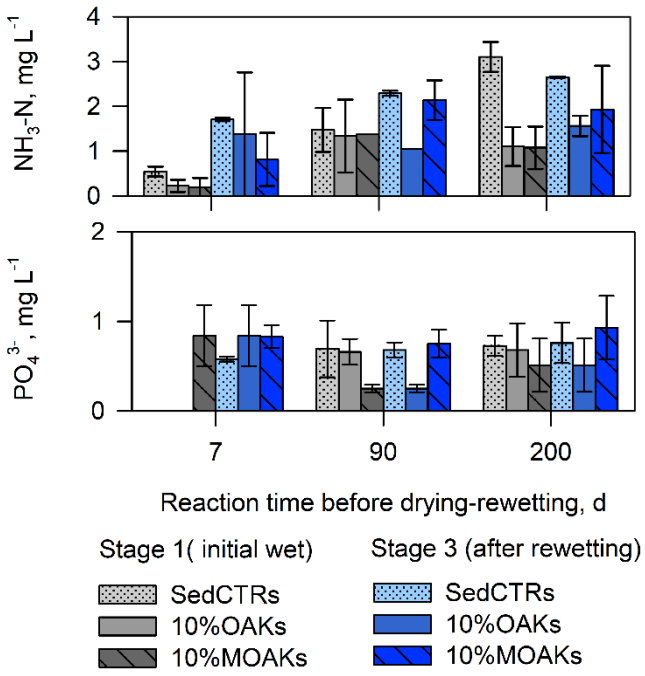

Fig. B 4 Concentrations of NH_3-N and PO_4^{3-} in soil controls (SedCTRs), OAK-amended (10%OAKs) and MOAK-amended systems (10%MOAKs) in Stage 1 (grey bars) and their corresponding systems in Stage 3 (blue bars).

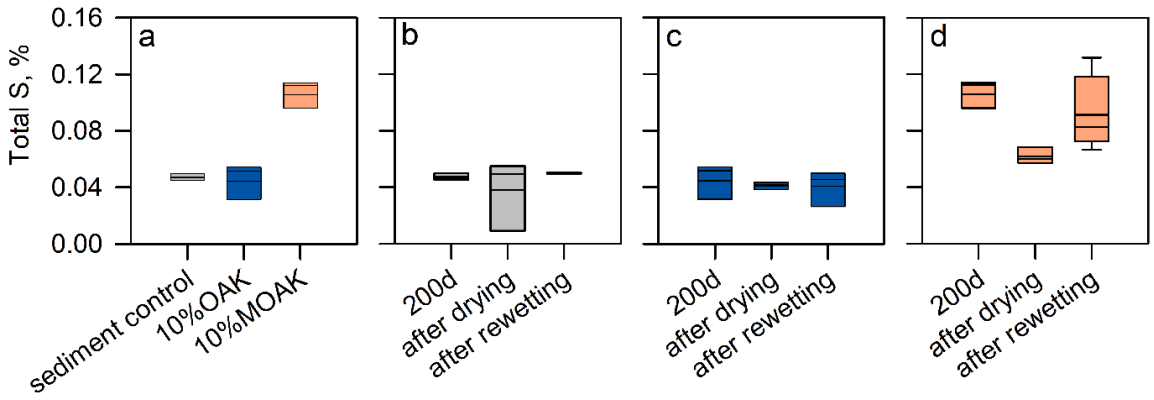

Fig. B 5 Total S content in solid collected in Stages 1 to 3. Total S content in solid reacted for 200 d in Stage 1 (a). Total S content in solid after drying and rewetting compared to reacted for 200 d in Stage 1 for soil control (b), OAK-amended systems (c), and MOAK-amended systems (d). Black solid lines represent mean concentrations.

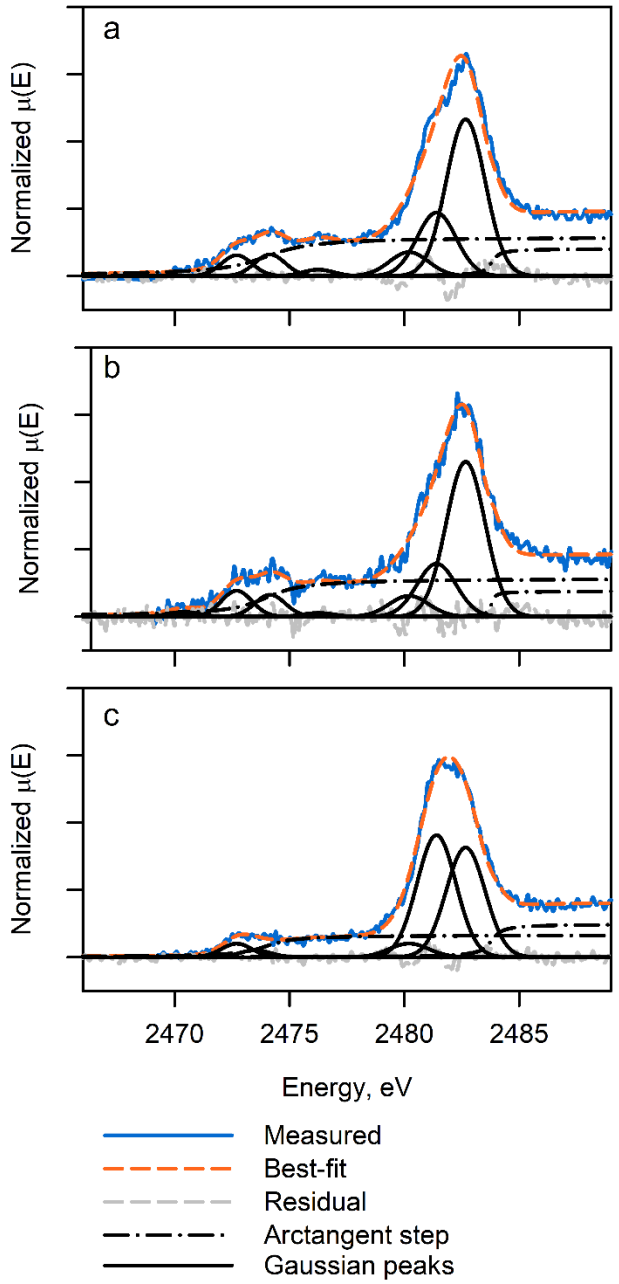

Fig. B 6 S K-edge X-ray absorption near edge structure (XANES) spectroscopy showing measured spectra (blue solid line) and best-fit (orange dash line) from Gaussian peak fitting for solid in soil control reacted for 200 d in Stage 1 (a) (NSS=6.27×10^{-3}) and its corresponding systems in Stages 2(b) (NSS=7.90×10^{-3}), and 3(c) (NSS=1.18×10^{-3}).

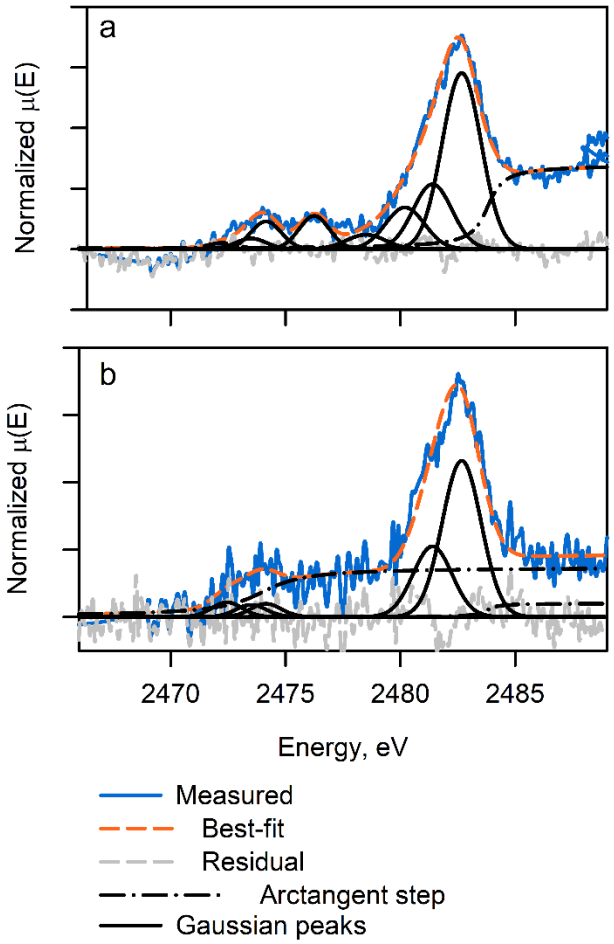

Fig. B 7 S K-edge X-ray absorption near edge structure (XANES) spectroscopy showing measured spectra (blue solid line) and best-fit (orange dash line) from Gaussian peak fitting for solid in 10%OAKs reacted for 200 d in Stage 2 (a) (NSS=9.96×10^{-3}) and its corresponding systems in Stages 3 (b) (NSS=3.06×10^{-2}).

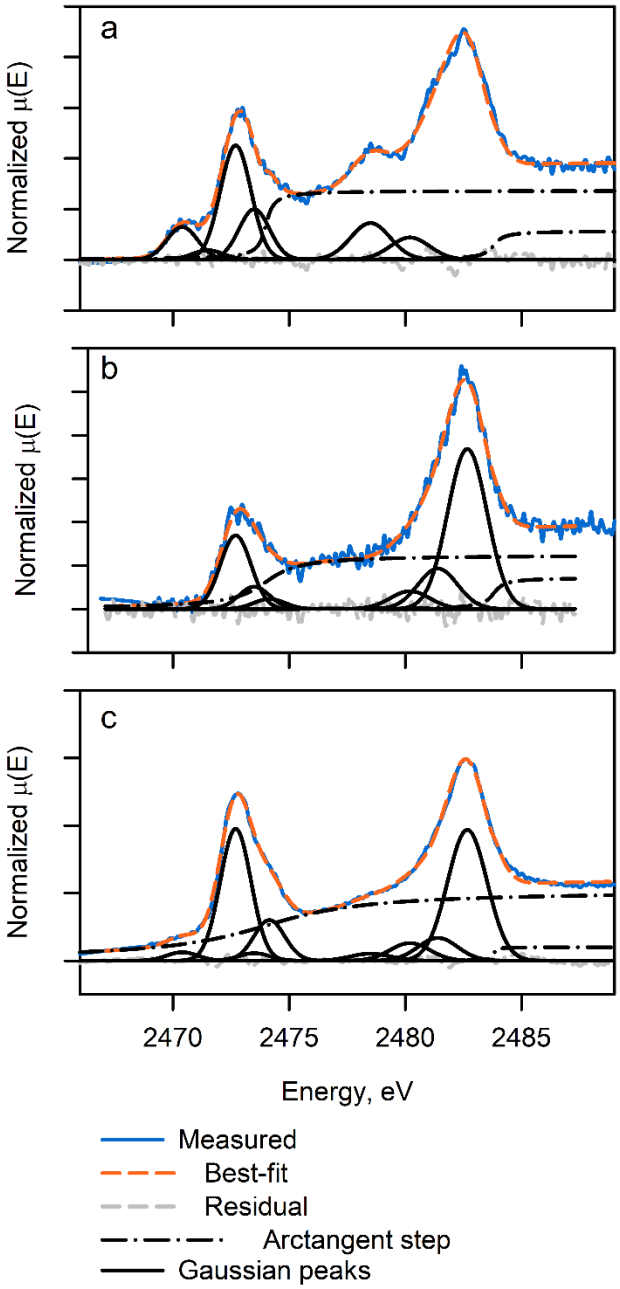

Fig. B 8 S K-edge X-ray absorption near edge structure (XANES) spectroscopy showing measured spectra (blue solid line) and best-fit (orange dash line) from Gaussian peak fitting for solid in s10%MOAKs reacted for 200 d in Stage 1 (a) (NSS=1.69×10^{-3}) and its corresponding systems in Stages 2(b) (NSS=4.11×10^{-3}), and 3(c) (NSS=6.83×10^{-4}).

Appendix C

Supporting Information for Chapter 4

Experimental Details

Text C 1: Analytical methods for (pH, Eh, alkalinity, S^{2-}, NH_4^+, PO_4^{3-}, $CH_{4(aq)}$, DOC, organic acids, anions, and trace elements)

Values of pH and Eh were determined immediately on unfiltered samples when aqueous samples were collected. pH values were determined using a ROSS combination electrode (Orion model 8156, Thermo Scientific) that was calibrated against three standard pH buffers at 7.01, 4.01, and 10.01 (Thermo Fisher Scientific) and checked at 7.01. The slope for the three-point calibration ranged between 98 and 100. Eh values were determined using a combination Pt Ag/AgCl electrode (Orion 9678, Thermo Scientific). The Eh electrodes were checked against Zoebell (Nordstrom, 1977) and Light (Light, 1972) solutions. All Eh values were relative to the standard H_2electrode. Concentrations of alkalinity were determined by titrating samples passing a 0.45-µm filter membrane using standardized 0.16 N H_2SO_4 (Hach LANGE, Dusseldorf, Germany) and bromocresol-green methyl red as an indicator.

Concentrations of total sulfide (S^{2-}), nitrogen, ammonia (NH_3-N), and reactive phosphorus (PO_4^{3-}) were determined using a spectrophotometer (DR 2800™, Hach LANGE, Dusseldorf, Germany) on samples passing 0.45-µm filter membranes within 8 h of collection. Concentrations of total sulfide were determined using the methylene blue method (Hach Method 10023) adapted from Standard Method 4500-S2-D for wastewater (APHA, 2005). Concentrations of NH_3-N were determined using LR Test'N Tube™ vials (Hach, VWR,

Mississauga, ON, Canada) following the salicylate method (Hach Method 10023) adapted from Reardon et al. (1966). Concentrations of PO_4^{3-} were determined using 10-mL phosphate reagent powder pillows following the PhosVer® 3 method (Method 8048 from Hach DR 2800 manual) adapted from Standard Method 4500-PE for wastewater (APHA, 2005). Concentrations of dissolved $CH_{4(aq)}$ were determined using a headspace method (Kampbell and Vandegrift, 1998) on a GC analyzer (7890B, Agilent)

Concentrations of trace elements were determined using inductively coupled plasma mass spectroscopy (ICP-MS) (X Series 2, Thermo Scientific), and concentrations of major cations were determined using inductively coupled plasma optical emission spectrometry (ICP-OES) (iCAP 6000, Thermo Scientific). Concentrations of DOC were determined using a oxidation method following US EPA method 415.3 (US EPA, 2009) on a TOC analyzer (Aurora 1030W TOC analyzer, OI Analytical, College Station, TX, USA). Concentrations of inorganic anions and organic acids were determined using ion chromatography (Dionex™, ICS-5000$^+$ DC, Thermo Fisher Scientific) with an analytical guard column (IonPac™ AS11, Thermo Fisher Scientific).

Text C 2: Pyrosequencing reaction

The 16S rRNA gene V4 variable region PCR primers 515/806 for soil control and biochar amendments were conducted at MR DNA Laboratory (Shallowater, TX, USA) in a single-step 30 cycle PCR using a HotStarTaq Plus Master Mix Kit (Qiagen, USA). The reaction conditions included 94 °C for 3 min, 28 cycles (5 cycles used on PCR products) of 94 °C for 3 s, 53 °C for 40 s, and 72 for 1 min, followed by a final elongation step at 72 °C for 5 min.

Sequencing was performed on an Ion Torrent PGM following the manufacturer's guidelines, and sequencing data were analyzed using an in-house analysis pipeline (MR DNA, Shallowater, TX, USA). Sequences were denoised by depleting barcodes and primers and removing sequence data with <150 bp, with ambiguous base calls, and with homopolymer runs exceeding 6 bp. Operational taxonomic units (OTUs) were generated by defining clusters at 97% similarity using a basic local alignment search tool (BLAST) against a curated database derived from Green Gennes (DeSantis et al., 2006), RDP (Wang et al., 2007), and NCBI (Benson et al., 2009; Sayers et al., 2009).

Tables and Figures

Table C 1Experimental setup for microcosm experiments showing reaction time in Stage 1 and selected reactors for Stages 2 and 3.

	SedCTR	10%DIG	10%DIS	10%75G25S	SRWCTR	Water
Description	20 g floodplain soil	20 g floodplain soil 2 g DIG	20 g floodplain soil 2 g DIS	20 g floodplain soil 2 g 75G25S	River water control	Ultrapure water control
Reaction time						
7 d	a*, b*, c	a*, b*, c	a*, b*, c	a*, b*, c	a	a
30 d	a	a	a	a, b		
60 d	a, b	a	a	a		
90 d	a*, b*, c	a*, b*, c	a*, b*, c	a*, b*, c	a	a
120 d	a	a, b	a	a		
160 d	a	a	a, b	a		
200 d	a*, b*, c	a*, b*, c	a*, b*, c	a*, b*, c	a	a

[a] *Replicate experiment 1*
[b] *Replicate experiment 2*
[c] *Replicate experiment* 3
[*] *Selected reactors for Stages 2-3*

Table C 2 Chemical equilibrium for Hg-S and MeHg-S used in PhreeqcI calculations

. Reactions	References
$MeHg^{+} + SH^{-} = MeHgSH^{0}$ $\log K = 14.6$	(Liem-Nguyen et al., 2017)
$MeHg^{+} + NOM - RS^{-}_{(aq,ads)} = MeHgSR - NOM$ $\log K = 15.6$	(Liem-Nguyen et al., 2017)
$Hg^{2+} + 2HS^{-} = Hg(SH)^{0}_{2}$ $\log K = 38.6$	(Liem-Nguyen et al., 2017)
$Hg^{2+} + HS^{-} = HgS_{(s)} + H^{+}$ $\log K = 38.6 - 37.6$	(Liem-Nguyen et al., 2017)
$Hg^{2+} + 2NOM - RS^{-}_{(aq,ads)} = Hg(NOM - RS)_{2(aq,ads)}$ $\log K = 40$	(Liem-Nguyen et al., 2017)
$NOM - RSH_{(aq,ds)} = NOM - RS^{-}_{(aq,ads)} + H^{+}$ $\log K = 8.5$	(Liem-Nguyen et al., 2017)
$H_sS_{(aq)} = HS^{-} + H^{+}$ $\log K = 7.0$	(Liem-Nguyen et al., 2017)
$HgS_{(s)} + H^{+} = Hg^{2+} + HS^{-}$ $\log K = -36.9$	(Drott et al., 2013)
$Hg^{2+} + 2HS^{-} = HgS_2H^{-} + H^{+}$ $\log K = 32.3$	(Drott et al., 2013)
$Hg^{2+} + 2HS^{-} = HgS_2^{2-} + 2H^{+}$ $\log K = 23.2$	(Drott et al., 2013)
$4H_2O + 4S^{(0)} = SO_4^{2-} + 5H^{+} + 3HS^{-}$ $\log K = -7.18$	(Lovley and Phillips, 1994)

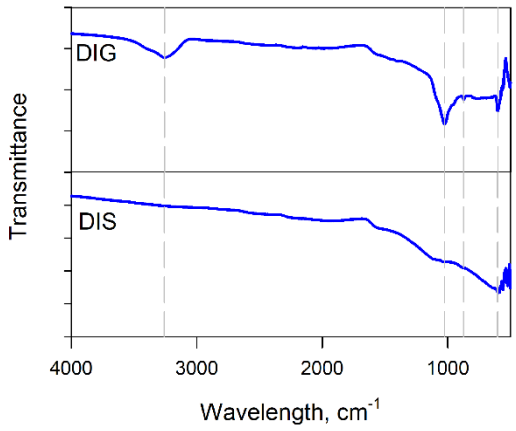

Fig. C 1 FTIR spectra for anaerobic digestate biochar (DIG) and distillers' grains biochar (DIS). Dashed lines at 3257, 1026, 874, and 602 cm^{-1} indicate vibration stretches attributed to the biochars.

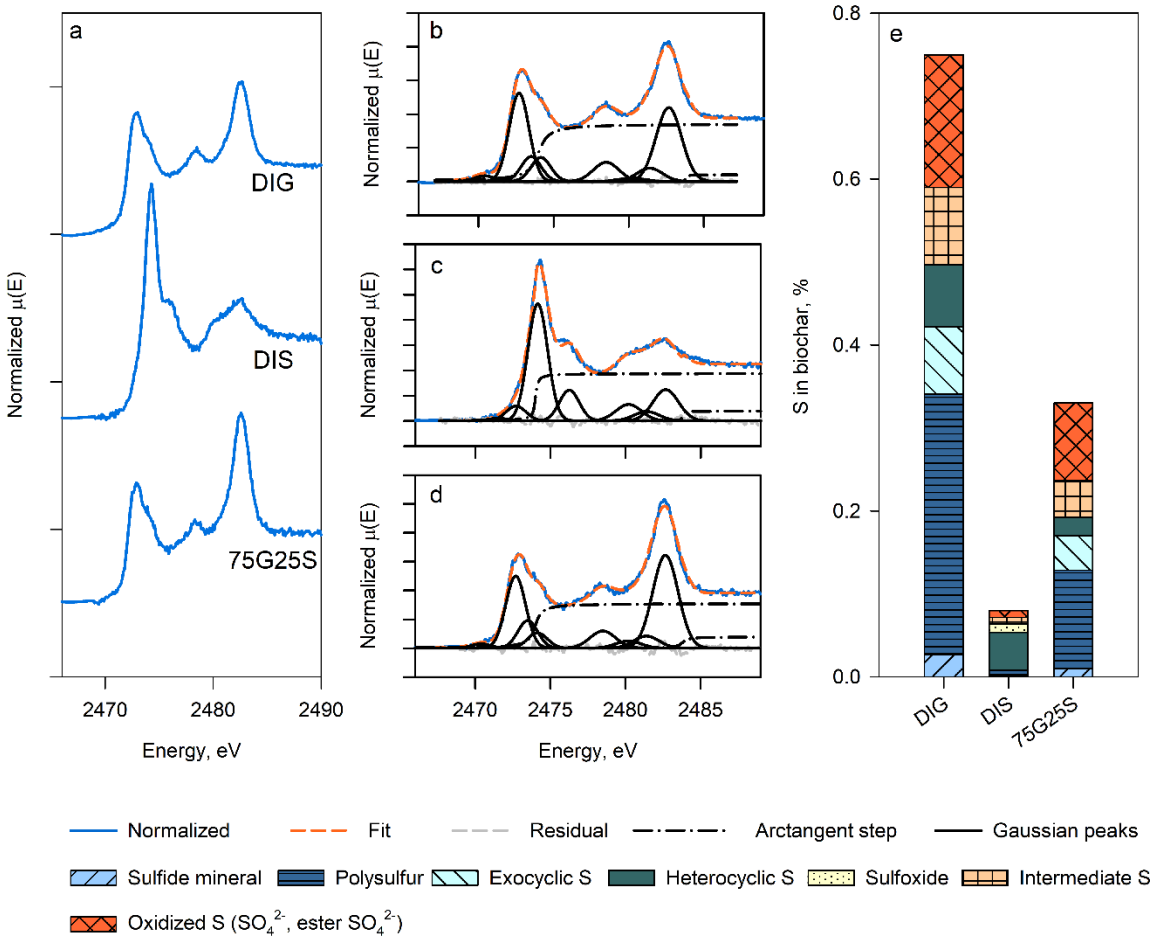

Fig. C 2 Normalized sulfur K-edge X-ray absorption near edge structure (XANES) for biochar used in this study (a). Gaussian peak fitting of S K-edge XANES spectra and the best-fit (orange dash line) for DIG (b, NSS = 6.7×10^{-4}), DIS (c, NSS = 1.3×10^{-3}), and 75G25S (d, NSS = 1.5×10^{-3}). Fractions of S obtained from the best-fit corrected with total S in biochar for DIG, DIS, and 75G25S (e).

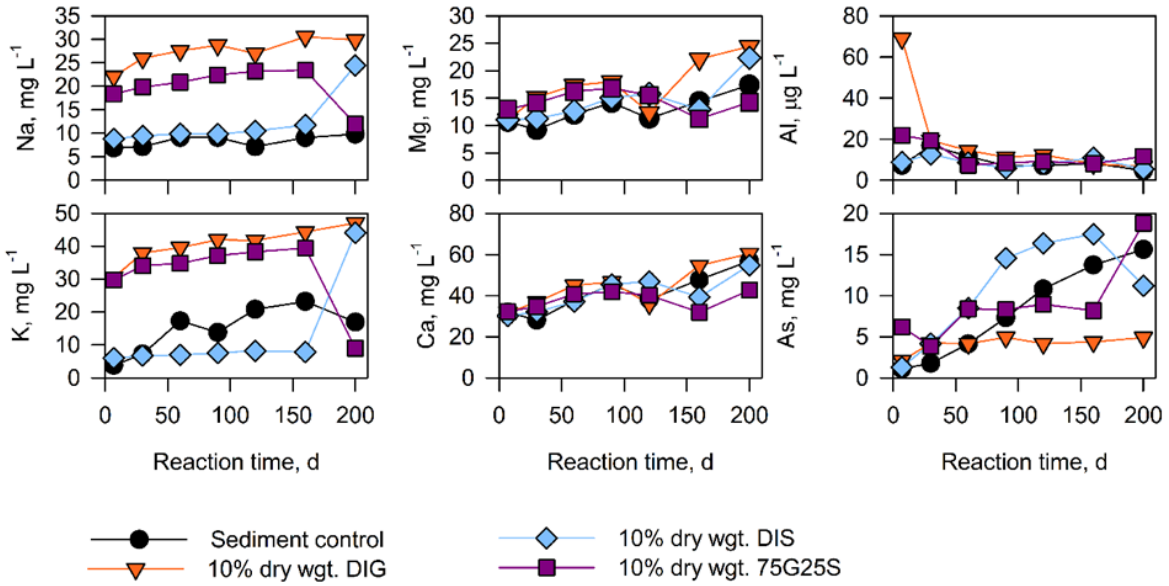

Fig. C 3 Concentrations of Na, Mg, Al, K, Ca, and As in soil control and biochar-amended systems in Stage 1.

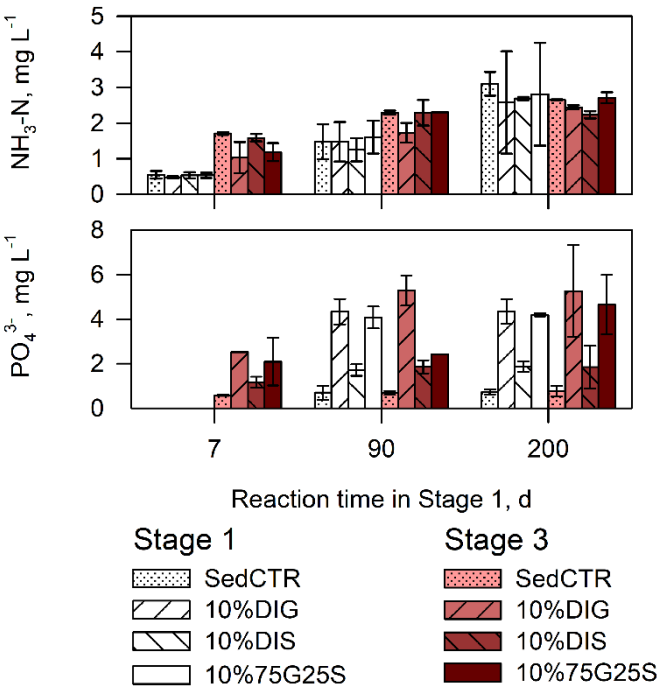

Fig. C 4 Concentrations of NH_3-N and PO_4^{3-} in soil control (SedCTR) and biochar-amended systems in Stage 3 (red bars) compared to their corresponding systems in Stage 1 (white bars). Error bars represent the standard deviation from replicate experiments. Results for SedCTR are from Chapter 3.

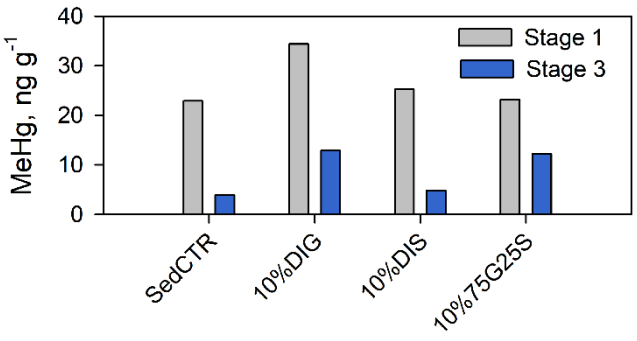

Fig. C 5 Solid MeHg in systems reacted for 200 d in Stage 1 (grey bars) and their corresponding systems in Stage 3 (blue bars). Error bars represent the standard deviation from replicate experiments. Results for soil control (SedCTR) are from Chapter 3.

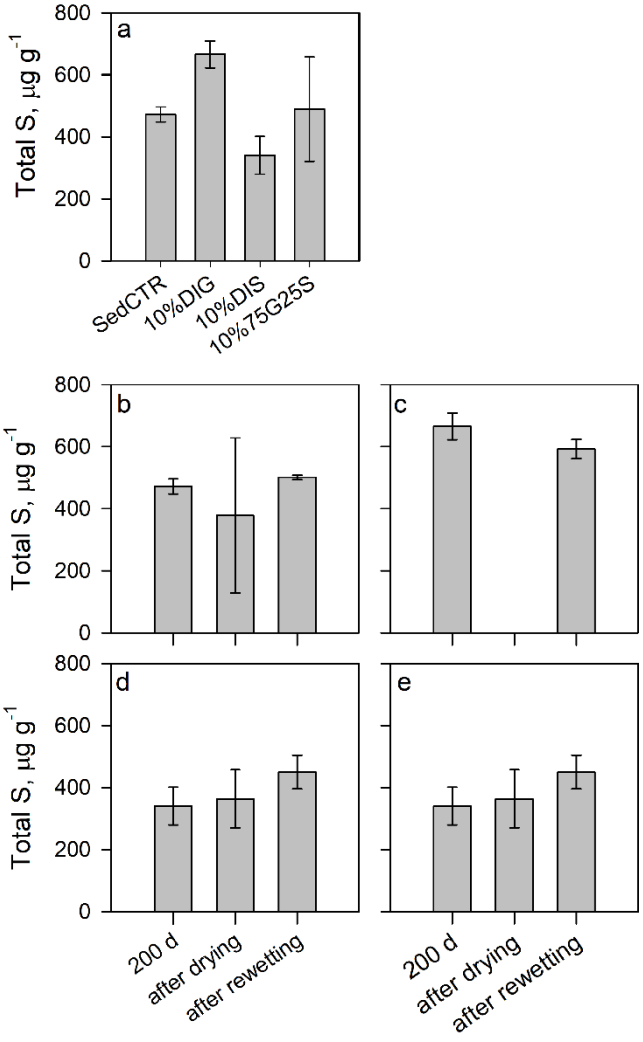

Fig. C 6 Total S in soil control and biochar-amended systems. (a) After equilibrating 200 d in Stage 1. (b-e) S content in systems in wetted for 200 d and the corresponding soil control (b), 10%DIG (c), 10%DIS (d), and 10%75G25S (e) systems.

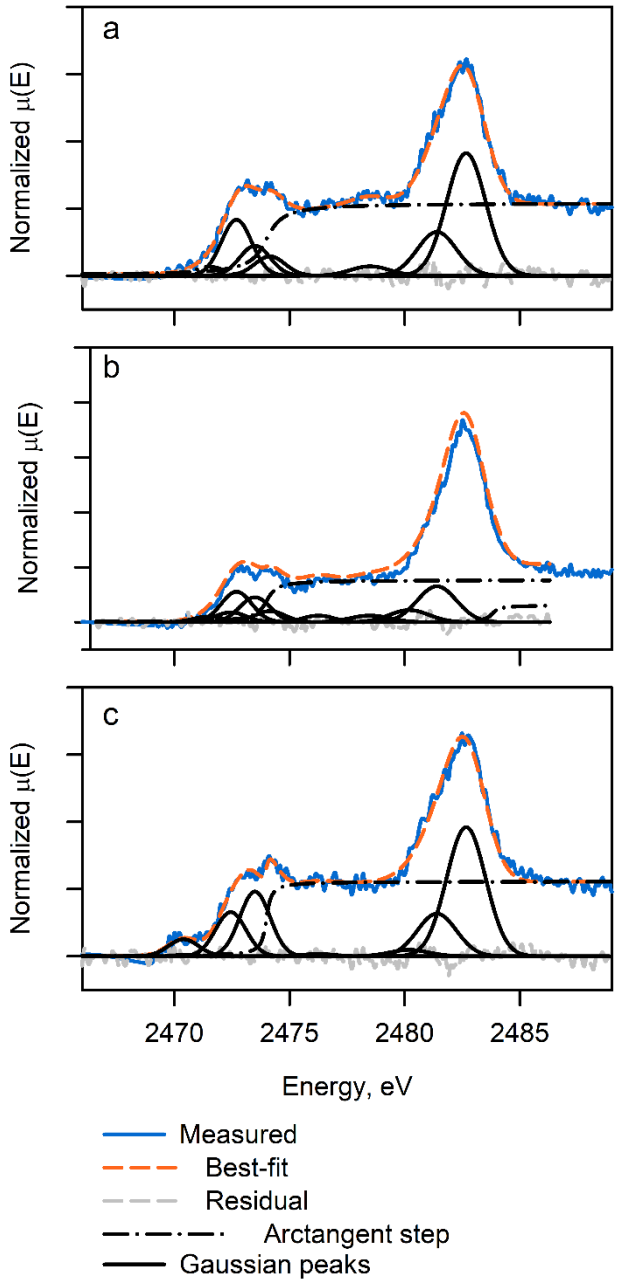

Fig. C 7 S K-edge X-ray absorption near edge structure (XANES) spectroscopy showing measured spectra (blue solid line) and best-fit (orange dash line) from Gaussian peak fitting for solid in 10%DIG reacted for 200 d in Stage 1 (a) (NSS=2.61×10^{-3}) and its corresponding systems in Stages 2(b) (NSS=1.12×10^{-2}), and 3(c) (NSS=3.78×10^{-3}).

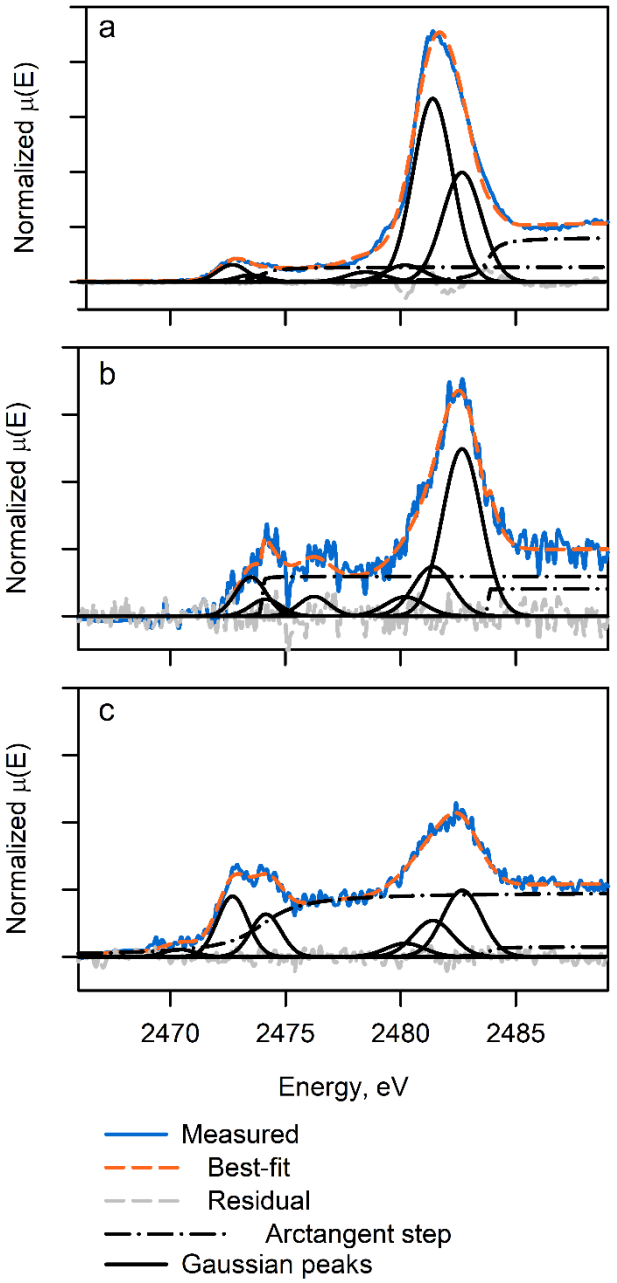

Fig. C 8 S K-edge XANES spectroscopy showing measured spectra (blue solid line) and best-fit (orange dash line) from Gaussian peak fitting for solid in 10%DIS reacted for 200 d in Stage 1 (a) (NSS=3.12×10^{-3}) and its corresponding systems in Stages 2(b) (NSS=1.50×10^{-2}), and 3(c) (NSS=4.22×10^{-3}).

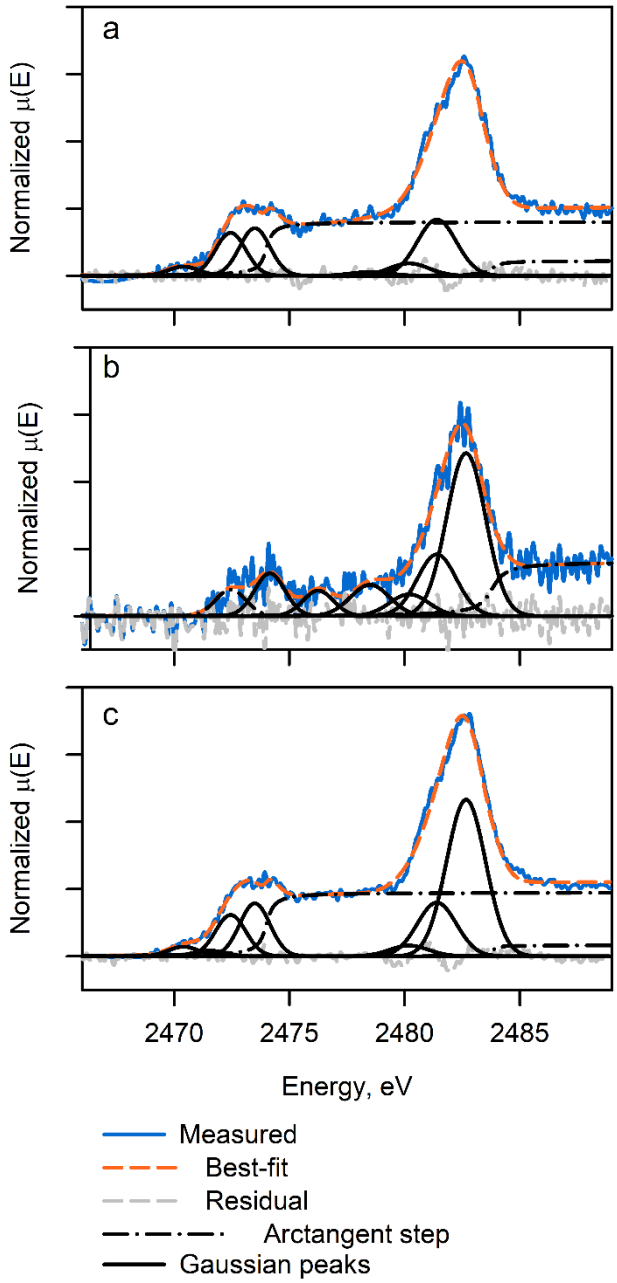

Fig. C 9 S K-edge XANES spectroscopy showing measured spectra (blue solid line) and best-fit (orange dash line) from Gaussian peak fitting for solid in 10%75G25S reacted for 200 d in Stage 1 (a) (NSS=3.58×10^{-3}) and its corresponding systems in Stages 2(b) (NSS=2.74×10^{-2}), and 3(c) (NSS=2.39×10^{-3}).

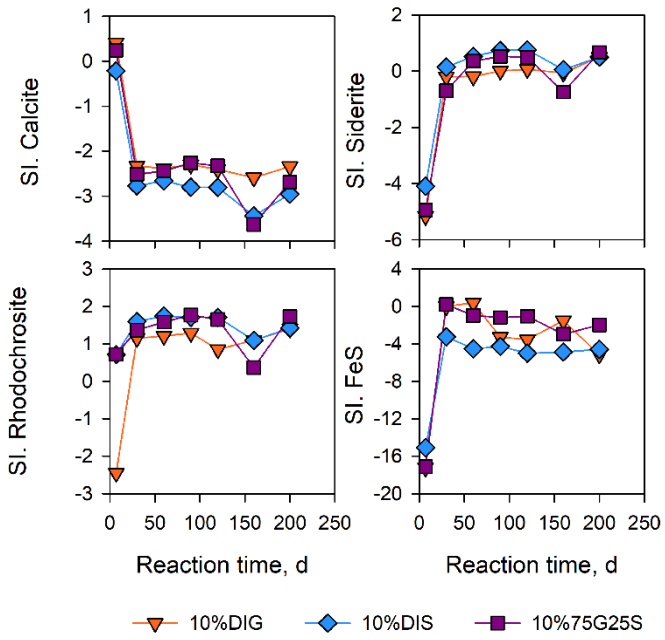

Fig. C 10 Saturation index for calcite ($CaCO_3$), siderite ($FeCO_3$), rhodochrosite ($MnCO_3$), and FeS in biochar-amended systems.

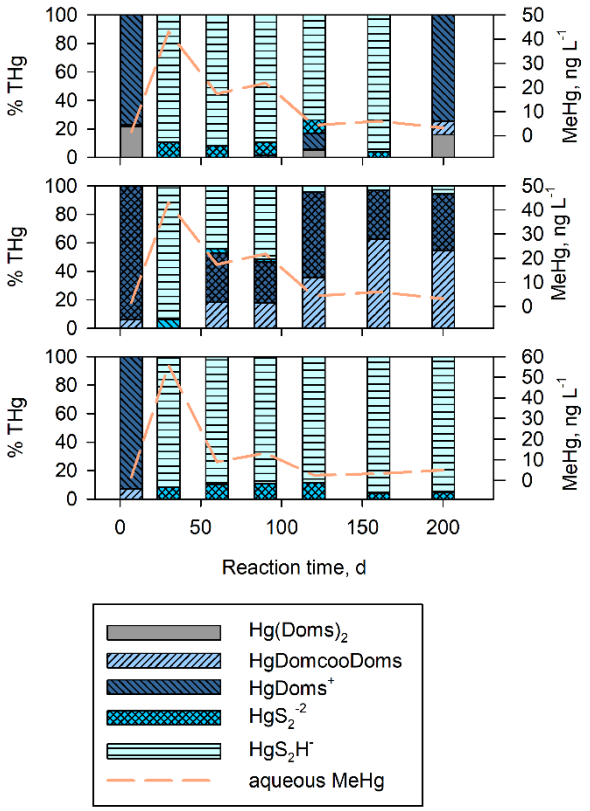

Fig. C 11 Results of geochemical calculation showing fractions of different Hg species of THg and their relations to aqueous MeHg in Stage 1 for 10%DIG (a), 10%DIS (b), and 10%75G25S (c) systems.

Appendix D

Supporting Information for Chapter 5

Experimental Details

Text D 1: Analytical information for aqueous parameters

pH, Eh, and alkalinity were determined immediately after sample collection. pH and Eh were collected on unfiltered aqueous samples. pH was determined using a combination Ross electrode (Orion model 8156, Thermo Scientific) with three-point calibrations (pH 7.00, 4.01, and 10.01) (Thermo Fisher Scientific), where calibration slopes were between 98 and 100%. Eh was determined using a combination platinum Ag/AgCl electrode (Orion 9678, Thermo Scientific) checked against Zobell's (Nordstrom, 1977) and Light's (Light, 1972) solutions. Eh was corrected to a standard hydrogen electrode. Alkalinity (as $CaCO_3$ mg L^{-1}) was determined by titrating an aqueous sample passing a 0.45-µm filter membrane using a digital titrator, 0.16 N H_2SO_4 (HACH), and bromocresol green/methyl red as an indicator.

Concentrations of S^{2-}, nitrogen ammonia (NH_3-N), and reactive phosphorous (PO_4^{3-}) were determined within 24 h of sample collection. Concentrations of dissolved $H_2S_{(g)}$ were determined on 10-mL 0.45-µm filtered samples using the methylene blue method (Method 10023 from Hach DR 2800 manual). Concentrations of NH_3-N were determined using LR Test'n Tube™ vials (Hach) following the salicylate method (Method 10023, Hach DR 2800 manual). Concentrations of reactive phosphorus (PO_4^{3-}) were determined using the PhosVer 3® (ascorbic acid) method (Method 8048, Hach DR 2800 manual). Concentrations of

dissolved $CH_{4(aq)}$ were determined using a headspace method (Kampbell and Vandegrift, 1998) and gas chromatography (GC) (7890B, Agilent).

Concentrations of unfiltered and 0.45-µm THg were determined using cold vapor atomic fluorescence spectroscopy (CVAFS, Tekran®2600, Tekran Instruments Corp., Scarborough, ON, Canada) following US EPA Method 1631 Revision E (US EPA, 2002). The instrumental method detection limit (n=5) was 0.18±0.03 ng L^{-1}. The relative percent difference (RPD%) for duplicate analyses and matrix spikes was 0.2-5.6% and 0.2-3%, respectively. Recovery for reference material (NIST 1641 e) was 102-108%.

Concentrations of MeHg were analyzed at the Biotron Experimental Climate Change Research Centre (University of Western Ontario, London, ON, Canada) following US EPA Method 1630 (US EPA, 2001). The instrumental method detection limit (n=3) was 0.006-0.008 ng L^{-1}. The percent recovery of matrix spikes was 78-82%. RPD% for duplicate analysis was 7-12%.

Concentrations of inorganic anions and organic acids were determined using ion chromatography (Dionex™, ICS-5000^{+} DC, Thermo Fisher Scientific) with an analytical guard column (IonPac™ AS11, Thermo Fisher Scientific). The relative standard deviation (RSD%) for duplicate analyses (n=4) targeting NO_3^- (>0.5 mg L^{-1}) and SO_4^{2-} was <5%. Concentrations of major cations were determined using inductively coupled plasma optical emission spectrometry (ICP-OES, iCAP 6000, Thermo Scientific), and concentrations of trace elements were determined using inductively coupled plasma mass spectroscopy (ICP-MS, X Series 2, Thermo Scientific). The RSD% for duplicate analyses (n=2) targeting Ca

was 1%. Concentrations of DOC were determined on a TOC analyzer (Aurora 1030W TOC analyzer, OI Analytical, College Station, TX, USA) using a wet oxidation method following US EPA Method 415.3 (US EPA, 2009). RPD% for duplicate analyses (n=7) was 0.37-2.84%. Recovery for certified materials (CRM Mauri-09) was 98-109%.

Text D 2: Details for pyrosequencing analysis

16S rRNA gene V4 variable region PCR primers 515/806 for soil control (HCSed) and biochar-amended systems were conducted by MR DNA Laboratory (Shallowater, TX, USA) in a single-step 30 cycle PCR using a HotStarTaq Plus Master Mix Kit (Qiagen, USA). The reaction conditions were 94 °C for 3 min, 28 cycles (5 cycles used on PCR products) at 94 °C for 3 s, 53 °C for 40 s, and 72 for 1 min, followed by a final elongation step at 72 °C for 5 min. Sequencing was performed on an Ion Torrent Personal Genome Machine (PGM) following the manufacturer's guidelines, and sequencing data were analyzed using an in-house analysis pipeline (MR DNA, Shallowater, TX). Sequences were denoised by depleting barcodes and primers and removing sequence data with <150 bp, with ambiguous base calls, and with homopolymer runs exceeding 6 bp. Operational taxonomic units (OTUs) were generated by defining clusters at 97% similarity using a basic local alignment search tool (BLAST) against a curated database derived from Green Gennes (DeSantis et al., 2006), RDP (Wang et al., 2007), and NCBI (Benson et al., 2009; Sayers et al., 2009).

Figures and Tables

Table D 1 Concentrations of THg for analyzed leachate samples passing through 0.2-µm filter membranes and corresponding pore water concentrations for soil control (HCSed), DIG- (HCDIG), and MOAK-amended systems (HCMOAK). Error bars represent standard deviation for pore water samples collected at two pore water ports in each humidity cell column.

HCSed			HCDIG			HCMOAK		
Wet-dry cycles	Leachate (0.2-µm) ng L^{-1}	Pore water ng L^{-1}	Wet-dry cycles	Leachate 0.2-µm ng L^{-1}	Pore water ng L^{-1}	Wet-dry cycles	Leachate 0.2-µm ng L^{-1}	Pore water ng L^{-1}
3	76	65±9	1	927	218	2	2251	NA
4	63	61±7	6	129	61±7	5	58	31
7	71	48±3	10	70	56±5	10	39	15

NA, Not analyzed

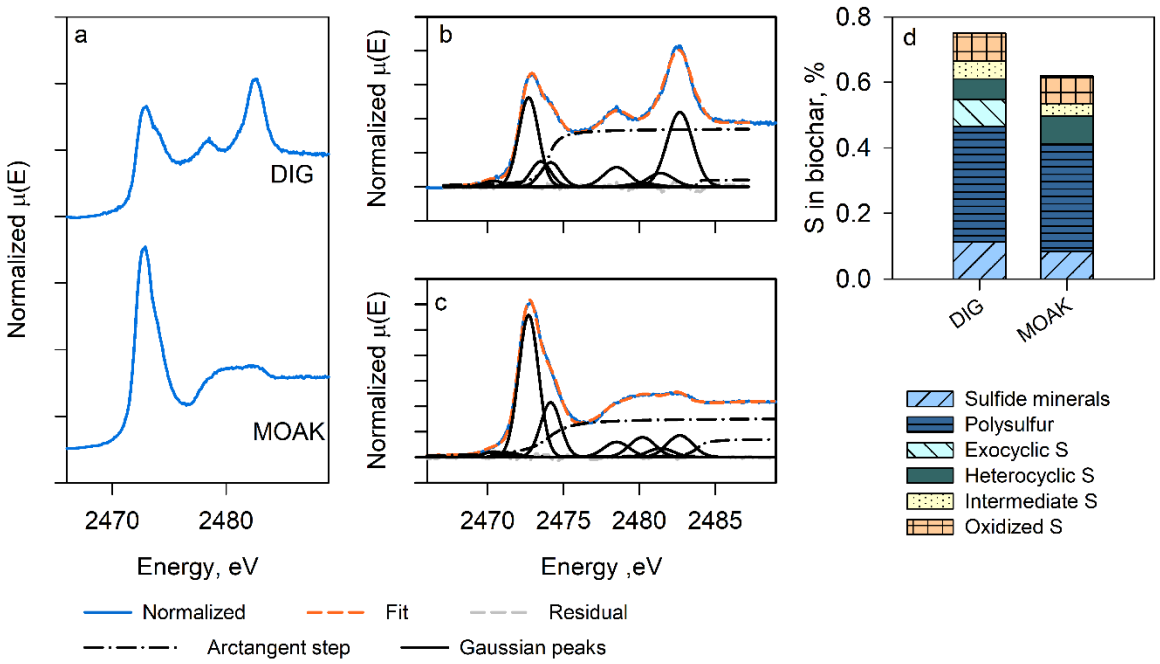

Fig. D 1 Normalized S K-edge X-ray absorption near edge structure (XANES) for biochar prepared from anaerobic digestion (DIG) and sulfurized hardwood biochar (MOAK) (a). S K-edge XANES spectra for DIG (b, NSS=6.70×10^{-4}) and MOAK (c, NSS=4.75×10^{-4}) were decomposed and analyzed using Gaussian peak fitting. Results of Gaussian peak fitting represent different S forms on biochars (d). Results for DIG and MOAK are from Chapters 3 and 4.

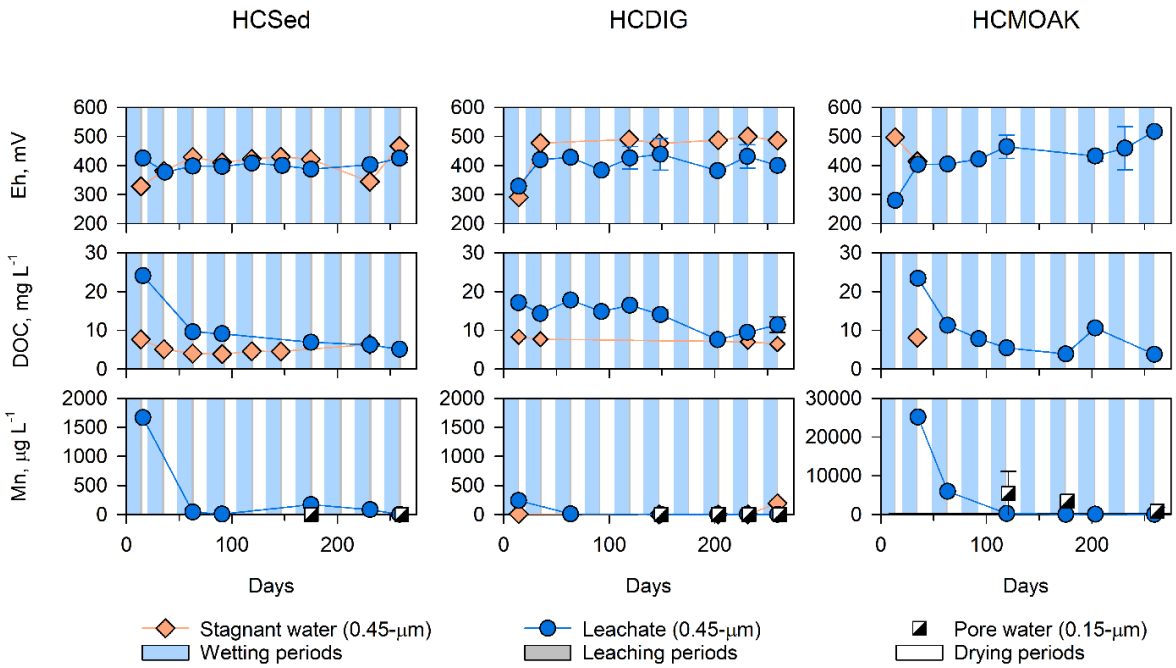

Fig. D 2 Eh and concentrations of DOC and Mn for soil control (HCSed), DIG- (HCDIG), and MOAK-amended systems (HCMOAK) as the number of wetting and drying cycles increased. Error bars for leachate represent the standard deviation for concentrations collected within 24 h after leaching started. Error bars for pore water represent the standard deviation for concentrations collected from two pore water collection ports in each column.

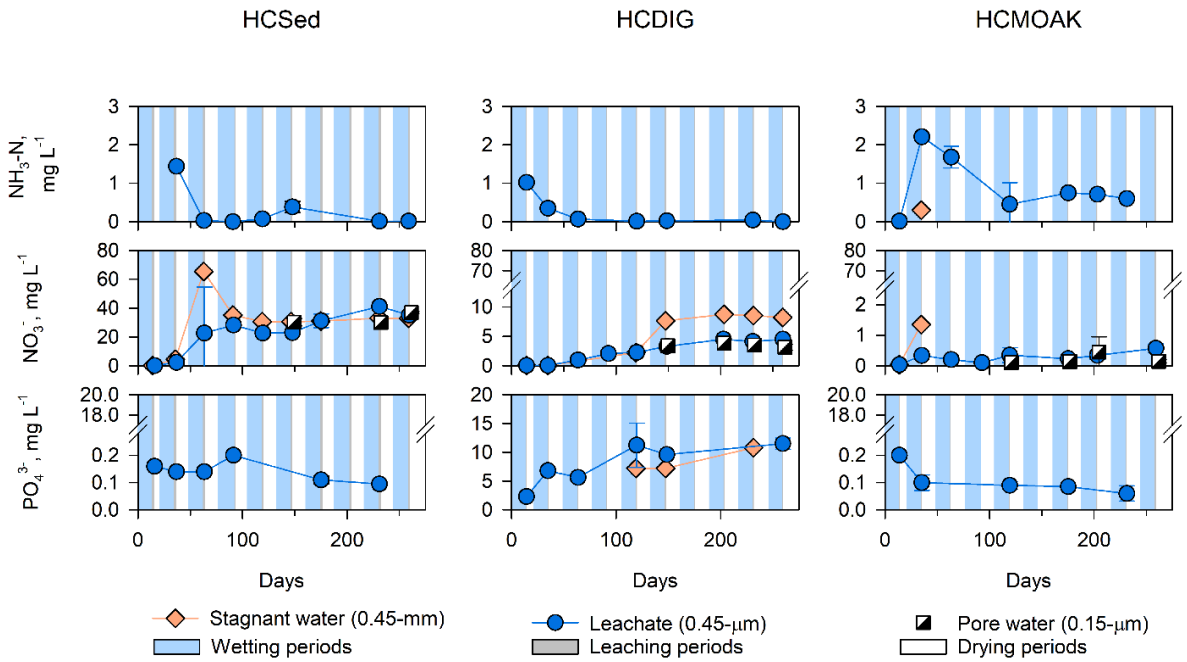

Fig. D 3 Concentrations of NH_3-N, NO_3^-, and PO_4^{3-} for soil control (HCSed), DIG-(HCDIG), and MOAK-amended systems (HMOAK) as the number of wetting and drying cycles increased. Error bars for leachates represent concentrations collected within 24 h after leaching. Error bars for pore water represent concentrations collected in two pore water collection ports for each column.

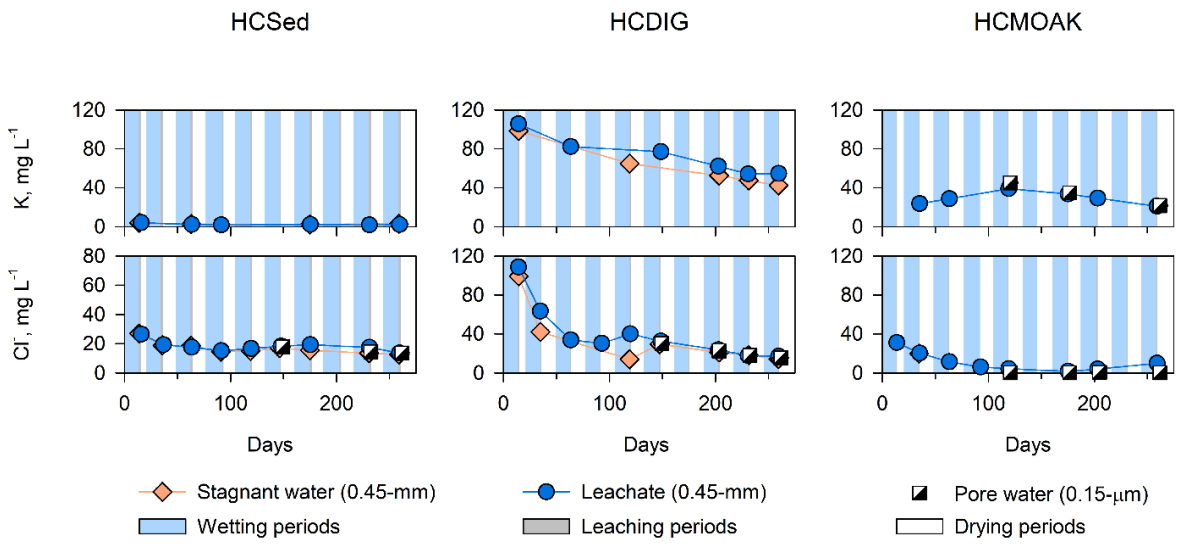

Fig. D 4 Concentrations of K and Cl in soil control (HCSed), DIG- (HCDIG), and MOAK-amended systems (HCMOAK) as the number of wetting and drying cycles increased. Error bars for leachate represent concentrations collected within 24 h after leaching started. Error bars for pore water represent concentrations collected in two pore water collection ports on each column.